
**Pacific Northwest
National Laboratory**

Operated by Battelle for the
U.S. Department of Energy

Hanford Tanks 241-AY-102 and 241-BX-101: Sludge Composition and Contaminant Release Data

K. M. Krupka
W. J. Deutsch
M. J. Lindberg
K. J. Cantrell

N. J. Hess
H. T. Schaefer
B. W. Arey

May 2004

Prepared for CH2M HILL Hanford Group, Inc.
and the U.S. Department of Energy
under Contract DE-AC06-76RL01830



DISCLAIMER

This report was prepared as an account of work sponsored by an agency of the United States Government. Neither the United States Government nor any agency thereof, nor Battelle Memorial Institute, nor any of their employees, makes **any warranty, express or implied, or assumes any legal liability or responsibility for the accuracy, completeness, or usefulness of any information, apparatus, product, or process disclosed, or represents that its use would not infringe privately owned rights.** Reference herein to any specific commercial product, process, or service by trade name, trademark, manufacturer, or otherwise does not necessarily constitute or imply its endorsement, recommendation, or favoring by the United States Government or any agency thereof, or Battelle Memorial Institute. The views and opinions of authors expressed herein do not necessarily state or reflect those of the United States Government or any agency thereof.

PACIFIC NORTHWEST NATIONAL LABORATORY

operated by

BATTELLE

for the

UNITED STATES DEPARTMENT OF ENERGY

under Contract DE-AC06-76RL01830

Printed in the United States of America

Available to DOE and DOE contractors from the

Office of Scientific and Technical Information,

P.O. Box 62, Oak Ridge, TN 37831-0062;

ph: (865) 576-8401

fax: (865) 576-5728

email: reports@adonis.osti.gov

**Available to the public from the National Technical Information Service,
U.S. Department of Commerce, 5285 Port Royal Rd., Springfield, VA 22161**

ph: (800) 553-6847

fax: (703) 605-6900

email: orders@ntis.fedworld.gov

online ordering: <http://www.ntis.gov/ordering.htm>



This document was printed on recycled paper.

**Hanford Tanks 241-AY-102 and 241-BX-101:
Sludge Composition and Contaminant Release Data**

K. M. Krupka	N. J. Hess
W. J. Deutsch	H. T. Schaefer
M. J. Lindberg	B. W. Arey
K. J. Cantrell	

May 2004

Prepared for
CH2M HILL Hanford Group, Inc. and
the U.S. Department of Energy
under Contract DE-AC06-76RL01830

Pacific Northwest National Laboratory
Richland, Washington 99352

Summary

This report describes the results of testing sludge samples from Hanford tanks 241-AY-102 (AY-102) and 241-BX-101 (BX-101). These tests were conducted to characterize the sludge and assess the water leachability of contaminants from the solids. A key finding of these tests is that technetium-99 is not completely water leachable and mobile from some of the tank sludges. In the case of tank AY-102, only 25% of the technetium-99 is water leachable, whereas for tank BX-101 all of it is water leachable. This work is being conducted to support the tank closure risk assessments being performed by CH2M HILL Hanford Group, Inc. for the U.S. Department of Energy. This is the first report of testing of BX-101 sludge and the second report of testing of AY-102. Lindberg and Deutsch (2003) described the first phase of testing on AY-102 material.

Initial (Tier 1) testing of BX-101 sludge consisted of acid digestion to determine the composition of the sludge and water leaching to estimate the soluble portion of the sludge. Subsequent analyses of samples from both BX-101 and AY-102 consisted of X-ray diffraction (XRD) to identify crystalline solids, scanning electron microscopy/energy-dispersive X-ray spectrometry (SEM/EDS) to view and measure the composition of the solids, and oxidation and reduction capacity measurements to evaluate the redox condition of the sludge. In addition to these tests, the composition of the sludge from AY-102 was measured by fusion analysis and the water leachability of the sludge was evaluated using periodic replenishment and selective extraction tests. The drainable liquid from tank AY-102 was tested using the X-ray absorption near edge structure (XANES) technique to determine redox state of the dissolved technetium.

The acid digestion and analysis of BX-101 showed that the predominant metals are aluminum, sodium, uranium-238, iron, manganese, and chromium. The predominant anions are carbonate/bicarbonate, nitrate, nitrite, sulfate, phosphate, and oxalate. In comparison with sludge from tank BX-101, AY-102 (previously analyzed) has higher concentrations of iron(8x), manganese(4x), nickel(20x), and sodium(2x), and lower concentrations of aluminum(1.7x) and uranium-238(31x).

Uranium-238 and technetium-99 are two of the primary tank waste contaminants of concern because of their long-half lives and relatively high mobility in the environment. The water leachabilities of these two radionuclides from the tank sludges were very different. Leach tests on BX-101 sludge showed that all of the technetium-99 but less than 10% of the uranium-238 was water leachable compared to leachabilities of only 20% of the technetium-99 and greater than 60% of the uranium-238 in sludge from AY-102. These results show the heterogeneities in tank compositions and the variabilities that exist in contaminant leaching.

The results of the XRD and SEM/EDS analyses of the AY-102 and BX-101 sludge samples are listed in Table 3-23. The crystalline phases (minerals) identified in AY-102 sludge were hematite, gibbsite, dawsonite and cancrinite (tentative). In BX-101, the primary mineral was gibbsite with a trace amount of cancrinite. There is good agreement between the phases identified by XRD and the compositions of the different types of particles identified by SEM/EDS. Generally, the SEM/EDS studies identified several additional phases that were not detected in the XRD patterns. This was expected because, as a rule of thumb, crystalline phases need to be present at greater than 5 wt% of the total sample mass (greater than

1 wt% under optimum conditions) to be detected by XRD. In addition to the crystalline phases, the SEM/EDS analyses identified a significant amount of solids in the sludge that may be amorphous because they lack external crystal faces. SEM/EDS analyses of the sludge samples did not identify any phases containing detectible concentrations of technetium, iodine, or nitrogen.

Periodic water replenishment (sequential leach) tests were conducted to evaluate whether or not the limited leachability of technetium-99 in AY-102 sludge was due to solubility control by a moderately-soluble salt. It was found that after the first water contact, in which 20% of the technetium-99 dissolved into the water, very little additional technetium-99 could be dissolved by contacting the solid with fresh, deionized water. These water leach tests were followed by selective extractions with stronger solvents to dissolve the carbonate and iron/aluminum oxyhydroxide minerals identified as components of the sludge. Very little additional technetium-99 was found in solution after dissolving the carbonate minerals. An additional 33% of the technetium-99 was found in solution when similar amounts of the iron and aluminum oxyhydroxide solids were dissolved by strong acid selective extraction. This shows the very recalcitrant nature of technetium-99 in the AY-102 sludge.

Sludges from tanks AY-102 and BX-101 were oxidized with hydrogen peroxide to test whether or not strong oxidation of the sludges would increase the release of technetium-99. Oxidation did not increase the amount of technetium-99 that was water leached from the sludges compared to amounts released by the sludges without oxidation treatment.

XANES analysis of the drainable liquid from tank AY-102 showed that the dissolved technetium was present as either the oxidized pertechnetate [Tc(VII)] or Tc(V) valence states, but not as reduced Tc(IV). This is consistent with the measurement of a low reduction capacity (28 $\mu\text{eq/g}$) for the AY-102 sludge.

Acknowledgments

The authors wish to acknowledge M. Connelly and T. E. Jones at CH2M HILL Hanford Group, Inc. (Richland, Washington) for providing project funding and technical guidance. We greatly appreciate the technical reviews provided by F. M. Mann (CH2M HILL), M. I. Wood (Fluor Hanford, Inc., Richland, Washington), R. J. Serne (PNNL), and W. Um (PNNL). The authors would also like to thank the PNNL staff S. R. Baum, K. M. Geiszler, I. V. Kutnyakov, and R. D. Orr for completing the chemical and radiochemical analyses of the solution samples from our studies. We are also particularly grateful to J. R. Zohn and L. F. Morasch (PNNL) for completing the editorial review and K. R. Neiderhiser (PNNL) for final work processing of our technical report.

The authors also wish to extend their appreciation for access to the resources provided by the Pacific Northwest Consortium – collaborative access team (PNC-CAT) at the Advanced Photon Source (Argonne National Laboratory, Argonne, Illinois) to complete the XAS analysis of the technetium redox state in the drainable liquid sample. The PNC-CAT project is supported by funding from the U.S. Department of Energy Basic Energy Sciences, the University of Washington, Simon Fraser University, and the NSERC in Canada. Use of the Advanced Photon Source is supported by the U. S. Department of Energy, Office of Science, Office of Basic Energy Sciences, under Contract No. W-31-109-Eng-38.

Acronyms and Abbreviations

AE	sample that has undergone the EPA acid digestion (or extraction) procedure
ASTM	American Society for Testing and Materials
am	amorphous
bse	backscattered electron
CCV	continuing calibration verification
DDI	distilled deionized (water)
DOE	U.S. Department of Energy
DUP	duplicate sample
EDS	energy-dispersive X-ray spectrometry
EMSP	DOE's Environmental Management Science Program
EPA	U.S. Environmental Protection Agency
ESL	Environmental Science Laboratory
EXAFS	extended X-ray absorption fine structure
FUS	sample that has undergone the KOH-KNO ₃ fusion treatment
GEA	gamma energy analysis
HLW	high-level radioactive waste
ICP-AES	inductively coupled plasma-atomic emission spectroscopy (same as ICP-OES)
ICP-MS	inductively coupled plasma-mass spectroscopy (spectrometer)
ICP-OES	inductively coupled plasma-optical emission spectroscopy (same as ICP-AES)
ICDD	International Center for Diffraction Data, Newtown Square, Pennsylvania
JCPDS	Joint Committee on Powder Diffraction Standards
LOQ	limit of quantification
ND	not determined
PDF TM	powder diffraction file
PNC-CAT	Pacific Northwest Consortium – collaborative access team
PNNL	Pacific Northwest National Laboratory
QA	quality assurance
QC	quality control
RPL	Radiochemical Processing Laboratory
se	secondary electron
SEM	scanning electron microscopy (or microscope)
TEM	transmission electron microscopy (or microscope)
TIC	total inorganic carbon
TOC	total organic carbon
WE	sample that has undergone a water extraction procedure
XAS	X-ray absorption spectroscopy
XANES	X-ray absorption near edge structure
XRD	X-ray powder diffractometry analysis (commonly called X-ray diffraction)

Units of Measure

Å	angstrom
θ	angle of incidence (Bragg angle)
$\Delta_f G_{298}^\circ$	Gibbs energy of formation from the elements in their reference states at 298.15 K
°C	temperature in degrees Celsius [$T(^{\circ}\text{C}) = T(\text{K}) - 273.15$]
eV	electron volt
g	gram
K	temperature in degrees (without degree symbol) Kelvin [$T(\text{K}) = T(^{\circ}\text{C}) + 273.15$]
K_{298}°	equilibrium constant at 298.15 K
kcal	kilocalorie, one calorie equals 4.1840 joules
keV	kilo-electron volt
kJ	kilojoule, one joule equals 4.1840 thermochemical calories
L	liter
μ	micro (prefix, 10^{-6})
μeq	microequivalent
μg	microgram
μm	micrometer
M	molarity, mol/L
mg	milligram
mL	milliliter
mM	molarity, millimol/L
mol	mole
rpm	revolution per minute
μmol	micromol
I/I_0	relative intensity of an XRD peak to the most intense peak
λ	wavelength
wt%	weight percent

Contents

Summary	iii
Acknowledgments.....	v
Acronyms and Abbreviations	vii
Units of Measure.....	ix
1.0 Introduction.....	1.1
2.0 Methods and Materials.....	2.1
2.1 AY-102 and BX-101 Sludge Samples.....	2.1
2.2 Fusion Analysis and Supporting EPA Acid Digestion – AY-102.....	2.3
2.3 XRD Analysis – AY-102 and BX-101	2.4
2.4 SEM/EDS Analysis – AY-102 and BX-101.....	2.6
2.5 XAS Analysis – AY-102 Drainable Liquid.....	2.7
2.6 Tier 1 Tests – BX-101	2.10
2.6.1 Moisture Content	2.10
2.6.2 Water Extracts	2.11
2.6.3 Acid Extracts	2.11
2.6.4 pH	2.11
2.6.5 Anion Analysis	2.11
2.6.6 Cations and Trace Metals	2.11
2.6.7 Alkalinity	2.12
2.6.8 Radioanalytical	2.12
2.7 Periodic Replenishment Tests – AY-102	2.12
2.8 Selective Extraction Tests – AY-102	2.13
2.9 Oxidation Test – AY-102 and BX-101.....	2.16
2.10 Reduction Capacity Test – AY-102 and BX-101	2.17

3.0	Results.....	3.1
3.1	Fusion and Acid Digestion Results – AY-102	3.1
3.2	XRD Results – AY-102 and BX-101	3.11
3.3	SEM/EDS Results – AY-102 and BX-101	3.17
3.3.1	Unleached AY-102 Sludge.....	3.17
3.3.2	Water-Leached AY-102 Sludge	3.40
3.3.3	Unleached BX-101 Sludge	3.51
3.3.4	General Observations	3.65
3.3.5	Comparison of XRD and SEM/EDS Results to Published Results of Others	3.66
3.4	XAS Results – AY-102 Drainable Liquid.....	3.70
3.5	Tier 1 Results – BX-101	3.71
3.5.1	Digestion Factors and Moisture Contents.....	3.71
3.5.2	Water Extract pH and Alkalinity	3.72
3.5.3	Technetium-99 and Uranium-238 – Water and Acid Extracts	3.73
3.5.4	Selected Metal Concentrations – Water and Acid Extracts	3.74
3.5.5	Anion Concentrations – Water Extracts	3.74
3.5.6	BX-101 Tier 1 Radioanalytical Results.....	3.75
3.6	Periodic Replenishment Test Results – AY-102	3.76
3.7	Selective Extraction Results – AY-102	3.77
3.8	Oxidation Test Results – AY-102 and BX-101	3.79
3.9	Reduction Capacity Test Results – AY-102 and BX-101	3.80
4.0	Conclusions.....	4.1
5.0	References.....	5.1
	Appendix A – As-Measured XRD Patterns for Sludge Samples.....	A.1
	Appendix B – EDS Results and Spectra for Unleached AY-102 Sludge	B.1
	Appendix C – EDS Results and Spectra for Water-Leached AY-102 Sludge.....	C.1
	Appendix D – EDS Results and Spectra for Unleached BX-101 Sludge	D.1

Figures

2-1	Unleached AY-102 tank sludge	2.2
2-2	Unleached BX-101 tank sludge.....	2.2
2-3	Exploded schematic view of the XRD sample holder.....	2.5
2-4	XRD pattern for collodion film measured in the absence of any sludge material.....	2.6
2-5	Components of primary container for solution samples	2.9
2-6	Components of secondary containment for solution and solid samples.....	2.10
2-7	Extraction sequence to determine association of technetium in readily soluble salts and dawsonite.....	2.15
2-8	Extraction sequence to determine association of technetium-99 in iron and aluminum oxyhydroxides	2.16
3-1	Background-subtracted XRD pattern measured for unleached AY-102 sludge sample using a copper radiation source.....	3.12
3-2	Background-subtracted XRD pattern measured for water-leached AY-102 sludge sample using a copper radiation source.....	3.12
3-3	Background-subtracted XRD pattern measured for unleached AY-102 sludge sample using a copper radiation source.....	3.13
3-4	Background-subtracted XRD pattern measured for unleached BX-101 sludge sample using a copper radiation source.....	3.13
3-5	XRD patterns for the unleached and water-leached AY-102 sludge samples compared to the database patterns for dawsonite, hematite, and gibbsite.....	3.14
3-6	XRD pattern for the unleached AY-102 sludge sample compared to the database patterns for dawsonite, gibbsite, hematite, and cancrinite	3.15
3-7	XRD pattern for the unleached BX-101 sludge sample compared to the database pattern for gibbsite and cancrinite.....	3.15
3-8	Low magnification scanning electron micrograph showing general morphology of particles in subsample “unleached 15935-1”	3.20
3-9	Micrograph showing at higher magnification the area indicated by the yellow-dotted square in Figure 3-8 of subsample “unleached 15935-1”	3.20

3-10	Micrograph showing at higher magnification the large lath-shaped crystal at the center of the previous figure of subsample “unleached 15935-1”	3.21
3-11	Micrograph showing various particle types that comprise subsample “unleached 15935-1”	3.21
3-12	Micrograph showing various particle types that comprise subsample “unleached 15935-1”	3.22
3-13	Micrograph showing various particle types that comprise subsample “unleached 15935-1”	3.22
3-14	Micrograph showing at higher magnification botryoidal aggregate of iron-rich, sodium-containing oxide particles in subsample “unleached 15935-1”	3.23
3-15	Backscatter electron micrograph in showing various particle types that comprise subsample “unleached 15935-1”	3.23
3-16	Backscatter electron micrograph in showing various particle types that comprise subsample “unleached 15935-1”	3.24
3-17	Backscatter electron micrograph in showing various particle types that comprise subsample “unleached 15935-1”	3.24
3-18	Backscatter electron micrograph in showing at higher magnification the particles labeled by “eds23” in Figure 3-17 of subsample “unleached 15935-1”	3.25
3-19	Low magnification scanning electron micrograph showing general morphology of large aggregate particles in subsample “unleached 15935-2”	3.27
3-20	Micrograph showing at higher magnification the area indicated by the yellow-dotted square #1 in Figure 3-19 of subsample “unleached 15935-2”	3.27
3-21	Micrograph showing at higher magnification the area indicated by the yellow-dotted square #2 in Figure 3-19 of subsample “unleached 15935-2”	3.28
3-22	Micrograph showing typical large aggregate particle in subsample “unleached 15935-2”	3.28
3-23	Micrograph showing at higher magnification the area indicated by the yellow-dotted square in Figure 3-22 of subsample “unleached 15935-2”	3.29
3-24	Micrograph showing range of particle types in subsample “unleached 15935-2”	3.29
3-25	Micrograph showing typical silver-oxide and iron, sodium-oxide particles and range of particle types in subsample “unleached 15935-2”	3.30
3-26	Micrograph showing large carbon-rich particle in subsample “unleached 15935-2”	3.30

3-27	Micrograph showing at higher magnification the area indicated by the yellow-dotted square of the large carbon-rich particle in Figure 3-26 of subsample “unleached 15935-2”	3.31
3-28	Low magnification scanning electron micrograph showing general morphology of large aggregate particles, including large carbon-rich particles, in subsample “unleached 15935-3”	3.33
3-29	Micrograph showing at higher magnification the area indicated by the yellow-dotted square of the large carbon-rich particle in Figure 3-28 of subsample “unleached 15935-3”	3.33
3-30	Secondary electron micrograph showing crust-like fragments of sludge solid in subsample “unleached 15935-3”	3.34
3-31	Backscatter electron micrograph showing area enriched in uranium in crust-like fragments of sludge solid in subsample “unleached 15935-3”	3.34
3-32	Electron micrograph showing at higher magnification area enriched in uranium in sludge solid in subsample “unleached 15935-3”	3.35
3-33	Electron micrograph showing at higher magnification section of crust-like fragment in bottom right corner of Figure 3-32 in subsample “unleached 15935-3”	3.35
3-34	Micrograph showing range of typical particle aggregate and types of individual particles in subsample “unleached 15935-3”	3.36
3-35	Micrograph showing at higher magnification lath- and prismatic-shaped particles on upper left edge of large particle aggregate in Figure 3-34 of subsample “unleached 15935-3”	3.36
3-36	Micrograph showing range of particle types in subsample “unleached 15935-3”	3.37
3-37	Micrograph showing range of particle types in subsample “unleached 15935-3”	3.37
3-38	Micrograph showing range of particle types in subsample “unleached 15935-3”	3.38
3-39	Low magnification scanning electron micrograph showing general morphology of particles in subsample “leached 15935-1”	3.42
3-40	Micrograph showing at higher magnification the area indicated by the yellow-dotted square in Figure 3-39 of subsample “leached 15935-1”	3.42
3-41	Micrograph showing range of typical particle types in subsample “leached 15935-1”	3.43
3-42	Micrograph showing range of typical particle types in subsample “leached 15935-1”	3.43
3-43	Micrograph showing range of typical particle types in subsample “leached 15935-1”	3.44

3-44	Micrograph showing range of typical particle types in subsample “leached 15935-1”	3.44
3-45	Micrograph showing range of typical particle types and crust-like aggregate in subsample “leached 15935-1”	3.45
3-46	Micrograph showing at higher magnification crust-like particle aggregate in center of Figure 3-45 of subsample “leached 15935-1”	3.45
3-47	Low magnification scanning electron micrograph showing general morphology of particles in subsample “leached 15935-2”	3.47
3-48	Micrograph showing at higher magnification the crust-like particle aggregate in Figure 3-47 of subsample “leached 15935-2”	3.47
3-49	Micrograph showing at higher magnification particles in area indicated by the yellow-dotted square #2 in Figure 3-47 of subsample “leached 15935-2”	3.48
3-50	Low magnification scanning electron micrograph showing general morphology of particle aggregates in subsample “leached 15935-2”	3.48
3-51	Micrograph showing at higher magnification particles in area indicated by the yellow-dotted square in Figure 3-50 of subsample “leached 15935-2”	3.49
3-52	Low magnification scanning electron micrograph showing general morphology of particles in subsample “unleached 16503-1”	3.53
3-53	Micrograph showing prismatic-like particles with hexagonal-like symmetry features in subsample “unleached 16503-1”	3.53
3-54	Micrograph showing range of typical particle types, including large needle-like grains, in subsample “unleached 16053-1”	3.54
3-55	Micrograph showing at higher magnification particles, including “ball-of-twine”-like crystals, in area indicated by the yellow-dotted square in Figure 3-54 of subsample “unleached 16503-1”	3.54
3-56	Micrograph showing typical botryoidal-shaped, uranium-rich particle aggregates in subsample “unleached 16503-1”	3.55
3-57	Micrograph showing at higher magnification botryoidal-shaped, uranium-rich particles at center of Figure 3-56 of subsample “unleached 16503-1”	3.55
3-58	Micrograph showing botryoidal-shaped, uranium-rich particles in subsample “unleached 16503-1”	3.56
3-59	Micrograph showing typical particle types in subsample “unleached 16503-1”	3.56
3-60	Micrograph showing typical particle types in subsample “unleached 16503-1”	3.57

3-61	Micrograph showing typical large particle aggregate in subsample “unleached 16503-1”	3.57
3-62	Micrograph showing range of typical particle types, including large needle-like grains, in subsample “unleached 16053-2”	3.59
3-63	Micrograph showing at higher magnification particles, including botryoidal-shaped, uranium-rich particle aggregate, in area indicated by the yellow-dotted square in Figure 3-62 of subsample “unleached 16503-2”	3.59
3-64	Micrograph showing typical particle types and aggregates in subsample “unleached 16053-2”	3.60
3-65	Micrograph showing at higher magnification particles, including “ball-of-twine”-like crystals, in area indicated by the yellow-dotted square #1 in Figure 3-64 of subsample “unleached 16503-2”	3.60
3-66	Micrograph showing at higher magnification “ball-of-twine”-like crystals in left-center area of Figure 3-65 in subsample “unleached 16503-2”	3.61
3-67	Micrograph showing at higher magnification botryoidal-shaped, uranium-rich particle aggregate in area indicated by the yellow-dotted square #2 in Figure 3-64 of subsample “unleached 16503-2”	3.61
3-68	Micrograph showing botryoidal-shaped, uranium-rich particles in subsample “unleached 16503-2”	3.62
3-69	Micrograph showing typical particle types in subsample “unleached 16503-2”	3.62
3-70	Micrograph showing at higher magnification “ball-of-twine”-like crystals in area indicated by the yellow-dotted square #1 in Figure 3-69 of subsample “unleached 16503-2”	3.63
3-71	Micrograph showing at higher magnification prismatic-shaped crystals in the area indicated by the yellow-dotted square #2 in Figure 3-69 of subsample “unleached 16503-2”	3.63
3-72	Estimated sizes of interaction volumes resulting from electron-beam penetration in four types of solids identified in the SEM/EDS analyses	3.67
3-73	Technetium K-edge XANES spectra	3.70

Tables

2-1	Summary of the sludge samples analyzed by XRD and SEM/EDS.....	2.2
2-2	Digestion factors for samples of AY-102 sludge solid used for the EPA acid digestion and KOH-KNO ₃ fusion treatments.....	2.4
2-3	Contact times and pH values for periodic replenishment test on tank AY-102 sludge.....	2.13
3-1	Concentrations of elements measured by ICP-OES per gram of dry sludge	3.3
3-2	Concentrations of elements measured by ICP-OES per gram of dry sludge (continued).....	3.4
3-3	Concentrations of elements measured by ICP-OES per gram of dry sludge (continued).....	3.5
3-4	Concentrations of elements determined from ICP-MS analysis per gram of dry sludge.....	3.6
3-5	Concentrations of elements determined from ICP-MS analysis per gram of dry sludge (continued)	3.7
3-6	Concentrations of technetium-99, uranium-238, and actinides measured by ICP-MS per gram of dry sludge	3.8
3-7	Gamma energy analysis in microcuries per gram of dry sludge	3.8
3-8	Gamma energy analysis in micrograms per gram of dry sludge.....	3.9
3-9	Total beta and total alpha activities and strontium-90 concentrations per gram of dry sludge	3.9
3-10	Summary of the average concentrations from the EPA acid digestion and KOH-KNO ₃ fusion analyses for the composition of unleached AY-102 sludge	3.10
3-11	Comparison of cadmium, chromium, and lead concentrations determined by ICP-MS and ICP-OES per gram of dry sludge.....	3.11
3-12	Mineral phases identified by XRD in AY-102 and BX-101 sludge samples.....	3.14
3-13	Summary of SEM/EDS data recorded in this study and listed in this report for the three subsamples of unleached AY-102 sludge	3.17
3-14	Qualitative compositions determined by SEM/EDS that include the emission peak for carbon for particles observed in unleached subsample 15935-1 of AY-102 tank sludge	3.26
3-15	Qualitative compositions determined by SEM/EDS that include the emission peak for carbon for particles observed in unleached subsample 15935-2 of AY-102 tank sludge	3.32

3-16	Qualitative compositions determined by SEM/EDS that include the emission peak for carbon for particles observed in unleached subsample 15935-3 of AY-102 tank sludge	3.39
3-17	Summary of SEM/EDS data recorded in this study and listed in this report for the two subsamples of water-leached AY-102 sludge	3.40
3-18	Qualitative compositions determined by SEM/EDS that include the emission peak for carbon for particles observed in leached subsample 15935-1 of AY-102 tank sludge	3.46
3-19	Qualitative compositions determined by SEM/EDS that include the emission peak for carbon for particles observed in leached subsample 15935-2 of AY-102 tank sludge	3.50
3-20	Summary of SEM/EDS data recorded in this study and listed in this report for the two subsamples of unleached BX-101 sludge.....	3.51
3-21	Qualitative compositions determined by SEM/EDS that include the emission peak for carbon for particles observed in unleached subsample 16503-1 of BX-101 tank sludge.....	3.58
3-22	Qualitative compositions determined by SEM/EDS that include the emission peak for carbon for particles observed in unleached subsample 16503-2 of BX-101 tank sludge.....	3.64
3-23	Comparison of XRD and SEM/EDS results for this study and for Bechtold et al. (2003)	3.68
3-24	Preparation data and moisture content	3.71
3-25	Water extract pH values	3.72
3-26	Alkalinities from water extracts	3.72
3-27	Technetium-99 and uranium-238 concentrations in BX-101 sludge from water and acid extracts	3.73
3-28	Water leachable percentages of technetium-99 and uranium-238 in BX-101 and AY-102 sludge samples	3.73
3-29	Metal concentrations in BX-101 sludge – ICP-OES analysis.....	3.74
3-30	Anion concentrations in BX-101 sludge from water extracts	3.75
3-31	BX-101 Gamma Energy Analysis.....	3.75
3-32	BX-101 Gross Alpha and Beta Analysis from water and acid extracts	3.76
3-33	Percentages of radionuclides in Tank AY-102 sludge that are soluble in sequential water leaches	3.76
3-34	Percentages of metals in Tank AY-102 sludge that are soluble in sequential water leaches	3.77

3-35	Selective extraction results for a NaHCO ₃ /Al extractant solution followed by an acetate buffer solution	3.78
3-36	Selective extraction results for a sequence of extractions starting with an acetate buffer, followed by a formate buffer, and then 8 M HNO ₃	3.78
3-37	Batch oxidation leach results.....	3.80

1.0 Introduction

This report describes the characterization and testing of sludge samples from Hanford tanks 241-AY-102 (AY-102) and 241-BX-101 (BX-101). This work was conducted to aid in the development of realistic contaminant source terms for residual waste in Hanford tanks at closure. These source terms are necessary for accurate risk assessment models.

Sludge samples from the tanks (and a drainable liquid sample from AY-102) were supplied to Pacific Northwest National Laboratory (PNNL) by CH2M HILL Hanford Group, Inc. Initial (Tier 1) tests to characterize the BX-101 sludge and identify water leachable constituents were conducted. The Tier 1 tests on AY-102 sludge were conducted previously and reported in Lindberg and Deutsch (2003); however, a comparison of some of the results of Tier 1 testing of the sludges from the two tanks is provided in this report. The Tier 1 tests consist primarily of acid digestion of the sludge to measure elemental concentrations in the solid and water leaching of the sludge to evaluate contaminant mobility in infiltrating water.

Based on the results of the Tier 1 tests, additional testing and analysis was performed to augment the characterization of the material and elucidate the controlling mechanism(s) for the release of technetium-99, which is one of the most important sludge constituents from a long-term risk perspective. These Tier 2 tests consisted of:

- AY-102 sludge fusion analysis
- AY-102 and BX-101 sludge X-ray powder diffractometry (XRD) analysis
- AY-102 and BX-101 sludge scanning electron microscopy/energy-dispersive X-ray spectrometry (SEM/EDS) analysis
- AY-102 drainable liquid X-ray absorption spectroscopy (XAS) analysis
- AY-102 sludge periodic (water) replenishment tests
- AY-102 sludge selective extraction tests
- AY-102 and BX-101 sludge oxidation tests
- AY-102 and BX-101 sludge reduction capacity measurements

The testing procedures are described in Section 2 of this report and the results are provided in Section 3. The conclusions are listed in Section 4.

2.0 Methods and Materials

2.1 AY-102 and BX-101 Sludge Samples

Archived samples of waste from tank AY-102 were shipped from the 222-S Laboratory to the PNNL Radiochemical Processing Laboratory (RPL) on December 16, 2002. These samples consisted of four jars of sludge (jars 15935, 17785, 18686, and 18761) and two jars of drainable liquid (jars 19332 and 18544). The samples used for the Tier 2 tests described in this report came from jars 15935 and 18686 (sludges) and jar 19332 (drainable liquid). These samples of sludge were used because they represent discrete intervals in the cores collected from tank AY-102 and are not composites of core segments. Jar 15935 material came from core number 270, segment 10 (LABCORE Number S00T000035) and jar 18686 material came from core number 281, segment 11 (LABCORE Number S01T000153). The remaining unused material from tank AY-102 is stored in the RPL.

Tier 1 tests (described in Section 2.6) were conducted on three Auger samples from tank BX-101. The sampling points and the laboratory identifiers are as follows:

- 94-AUG-004 Auger Subsample A – S02T001253
- 94-AUG-004 Auger Subsample B – S02T001254
- 94-AUG-005 Auger Subsample B – S02T001255

Auger samples numbered 94-AUG-004 were sampled from BX-101 Riser 1 and 94-AUG-005 samples were collected from BX-101 Riser 7. The samples were initially broken down in the 222 S hot cells on June 20, 1994 (94-AUG-004) and June 21, 1994 (94-AUG-005). Subsamples were then shipped to the RPL. The samples were later delivered to the Environmental Science Laboratory (ESL 3720 building, 300 Area). At the end of fiscal year 2003, the instrumentation, staff supporting these studies, and Auger samples 94-AUG-044 and 94-AUG-005 were moved to the RPL in preparation for the closure and decommissioning of the 3720 building.

Lindberg and Deutsch (2003) provide further description of the unleached (raw) AY-102 (jar 15935) sludge sample and of the results of Tier 1 testing of AY-102 material. Photographs of the unleached (raw) AY-102 (jar 15935) and BX-101 (jar 16503) sludge samples are shown in Figure 2-1 and Figure 2-2, respectively. Materials characterized by XRD and SEM/EDS are listed in Table 2-1. The water-leached sample of AY-102 (jar 15935) sludge used for XRD and SEM/EDS analyses was taken from the periodic replenishment tests (see Section 2.7). The water-leached sample had undergone all sequential contacts listed in Table 2-3. The resulting solid was then placed in a tube, contacted with 30 mL distilled deionized (DDI) water, and allowed to react for 36 additional days at which time the liquid was removed and the solid material was prepared for XRD and SEM/EDS analyses.

Table 2-1. Summary of the sludge samples analyzed by XRD and SEM/EDS

Sludge Sample	Analysis by XRD	Analysis by SEM/EDS
Unleached (raw) AY-102 (jar 15935) sludge	X	X
Water-leached AY-102 (jar 15935) sludge	X	X
Unleached (raw) AY-102 (jar 18686) sludge	X	
Unleached (raw) BX-101 (jar 16503) sludge	X	X

SEM/EDS = Scanning electron microscopy/energy-dispersive X-ray spectrometry.
XRD = X-ray powder diffractometry analysis.



Figure 2-1. Unleached (raw) AY-102 tank sludge (from jar 15935)



Figure 2-2. Unleached (raw) BX-101 tank sludge (from jar 16503)

2.2 Fusion Analysis and Supporting EPA Acid Digestion – AY-102

The bulk composition of the untreated (raw) AY-102 (jar 15935) sludge solid was determined using accepted PNNL internal procedure AGG-ESL-001, *Solubilization of Metals from Solids Using a KOH-KNO₃ Fusion*.¹ The KOH-KNO₃ fusion-dissolution procedure is the most commonly used method for solubilization of Hanford tank sludge samples for their chemical analysis by inductively coupled plasma-mass spectroscopy (ICP-MS) and other instrument methods (De Lorenzo et al. 1994; Simpson 1994; Fiskum et al. 2000; Smith et al. 2001). Benefits of using this procedure include the following: effective metathesizing of insoluble salts, such as SrSO₄, PuPO₄, PuF₃, and ThF₃, into acid soluble hydroxides; fusion is completed at relatively low temperature (550°C) compared to other fluxing agents, such as 1100°C for the LiBO₂ (lithium metaborate) fluxing agent; and nickel or zirconium crucibles, as opposed to the more costly platinum crucibles, can be used for the fusion.²

The KOH-KNO₃ fusion-dissolution procedure consists of chemical analyses of a solution resulting from water and acid dissolutions of a solid that has been fused at a high temperature with a caustic fluxing agent. In this procedure, 300 mg of the tank waste sludge material was mixed with a fluxing agent of 2.0 g KOH – 0.2 g KNO₃ in a nickel crucible. The crucible was then covered and transferred to a muffle furnace preheated to 550°C. Fusion was accomplished by heating the sample-flux mixture for 60 minutes at the required temperature. After this period of time, the crucible was removed from the furnace and allowed to cool to ambient room temperature. The fused solid was then dissolved in DDI water. The resulting solution was transferred to a 100-mL volumetric flask to which 1 mL of 1.0 M hydroxylamine HCl was added. Ten milliliters of an 8 M nitric acid solution was added to the crucible to dissolve any remaining residual solid. The resulting solution was also added to the volumetric flask. The crucible was then triple rinsed with DDI water, and these solutions were also added to the volumetric flask. There were no residual solids present in the crucible after the various dissolution and rinse steps had been completed. The resulting solution was then diluted up to a total volume of 100 mL with DDI water. Prior to chemical analysis, the final 100-mL solution was passed through a 0.45-µm pore-size syringe filter to remove a light-brown flocculent observed when the nitric acid solution was added to the volumetric flask. The insoluble fraction was not characterized by XRD or SEM/EDS due to its limited quantity and the inability to remove it from the filter media.

Chemical analyses of an acid digestion of untreated (raw) AY-102 (jar 15935) sludge solid were also completed for the purpose of comparison to the KOH-KNO₃ fusion procedure for digesting and determining the bulk composition of sludge material. Duplicate samples of the untreated AY-102 (jar 15935) sludge were digested following the basic procedure described in U.S. Environmental Protection Agency (EPA) SW-846 Method 3050B (EPA 1996) for the acid digestion of sediments, sludges, and soils. This digestion is accomplished by the addition of 8 M nitric acid and H₂O₂ to samples of each sludge solid. Method 3050B was used with the following exceptions. All reagent volumes were reduced by 50% because safety considerations necessitated the use of smaller sample masses due to the high radioactivity levels associated with these sludge solids. HCl was not added during the digestion to allow analysis of

¹ Lindberg, MJ. 2003. *Solubilization of Metals from Solids Using a KOH-KNO₃ Fusion*. AGG-ESL-001 (Rev. 0), unpublished PNNL Technical Procedure, Pacific Northwest National Laboratory, Richland, Washington.

² William (Bill) I. Winters, CH2M HILL Hanford Group, Inc., Richland, Washington. Personal communication on December 22, 2003.

the resulting solutions by ICP-MS. If HCl is used, an ArCl^+ species is formed during ICP-MS analysis, which creates a spectral interference that impedes analysis of certain analytes. Throughout the remainder of this report, this treatment of AY-102 (jar 15935) sludge solid will be referred to as the “EPA acid digestion.” An insoluble fraction was observed at completion of the acid digestion. This solid consisted of very fine particles and had the same rusty-brown color as the starting material. The particles in the insoluble fraction were not analyzed due to the limited quantity and the inability to remove them from the filter material.

Table 2-2 lists the digestion factors (wet solid-to-solution ratios) for the samples of AY-102 (jar 15935) sludge solid used for the EPA acid digestion and KOH-KNO₃ fusion treatments. These factors were calculated from the wet weight of sludge material divided by the volume of extracting solution. The digestion factors were then multiplied by the percent solids, as determined from moisture content analysis, to convert to a dry weight basis. All EPA acid-digestion and fused-sample solutions were filtered using 0.45- μm pore-size syringe filters prior to analysis. The dissolved metal concentrations and the total beta and total alpha activities for the filtered solutions were then analyzed by a combination of methods, including ICP-MS, inductively coupled plasma-optical emission spectroscopy (ICP-OES), and several radiochemical analytical techniques. These analytical methods are described in Lindberg and Deutsch (2003).

Table 2-2. Digestion factors for samples of AY-102 (jar 15935) sludge solid used for the EPA acid digestion and KOH-KNO₃ fusion treatments

Treatment	Sample Number	Dry Weight Corrected Digestion Factor (g/L)
EPA acid digestion	15935-1 AE	6.1504
	15935-1 AE DUP	7.6880
KOH-KNO ₃ fusion	15935-1 FUS	2.5302
	15935-1 FUS DUP	2.6243
AE = A sample that has undergone the EPA acid digestion (or extraction) procedure. DUP = “Duplicate” sample. FUS = A sample that has undergone the KOH-KNO ₃ fusion treatment.		

2.3 XRD Analysis – AY-102 and BX-101

Crystalline phases present in the unleached (raw) AY-102 (jars 15935 and 18686) and BX-101 (jar 16503) sludge samples, and the water-leached AY-102 (jar 15935) sludge sample were characterized by standard powder XRD techniques. Because the sludge samples were highly radioactive dispersible powders, the XRD mounts of the sludge samples were prepared inside a fumehood regulated for the handling of radioactive materials. Sludge samples were prepared for XRD analysis by placing milligram quantities of each sample into a mixture of water and collodion solution. The collodion solution consists of 2% nitrocellulose dissolved in amyl acetate. It is an X-ray amorphous, viscous binder that is commonly used to make random-powder mounts for XRD when only a limited amount of sample is available. The slurry was pipetted onto a circular-shaped platform (1-cm diameter) and placed on top of the post located on the base inside the disposable XRD specimen holder shown schematically in

Figure 2-3. This specimen holder was designed specifically for safe handling of dispersible powders containing highly radioactive or hazardous materials (Strachan et al. 2003). After allowing samples to air dry overnight, the holder was assembled and a piece of Kapton[®] film was placed between the cap and the retainer. The holder was sealed with wicking glue and removed from the fumehood.

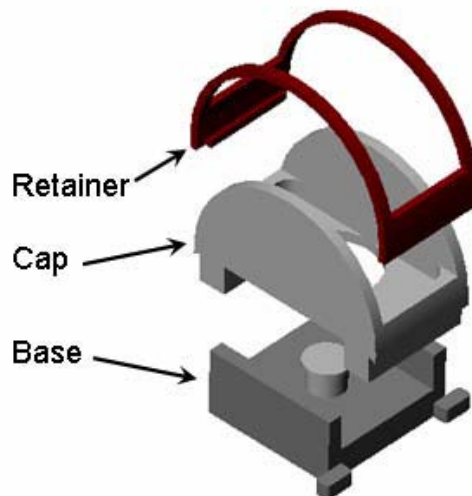


Figure 2-3. Exploded schematic view of the XRD sample holder [Kapton[®] film not shown]

Each specimen of sludge was analyzed using a Scintag XRD unit equipped with a Pelter thermoelectrically cooled detector and a copper X-ray tube. The diffractometer was operated at 45 kV and 40 mA. Individual scans were obtained from 2 to 65° 2 θ with a dwell time of 4 and 14 seconds. Scans were collected electronically and processed using the JADE[®] XRD pattern-processing software.

A sample consisting of only a dry film of the collodion solution was also prepared and analyzed by XRD so that its contribution relative to the background signals of the XRD patterns for the sludge samples could be quantified. The resulting XRD pattern for the collodion-solution film is shown in Figure 2-4. The most obvious feature of this diffraction pattern is the broad peak positioned between 10 and 30° 2 θ . The symmetry of this peak is characteristic of those resulting from the XRD of amorphous (non-crystalline) material. Although subtracting the collodion background from sludge XRD patterns allows for better phase matching, this process may eliminate minor reflections and inconspicuous features of a pattern. Therefore, each as-measured XRD pattern (Appendix A) was examined before and after background subtraction to ensure that the integrity of the pattern was maintained. For background subtraction, the JADE[®] software provides the user with control over the selection of background-subtraction points. This process allows a better fit to 2 θ regions under broad reflections, such as those resulting from amorphous materials. On average, 30 to 40 background points were selected from each XRD pattern, and a cubic-spline curve was then fit through each set of points. Adjustments to this curve were made by selecting additional background points in regions of a pattern that were difficult to fit. Once a well-matched curve was fitted to a pattern, the background was subtracted from each as-measured XRD pattern resulting in a smooth tracing.

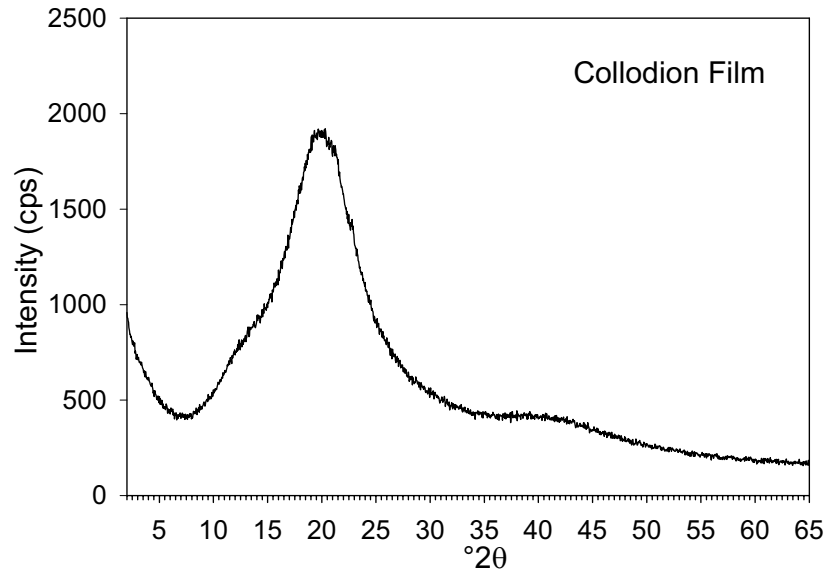


Figure 2-4. XRD pattern for collodion film measured in the absence of any sludge material

Identification of the mineral phases in the background-subtracted patterns was based on a comparison of the XRD patterns measured for the sludge samples with the mineral powder diffraction files (PDF™) published by the Joint Committee on Powder Diffraction Standards (JCPDS) International Center for Diffraction Data (ICDD). As a rule of thumb, a crystalline phase must be present at greater than 5 wt% of the total sample mass (greater than 1 wt% under optimum conditions) to be readily detected by XRD. In general, the measured peak intensities depend on several factors, including the combined mass of each crystalline phase in the sample. Due to the physical characteristics of these tank sludge samples, such as high radioactivity, high dispersibility, and variable moisture content, the mass of tank sludge combined with the collodion solution for each XRD mount could not be controlled or easily determined. Additionally, dissimilarities in mineral segregation (settling) resulting from the different densities of minerals mixed with the collodion solution and associated effects on relative peak intensities also influence the overall pattern intensity. Therefore, the combined effect of these factors had some impact on the characteristic mineral peak intensities, which precluded quantitative comparisons of peak intensities for equivalent reflections in background-subtracted XRD patterns for different sludge samples.

2.4 SEM/EDS Analysis – AY-102 and BX-101

Samples of unleached (raw) and water-leached AY-102 (jar 15935) sludge, and of the unleached (raw) BX-101 (jar 16503) sludge were characterized by SEM/EDS. Three mounts were prepared of each sample to compensate for the possibility that one or more less-than-optimum mounts of a sample might occur, thus improving the likelihood of obtaining representative SEM imaging of each sample. The mounts used for SEM/EDS consisted of double-sided carbon tape attached to standard aluminum mounting stubs. For each mount, small aliquots of each sludge sample were placed on the exposed upper surface of the carbon tape using a micro spatula. Each mount was then coated with carbon using a vacuum-sputter coater to improve the conductivity of the samples and thus the quality of the SEM images and EDS signals.

A JEOL JSM-840 SEM was used for high-resolution imaging of micrometer/submicrometer-sized particles from AY-102 and BX-101 sludge samples. The SEM system is equipped with an Oxford Links ISIS 300 EDS that was used for qualitative elemental analysis. Operating conditions consisted of 10 to 20 keV for SEM imaging, and 20 keV, 100 live seconds¹ for the EDS analyses. The EDS analyses of particles are limited to elements with atomic weights heavier than boron. Photomicrographs of high-resolution secondary-electron (se) images and backscattered electron (bse) images were obtained as digital images and stored in electronic format. To help identify particles that contain elements with large atomic number, such as uranium, the SEM was typically operated in the bse mode. Secondary electrons are low-energy electrons ejected from the probed specimen as a result of inelastic collisions with beam electrons, whereas backscattered electrons are primary electrons emitted as a result of elastic collisions. Backscattered electron emission intensity is a function of the specimen's atomic number, i.e., the larger the atomic number, the brighter the signal. Backscattered electron images are obtained in exactly the same way as secondary-electron images.

The SEM micrographs included in this report were selected because they show typical morphologies, sizes, and surface textures of particles in the sludge subsample mounts. The name of each digital image file, sample identification number, and a size scale bar are given, respectively, at the bottom left, center, and right of each SEM micrograph in this report. Micrographs labeled by "bse" to the immediate right of the digital image file name indicate that the micrograph was collected with backscattered electrons. Areas outlined by a yellow dotted-line square in a micrograph designate sample material that is imaged at higher magnification, which is typically shown in the next figure of the series for that subsample.

Areas labeled by "eds" in SEM micrographs in this report indicate areas of particles for which EDS spectra were recorded and qualitative compositions were calculated and tabulated in this report. Compositions determined by EDS are qualitative and have large uncertainties resulting from alignment artifacts caused by the variable sample and detector configurations that exist when different particles are imaged by SEM. The calculated weight percentages listed in the EDS composition tables in this report have been normalized to 100 wt%. The combined process of calculation of the qualitative compositions from the EDS peak areas and normalization to 100 wt% may result in negative weight percentages being listed for a few elements present at trace concentrations (e.g., less than 1 wt%).

2.5 XAS Analysis – AY-102 Drainable Liquid

X-ray absorption spectroscopy (XAS) is an element-specific probe that can be used to determine the local structure around the selected absorbing element. The X-ray absorption spectrum can be divided into two main parts: the lower energy X-ray absorption near edge structure (XANES) region, which contains oxidation state and symmetry information, and the higher energy extended X-ray absorption fine structure (EXAFS) region, which can be modeled to give information on the identity, coordination number, and distance to nearest and next nearest neighbor atoms. XAS investigations of solution, solid, sorbates, and

¹ Live time is the time (real time less dead time) that the EDS system is available to detect incoming X-ray photons. Dead time is the portion of the total analyzing time that is actually spent processing or measuring X-rays. During the time that each X-ray pulse is being measured, the system cannot measure another X-ray that may enter the detector and is therefore said to be "dead."

gas phase samples are possible without need for prior chemical separations or sample dissolution. Brown et al. (1988) provides an excellent review of XAS and its applications in geochemistry and environmental science.

The XANES region is further divided into a pre-edge region, which extends from about 10 eV below the main absorption edge energy to a few eV above it, and an intermediate energy region, which extends a few eV above the pre-edge region to 50 eV above the absorption edge. Features in the pre-edge region originate from the energy-matched electronic transitions of the ejected photoelectron to empty bound states, which can be localized atomic orbitals or de-localized molecular orbitals. The transition probability to empty bound states is governed by the selection rules for dipolar electronic transitions just as in visible and vibrational spectroscopy. Thus the pre-edge region can give information about the site symmetry of the absorbing atom. Features in the intermediate energy region originate from multiple scattering events of the ejected photoelectron with low kinetic energy to continuum states involving nearest and next nearest neighbors. The interpretation of features in this region is more complex due to the multiple-scattering phenomenon, but empirical and recent theoretical efforts have demonstrated that information on the geometry of the coordination environment of the absorbing atom can be obtained. The oscillations in the EXAFS region originate from the interference of the outgoing ejected photoelectron with high kinetic energy and backscattered photoelectrons from nearest and next nearest neighbor atoms. Analysis of the EXAFS region requires higher signal-to-noise than for analysis of the XANES and was not conducted.

Because the technetium K-edge occurs at high energy, 21,044 eV, the incident X-rays are capable of penetrating sample containment necessary for radioactive samples. For samples containing technetium, the estimated detection limits for XANES and EXAFS analysis of technetium are approximately 5-10 and 100 μmol , respectively, based on these results and those published in the literature for similar samples (Blanchard et al. 1997). The low detection limit, elemental specificity, and wide variety of possible sample types make XAS analysis a versatile probe for the determination of radionuclide oxidation states in chemically complex high-level waste.

Approximately 0.3 mL each of drainable liquid, 1 mmol pertechnetate solution, and 0.04 mmol technetium in 0.3 M HCO_3^- solution was injected into the XAS sample cells shown in Figure 2-5. The technetium-bicarbonate sample is from an ongoing study funded by the U.S. Department of Energy Environmental Management Science Program (EMSP) on technetium chemistry in high-level radioactive waste (HLW), and was used as a Tc(V) standard for this report. The technetium-bicarbonate sample was prepared by equilibrating 20 mL of distilled, de-ionized, degassed, iron-equilibrated water containing 0.3 M NaHCO_3 and 0.02 M hydrazine at pH 9.4 in the presence of 5 mg of $\text{TcO}_2 \cdot 1.6\text{H}_2\text{O}$ (am) for approximately 500 days in an argon atmosphere. Approximately 2.5 mL of the equilibrated solution was removed, centrifuged and filtered for use as the XAS sample. The total concentration and oxidation state of technetium in the equilibrated technetium-bicarbonate solution were determined using a combination of solvent extraction based on tetraphenylphosphonium chloride in chloroform (Kopunec et al. 1998) and scintillation counting. The measured solution concentrations of total technetium and Tc(VII) were determined to be 4.4×10^{-5} and 9.1×10^{-7} mol/L, respectively, which indicates that reduced technetium species constituted 98% of the XAS sample.

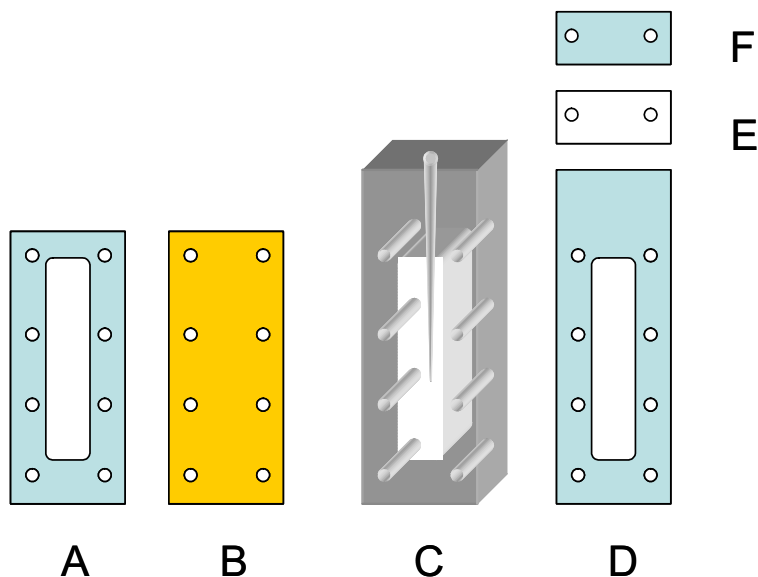


Figure 2-5. Components of primary container for solution samples. Part A is a steel frame drilled to accommodate bolts. The mating surface with Kapton[®] window (Part B) has a machined groove to form a seal (not shown). Part B is a 0.3-mm thick Kapton[®] window. Part C is a machined Teflon block with recessed sample cavity. There is an additional hole on the top surface for injection of liquid samples. Kapton[®] window seals the sample in the cavity. Part D is a steel frame drilled to accommodate bolts. Part E is a Teflon film. Part F is a steel cap. After assembly of parts A through D, the liquid sample is injected into the top hole in C. Parts E and F are then secured.

The cells were loaded into a secondary container which can accommodate up to eight samples (Figure 2-6). The secondary container was installed on the Pacific Northwest Consortium – collaborative access team (PNC-CAT) bending-magnet line at the Advanced Photon Source (Argonne National Laboratory, Argonne, Illinois) at 45° to the incident X-ray beam. The XANES spectrum was collected in fluorescence mode using a 13-channel germanium detector at the technetium K-edge. Due to the low concentration of technetium in the drainable liquid and bicarbonate samples, data were collected over a 10-hour period to obtain an acceptable signal-to-noise ratio. The energy position of the incident beam monochromator was calibrated using the transmission data for a zirconium foil and assigning the first inflection point of the absorption edge to 17,995 eV. Normalization of the absorption spectrum was accomplished by fitting polynomials through the pre- and post-edge regions, setting the value of the extrapolated pre-edge to zero at E_0 , defined as 21,044 eV for the technetium K-edge. The difference between the extrapolations of the pre- and post-edge polynomials was set to unity at E_0 .

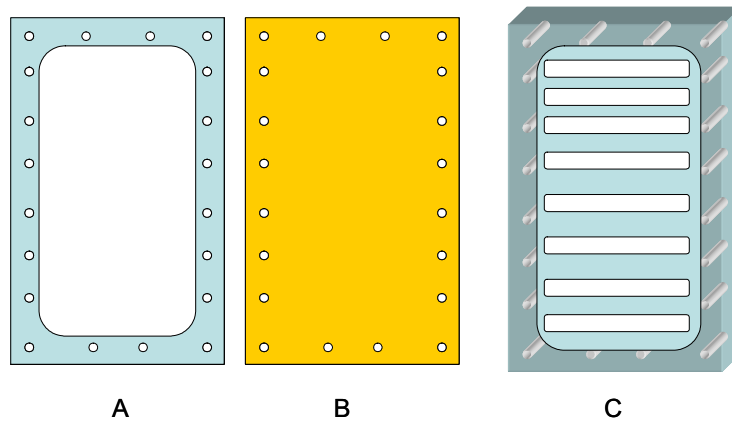


Figure 2-6. Components of secondary containment for solution and solid samples. Part A is a steel frame drilled to accommodate bolts. Part B is a 0.3-mm thick Kapton[®] window. Part C is a machined aluminum block that accommodates 8 primary cells. Not shown on Part C are drilled holes that match the bolt hole pattern of the primary cells. This secures the primaries in the secondary. The mating surfaces with Kapton[®] windows (Part B) have a machined groove to accommodate O-rings, not shown. The back of Part C is sealed with a second steel frame and Kapton[®] window (duplicate parts A and B).

2.6 Tier 1 Tests – BX-101

Tank waste samples were analyzed in a tiered approach similar to the one developed for investigating contaminant fate and transport issues associated with past single-shell tank leaks in the vadose zone. Such an approach allows for initial screening (the Tier 1 test described in this report) of samples using relatively inexpensive analytical techniques. This is followed by an analysis of the data to determine the need for further analysis (Tier 2). At this time, the need for further testing of material from BX-101 has not been established and additional tests are not scheduled.

The tests described below were conducted on the three sludge samples from BX-101 designated S02T001253, S02T001254, S02T001255. In several cases, a duplicate analysis was conducted using sample number S02T001253.

2.6.1 Moisture Content

The moisture contents of the tank waste samples were measured in order to calculate dry weight concentrations for constituents in the waste. Dry weight concentrations provide a consistent measurement unit for comparison purposes that eliminates the effect of variable water content on sample concentrations.

Gravimetric water contents of the waste material were determined using PNNL laboratory procedures. This procedure is based on the American Society for Testing and Materials procedure *D2216-98 Standard Test Method for Laboratory Determination of Water (Moisture) Content of Soil and Rock by Mass* (ASTM 1998). Samples for measurement were placed in tared containers, weighed, and dried in an oven at 105°C until constant weight had been achieved, usually within 24 to 48 hours. The containers

were then removed from the oven, sealed, cooled, and weighed. After an additional 24 hours of heating, at least two weighings were performed to ensure that all moisture had been removed. All weighings were performed using a calibrated balance. The gravimetric water content is computed as the percentage change in soil weight before and after oven drying (i.e., $[(\text{wet weight} - \text{dry weight})/\text{dry weight}]$).

2.6.2 Water Extracts

Water-soluble inorganic constituents were determined using a DDI water extract method. The extracts were prepared by adding an exact 30-mL volume of DDI water to 0.200 to 0.600 g of each sample contained in a polypropylene bottle. The polypropylene bottles were sealed and briefly shaken by hand, and then placed on a mechanical orbital shaker for one hour. After shaking for one hour, the slurries were allowed to settle until the supernatant liquid was fairly clear. The supernatant was carefully decanted and filtered through 0.45- μm pore size membranes for anion, cation, carbon, pH determinations, and radionuclide analyses. More details can be found in ASTM Procedure *D3987-85 Standard Test Method for Shake Extraction of Solid Waste with Water* (ASTM 1999).

2.6.3 Acid Extracts

Acid digestions were performed on the samples according to EPA SW-846 Method 3050B (EPA 2000) with exceptions. The exceptions include reduced sample size (0.200 to 0.600 g) and adjusted reagent volumes for the smaller samples. Also, HCl acid was not added in the final steps of digestion to allow the use of one extract for ICP-OES and ICP-MS analysis. Gross alpha/beta and gamma energy analysis (GEA) were also performed on the acid extracts.

2.6.4 pH

Approximately 3-mL aliquots of the unfiltered supernatant from the water-leach tests were used for pH measurements. Solution pH values were measured with a solid-state pH electrode and a pH meter calibrated with buffers 4, 7, and 10.

2.6.5 Anion Analysis

The filtered water leachates were analyzed for anions using an ion chromatograph. Fluoride, acetate, formate, chloride, nitrite, bromide, nitrate, nitrite, carbonate, phosphate, sulfate, and oxalate were separated on a Dionex AS17 column with a gradient elution technique from 1 mM to 35 mM NaOH and measured using a conductivity detector. This methodology is based on *Test Methods for Evaluating Solid Wastes: Physical/Chemical Methods* (EPA SW-846 Method 9056) (EPA 2000) with the exception of using gradient elution with NaOH.

2.6.6 Cations and Trace Metals

Major cation analysis (including aluminum, silicon, calcium, magnesium, sodium, potassium, iron, and manganese) of the water leachates and drainable liquid were performed by ICP-OES. High-purity calibration standards were used to generate calibration curves and verify continuing calibration during the analysis run. Dilutions of 10x and 5x were made for each sample and analyzed to investigate and correct

for matrix interferences. Details are found in EPA Method 6010B (EPA 2000). An ICP-MS was used to analyze trace metals including chromium, molybdenum, arsenic, selenium, cadmium, silver, lead, technetium-99, uranium isotopes, and several transuranics in the acid and water leachates. This method is similar to EPA Method 6020 (EPA 2000).

2.6.7 Alkalinity

The alkalinities of the water leaches were measured by standard titration with acid. The alkalinity procedure is equivalent to Standard Method 2320 B (Clesceri et al. 1998).

2.6.8 Radioanalytical

In addition to the radionuclides listed above that were analyzed in solution by ICP-MS, short-lived radionuclides were analyzed by conventional counting methods. Cesium-137, cobalt-60, and the europium isotopes were measured by GEA (using methods discussed below under Section 2.6.8.1).

2.6.8.1 Gamma Energy Analysis

All samples for GEA were analyzed using 60%-efficient intrinsic-germanium gamma detectors. All germanium counters were efficiency calibrated for distinct geometries using mixed gamma standards traceable to the National Institute of Standards and Technology. Direct solids, acid extracts and water extracts were analyzed for gamma energy. Spectral analysis was conducted using libraries containing most mixed-fission products, activation products, and natural-decay products. Control samples were run throughout the analysis to ensure correct operation of the detectors. The controls contained isotopes with photo peaks spanning the full detector range and were monitored for peak position, counting rate, and full-width half-maximum. Details are found in procedure RRL-001.¹

2.6.8.2 Gross Alpha and Beta Analysis

Gross alpha and beta measurement were made on both the water and acid extracts. For each extract, 0.100 mL sample volume was placed in a 20-mL liquid scintillation vial containing 15-mL of scintillation cocktail.² The samples were then mixed and counted on a Wallace model 1415 liquid scintillation counter as prescribed in procedure AGG-RRL-002.³

2.7 Periodic Replenishment Tests – AY-102

Duplicate periodic replenishment tests were conducted on samples of sludges from tank AY-102 (jar 15935). In these tests, the water leachate solutions were periodically removed and replaced with an equal volume of fresh solution. These tests were conducted to evaluate whether or not the technetium-99

¹ RRL-001. *Gamma Energy Analysis, Operation, and Instrument Verification using Genie2000 Support Software*, unpublished PNNL Technical Procedure, Pacific Northwest National Laboratory, Richland, Washington.

² The scintillation cocktail used is Packard Optifluor, which is based on the high flash-point solvent LAB (Linear Alkylbenzene) (<http://las.perkinelmer.com/catalog/Product.aspx?ProductId=6013199>)

³ AGG-RRL-002. *Liquid Scintillation Counting and Instrument Verification using the 1400 DSA™ Support Software*, unpublished PNNL Technical Procedure, Pacific Northwest National Laboratory, Richland, Washington.

solution concentrations might be limited by the solubility of one or more of the solid phases. In particular, these tests were conducted to determine if the low release of technetium-99 (25%) from the AY-102 sludge was due to solubility constraints.

Approximately 0.3 g of sludge was contacted with 30 mL of DDI water a total of five times. The contact periods ranged from one to four days, and are the length of time between each replenishment of water leachate solution. Table 2-3 lists the contact duration and the average pH values for the duplicate samples.

The solutions from each extraction were analyzed for metals and radionuclides by ICP-MS and ICP-OES.

Table 2-3. Contact times and pH values for periodic replenishment test on tank AY-102 sludge (jar 15935)

Sequential Contacts	Contact Duration (days)	pH (average)
1	1	10.11
2	2	9.18
3	3	8.73
4	3	8.36
5	4	8.22

2.8 Selective Extraction Tests – AY-102

Tier 1 testing of AY-102 sludge showed that only 25% of the technetium-99 was water leachable (Lindberg and Deutsch 2003). This is contrary to previous assumptions that technetium-99 is completely water soluble. The objectives of the Tier 2 sequential extractions were to determine 1) if the 25% technetium that is readily mobilized is associated with dawsonite or is simply precipitated during evaporation of entrained salt solution associated with the sludge, or 2) if the immobile technetium (but acid extractable by Method 3050B) is associated with the aluminum or iron oxyhydroxides.

Using results from the acid digestion (Method 3050B) and the total inorganic carbon (TIC) content of the sludge, mass balance calculations indicate that AY-102 sludge contains 2.1% by weight TIC, 11% aluminum, and 13% iron (average of sludge samples 15935 and 18686, Lindberg and Deutsch 2003). If it is assumed that all the TIC occurs as carbonate, 2.1% TIC would equate to 10.5% by weight carbonate. If it is assumed that all the carbonate occurs in the sludge as dawsonite $[\text{NaAl}(\text{CO}_3)(\text{OH}_2)]$ (identified as one of the most abundant crystalline minerals in the sludge by XRD), then the sludge would be 26% dawsonite. This amount of dawsonite would contain 5% of the available aluminum (percent weight sludge basis), leaving 6% of the aluminum in another phase. If the majority of remaining aluminum occurs as $\text{Al}(\text{OH})_3(\text{am})$, then the sludge would contain 17% $\text{Al}(\text{OH})_3(\text{am})$. (Note that a small amount of gibbsite [crystalline $\text{Al}(\text{OH})_3$] was identified by XRD in the AY-102 sample.)

If all the iron in the sludge occurs as hematite (identified in the sludge by XRD), the sludge would contain 19% by weight hematite. If the iron occurs as $\text{Fe}(\text{OH})_3(\text{am})$, the sludge would contain 25% by

weight $\text{Fe}(\text{OH})_3(\text{am})$. Clearly, dawsonite and these aluminum and iron oxyhydroxide phases make up major portions of the tank sludge. During Tier 1 testing, it was established that approximately 25% of technetium in the sludge was readily solubilized by leaching with water. This indicates that technetium may be associated with dawsonite (which dissolves during this water-leaching step) or is simply precipitated from the entrained salt solution during drying of the sludge. The remaining technetium did not solubilize during subsequent sequential water extractions.

The first reagent used to leach the sludge in the sequential extraction was a NaHCO_3/Al solution that is saturated with respect to dawsonite. If this extractant does not remove technetium, this would indicate that the readily soluble technetium is associated with dawsonite or the aluminum or iron oxide/hydroxide solids. If approximately 25% of the technetium is removed with this solution, this would indicate that the readily mobilized technetium was simply precipitated from the entrained salt solution in the sludge during drying.

The NaHCO_3/Al solution designed to be in equilibrium with dawsonite was made up as follows: 6.8×10^{-3} M in NaHCO_3 and 1.2×10^{-6} M in aluminum. The aluminum was added as $\text{Al}(\text{NO}_3)_3 \cdot 9\text{H}_2\text{O}$. These concentrations were determined by calculating the solubility of dawsonite [$\text{NaAlCO}_3(\text{OH})_2$] using the MINEQL+ geochemical code. The dawsonite solubility constant ($\log K_{298^\circ}$) at 298.15 K (25.0°C) chosen for inclusion in MINEQL+ was 5.984 for the reaction



This $\log K_{298^\circ}$ value was calculated from a Gibbs free energy of formation ($\Delta_f G_{298^\circ}$) of -426.9 kcal/mol (-1786.0 kJ/mol) reported for dawsonite by Ferrante et al. (1976), and accepted in the compilation of thermodynamic values published by Robie and Hemingway (1995).

For each extraction step, 0.3 g sludge and 30 mL of extractant (pH ~ 8.6) was used and the contact time was approximately 24 hours. The second extraction step in this sequential extraction process used a buffer solution of 0.1 M acetic acid/0.1 M acetate (pH ~ 4.6) for removal of dawsonite. After extraction, the pH values of the solutions were measured and each solution was analyzed for technetium-99, aluminum, and iron. The first sequence of extractions is as follows:

- Day 1: NaHCO_3/Al solution for soluble salt removal
- Day 2: NaHCO_3/Al solution for soluble salt removal
- Day 3: 0.1 M acetic acid/0.1 M acetate buffer (pH ~ 4.6) for dawsonite removal
- Day 4: 0.1 M acetic acid/0.1 M acetate buffer (pH ~ 4.6) for dawsonite removal

Figure 2-7 shows this sequence of extractions schematically.

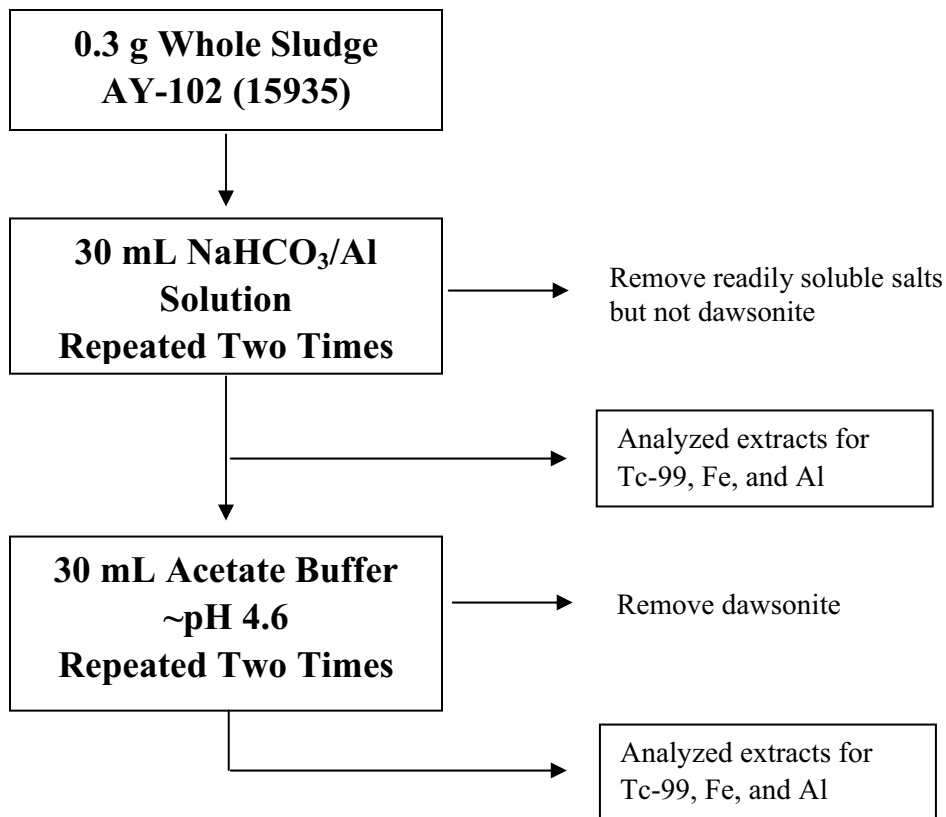


Figure 2-7. Extraction sequence to determine association of technetium in readily soluble salts and dawsonite

The second sequence of extractions was designed to remove the dawsonite with minimal dissolution of the aluminum and iron oxyhydroxides followed by aluminum oxyhydroxides removal with minimal iron hydroxides/oxides removal, and then finally complete dissolution of the sludge (Figure 2-8). The dawsonite was removed prior to the formate buffer treatment so that the formate buffer capacity was not significantly diminished by the release of carbonate from dawsonite. Each of the extract solutions was analyzed for pH, technetium-99, iron, and aluminum. For these extractions, 0.3 g sludge and 30 mL of each extractant was used.

A contact time of approximately 24 hours was used for each step. The sequence of extractions was conducted according to the following schedule:

- Day 1: 0.1 M acetic acid/0.1 M acetate buffer (pH 4.6) for dawsonite removal
- Day 2: 0.1 M acetic acid/0.1 M acetate buffer (pH 4.6) for dawsonite removal
- Day 3: 0.1 M formic acid/0.1 M formate buffer (pH 3.6) for aluminum oxyhydroxide removal
- Day 4: 0.1 M formic acid/0.1 M formate buffer (pH 3.6) for aluminum oxyhydroxide removal

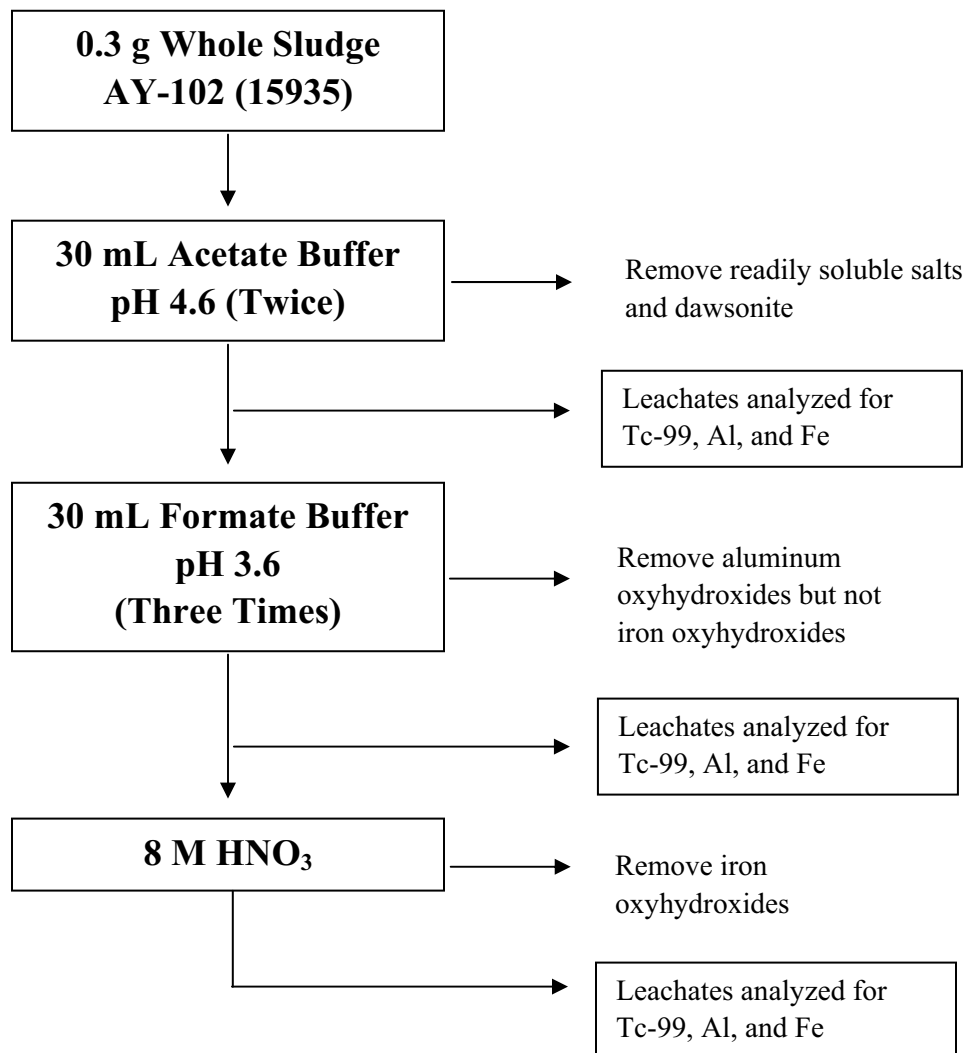


Figure 2-8. Extraction sequence to determine association of technetium-99 in iron and aluminum oxyhydroxides

- Day 5: 0.1 M formic acid/0.1 M formate buffer (pH 3.6) for aluminum oxyhydroxide removal
- Day 6: 8 M HNO₃ for iron oxyhydroxide removal

2.9 Oxidation Test – AY-102 and BX-101

Previous work conducted as part of the Tier 1 characterization of sludge from tank AY-102 indicated that only 25% of the technetium-99 in the sludge is water leachable. A set of batch oxidation experiments was designed to determine if the unleachable technetium-99 could have been incorporated into an organic phase in the sludge. The AY-102 sludge was found to contain between 0.2% and 0.4% organic carbon. If technetium-99 is contained within an organic phase, then oxidation of that phase would likely release the

technetium-99. To selectively remove any solid organic phases and to oxidize any reduced technetium-99 within the organic phases, sludge samples were treated with a 3% H₂O₂ solution in a batch process. Other chemical oxidation methods were not considered because acidic conditions are required with these methods and the acid would dissolve other solid phases potentially containing technetium-99.

The batch oxidation experiments were conducted through sequential leaching with three separate leachate solutions. Two different sludge samples were used, one from AY-102 (15935) and one from BX-101 (16503). In the first two leaching steps, the sludge was contacted with the 3% H₂O₂ solution for one day each. In the last leaching step, the contact time was five days. The leaching process was conducted by adding approximately 0.3 g of sludge to a 50 mL centrifuge tube and then adding a measured volume of 3% H₂O₂. It was originally intended to add 40 mL of the 3% H₂O₂ solution for each leach. However, due to excessive outgassing that resulted from decomposition of H₂O₂ during initial contact with the sludge, a reduced volume of solution was added during the first leach step. After addition of the 3% H₂O₂ solution to the centrifuge tube, the solution and sludge were mixed by rotating the tubes for approximately 24 hours. The tubes were then centrifuged at the end of this contact period. The solution was removed after centrifugation, and analyzed for technetium by ICP-MS. For the second and third leaches, 40 mL of 3% H₂O₂ solution was added to the tube containing the sludge and the tubes rotated again for the appropriate time.

2.10 Reduction Capacity Test – AY-102 and BX-101

The reductive capacities of sludge samples from tanks AY-102 and BX-101 were measured to evaluate the ability of the solids to reduce (and potentially immobilize) some of the contaminants such as technetium, uranium, and chromium. A slight modification of the method described by Lee et al. (2000, 2003) was used for the test. To two plastic centrifuge cones, were added approximately 0.3 g of sludge and 3 mL of chromate solution (other quantities can be used as long as the solution volume/solid weight ratio is maintained at 10). The chromate solution consisted of 5.75 mM chromate solution containing 10 mM NaHCO₃ (0.846 g K₂Cr₂O₇ and 0.84 g NaHCO₃ per liter). The pH of the slurry was adjusted to 7 after addition of chromate solution with additions of 1 M H₂SO₄ or 1 M NaOH as necessary. The vials were then capped and agitated for four days. After four days, 0.0142 g Na₂SO₄ was added to each vial for each mL of chromate solution and rotated for another day to remove any surface adsorbed chromate. The vials were then centrifuged at 2800 rpm for 100 minutes. The solution was next filtered through a 0.2- μ m membrane filter, and analyzed for chromate by ICP-OES and technetium by ICP-MS. The reduction capacity was calculated by dividing the difference between the initial mass of added chromate and remaining mass of chromate by the mass of solids that were reacted.

3.0 Results

This section provides the results of the following tests conducted on sludge samples from tanks AY-102 and BX-101, and drainable liquid from tank AY-102:

- Fusion and acid digestion of AY-102 sludge to measure composition
- XRD analysis of sludge from both tanks to identify crystalline solids
- SEM/EDS analysis of sludge from both tanks to view solids and estimate composition
- XAS study of drainable liquid from AY-102 to determine oxidation state of technetium-99
- Tier 1 testing of BX-101 sludge to measure total concentrations and water leachable fractions
- Periodic water replenishment testing of AY-102 sludge to evaluate longer-term contaminant release
- Selective extraction of AY-102 solids to identify phases limiting the release of technetium-99
- Oxidation testing of AY-102 and BX-101 sludges to test the effect of oxidation on the release of technetium-99
- Measurement of the reduction capacities of AY-102 and BX-101 sludges

3.1 Fusion and Acid Digestion Results – AY-102

The dissolved element concentrations and total beta and total alpha activities measured for the filtered solutions from the EPA acid digestion and KOH-KNO₃ fusion treatments of AY-102 (jar 15935) sludge are given in the following tables:

Table 3-1 to Table 3-3	Concentrations of elements measured by ICP-OES per gram of dry sludge
Table 3-4 to Table 3-5	Concentrations of elements measured by ICP-MS per gram of dry sludge
Table 3-6	Concentrations of technetium-99, uranium-238, and actinides measured by ICP-MS per gram of dry sludge
Table 3-7 to Table 3-8	GEA of dry sludge in units of $\mu\text{Ci/g}$ and $\mu\text{g/g}$, respectively
Table 3-9	Total beta and total alpha activities, and strontium-90 concentrations per gram of dry sludge
Table 3-10	Summary of average concentrations from the EPA acid digestion and KOH-KNO ₃ fusion analyses for unleached AY-102 sludge

Table 3-11

Comparison of cadmium, chromium, lead, arsenic, and molybdenum concentrations determined by ICP-MS and ICP-OES per gram of dry sludge.

Concentrations listed in parentheses in Table 3-1 to Table 3-11 are defined as values that are less than the lowest limit of quantification (LOQ) and greater than a zero instrument signal. Values listed in parentheses are reported for informational purposes only. These values may reflect concentrations that are real and have larger associated uncertainties, or concentrations that were calculated from the instrument's background signal. The LOQ is the lowest calibration check standard used as a control for that particular analytical run. The LOQ of a particular analysis is determined by analyzing a suite of continuing calibration verification (CCV) standards at the beginning and end of each analytical run. The LOQ is calculated by multiplying the lowest CCV standard that was measured to be within $\pm 10\%$ of its certified value throughout the run by the dilution factor performed on the sample set being analyzed. Multiple LOQ values are possible for a particular run if the samples require different levels of dilution to measure the analyte of interest in the appropriate analytical range. The LOQ can vary with every analysis depending on sample matrix, instrument calibration, and quality assurance/quality control (QA/QC) requirements and recoveries.

Concentrations listed as less than (<) values in Table 3-1 to Table 3-9 refer to instrument values that are less than zero. In these instances, the reported analyte concentration is assigned a value of "<LOQ" using the LOQ value appropriate for that particulate analyte and set of analysis conditions.

The element concentrations in Table 3-4 and Table 3-5 were derived from the ICP-MS analyses of the indicated isotopes and the known relative natural abundance of each of these isotopes. The accuracy of the ruthenium concentrations determined by ICP-MS (Table 3-5) is suspect due to fission product yields of the listed ruthenium isotopes being different than their natural abundances.

Average concentrations calculated from analyses by Lindberg and Deutsch (2003) for the filtered solutions from a similar EPA acid digestion (i.e., nitric acid) treatment of duplicate samples of AY-102 (jar 15935) sludge are given near the top of Table 3-1 to Table 3-9. These average concentrations are in good agreement with the average concentrations determined in this study for the EPA acid digestion solutions.

Comparison of the average concentrations in Table 3-10 for the solutions from the EPA acid digestion and KOH-KNO₃ fusion treatments indicates relatively good correspondence (within 20%) for the two methods. Elements that are not measured at similar concentrations for these two methods are silicon, boron, selenium, phosphorus, copper, nickel, arsenic, bismuth, lithium, and strontium. In the cases of silicon, boron, selenium, copper, arsenic, and bismuth, the fusion values are greater than the acid digestion values, and likely represent the greater effective dissolution of the sludge sample by the fusion method. It is not clear why the values for phosphorus, nickel, lithium, and strontium are significantly higher in the acid digestion measurement compared to the fusion analysis.

Table 3-1. Concentrations of elements measured by ICP-OES per gram of dry sludge

Sample Number	Al	As	B	Ba	Be	Bi	Ca	Cd	Co	Cr
	----- µg/g -----									
EPA Acid Digestion (Lindberg and Deutsch 2003)										
Average for duplicate "15935 AE" samples	1.21E+05	ND	(6.48E+03)	(1.39E+03)	(7.63E+01)	(7.74E+03)	(1.12E+04)	(4.62E+02)	(1.68E+02)	(5.77E+03)
EPA Acid Digestion (This Study)										
15935-1 AE	9.02E+04	(6.61E+02)	(4.30E+03)	1.03E+03	(2.34E+01)	(3.17E+02)	5.56E+03	(1.55E+02)	(2.62E+02)	3.38E+03
15935-1 AE Dup	9.13E+04	(1.03E+02)	(3.33E+03)	1.12E+03	(1.24E+01)	(2.03E+02)	5.52E+03	(1.62E+02)	(2.38E+02)	3.46E+03
Average	9.07E+04	(3.82E+02)	(3.82E+03)	1.07E+03	(1.79E+01)	(2.60E+02)	5.54E+03	(1.58E+02)	(2.50E+02)	3.42E+03
Fusions (This Study)										
15935-1 FUS	8.99E+04	(2.52E+03)	(9.46E+03)	6.67E+02	(3.24E+01)	(1.54E+03)	(5.24E+03)	(1.44E+02)	(4.38E+02)	3.05E+03
15935-1 FUS Dup	8.11E+04	(1.48E+03)	(8.21E+03)	9.89E+02	(3.19E+01)	(1.25E+03)	(4.96E+03)	(1.59E+02)	(3.26E+02)	2.82E+03
Average	8.55E+04	(2.00E+03)	(8.83E+03)	8.28E+02	(3.22E+01)	(1.40E+03)	(5.10E+03)	(1.52E+02)	(3.82E+02)	2.94E+03
Percentage Leached by EPA Acid Digestion (Average This Study) Relative to Average Fusion Results										
	106%	19.1%	43.2%	130%	55.6%	18.6%	109%	104%	65.4%	117%

Table 3-2. Concentrations of elements measured by ICP-OES per gram of dry sludge (continued)

Sample Number	Cu	Fe	K	Li	Mg	Mn	Mo	Ni	P	Pb
	----- µg/g -----									
EPA Acid Digestion (Lindberg and Deutsch 2003)										
Average for duplicate "15935 AE" samples	(4.49E+02)	1.41E+05	ND	(1.80E+04)	(1.82E+03)	7.09E+04	(1.20E+03)	9.56E+03	(5.13E+03)	(9.68E+03)
EPA Acid Digestion (This Study)										
15935-1 AE	(2.16E+03)	1.29E+05	1.47E+05	(2.39E+02)	(1.27E+03)	4.88E+04	(4.71E+02)	(7.23E+03)	9.21E+03	8.61E+03
15935-1 AE Dup	(1.79E+03)	1.30E+05	6.27E+04	(4.17E+02)	(1.39E+03)	4.93E+04	(4.99E+02)	(7.16E+03)	9.10E+03	8.60E+03
Average	(1.98E+03)	1.29E+05	1.05E+05	(3.28E+02)	(1.33E+03)	4.91E+04	(4.85E+02)	(7.20E+03)	9.15E+03	8.61E+03
Fusions (This Study)										
15935-1 FUS	(3.90E+03)	1.48E+05	4.10E+06	(9.12E+02)	(1.26E+03)	4.61E+04	(4.93E+02)	(2.84E+03)	7.36E+03	7.56E+03
15935-1 FUS Dup	(3.26E+03)	1.41E+05	3.72E+06	(3.22E+02)	(1.33E+03)	4.25E+04	(6.30E+02)	(2.71E+03)	4.72E+03	6.89E+03
Average	(3.58E+03)	1.44E+05	3.91E+06	(6.17E+02)	(1.30E+03)	4.43E+04	(5.62E+02)	(2.78E+03)	6.04E+03	7.23E+03
Percentage Leached by EPA Acid Digestion (Average This Study) Relative to Average Fusion Results										
	55.2%	89.6%	2.7%	53.2%	103%	111%	86.3%	259%	152%	119%

Table 3-3. Concentrations of elements measured by ICP-OES per gram of dry sludge (continued)

Sample Number	Se	Sr	Tl	V	Zn	Na	Si	S	Ti	Zr
	----- µg/g -----									
EPA Acid Digestion (Lindberg and Deutsch 2003)										
Average for duplicate "15935 AE" samples	ND	(7.49E+02)	(3.09E+03)	(6.34E+03)	(1.94E+03)	2.13E+05	(9.17E+03)	(3.21E+03)	(1.88E+02)	(5.06E+02)
EPA Acid Digestion (This Study)										
15935-1 AE	(1.58E+03)	4.17E+02	<1.62 E+04	(2.34E+02)	9.76E+02	1.37E+05	(9.71E+02)	(4.23E+03)	(1.57E+02)	(1.23E+03)
15935-1 AE Dup	(9.87E+02)	4.25E+02	<1.30 E+04	(2.52E+02)	8.54E+02	1.39E+05	(8.79E+02)	(1.45E+03)	(1.67E+02)	(4.19E+02)
Average	(1.28E+03)	4.21E+02		(2.43E+02)	9.15E+02	1.38E+05	(9.25E+02)	(2.84E+03)	(1.62E+02)	(8.24E+02)
Fusions (This Study)										
15935-1 FUS	(6.61E+03)	2.17E+02	<3.95 E+04	(4.44E+02)	(1.40E+03)	1.21E+05	(2.98E+04)	(3.94E+03)	(1.81E+02)	(6.49E+02)
15935-1 FUS Dup	(8.84E+03)	3.06E+02	<3.81 E+04	(2.96E+02)	1.62E+03	1.11E+05	(2.64E+04)	(2.54E+03)	(1.97E+02)	(7.65E+02)
Average	(7.73E+03)	2.61E+02		(3.70E+02)	1.51E+03	1.16E+05	(2.81E+04)	(3.24E+03)	(1.89E+02)	(7.07E+02)
Percentage Leached by EPA Acid Digestion (Average This Study) Relative to Average Fusion Results										
	16.6%	161%		65.8%	60.5%	119%	3.3%	87.7%	85.8%	117%

Table 3-4. Concentrations of elements determined from ICP-MS analysis per gram of dry sludge

Sample Number	Cr - total based on		As - total based on	Se - total based on	Mo - total based on		
	Cr-52	Cr-53	As-75	Se-82	Mo-95	Mo-98*	Mo-100
----- µg/g -----							
EPA Acid Digestion (Lindberg and Deutsch 2003)							
Average for duplicate "15935 AE" samples	4.28E+03	4.19E+03	1.60E+01	9.63E+00		1.59E+01	2.14E+01
EPA Acid Digestion (This Study)							
15935-1 AE	3.08E+03	3.07E+03	(1.08E+01)	<4.06E+01	NR	9.56E+00	(1.33E+01)
15935-1 AE Dup	3.08E+03	3.08E+03	(1.09E+01)	(2.26E+00)	NR	1.06E+01	(1.29E+01)
Average	3.08E+03	3.08E+03	(1.09E+01)		NR	1.01E+01	(1.31E+01)
Fusions (This Study)							
15935-1 FUS	2.74E+03	2.78E+03	(2.77E+00)	<9.88E+01	NR	(1.35E+01)	(1.84E+01)
15935-1 FUS Dup	2.59E+03	2.61E+03	(4.46E+00)	<9.53E+01	NR	(1.36E+01)	(1.74E+01)
Average	2.66E+03	2.70E+03	(3.61E+00)		NR	(1.35E+01)	(1.79E+01)
Percentage Leached by EPA Acid Digestion (Average This Study) Relative to Average Fusion Results							
	116%	114%	301%	22.1%		74.5%	73.3%
<p>"NR" refers to "not reported." *The indicated isotope is the suggested isotope for use to quantify the total concentration of that element.</p>							

Table 3-5. Concentrations of elements determined from ICP-MS analysis per gram of dry sludge (continued)

Sample Number	Ru ^{**} -total based on		Ag - total based on		Cd - total based on		Pb - total based on		
	Ru-101	Ru-102*	Ru-104	Ag-107	Ag-109*	Cd-111	Cd-114*	Pb-206	Pb-208*
----- µg/g -----									
EPA Acid Digestion (Lindberg and Deutsch 2003)									
Average for duplicate "15935 AE" samples	NR	2.13E+02	2.01E+02	1.50E+03	1.53E+03	2.39E+02	2.17E+02	8.97E+03	1.00E+04
EPA Acid Digestion (This Study)									
15935-1 AE	8.54E+02	3.97E+02	3.75E+02	1.64E+03	1.67E+03	1.65E+02	1.47E+02	7.55E+03	8.49E+03
15935-1 AE Dup	8.05E+02	3.76E+02	3.59E+02	1.65E+03	1.69E+03	1.70E+02	1.55E+02	7.60E+03	8.55E+03
Average	8.30E+02	3.87E+02	3.67E+02	1.65E+03	1.68E+03	1.67E+02	1.51E+02	7.57E+03	8.52E+03
Fusions (This Study)									
15935-1 FUS	1.01E+03	4.73E+02	4.43E+02	1.54E+01	1.34E+01	1.37E+02	1.25E+02	6.39E+03	7.13E+03
15935-1 FUS Dup	9.29E+02	4.35E+02	4.07E+02	1.43E+01	1.27E+01	1.33E+02	1.20E+02	5.93E+03	6.62E+03
Average	9.72E+02	4.54E+02	4.25E+02	1.49E+01	1.30E+01	1.35E+02	1.22E+02	6.16E+03	6.88E+03
Percentage Leached by EPA Acid Digestion (Average This Study) Relative to Average Fusion Results									
	85.4%	85.2%	86.3%	11,100%	12,900%	124%	123%	123%	124%
NR = Not reported.									
*The indicated isotope is the suggested isotope for use to quantify the total concentration of that element.									
**The accuracy of the ruthenium concentrations is suspect due to fission product yields being different than natural abundances.									

Table 3-6. Concentrations of technetium-99, uranium-238, and actinides measured by ICP-MS per gram of dry sludge

Sample Number	Tc-99	U-238	Am-241	Pu-239	Np-237
	----- $\mu\text{g/g}$ -----				
EPA Acid Digestion (Lindberg and Deutsch 2003)					
Average for duplicate "15935 AE" samples	4.82E+00	1.61E+03	3.51E+00	5.74E+01	1.86E+01
EPA Acid Digestion (This Study)					
15935-1 AE	3.24E+00	1.25E+03	2.48E+00	4.10E+01	1.06E+01
15935-1 AE Dup	3.21E+00	1.33E+03	2.68E+00	4.31E+01	1.14E+01
Average	3.23E+00	1.29E+03	2.58E+00	4.20E+01	1.10E+01
Fusions (This Study)					
15935-1 FUS	3.12E+00	9.54E+02	2.06E+00	3.66E+01	5.41E+00
15935-1 FUS Dup	2.59E+00	9.80E+02	2.11E+00	2.75E+01	8.52E+00
Average	2.86E+00	9.67E+02	2.08E+00	3.21E+01	6.97E+00
Percentage Leached by EPA Acid Digestion (Average This Study) Relative to Average Fusion Results					
	113%	133%	124%	131%	158%

Table 3-7. Gamma energy analysis (GEA) in microcuries per gram of dry sludge

Sample Number	K-40	Co-60	Cs-137	Eu-154	Eu-155
	----- $\mu\text{Ci/g}$ -----				
Untreated (Raw) Solid (Lindberg and Deutsch 2003)					
"15935_solid"	1.231E+00	9.973E-01	9.304E+02	1.705E+01	2.207E+02
EPA Acid Digestion (Lindberg and Deutsch 2003)					
Average for duplicate "15935 AE" samples	ND	ND	7.810E+02	1.214E+01	2.777E+02
EPA Acid Digestion (This Study)					
15935-1 AE	ND	5.322E-01	4.570E+02	6.707E+00	7.840E+01
15935-1 AE Dup	ND	5.049E-01	4.636E+02	7.650E+00	6.292E+01
Average		5.186E-01	4.603E+02	7.178E+00	7.066E+01
Fusions (This Study)					
15935-1 FUS	ND	4.699E-01	4.031E+02	4.416E+00	7.103E+01
15935-1 FUS Dup	ND	3.446E-01	3.457E+02	5.157E+00	6.779E+01
Average		4.073E-01	3.744E+02	4.786E+00	6.941E+01
Percentage Leached by EPA Acid Digestion (Average This Study) Relative to Average Fusion Results					
		127%	123%	150%	102%
"ND" refers to "not determined."					

Table 3-8. Gamma energy analysis (GEA) in micrograms per gram of dry sludge

Sample Number	K-40	Co-60	Cs-137	Eu-154	Eu-155
	----- µg/g -----				
Untreated (Raw) Solid (Lindberg and Deutsch 2003)					
“15935_solid”	1.75E+05	8.82E-04	1.07E+01	6.31E-02	4.54E-01
EPA Acid Digestion (Lindberg and Deutsch 2003)					
Average for duplicate “15935 AE” samples	ND	ND	9.02E+00	4.49E-02	5.72E-01
EPA Acid Digestion (This Study)					
15935-1 AE	ND	4.70E-04	5.28E+00	2.48E-02	1.61E-01
15935-1 AE Dup	ND	4.46E-04	5.36E+00	2.83E-02	1.30E-01
Average		4.58E-04	5.32E+00	2.66E-02	1.46E-01
Fusions (This Study)					
15935-1 FUS	ND	4.15E-04	4.66E+00	1.63E-02	1.46E-01
15935-1 FUS Dup	ND	3.05E-04	3.99E+00	1.91E-02	1.40E-01
Average		3.60E-04	4.33E+00	1.77E-02	1.43E-01
Percentage Leached by EPA Acid Digestion (Average This Study) Relative to Average Fusion Results					
		127%	123%	150%	102%
“ND” refers to “not determined.”					

Table 3-9. Total beta and total alpha activities and strontium-90 concentrations per gram of dry sludge

Sample Number	Gross Beta	Gross Alpha	Sr-90*	
	----- µCi/g -----		-----µCi/g -----	µg/g
EPA Acid Digestion (Lindberg and Deutsch 2003)				
Average for “15935 AE” samples	2.842E+04	7.919E+03	1.992E+04	1.43E+02
EPA Acid Digestion (This Study)				
15935-1 AE	1.004E+04	6.473E+03	1.233E+02	8.87E-01
15935-1 AE Dup	8.642E+03	6.682E+03	7.035E+01	5.06E-01
Average	9.340E+03	6.577E+03	9.682E+01	6.97E-01
Fusions (This Study)				
15935-1 FUS	9.692E+03	2.269E+03	9.922E+02	7.14E+00
15935-1 FUS Dup	1.204E+04	2.150E+03	1.214E+03	8.73E+00
Average	1.086E+04	2.209E+03	1.103E+03	7.93E+00
Percentage Leached by EPA Acid Digestion (Average This Study) Relative to Average Fusion Results				
	86.0%	298%	8.8%	8.8%
*The concentrations of Sr-90 are derived from the measurement of gross beta. The calculated concentration of Sr-90 represents at best a qualitative estimate of the maximum concentration limit for Sr-90, because the gross beta measurements likely include activity contributed from other beta emitters.				

Table 3-10. Summary of the average concentrations from the EPA acid digestion and KOH-KNO₃ fusion analyses for the composition of unleached AY-102 (jar 15935) sludge

Analyte	Average Concentration (µg/g)		Analyte	Average Concentration (µg/g)	
	EPA Acid Digestion	KOH-KNO ₃ Fusion		EPA Acid Digestion	KOH-KNO ₃ Fusion
Fe	129,000	144,000	Mg	(1,330)	(1,300)
Na	138,000	116,000	U-238	1,290	967
Al	90,700	85,500	Ba	1,070	828
Mn	49,100	44,300	Zr	(824)	(707)
Si	(925)	(28,100)	Li	(328)	(617)
B	(3,820)	(8,830)	Mo	(485)	(562)
Se	(1,280)	(7,730)	Co	(250)	(382)
Pb	8,610	7,230	V	(243)	(370)
P	9,150	6,040	Sr	421	261
Ca	5,540	(5,100)	Ti	(162)	(189)
Cu	(1,980)	(3,580)	Cd	(158)	(152)
S	(2,840)	(3,240)	Be	(17.9)	(32.2)
Cr	3,420	2,940	Pu-239	42.0	32.1
Ni	(7,200)	(2,780)	Np-237	11.0	6.97
As	(382)	(2,000)	Tc-99	3.23	2.86
Zn	915	1,510	Am-241	2.58	2.08
Bi	(260)	(1,400)			

The measured concentrations of dissolved silver in the EPA acid digestion and KOH-KNO₃ fusion solutions were especially inconsistent. The silver concentrations determined from ICP-MS measurements of dissolved silver-107 and silver-109 in the KOH-KNO₃ fusion solutions were only slightly greater than the silver concentrations for the blank, and were two orders of magnitude lower than those for the EPA acid digestion solutions. This discrepancy in the silver concentrations resulted in relative recovery percentages of 11,100% and 12,900% based on silver-107 and silver-109 analyses, respectively. These results suggest that a sparingly soluble silver compound, such as silver chloride, may have precipitated during the KOH-KNO₃ fusion treatment possibly with the addition of 1.0 M hydroxylamine HCl solution. The potential of low silver recovery resulting from silver chloride precipitation in the analysis of Hanford tank wastes has been discussed previously by Fiskum et al. (2000) and Patello et al. (2001).

Table 3-11 shows a comparison of the concentrations of cadmium, chromium, and lead in the EPA acid digestion and KOH-KNO₃ fusion solutions as determined by ICP-MS and ICP-OES. Although some of these comparisons are based on values that were less than the lowest LOQ (concentrations listed in parentheses), these results suggest that the ICP-MS and ICP-OES analyses for cadmium, chromium, and

Table 3-11. Comparison of cadmium, chromium, and lead concentrations determined by ICP-MS and ICP-OES per gram of dry sludge

Sample Number	Cd - total based on		Cr - total based on		Pb - total based on	
	Cd-111	Cd-114*	Cr-52	Cr-53	Pb-206	Pb-208*
EPA Acid Digestion (ICP-MS)						
15935-1 AE	1.65E+02	1.47E+02	3.08E+03	3.07E+03	7.55E+03	8.49E+03
15935-1 AE Dup	1.70E+02	1.55E+02	3.08E+03	3.08E+03	7.60E+03	8.55E+03
Average	1.67E+02	1.51E+02	3.08E+03	3.08E+03	7.57E+03	8.52E+03
EPA Acid Digestion (ICP-OES)						
15935-1 AE	(1.55E+02)		3.38E+03		8.61E+03	
15935-1 AE Dup	(1.62E+02)		3.46E+03		8.60E+03	
Average	(1.58E+02)		3.42E+03		8.61E+03	
Percent Difference between Average EPA Acid Digestion ICP-MS and ICP-OES Values						
	0.63%		11.0%		7.0%	
Fusions (ICP-MS)						
15935-1 FUS	1.37E+02	1.25E+02	2.74E+03	2.78E+03	6.39E+03	7.13E+03
15935-1 FUS Dup	1.33E+02	1.20E+02	2.59E+03	2.61E+03	5.93E+03	6.62E+03
Average	1.35E+02	1.22E+02	2.66E+03	2.70E+03	6.16E+03	6.88E+03
Fusions (ICP-OES)						
15935-1 FUS	(1.44E+02)		3.05E+03		7.56E+03	
15935-1 FUS Dup	(1.59E+02)		2.82E+03		6.89E+03	
Average	(1.52E+02)		2.94E+03		7.23E+03	
Percent Difference between Average Fusion ICP-MS and ICP-OES Values						
	18.3%		9.7%		10.9%	
*The indicated isotope is the suggested isotope for use to quantify the total concentration of that element.						

lead in the EPA acid digestion solutions and in KOH-KNO₃ fusion solutions are, respectively, in close agreement. Similar favorable comparisons of the concentrations for arsenic and molybdenum determined by ICP-MS and ICP-OES in the EPA acid digestion solutions and in KOH-KNO₃ fusion solutions were not justified because the determined values were near background concentrations (i.e., similar to the concentrations in the blanks) and almost all were less than the lowest LOQ values.

3.2 XRD Results – AY-102 and BX-101

The background-subtracted XRD patterns measured for the samples of unleached and water-leached AY-102 (jar 15935) sludge, unleached AY-102 (jar 18686) sludge, and unleached BX-101 (jar 16503) sludge are shown in Figure 3-1, Figure 3-2, Figure 3-3, and Figure 3-4, respectively. The as-measured XRD patterns prior to background subtraction are shown in Appendix A. Each pattern is shown as a function of 2θ based on Cu_{Kα} radiation (λ=1.5406 Å). The vertical axis in each pattern represents the intensity of the XRD peaks. The crystalline solid phases identified by XRD as being present in the AY-102 and BX-101 sludge samples are summarized in Table 3-12.

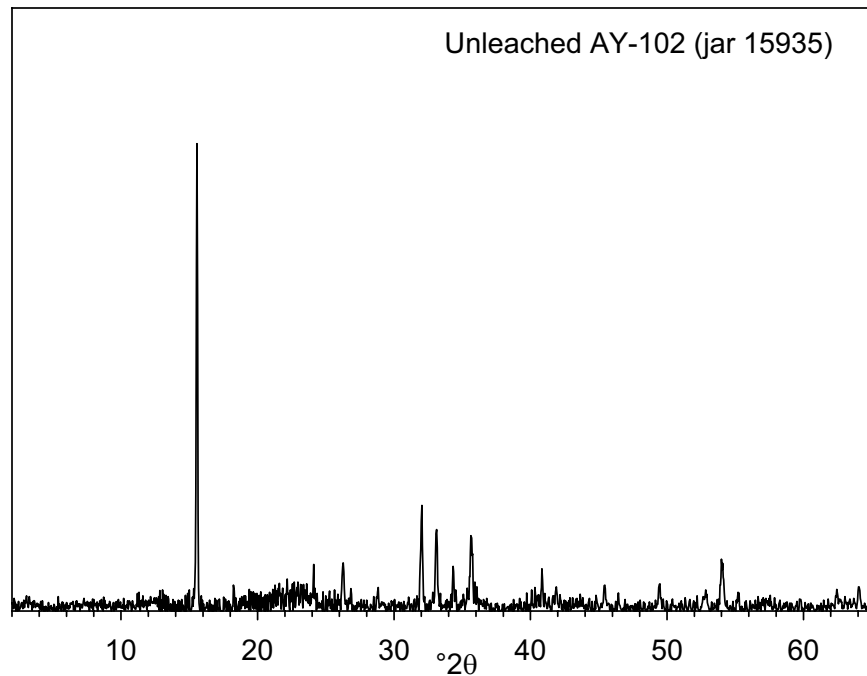


Figure 3-1. Background-subtracted XRD pattern measured for unleached AY-102 (jar 15935) sludge sample using a copper radiation source

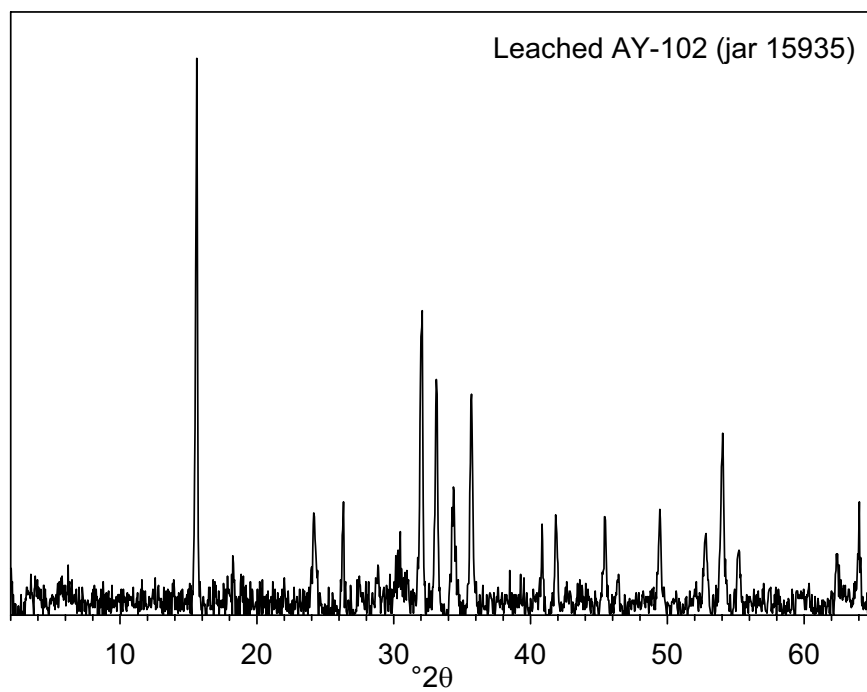


Figure 3-2. Background-subtracted XRD pattern measured for water-leached AY-102 (jar 15935) sludge sample using a copper radiation source

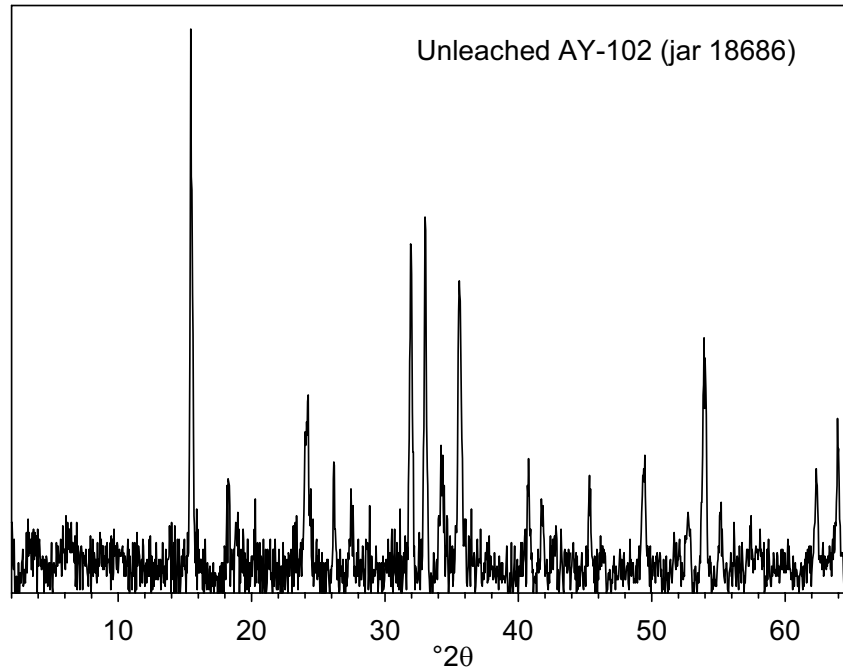


Figure 3-3. Background-subtracted XRD pattern measured for unleached AY-102 (jar 18686) sludge sample using a copper radiation source

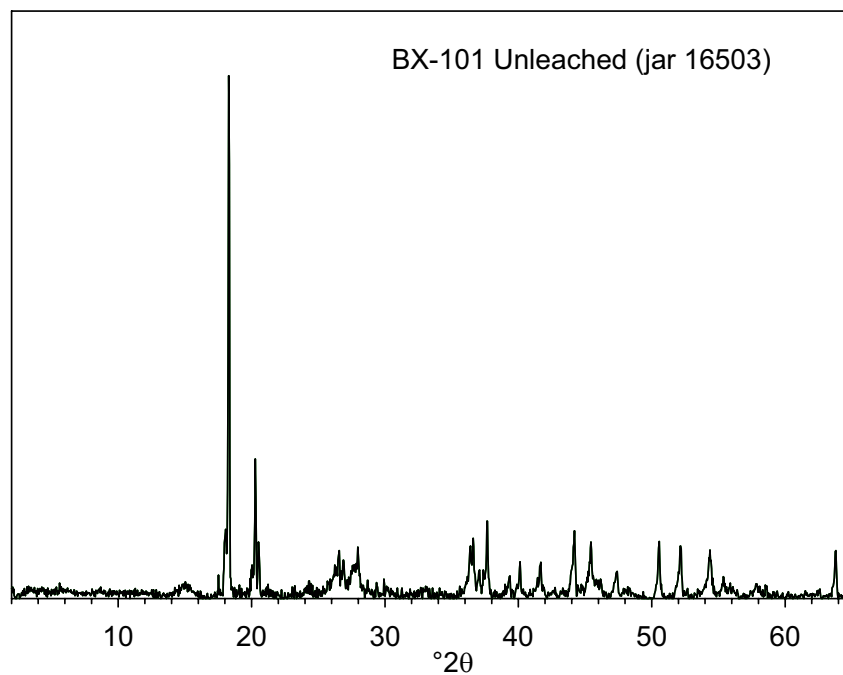


Figure 3-4. Background-subtracted XRD pattern measured for unleached BX-101 (jar 16503) sludge sample using a copper radiation source

Table 3-12. Mineral phases identified by XRD in AY-102 and BX-101 sludge samples

Sample Identification	Mineral Phases Identified by XRD
Unleached AY-102 (jar 15935) sludge	Dawsonite, hematite, gibbsite
Water-leached AY-102 (jar 15935) sludge	Dawsonite, hematite, gibbsite
Unleached AY-102 (jar 18686) sludge	Dawsonite, hematite, gibbsite, cancrinite
Unleached BX-101 (jar 16503) sludge	Gibbsite, cancrinite

Dawsonite [NaAlCO₃(OH)₂], hematite (Fe₂O₃), and gibbsite [Al(OH)₃] were identified as crystalline phases present in the unleached and water-leached AY-102 (jar 15935) sludge samples. For comparison, the XRD patterns for the unleached and water-leached AY-102 (jar 15935) samples are shown schematically in Figure 3-5 along with database patterns for dawsonite (PDF #45-1359), hematite (PDF #33-0664), and gibbsite (PDF #74-1775). In each schematic database (PDF) pattern shown in Figure 3-5, Figure 3-6, and Figure 3-7, the height of each line represents the relative intensity of an XRD peak [i.e., the most intense (the highest) peak has a relative intensity of 100%]. Quantitative analyses of the relative masses of individual phases present in each sludge sample were not calculated using these XRD patterns due to the factors discussed at the end of Section 2.3. However, the decrease in height of the major diffraction peak at 15.60° 2θ peak (Figure 3-5) suggests that less dawsonite is present in the water-leached sample compared to that in the unleached sample of AY-102 (jar 15935) sludge. There were no unassigned reflections in the background-subtracted XRD patterns for the samples of unleached and water-leached AY-102 (jar 15935) sludge. That is, all crystalline phases present at greater than 5-10 wt% in this sludge sample were identified by XRD.

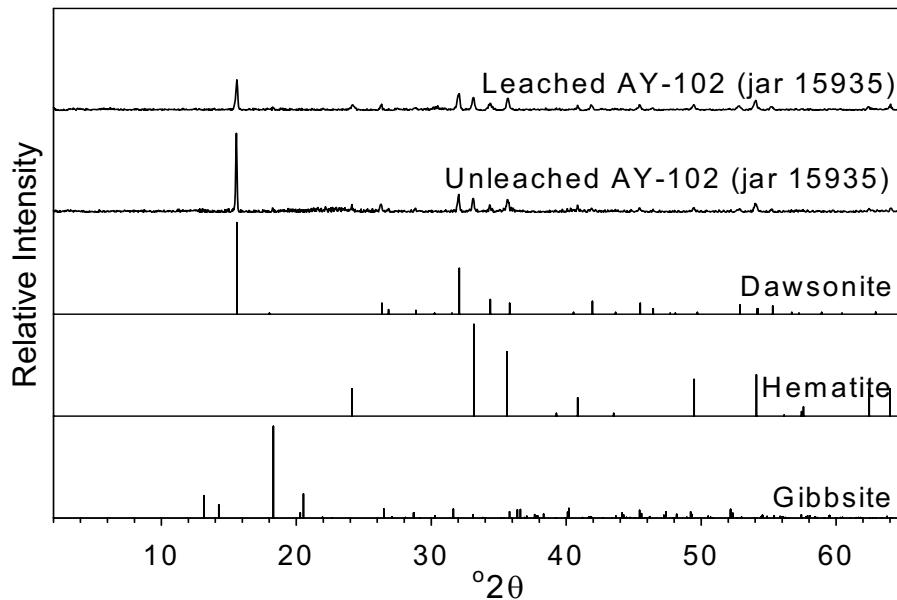


Figure 3-5. XRD patterns for the unleached and water-leached AY-102 (jar 15935) sludge samples compared to the database patterns for dawsonite (PDF #45-1359), hematite (PDF #33-0664), and gibbsite (PDF #74-1775)

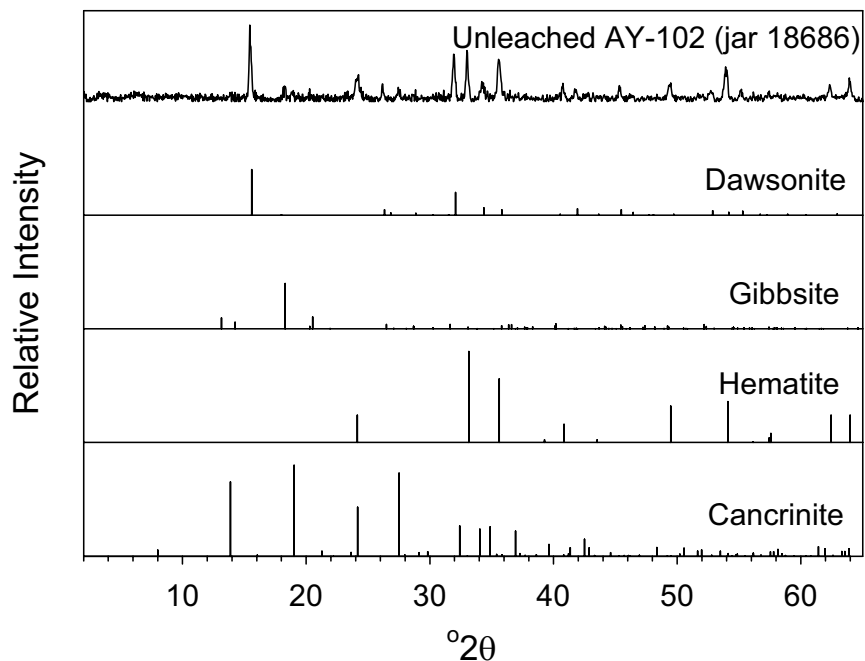


Figure 3-6. XRD pattern for the unleached AY-102 (jar 18686) sludge sample compared to the database patterns for dawsonite (PDF #45-1359), gibbsite (PDF #74-1775), hematite (PDF #33-0664), and cancrinite (PDF #71-0776)

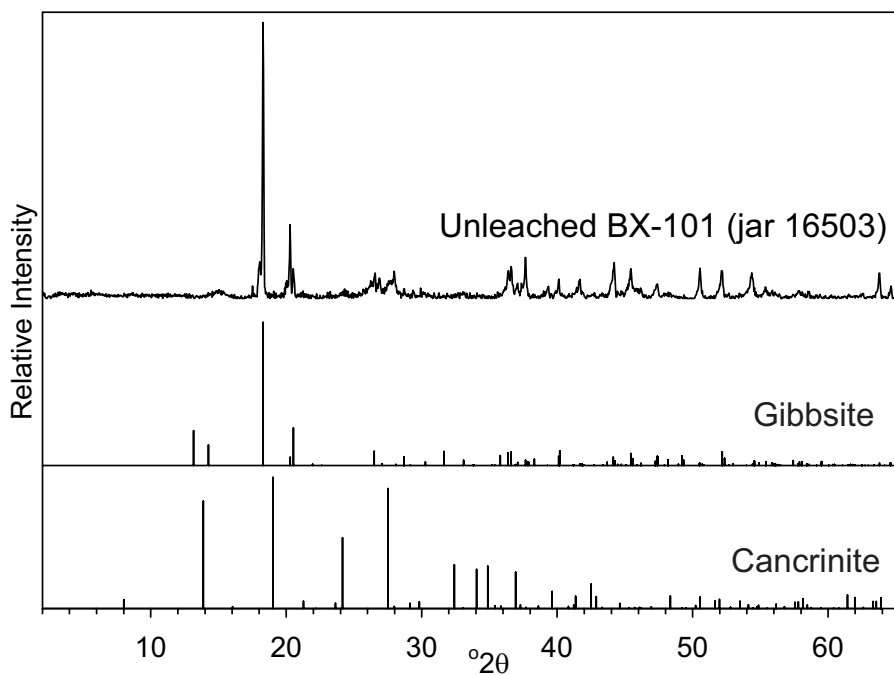


Figure 3-7. XRD pattern for the unleached BX-101 (jar 16503) sludge sample compared to the database pattern for gibbsite (PDF #74-1775) and cancrinite (PDF #71-0776)

Like the results for the AY-102 (jar 15935) sludge sample, dawsonite, hematite, and gibbsite were also identified in the unleached AY-102 (jar 18686) sludge sample (Figure 3-6). The silicate-carbonate phase cancrinite was also tentatively identified in the unleached AY-102 (jar 18686) sludge sample. This determination was based on matches of measured reflections to pattern PDF #71-0776 for the cancrinite composition $\text{Na}_6(\text{Al}_6\text{Si}_6\text{O}_{24})(\text{CaCO}_3)(\text{H}_2\text{O})_2$. This composition agrees well with the SEM/EDS analyses (Section 3.3), which show that these particles do not contain any detectable calcium or nitrogen (such as nitrate). Because the AY-102 (jar 18686) sludge sample was not analyzed by SEM/EDS, there are no additional data to corroborate the identification of cancrinite in this sludge sample. There were no unassigned reflections in the background-subtracted XRD pattern for the unleached AY-102 (jar 18686) sludge sample. This suggests that all the crystalline phases present at greater than 5-10 wt% in this sludge sample were identified by XRD.

In contrast to the XRD patterns for the AY-102 sludge samples, gibbsite was determined by XRD analysis based on pattern PDF #74-1775 to be the primary crystalline phase present in the unleached BX-101 (jar 16503) sludge sample (Figure 3-7). Minor reflections observed on the XRD pattern at 19.03, 24.14, and 27.5 °2θ correlated well with crystalline cancrinite [$\text{Na}_6(\text{Al}_6\text{Si}_6\text{O}_{24})(\text{CaCO}_3)(\text{H}_2\text{O})_2$] (PDF #71-0776), which suggested that a trace amount of this mineral was present in this sludge sample. The identification of cancrinite was based on a re-inspection of the measured XRD pattern for the unleached BX-101 (jar 16503) sludge after SEM/EDS analyses had shown the occurrence of silicon-containing particles with external morphologies and compositions consistent with what others in the literature had identified as cancrinite (see Section 3.3.3). After allowing for all possible XRD reflections for both gibbsite and cancrinite, there were several reflections (e.g., 17.45, 18.00, and 4.44 °2θ) unassigned. These reflections indicate one or more unidentified crystalline phase(s) are likely present in the BX-101 (jar 16503) sludge. Identification of these unknown phases was not possible without more extensive, detailed chemical characterization (e.g., transmission electron microscopy [TEM]) of this sludge sample.

The SEM/EDS analysis of the unleached BX-101 (jar 16503) sludge also indicates the presence of particles containing significant concentrations of uranium with lesser amounts of sodium and aluminum (see Section 3.3.3). Based on this information, the XRD pattern for the unleached BX-101 (jar 16503) sludge sample was re-evaluated for the presence of reflections that may have matched PDF patterns for any crystalline oxide or carbonate solids containing uranium, sodium, and possibly aluminum, such as $\text{Na}_2\text{U}_2\text{O}_7$ (PDF #43-0347) and clarkeite [PDF #08-0315, $(\text{Na,Ca,Pb})_2\text{U}_2(\text{O,OH})_7$]. The pattern search did not detect any reflections that could be unambiguously assigned to $\text{Na}_2\text{U}_2\text{O}_7$, clarkeite,¹ or any other uranium solid. The PDF file #43-0347 for $\text{Na}_2\text{U}_2\text{O}_7$ has a major reflection at 14.838 °2θ, which might correspond to a very broad reflection between 14 and 16 °2θ (see Figure 3-4). Unfortunately, the collodion solution used as a binder for our XRD samples has a large, broad reflection between approximately 12 and 32 °2θ (see Figure 2-4), which makes resolution of peaks in this 2θ region problematic for phases present in trace quantities. The other reflections listed in PDF file #43-0347 for $\text{Na}_2\text{U}_2\text{O}_7$ are all less than 50% of the intensity of the main peak at 14.838 °2θ, which makes them difficult to detect. Some of these reflections, moreover, overlap with reflections for gibbsite, which also prevents their identification. The same difficulties also affect the detection of most of the major reflections listed in pattern

¹ Clarkeite is isostructural with $\text{Na}_2\text{U}_2\text{O}_7$ and $\text{Na}_6\text{U}_7\text{O}_{24}$, and is therefore difficult to distinguish using XRD (Finch and Ewing 1997). Based on new chemical and structural data, Finch and Ewing (1997) suggest that the “ideal formula for the ideal end-member” clarkeite is $\text{Na}[(\text{UO}_2)\text{O}(\text{OH})](\text{H}_2\text{O})_{0.1}$.

PDF #08-0315 for clarkeite. In addition, major reflections at 21.711 °2θ (40% I/I₀), 46.084 °2θ (70% I/I₀), and 48.845 °2θ (60% I/I₀) were missing from the measured XRD pattern for unleached BX-101 (jar 16503) sludge.

3.3 SEM/EDS Results – AY-102 and BX-101

This section summarizes the results of the SEM/EDS analyses on 1) unleached (raw) AY-102 (jar 15935) sludge, 2) water-leached AY-102 (jar 15935) sludge, and 3) unleached (raw) BX-101 (jar 16503) sludge samples. SEM micrographs are presented that show the typical morphologies, sizes, and surface textures of particles in each sludge sample. Tables are also given of qualitative compositions (in wt%) calculated for particles probed by EDS from each sludge sample.

All of the particle compositions determined by SEM/EDS and discussed in this report contain oxygen, and possibly carbonate and/or hydrogen (unless otherwise noted). The concentrations of oxygen are listed in the EDS composition summary tables, and issues regarding the detection of hydrogen and the uncertainties associated with the calculated concentrations of carbon in the EDS analyses are discussed in later sections.

3.3.1 Unleached AY-102 Sludge

Three subsamples (i.e., three SEM mounts) of unleached AY-102 (jar 15935) sludge were inspected by SEM/EDS. The three subsamples were designated “unleached 15935-1,” “unleached 15935-2,” and “unleached 15935-3.” Table 3-13 summarizes the number of micrographs and EDS spectra recorded in this study for the three subsamples of unleached AY-102 (jar 15935) sludge, and identifies the specific figures, tables, and appendix containing the relevant results for these subsamples.

Unlike the other sludge samples examined in this study, there were differences in the particle types observed from the three mounts of unleached AY-102 (jar 15935) sludge. Subsample “unleached

Table 3-13. Summary of SEM/EDS data recorded in this study and listed in this report for the three subsamples of unleached AY-102 (jar 15935) sludge

	Subsample Identification		
	Unleached 15935-1	Unleached 15935-2	Unleached 15935-3
Number of recorded micrographs	17	11	19
Number of recorded EDS spectra	24	15	22
Figures of SEM micrographs showing typical particle morphologies and types	Figure 3-8 to Figure 3-18	Figure 3-19 to Figure 3-27	Figure 3-28 to Figure 3-38
Tables of calculated EDS compositions (with carbon)	Table 3-14	Table 3-15	Table 3-16
Appendix containing tables of calculated EDS compositions (without carbon) and figures of EDS spectra	Appendix B		

15935-1” contains a range of particles that are from a few tens of micrometers to submicrometers in size. Certain particles exhibit specific crystal habits, and may exist as aggregates of intergrown crystals (e.g., Figure 3-9). The large lath-shaped¹ crystals, for example as observed in Figure 3-10 (eds01), Figure 3-11 (eds06), and Figure 3-12 (eds11, eds12, and eds13), are one of the dominant types of particles observed in “unleached 15935-1.” In some areas of the SEM mount of “unleached 15935-1,” the lath-shaped crystals represent the majority of the sample mass (Figure 3-17). The lath-shaped crystals contain primarily sodium, and sometimes lesser concentrations of aluminum and/or iron (Table 3-14). The presence of crystal faces indicates that these lath-shaped particles are crystalline. Based on their abundance and compositions, the lath-shaped crystals are likely dawsonite.

Subsample “unleached 15935-1” also contained at least three other distinguishable types of particles. The globular or botryoidal² aggregates of particles observed in Figure 3-11 (eds08), Figure 3-12 (eds10), Figure 3-13 (eds15), and Figure 3-14 were composed of iron-rich particles that sometimes contained lesser amounts of sodium and manganese. The morphologies of these iron-rich aggregates and those in other subsamples of this sludge are similar to those shown in electron micrographs for hematite in Schwertmann and Cornell (1991). Aggregates of intergrown submicrometer crystals composed of sodium-iron-aluminum silicate [Figure 3-11, (eds09) and Figure 3-16 (eds20)] were also observed, but were rare in this sludge sample. Micrographs taken with backscattered electrons revealed the presence of silver-rich particles containing lesser concentrations of aluminum [see bright grains in Figure 3-15 (eds04) and Figure 3-16 (eds16)]. These silver-containing particles were not common, and did not have any distinguishing morphological features. None of the particles of “unleached 15935-1” examined by SEM/EDS contained any significant concentrations (i.e., >5 wt%) of uranium (see Table 3-14).

Subsample “unleached 15935-2” consisted primarily of large aggregates of submicron particles (Figure 3-19, Figure 3-22, and Figure 3-24). The aggregates were typically tens of micrometers or less in size, and appeared in some cases to be crusty or cemented together (Figure 3-21). Subsample “unleached 15935-2” also contained (in order of relative abundance) the lath-shaped (more rod-shaped in this subsample) sodium-rich crystals [Figure 3-23 (eds04)], botryoidal aggregates of iron-rich particles [Figure 3-23 (eds05), and Figure 3-24 (eds08)], and silver-containing particles [Figure 3-21 (eds01)]. These particles were not as well formed as those observed in “unleached 15935-1.” A large particle composed essentially of carbon was also observed in “unleached 15935-2.” The particle is shown at low and high magnification in Figure 3-26 and Figure 3-27, respectively. The particle is several hundred micrometers in length and coated with submicrometer-sized particles of the other phases present in this sludge sample. None of the particles of “unleached 15935-2” examined by SEM/EDS contained any significant concentrations (i.e., >5 wt%) of uranium (see Table 3-15).

Subsample “unleached 15935-3” was similar to “unleached 15935-2” in that it consisted primarily of aggregates of micrometer-to-submicrometer sized particles that were less well formed than those in “unleached 15935-1.” Like “unleached 15935-2,” subsample “unleached 15935-3” contained some large (hundreds of micrometers in size) particle fragments composed essentially of carbon [Figure 3-28 and Figure 3-29 (eds12)]. Subsample “unleached 15935-3” also contained (in order of relative abundance)

¹ Lath-shaped refers to crystals that are long and thin in shape with moderate to narrow widths.

² Botryoidal refers to a spherical or globular growth of an aggregate of particles.

rod-shaped sodium-rich crystals [Figure 3-38 (eds10)], botryoidal aggregates of iron-rich particles [Figure 3-35 (eds04)], and silver-containing particles [Figure 3-37 (eds17)]. Subsample “unleached 15935-3” also contained some thin, crust-like material (Figure 3-30 to Figure 3-33) not observed previously in “unleached 15935-1” or “unleached 15935-2.” Except for the fine particles attached to its surface, the crust-like phase appears to be relatively homogeneous. However, when imaged by secondary electrons (Figure 3-30) versus backscatter electrons (Figure 3-31), it is apparent that the compositions of the crusty material are not uniform. The bright area outlined by a yellow-dotted square in Figure 3-31 contains primarily uranium and sodium [see Figure 3-33 (eds05)], whereas the darker areas of the crusty material are composed primarily of sodium and silicon [see Figure 3-33 (eds06)]. Another particle containing uranium and a lesser concentration of sodium is shown in Figure 3-35 (eds01). This was the only subsample of unleached AY-102 (jar 15935) sludge in which uranium-containing particles were identified.

The major elements detected by EDS (Table 3-14, Table 3-15, and Table 3-16) for the three subsamples of unleached AY-102 (jar 15935) sludge are generally consistent with the major elements detected by bulk EPA acid digestion and KOH-KNO₃ fusion elemental analyses of this unleached sludge sample. The results of these analyses are reported in Section 3.1 and summarized in Table 3-10, which indicates the sludge contains primarily iron, sodium, aluminum, manganese, and silicon. All of the other metals detected in these analyses were present below 9,000 µg/g sludge. The EDS results also indicated that iron, sodium, aluminum, manganese, and silicon were major constituents of particles in the three subsamples of unleached AY-102 (jar 15935).

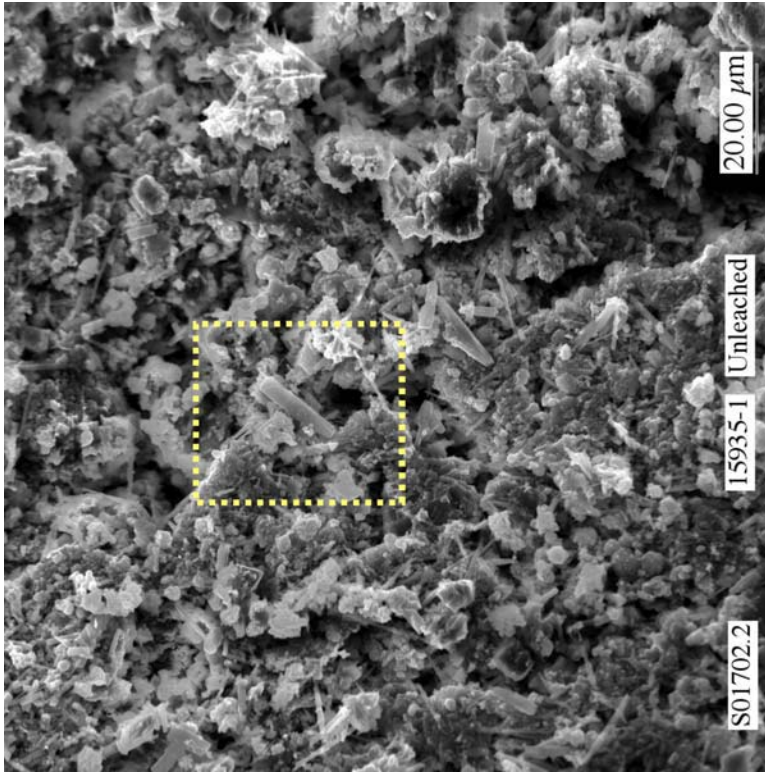


Figure 3-8. Low magnification scanning electron micrograph showing general morphology of particles in subsample “unleached 15935-1.” (A scale bar is given at the bottom right corner of this and all subsequent SEM micrographs.)

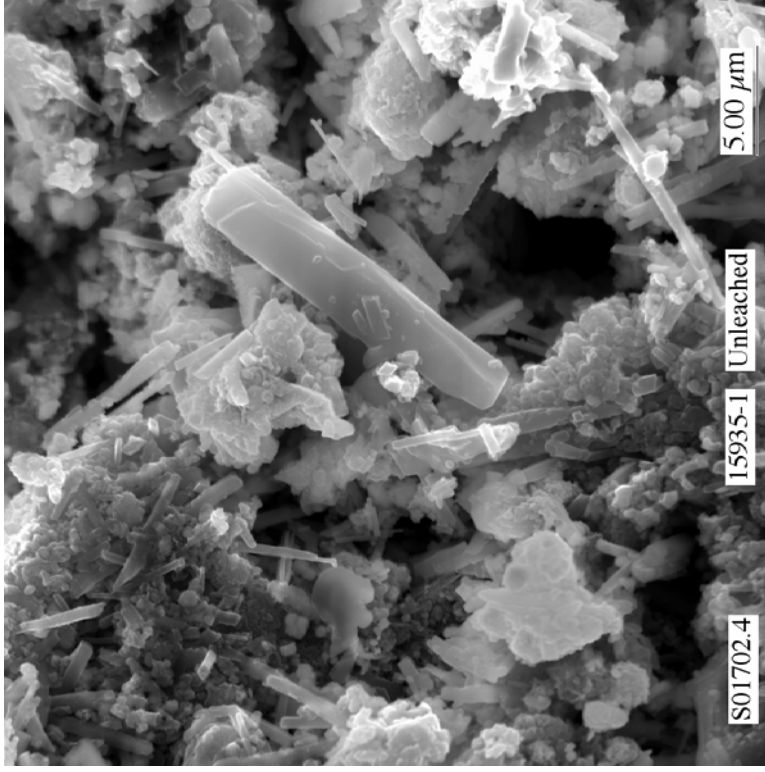


Figure 3-9. Micrograph showing at higher magnification the area indicated by the yellow-dotted square in Figure 3-8 of subsample “unleached 15935-1”

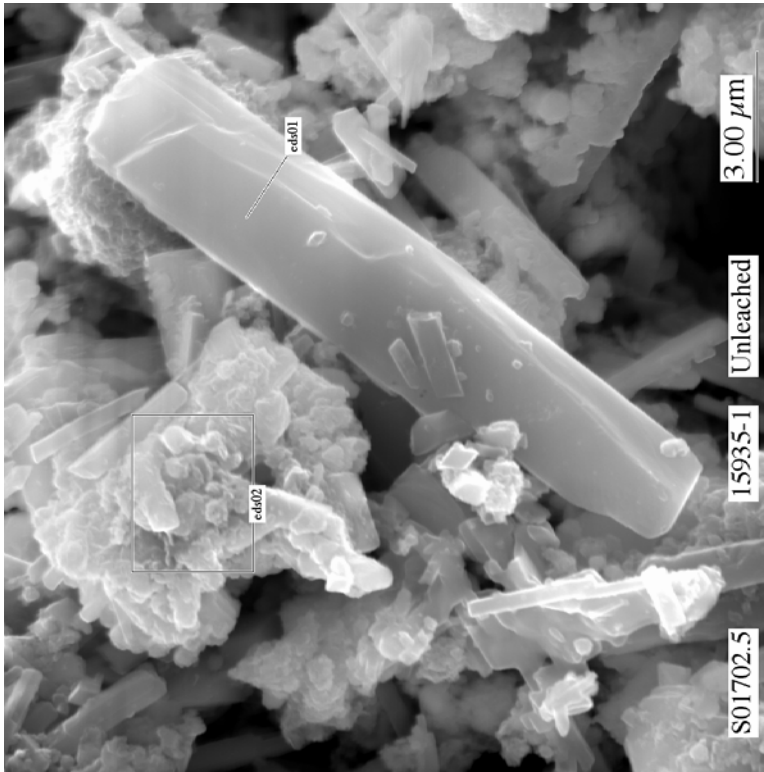


Figure 3-10. Micrograph showing at higher magnification the large lath-shaped crystal at the center of the previous figure of subsample “unleached 15935-1.” (Areas labeled by “eds” in this and all subsequent SEM micrographs indicate areas of sludge particles where EDS spectra were measured and recorded. The “eds” labels in these figures correspond to the same spectrum labels listed for the same sludge subsamples in tables of calculated EDS compositions.)

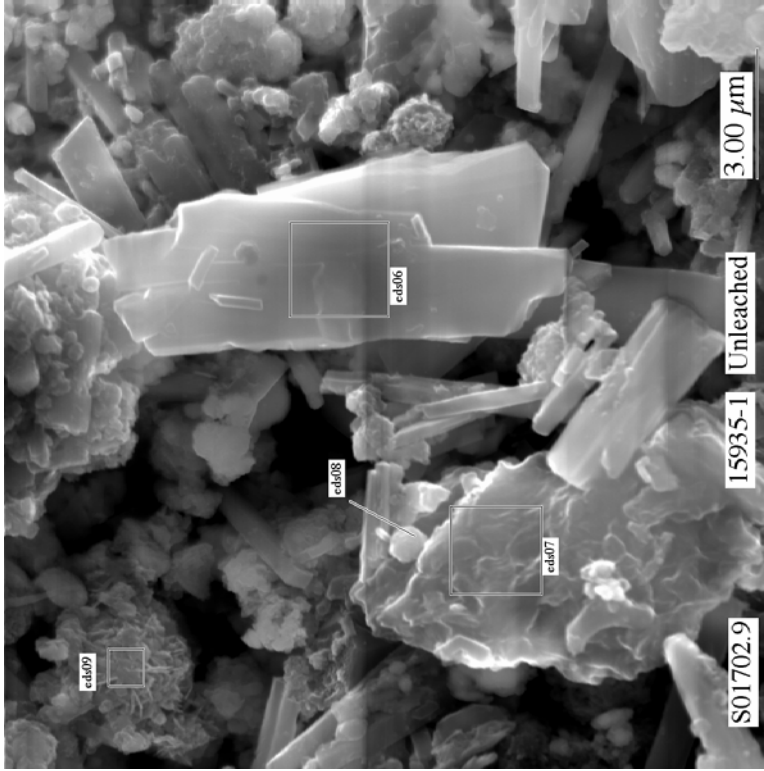


Figure 3-11. Micrograph showing various particle types that comprise subsample “unleached 15935-1”

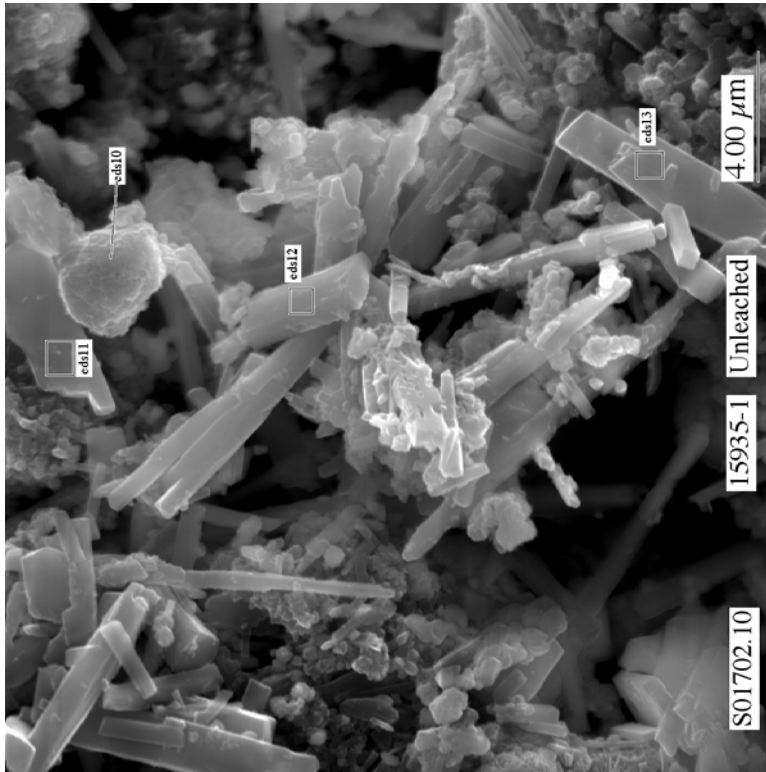


Figure 3-12. Micrograph showing various particle types that comprise subsample “unleached 15935-1”

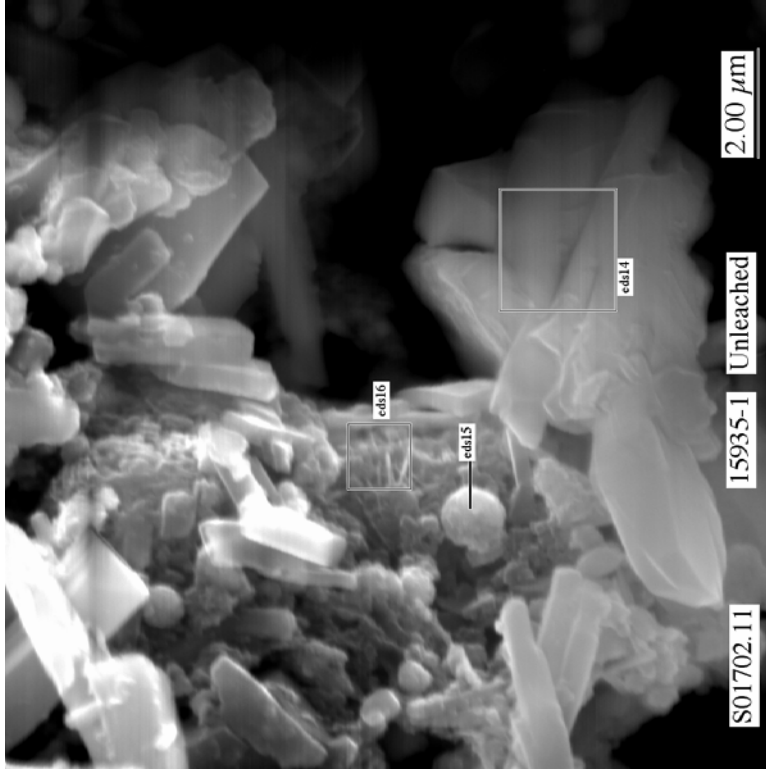


Figure 3-13. Micrograph showing various particle types that comprise subsample “unleached 15935-1”

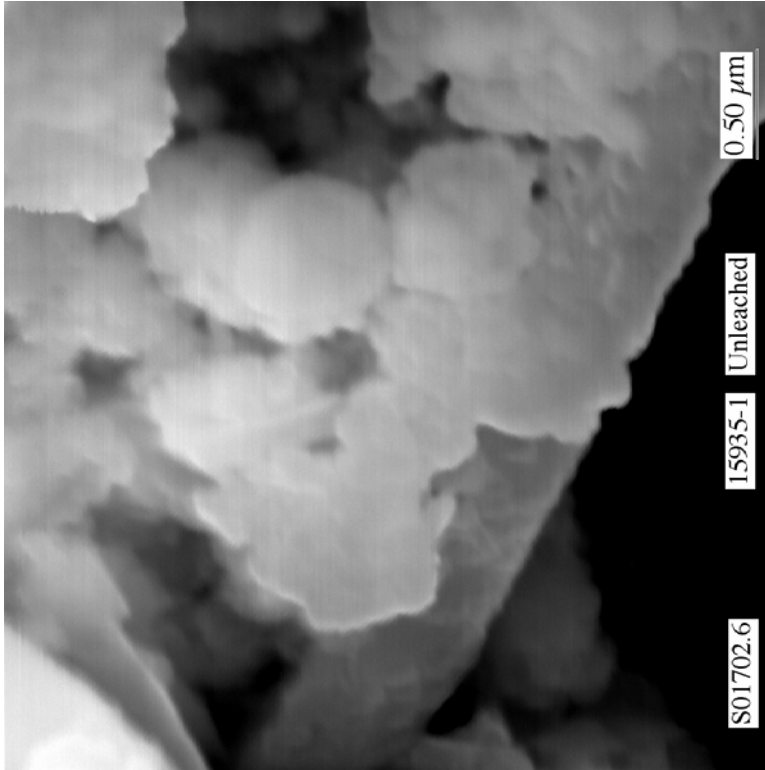


Figure 3-14. Micrograph showing at higher magnification botryoidal aggregate of iron-rich, sodium-containing oxide particles in subsample “unleached 15935-1”

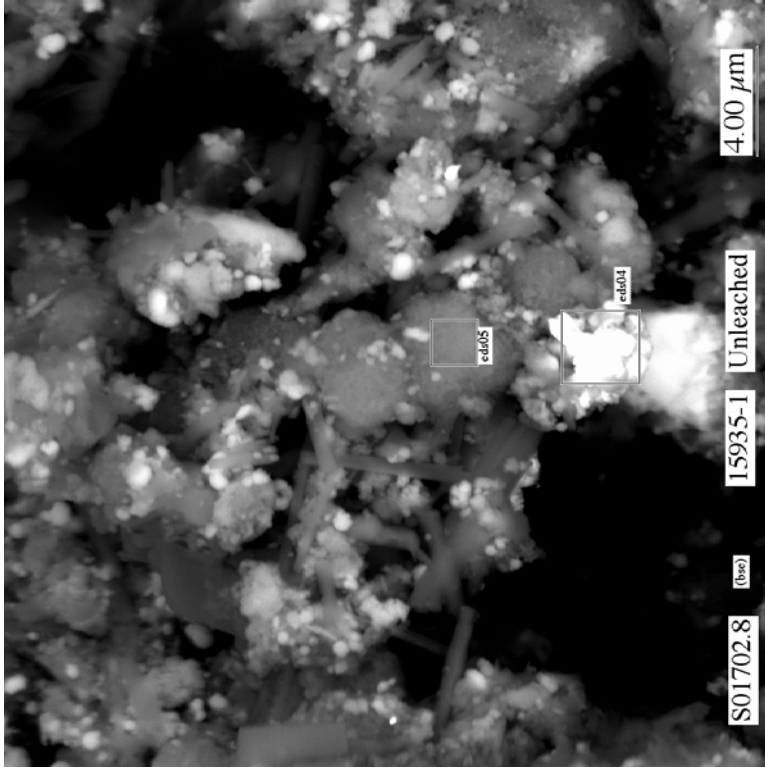


Figure 3-15. Backscatter electron micrograph in showing various particle types that comprise subsample “unleached 15935-1.” (The “bse” label on the bottom left of this and all subsequent micrographs signifies that the micrograph was collected backscattered electrons.)

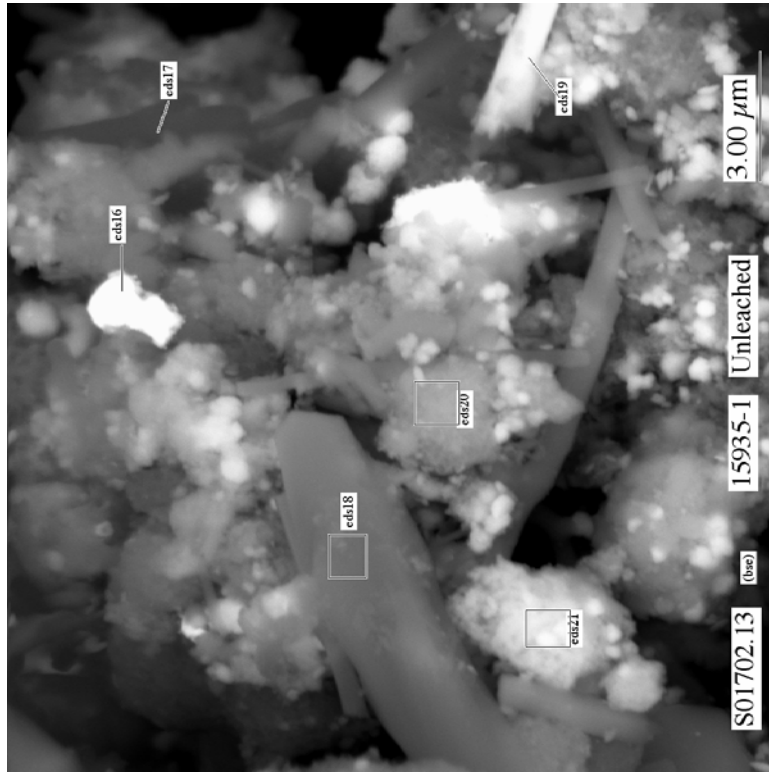


Figure 3-16. Backscatter electron micrograph in showing various particle types that comprise subsample “unleached 15935-1”

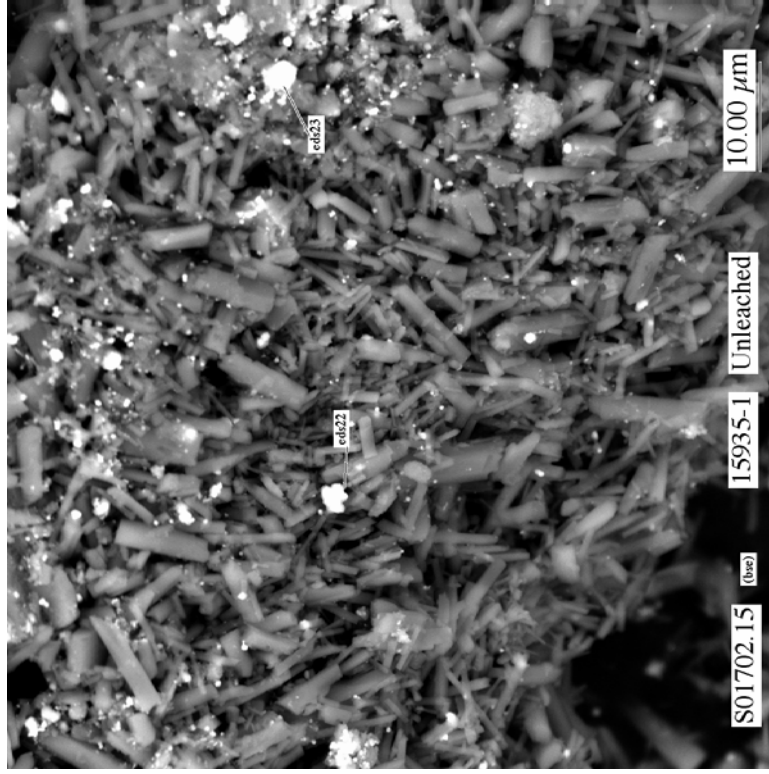


Figure 3-17. Backscatter electron micrograph in showing various particle types that comprise subsample “unleached 15935-1”

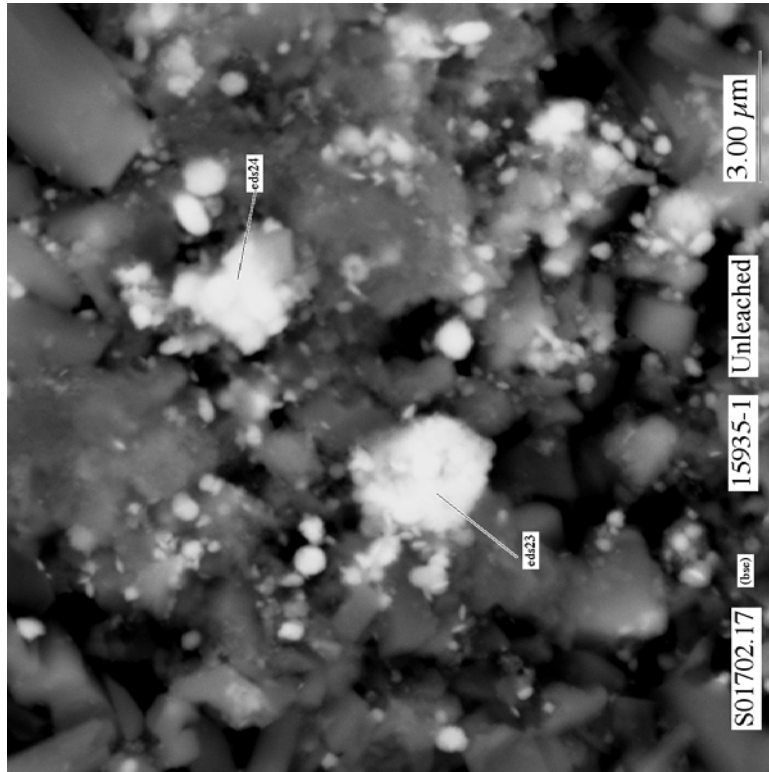


Figure 3-18. Backscatter electron micrograph in showing at higher magnification the particles labeled by “eds23” in Figure 3-17 of subsample “unleached 15935-1”

Table 3-14. Qualitative compositions determined by SEM/EDS that include the emission peak for carbon for particles observed in unleached subsample 15935-1 of AY-102 tank sludge (jar 15935)

Figure and Spectrum Label	Major Metals (>5 wt%)	----- wt% -----													
		C	O	Na	Al	Si	P	S	Ca	Cr	Mn	Fe	Ni	Ag	U
Figure 3-10 eds01	Na-Fe-Al-Si	12.4	42.7	13.0	8.9	5.8	1.0	0.3	0.2	0.2	4.0	11.3	0.4	0.1	-0.2
Figure 3-10 eds02	Na-Fe-Al	18.6	51.2	10.0	6.5	0.4	0.8	0.2	0.2	0.2	2.9	8.6	0.4	0.0	0.1
Fig. not shown eds03	Fe-Na-Mn-Al	7.6	33.5	9.5	7.7	2.8	1.4	0.7	0.7	0.4	8.2	25.6	1.1	0.8	0.2
Figure 3-15 eds04	Ag-Al	9.3	33.5	4.5	6.2	0.6	0.3	0.1	0.1	0.1	1.6	4.7	0.1	39.0	-0.1
Figure 3-15 eds05	Na-Al-Si	12.6	46.2	12.0	9.4	9.3	0.8	0.3	0.1	0.0	1.2	4.4	0.1	0.5	3.3
Figure 3-11 eds06	Na	16.8	52.0	21.0	2.2	0.4	0.3	0.1	0.1	0.1	1.9	4.9	0.2	0.1	0.0
Figure 3-11 eds07	Na	46.4	39.4	5.4	2.7	0.4	0.4	0.1	0.1	0.1	1.1	3.9	0.2	0.1	-0.1
Figure 3-11 eds08	Fe-Na	29.1	45.3	5.9	2.8	0.4	0.4	0.1	0.1	0.1	1.2	14.0	0.4	0.1	0.1
Figure 3-11 eds09	Fe-Na-Al-Si	17.6	40.7	9.5	7.2	6.7	0.9	0.2	0.2	0.3	3.6	12.1	0.7	0.1	0.2
Figure 3-12 eds10	Fe-Na	17.6	43.4	6.6	2.3	0.6	0.6	0.1	0.1	0.4	4.5	22.6	1.1	0.0	0.0
Figure 3-12 eds11	Na-Al-Fe	15.9	49.7	17.1	5.7	2.8	0.6	0.1	0.4	0.2	1.9	5.4	0.3	0.1	0.0
Figure 3-12 eds12	Na-Fe	16.2	50.3	20.5	3.4	1.0	0.6	0.1	0.1	0.1	2.1	5.2	0.3	0.1	0.0
Figure 3-12 eds13	Na-Fe	16.7	49.4	18.0	3.2	0.4	0.7	0.1	0.2	0.2	3.1	7.5	0.5	0.1	0.0
Figure 3-13 eds14	Na	18.1	48.1	23.8	2.8	1.3	0.3	0.0	0.1	0.0	1.5	4.1	0.2	0.1	-0.2
Figure 3-13 eds15	Fe-Na-Al	13.5	46.5	10.5	5.7	4.4	0.6	0.1	0.1	0.2	2.4	15.6	0.6	-0.1	-0.1
Figure 3-16 eds16	Ag-Al	20.8	36.7	3.8	5.2	0.4	0.2	0.1	0.0	0.0	0.8	2.6	0.1	29.1	0.3
Figure 3-16 eds17	Na	30.5	48.8	9.7	2.9	0.7	0.3	0.1	0.1	0.1	1.7	4.9	0.2	0.0	0.0
Figure 3-16 eds18	Na	20.9	51.4	17.9	2.9	1.3	0.4	0.1	0.1	0.1	1.4	3.2	0.2	0.2	0.1
Figure 3-16 eds19	Na	28.5	54.0	8.5	2.4	0.5	0.1	0.1	1.2	-0.6	0.6	3.7	0.2	0.7	0.1
Figure 3-16 eds20	Na-Al-Fe-Si	16.1	49.8	11.3	7.6	5.5	0.7	0.1	0.1	0.1	1.8	6.4	0.1	0.4	0.0
Figure 3-16 eds21	Fe-Na	16.1	44.2	7.6	4.2	1.7	0.7	0.2	0.1	0.5	2.8	20.8	0.9	0.1	0.1
Figure 3-17 eds22	Fe-Na	16.3	42.6	8.0	3.5	0.4	0.7	0.1	0.1	0.4	4.0	23.6	0.6	0.0	-0.2
Figure 3-18 eds23	Fe	8.2	5.6	2.1	0.7	0.4	0.6	0.1	0.1	1.1	4.9	76.0	0.7	-0.1	-0.2
Figure 3-18 eds24	Fe-Na	20.5	30.8	5.6	1.5	0.5	0.6	0.2	0.1	0.4	4.4	33.7	1.5	0.2	0.1

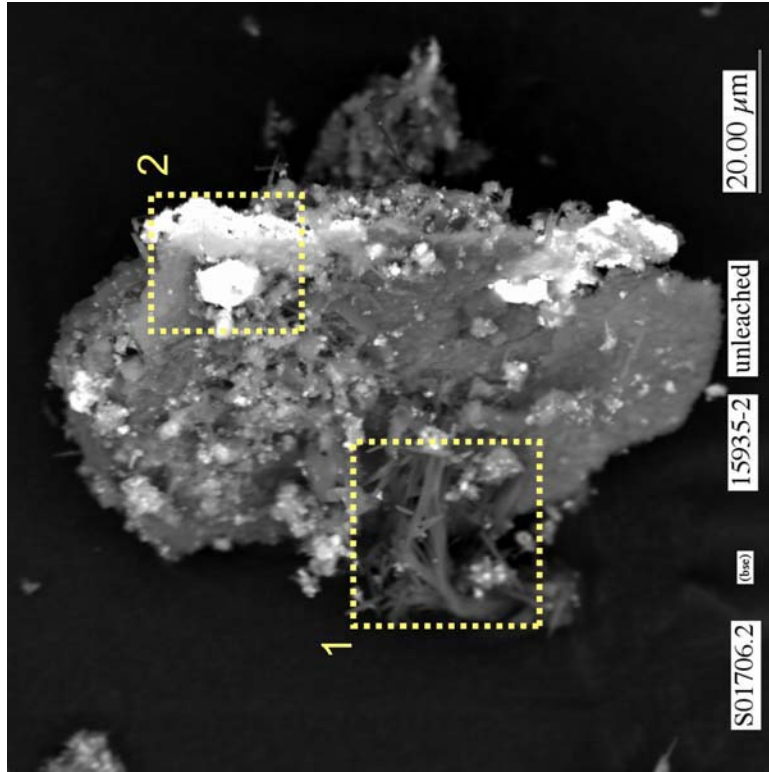


Figure 3-19. Low magnification scanning electron micrograph showing general morphology of large aggregate particles in subsample “unleached 15935-2”

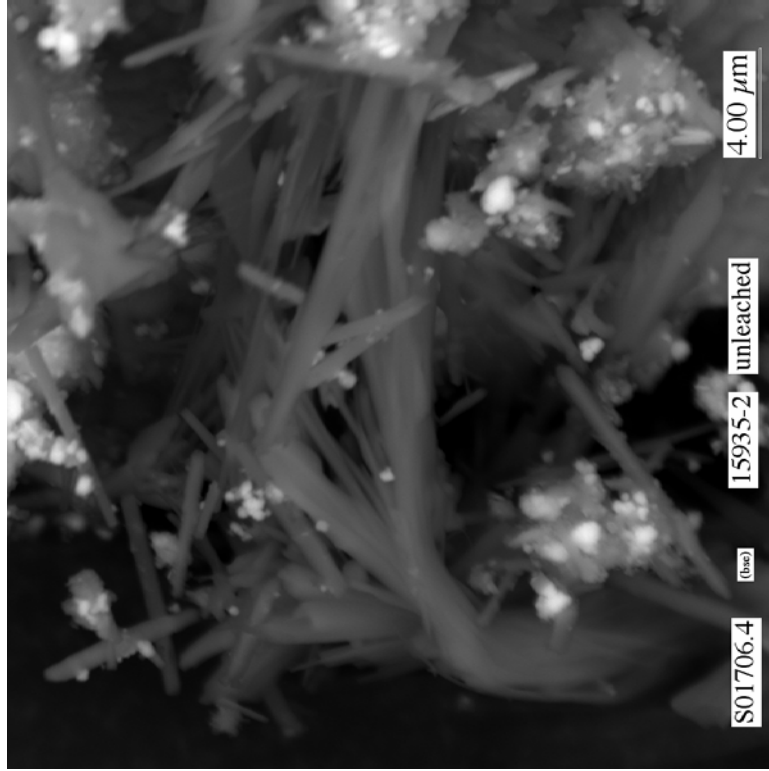


Figure 3-20. Micrograph showing at higher magnification the area indicated by the yellow-dotted square #1 in Figure 3-19 of subsample “unleached 15935-2”

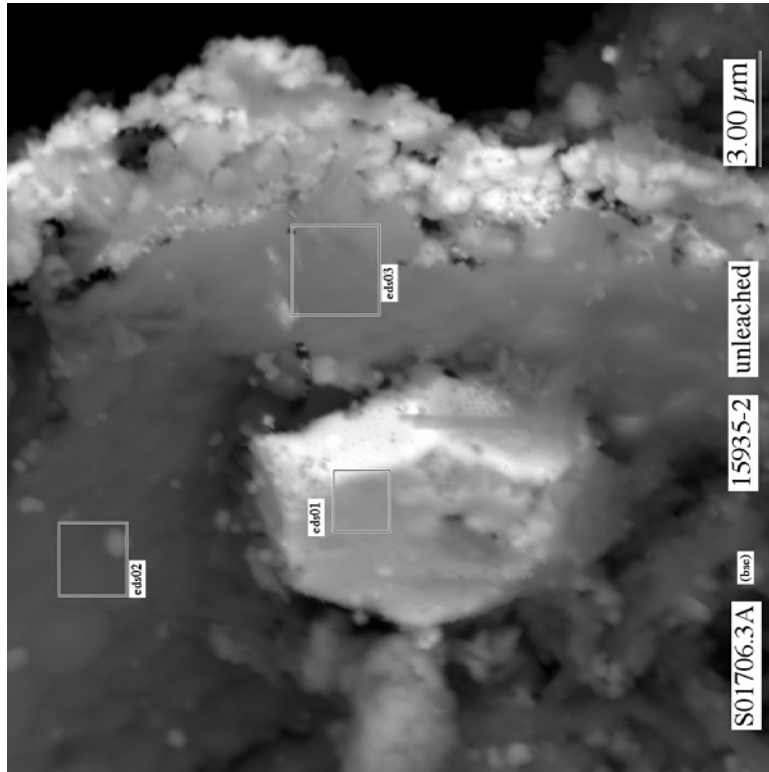


Figure 3-21. Micrograph showing at higher magnification the area indicated by the yellow-dotted square #2 in Figure 3-19 of subsample “unleached 15935-2”

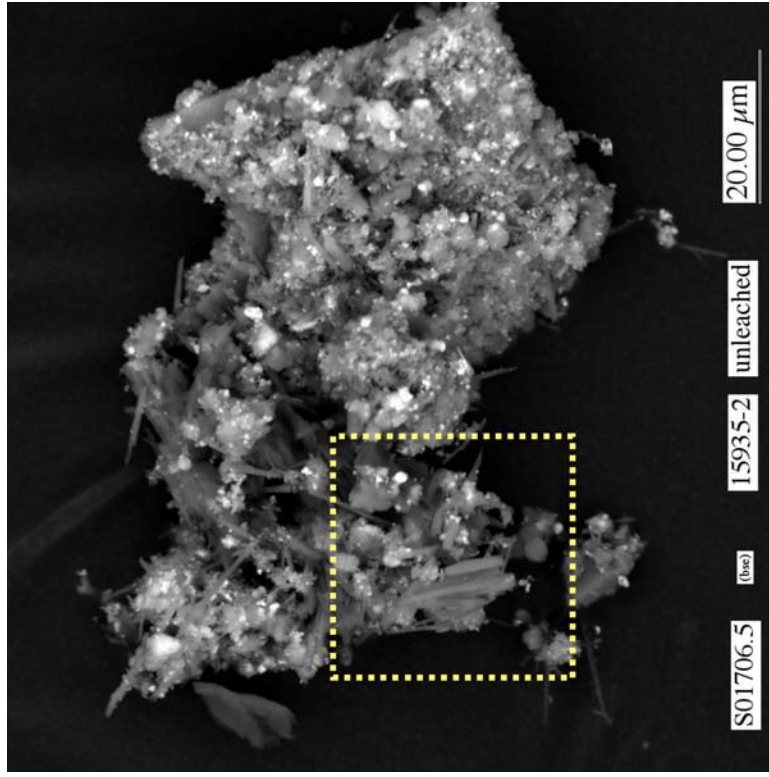


Figure 3-22. Micrograph showing typical large aggregate particle in subsample “unleached 15935-2”

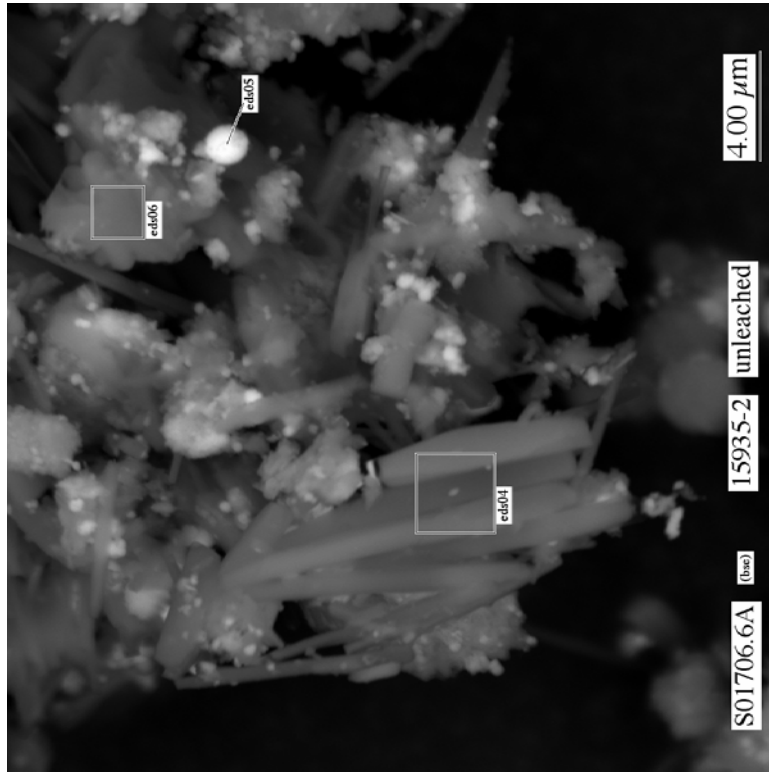


Figure 3-23. Micrograph showing at higher magnification the area indicated by the yellow-dotted square in Figure 3-22 of subsample “unleached 15935-2”

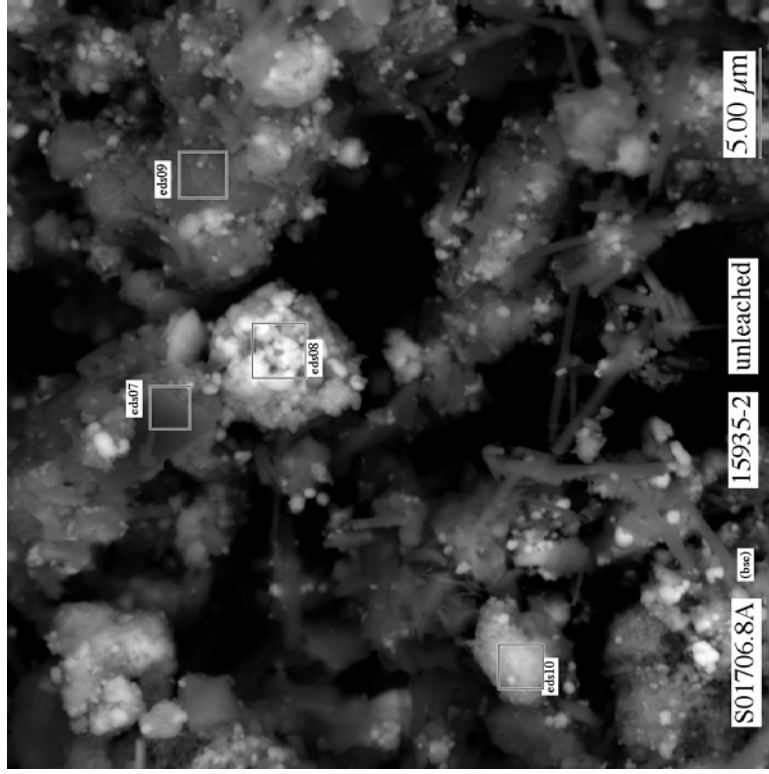


Figure 3-24. Micrograph showing range of particle types in subsample “unleached 15935-2”

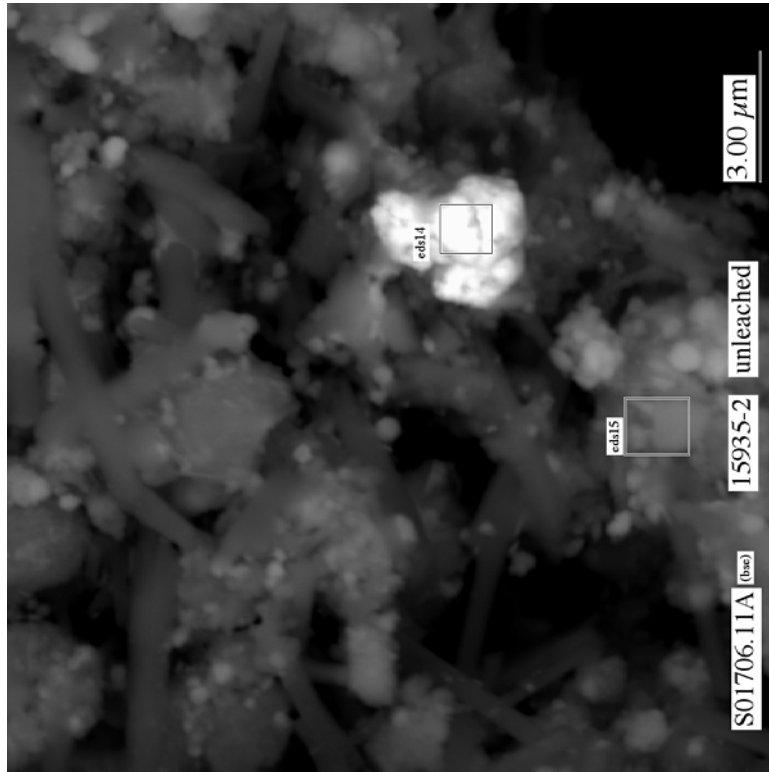


Figure 3-25. Micrograph showing typical silver-oxide and iron, sodium-oxide particles (eds14 and eds15, respectively) and range of particle types in subsample “unleached 15935-2”

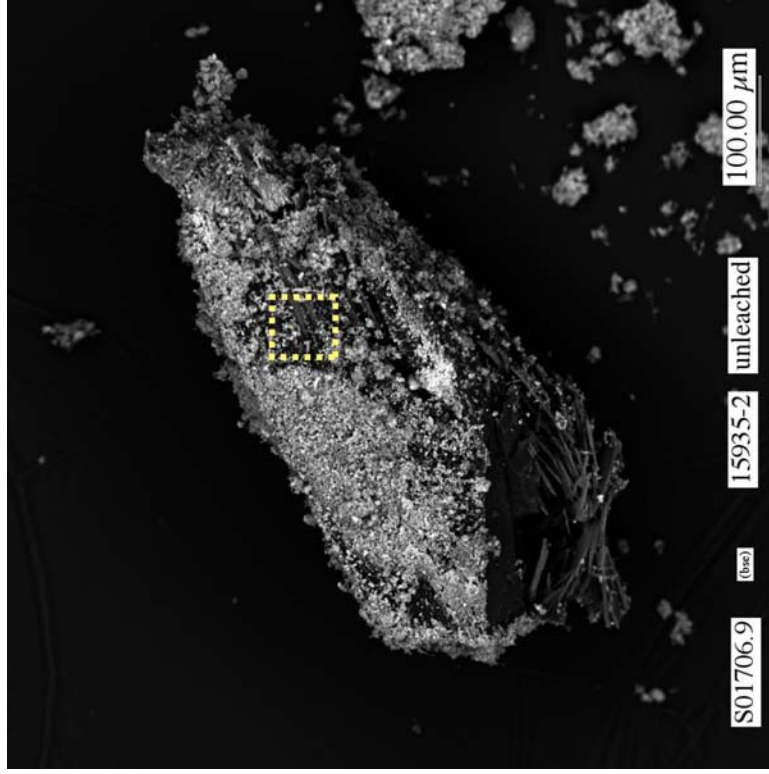


Figure 3-26. Micrograph showing large carbon-rich particle in subsample “unleached 15935-2”

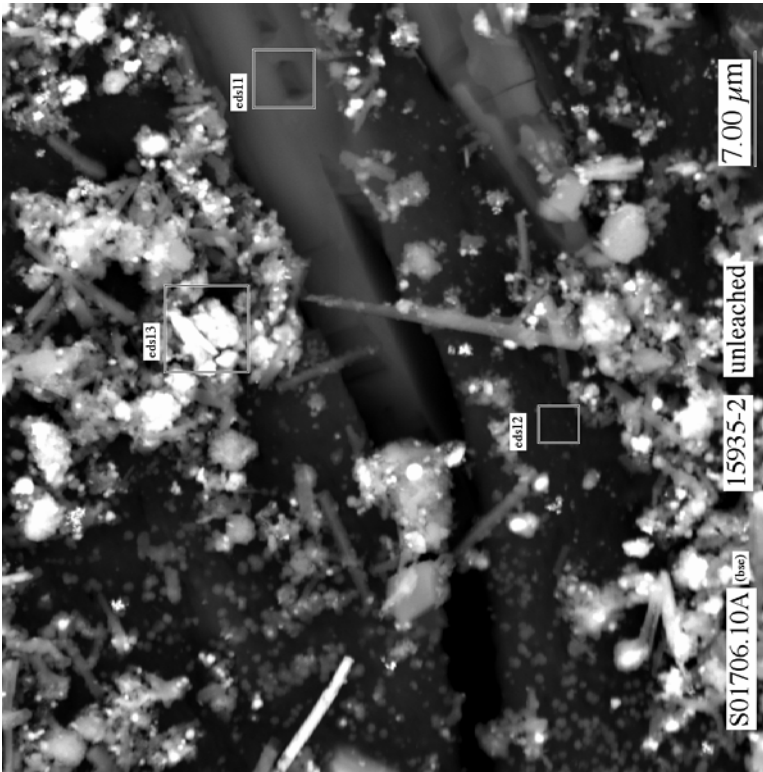


Figure 3-27. Micrograph showing at higher magnification the area indicated by the yellow-dotted square of the large carbon-rich particle in Figure 3-26 of subsample “unleached 15935-2”

Table 3-15. Qualitative compositions determined by SEM/EDS that include the emission peak for carbon for particles observed in unleached subsample 15935-2 of AY-102 tank sludge (jar 15935)

Figure and Spectrum Label	Major Metals (>5 wt%)	wt%													U
		C	O	Na	Al	Si	P	S	Ca	Cr	Mn	Fe	Ni	Ag	
Figure 3-21 eds01	Ag	17.5	29.1	2.1	3.8	0.5	0.2	0.1	0.2	0.0	0.6	2.1	0.3	40.2	3.5
Figure 3-21 eds02	Na-Si	28.9	49.7	6.8	2.5	5.6	1.1	0.0	0.4	0.1	1.0	3.5	0.2	0.3	-0.1
Figure 3-21 eds03	Ag	27.0	42.0	4.6	4.2	2.4	0.5	0.1	0.2	0.1	1.4	2.8	0.5	13.6	0.7
Figure 3-23 eds04	Na	26.7	49.7	20.2	0.9	0.3	0.1	0.0	0.1	0.0	0.5	1.5	0.1	0.1	-0.1
Figure 3-23 eds05	Fe-Na	18.2	23.3	8.7	1.2	0.3	0.4	0.2	0.1	0.3	3.2	43.2	0.7	0.0	0.1
Figure 3-23 eds06	Na	24.4	51.2	19.3	1.5	0.3	0.2	0.0	0.1	0.1	0.8	2.3	0.0	0.1	-0.1
Figure 3-24 eds07	Al-Na	15.1	54.0	11.7	12.2	0.4	0.4	0.1	0.1	0.1	1.4	4.1	0.3	0.1	0.0
Figure 3-24 eds08	Fe	12.5	39.6	3.5	1.6	0.3	0.6	0.3	0.1	0.2	2.7	38.0	0.5	0.1	0.0
Figure 3-24 eds09	Na-Fe-Al	25.0	44.5	9.4	5.8	4.9	0.9	0.2	0.1	0.1	2.1	6.6	0.2	0.1	0.1
Figure 3-24 eds10	Mn-Na-Fe	23.6	45.9	8.0	3.2	0.6	0.5	0.5	0.1	0.2	11.7	5.3	0.3	0.1	0.0
Figure 3-27 eds11	Na	7.1	54.1	24.7	4.1	0.8	0.4	-0.3	0.9	-1.0	1.0	2.3	0.5	2.8	2.8
Figure 3-27 eds12	Primarily C	59.2	29.6	7.5	1.4	0.1	0.9	0.2	0.1	0.2	-0.1	0.4	-0.1	0.3	0.3
Figure 3-27 eds13	Fe-Na	17.9	37.9	8.5	3.4	0.3	1.4	0.9	1.1	-0.2	4.9	20.3	1.3	1.1	1.0
Figure 3-25 eds14	Ag-Al	15.3	29.9	3.6	10.2	-0.1	0.2	0.1	0.0	0.1	1.0	2.5	0.2	36.8	0.3
Figure 3-25 eds15	Fe-Na	18.2	51.8	10.6	2.8	0.3	0.6	0.2	1.6	-0.4	3.1	10.7	0.3	0.3	-0.1

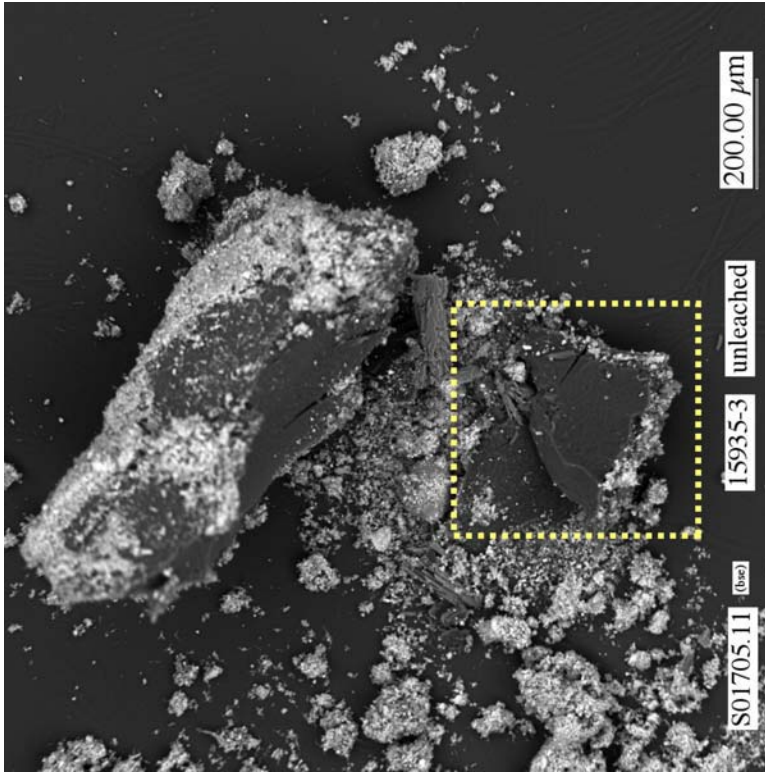


Figure 3-28. Low magnification scanning electron micrograph showing general morphology of large aggregate particles, including large carbon-rich particles (top center and lower center), in subsample “unleached 15935-3”

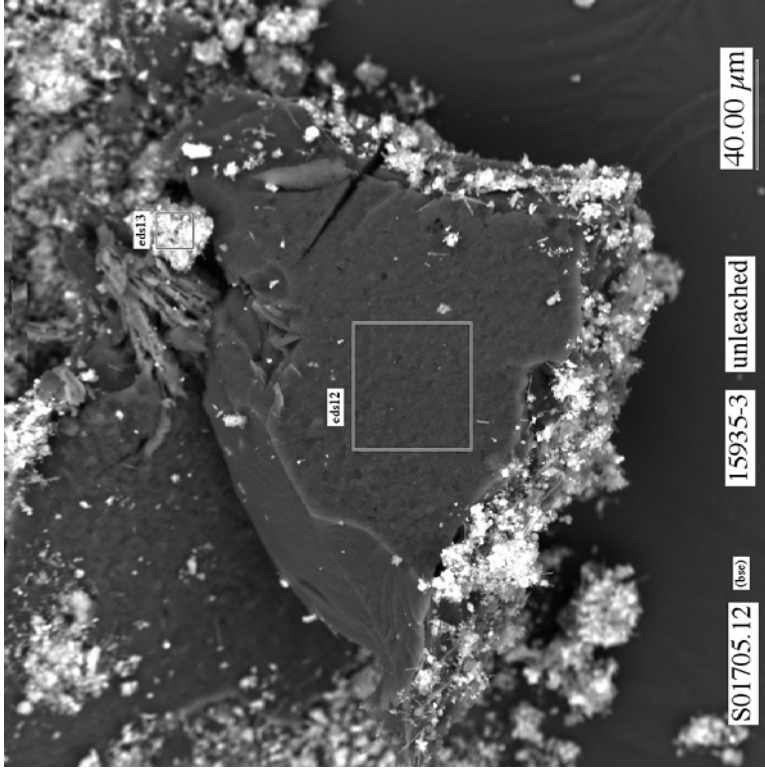


Figure 3-29. Micrograph showing at higher magnification the area indicated by the yellow-dotted square of the large carbon-rich particle in Figure 3-28 of subsample “unleached 15935-3”

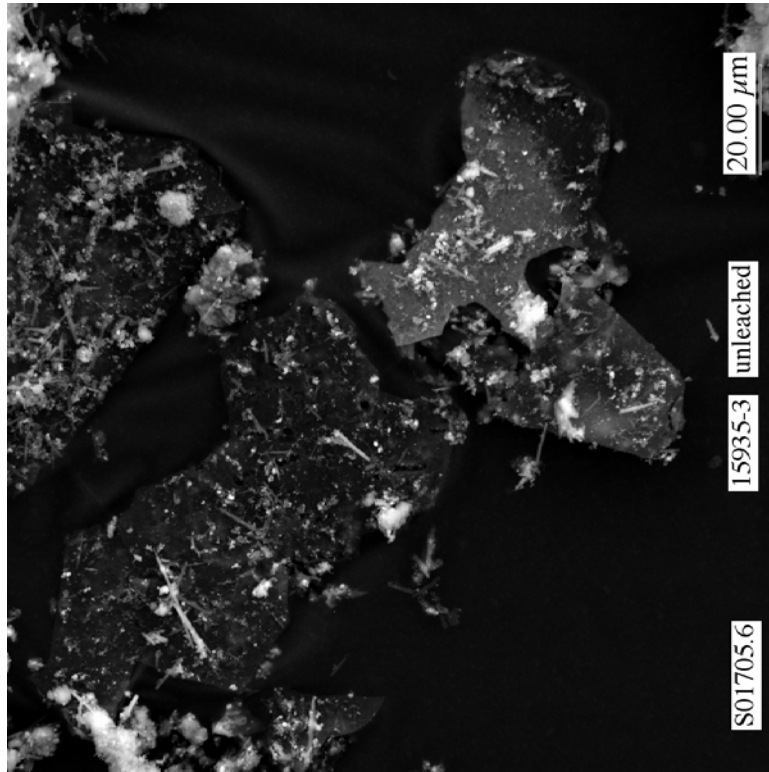


Figure 3-30. Secondary electron (se) micrograph showing crust-like fragments of sludge solid in subsample “unleached 15935-3”

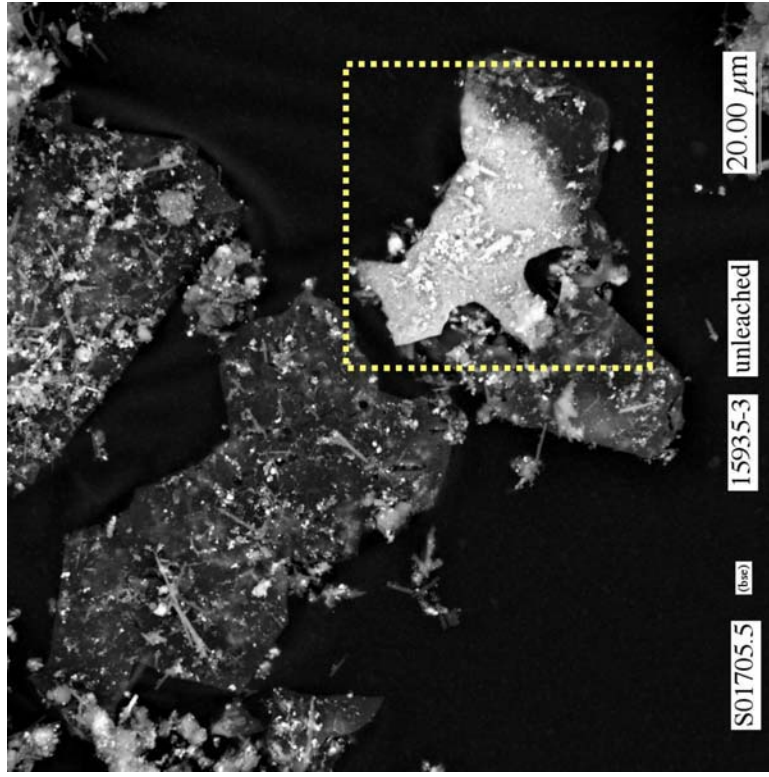


Figure 3-31. Backscatter (bse) electron micrograph showing area enriched in uranium (area marked by yellow-dotted square) in crust-like fragments of sludge solid in subsample “unleached 15935-3”

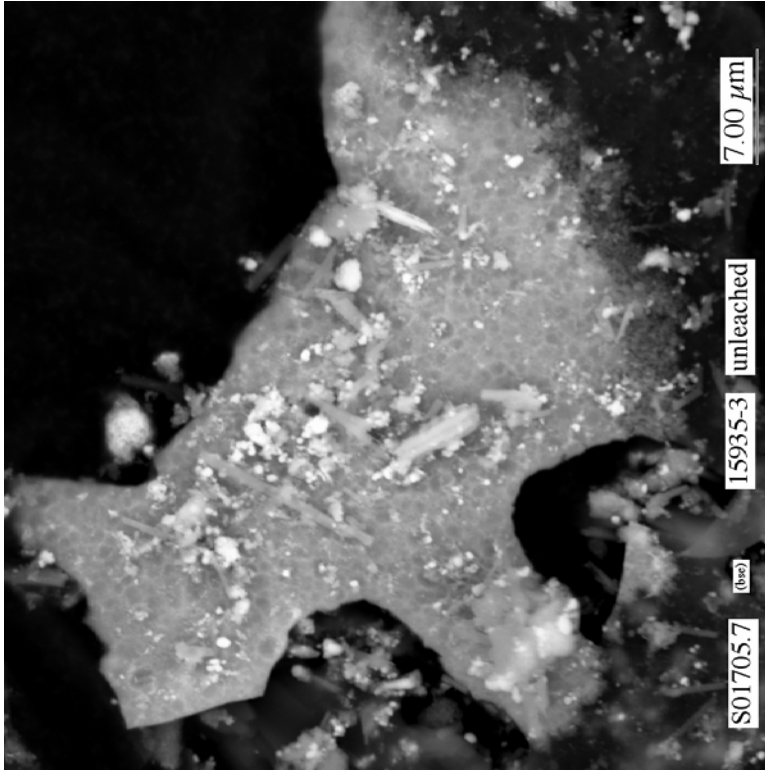


Figure 3-32. Electron micrograph showing at higher magnification area enriched in uranium (yellow-dotted square in Figure 3-31) in sludge solid in subsample “unleached 15935-3”

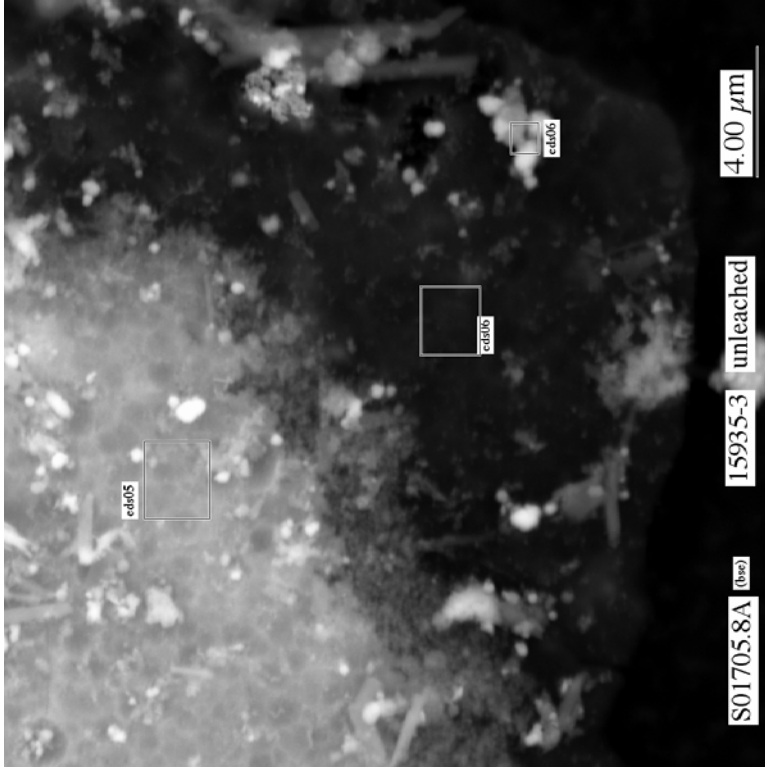


Figure 3-33. Electron micrograph showing at higher magnification section of crust-like fragment in bottom right corner of Figure 3-32 in subsample “unleached 15935-3.” (Section of crust enriched in uranium shows as bright area in upper left corner of this figure.)

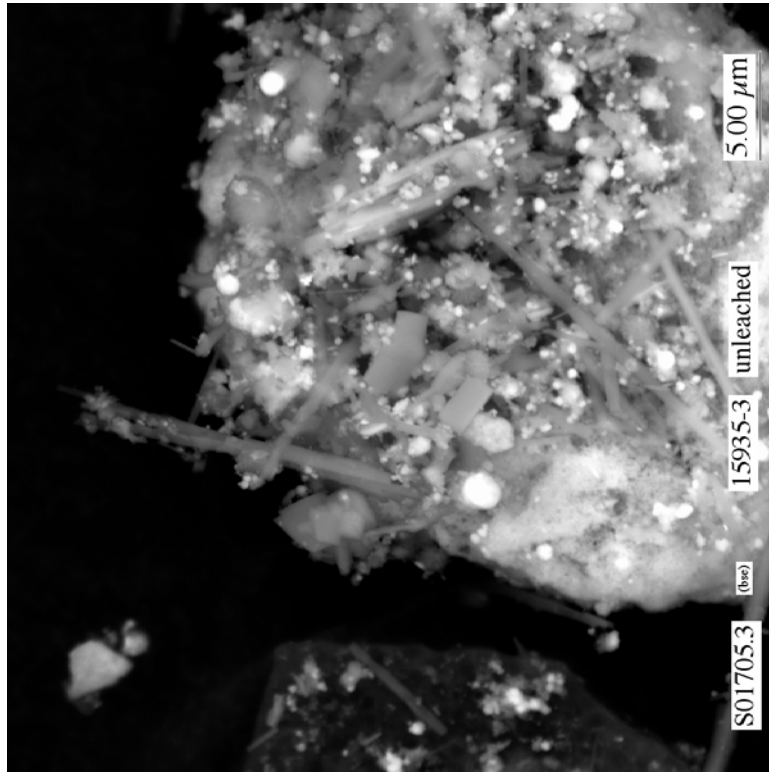


Figure 3-34. Micrograph showing range of typical particle aggregate and types of individual particles in subsample “unleached 15935-3”

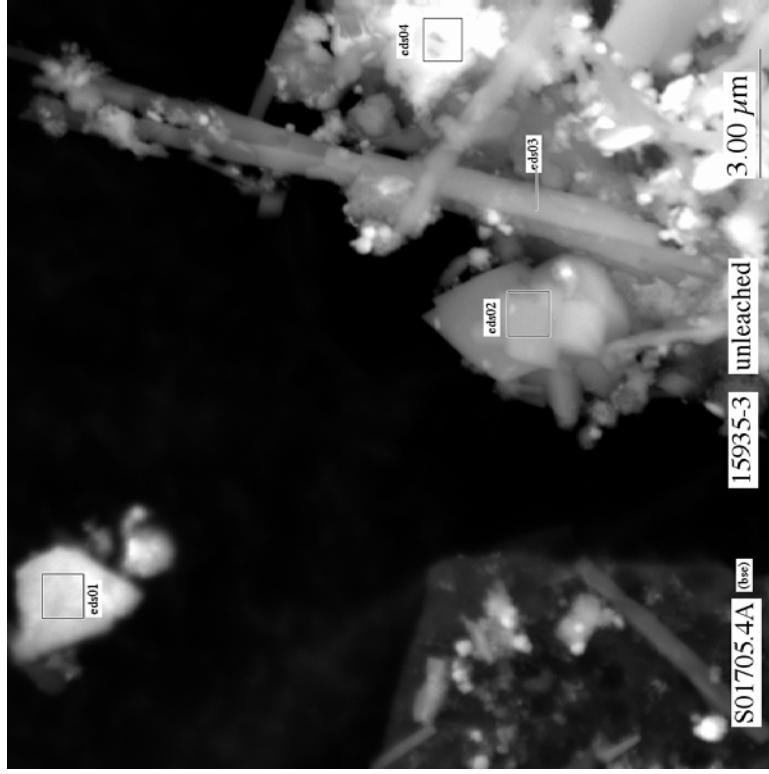


Figure 3-35. Micrograph showing at higher magnification lath- and prismatic-shaped particles on upper left edge of large particle aggregate in Figure 3-34 of subsample “unleached 15935-3”

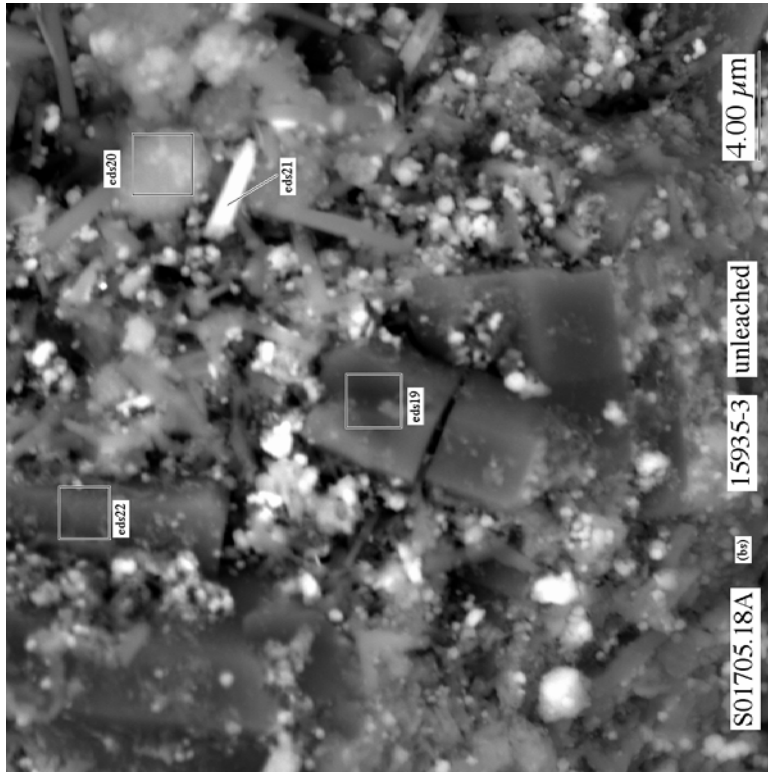


Figure 3-36. Micrograph showing range of particle types in subsample “unbleached 15935-3”

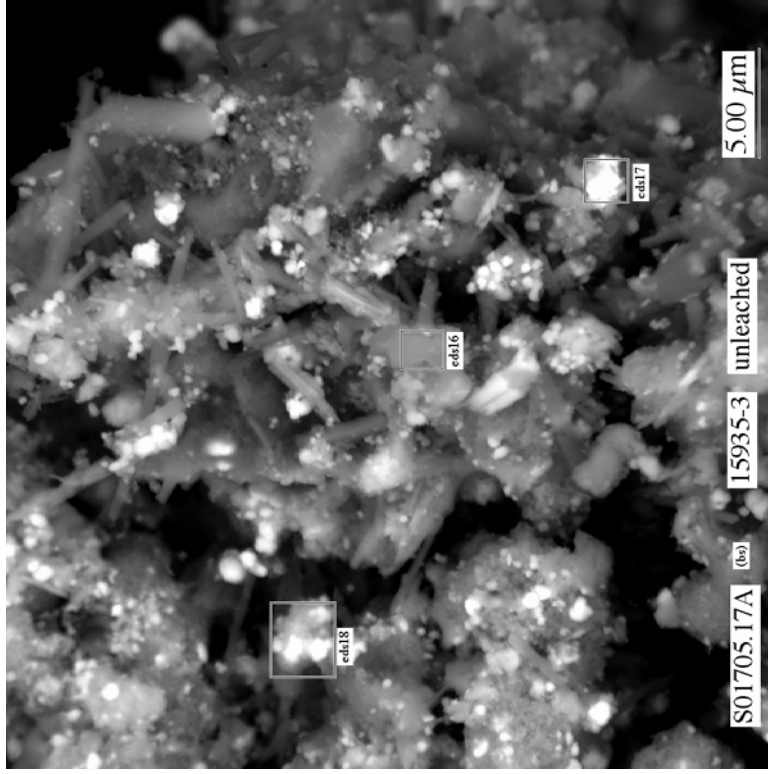


Figure 3-37. Micrograph showing range of particle types in subsample “unbleached 15935-3”

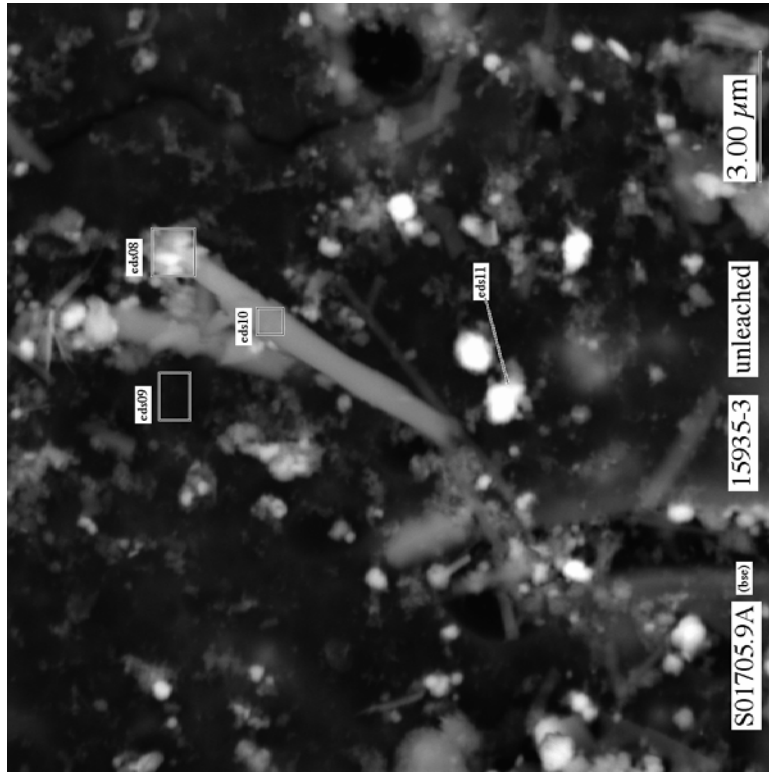


Figure 3-38. Micrograph showing range of particle types in subsample “unleached 15935-3”

Table 3-16. Qualitative compositions determined by SEM/EDS that include the emission peak for carbon for particles observed in unleached subsample 15935-3 of AY-102 tank sludge (jar 15935)

Figure and Spectrum Label	Major Metals (>5 wt%)	wt%														
		C	O	Na	Al	Si	P	S	Ca	Cr	Mn	Fe	Ni	Ag	U	
Figure 3-35 eds01	U	49.0	23.5	2.5	1.3	3.7	0.4	0.8	0.0	0.1	0.8	1.7	0.2	0.2	0.2	15.7
Figure 3-35 eds02	Al-Na-Fe	23.9	47.0	8.1	12.6	0.7	0.3	0.1	0.1	0.1	1.5	5.5	0.3	0.0	0.0	-0.1
Figure 3-35 eds03	Fe-Al-Na	27.4	34.7	6.2	6.8	0.7	0.4	0.1	0.1	0.6	3.4	19.0	0.4	0.1	0.1	0.0
Figure 3-35 eds04	Fe-Mn-Na	24.4	33.0	5.2	3.6	0.9	0.6	0.2	0.3	0.4	5.6	24.8	1.0	0.1	0.1	0.0
Figure 3-33 eds05	U-Na-Si	16.7	46.5	9.0	2.3	6.2	0.4	0.4	0.0	0.0	0.5	1.2	0.1	0.1	0.1	16.5
Figure 3-33 eds06	Si-Na	38.7	44.2	5.2	2.9	6.8	0.6	0.6	0.0	0.1	0.3	0.7	-0.1	-0.2	0.1	0.1
Figure 3-33 eds07	Fe	39.7	38.0	2.9	1.7	3.2	0.7	0.2	0.4	0.1	1.4	11.7	0.3	0.0	0.0	-0.2
Figure 3-38 eds08	Na-Fe	31.5	47.6	6.7	2.6	3.8	0.5	0.3	0.1	0.1	1.4	5.3	0.4	-0.1	-0.1	-0.1
Figure 3-38 eds09	Primarily C	46.6	42.0	3.4	1.8	5.4	0.4	0.5	0.0	0.0	0.1	0.2	0.0	-0.1	-0.1	-0.1
Figure 3-38 eds10	Na	29.0	49.7	8.5	3.9	3.4	0.7	0.3	0.1	0.1	1.5	2.8	0.2	0.0	0.0	0.0
Figure 3-38 eds11	Fe-Na	24.3	44.3	5.4	2.0	2.5	0.5	0.3	0.1	0.1	1.9	18.1	0.4	0.0	0.0	0.0
Figure 3-29 eds12	Primarily C	75.9	20.7	3.2	0.0	0.0	0.1	0.0	0.0	0.0	0.0	0.0	0.0	0.0	0.0	0.1
Figure 3-29 eds13	Fe-Na-Al	20.4	47.2	8.6	5.6	2.1	1.1	0.2	0.3	0.2	3.6	10.4	0.4	0.0	0.0	0.1
Fig. not shown eds14	Na-Fe	24.0	48.9	8.0	4.7	2.1	0.9	0.1	0.1	0.2	2.3	8.1	0.4	0.1	0.0	0.0
Fig. not shown eds15	U-Na-Fe	14.4	47.3	10.3	1.8	0.9	1.1	0.1	0.1	0.1	2.0	7.7	0.4	0.0	0.0	13.7
Figure 3-37 eds16	Fe-Na-Al	19.8	50.1	8.8	6.0	0.5	0.8	0.1	0.2	0.1	3.0	9.9	0.5	0.0	0.1	0.1
Figure 3-37 eds17	Ag-Na-Fe	19.1	46.9	6.9	4.9	0.3	0.6	0.1	0.1	0.1	2.4	5.6	0.3	13.0	-0.2	-0.2
Figure 3-37 eds18	Fe-Na-Mn	13.5	37.3	7.8	3.5	1.4	0.9	0.2	0.4	0.3	6.9	26.0	1.7	-0.1	0.0	0.0
Figure 3-36 eds19	Al	8.3	64.9	1.4	23.9	0.1	0.2	0.0	0.0	0.0	0.4	0.8	0.1	0.0	0.0	-0.1
Figure 3-36 eds20	Na-Al	20.0	51.0	11.0	6.2	4.8	0.5	0.2	0.1	0.1	1.3	4.7	0.2	0.0	0.0	0.0
Figure 3-36 eds21	Na-Fe	19.1	53.3	10.8	4.6	1.5	0.5	0.2	1.7	-0.5	1.6	6.5	0.4	0.3	0.2	0.2
Figure 3-36 eds22	Al	9.3	63.8	1.7	22.6	0.2	0.3	0.0	0.1	0.0	0.5	1.5	0.1	0.0	0.0	-0.1

3.3.2 Water-Leached AY-102 Sludge

Two subsamples (i.e., two SEM mounts) of water-leached AY-102 (jar 15935) sludge were inspected by SEM/EDS. The two subsamples were designated “leached 15935-1” and “leached 15935-2.” Table 3-17 summarizes the number of micrographs and EDS spectra recorded in this study for the two subsamples of water-leached AY-102 (jar 15935) sludge, and identifies the specific figures, tables, and appendix containing the relevant results for these subsamples.

The two mounts of water-leached AY-102 (jar 15935) sludge contained a similar variety of fine (micrometer to submicrometer in size) particle types. The following four differences are readily obvious in the SEM/EDS results for water-leached AY-102 (jar 15935) sludge samples relative to those for the unleached material (Section 3.3.1):

- The micrographs for particles in the water-leached AY-102 (jar 15935) sludge all appear “blurred” (indistinct) (e.g., Figure 3-40 and Figure 3-45) when compared to the SEM micrographs for the unleached AY-102 (jar 15935) sludge sample. Because all of the SEM mounts were prepared using the same procedure and mounting materials, this “blurred” effect is assumed to be due to the rounding of particle edges caused by dissolution during the water-leach treatment of this sludge and not an artifact of the SEM imaging or preparation of the SEM mount.
- Based on the EDS analyses (Table 3-18 and Table 3-19), there is a significant decrease in the sodium content of the water-leached AY-102 (jar 15935) sludge. This indicates that the sodium-containing solids in the unleached sludge might be more soluble during the water leach relative to the other solid phases present in this material.
- The majority of the particles in the water-leached AY-102 (jar 15935) sludge appear to contain iron with lesser amounts of manganese and/or aluminum.

Table 3-17. Summary of SEM/EDS data recorded in this study and listed in this report for the two subsamples of water-leached AY-102 (jar 15935) sludge

	Subsample Identification	
	Leached 15935-1	Leached 15935-2
Number of recorded micrographs	18	5
Number of recorded EDS spectra	18	8
Figures of SEM micrographs showing typical particle morphologies and types	Figure 3-39 to Figure 3-46	Figure 3-47 to Figure 3-51
Tables of calculated EDS compositions (with carbon)	Table 3-18	Table 3-19
Appendix containing tables of calculated EDS compositions (without carbon) and figures of EDS spectra	Appendix C	

The range of carbon content measured by EDS for particles from the water-leached AY-102 (jar 15935) sludge sample is 5 to 20 wt% (Table 3-18 and Table 3-19), which is lower than the 5 to 40 wt% (Table 3-14 to Table 3-16) determined for the carbon content of non-carbon rich particles in the unleached sludge sample.

The particles observed in the two subsamples of water-leached AY-102 (jar 15935) sludge were typically a few micrometers to submicrometer in size (See Figure 3-40, Figure 3-43, and Figure 3-49). The particles consisted of both discrete particles and aggregates of particles. A few larger, crusty-like sludge particles similar to those in the subsamples of unleached AY-102 sludge were also observed in the water leached subsamples (Figure 3-39, Figure 3-45, and Figure 3-51). Almost all of the particles imaged by SEM in the two subsamples of water-leached AY-102 sludge had indistinct surface features and morphologies, which is likely due to the water-leach treatment. The water-leached AY-102 (jar 15935) sludge sample contained a few lath- (or rod-) shaped crystals (Figure 3-41 [eds15], Figure 3-48, and Figure 3-49), which were similar to, but less common than, those observed by SEM in unleached samples. The subsamples of water-leached sludge also contained botryoidal aggregates of iron-rich particles (Figure 3-41 [eds16], Figure 3-44 [eds12], and Figure 3-48 [eds02]), and silver-containing particles (Figure 3-49 [eds04]). Based on both the SEM micrographs and the EDS analyses, the iron-rich particles appear to be one of the most abundant phases in the water-leached AY-102 (jar 15935) sludge. Although rare, a few particles containing calcium, iron, and phosphorus were identified by SEM/EDS (Figure 3-43 [eds08, eds09, and eds10]), but this type of particle was impossible to distinguish based on morphology by SEM from the iron-rich particles that contained little or no calcium or phosphorus. None of the particles of “leached 15935-1” and “leached 15935-2” examined by SEM/EDS contained any significant concentrations (i.e., >1 wt%) of uranium (see Table 3-18 and Table 3-19).

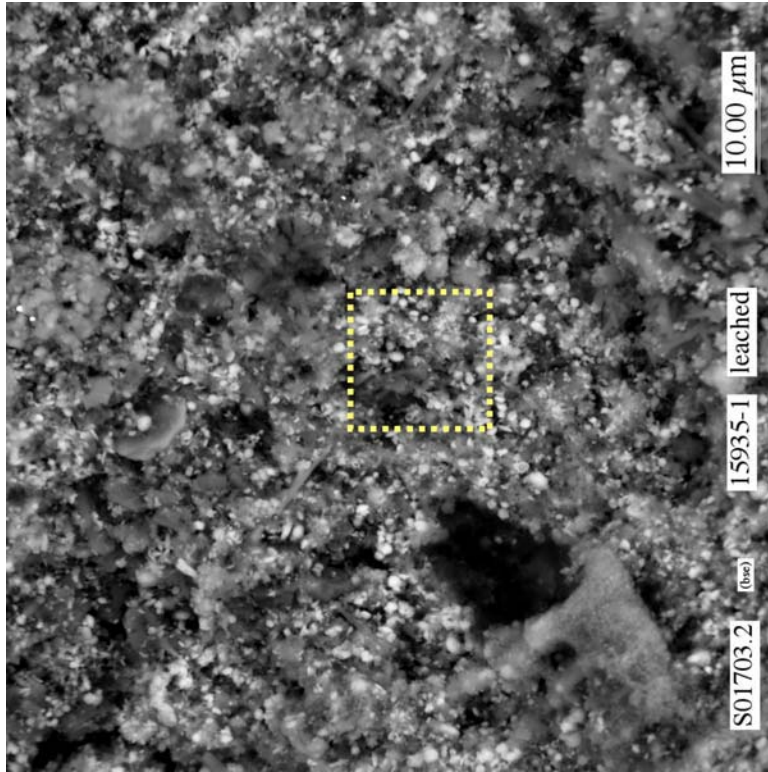


Figure 3-39. Low magnification scanning electron micrograph showing general morphology of particles in subsample “leached 15935-1”

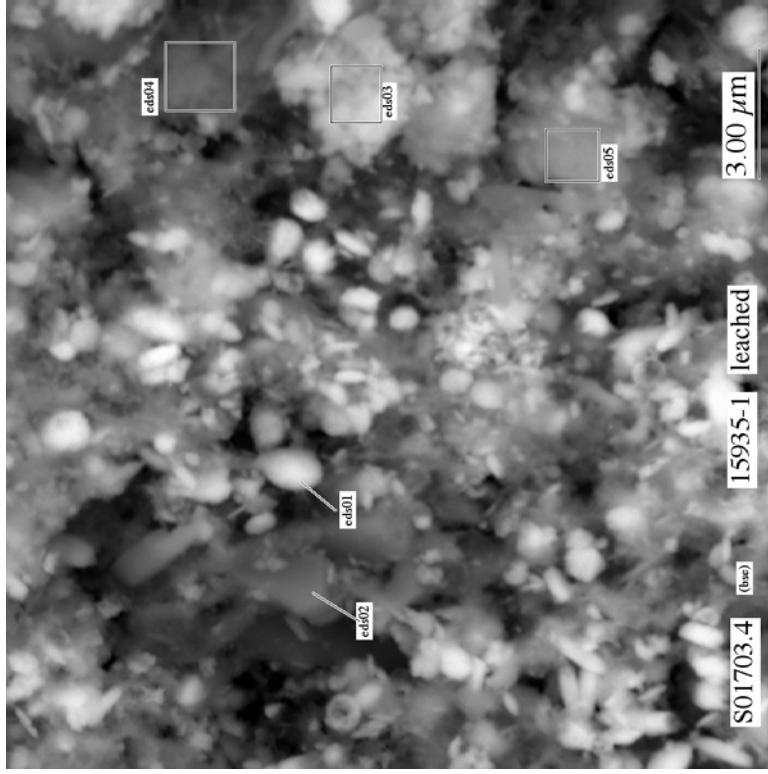


Figure 3-40. Micrograph showing at higher magnification the area indicated by the yellow-dotted square in Figure 3-39 of subsample “leached 15935-1”

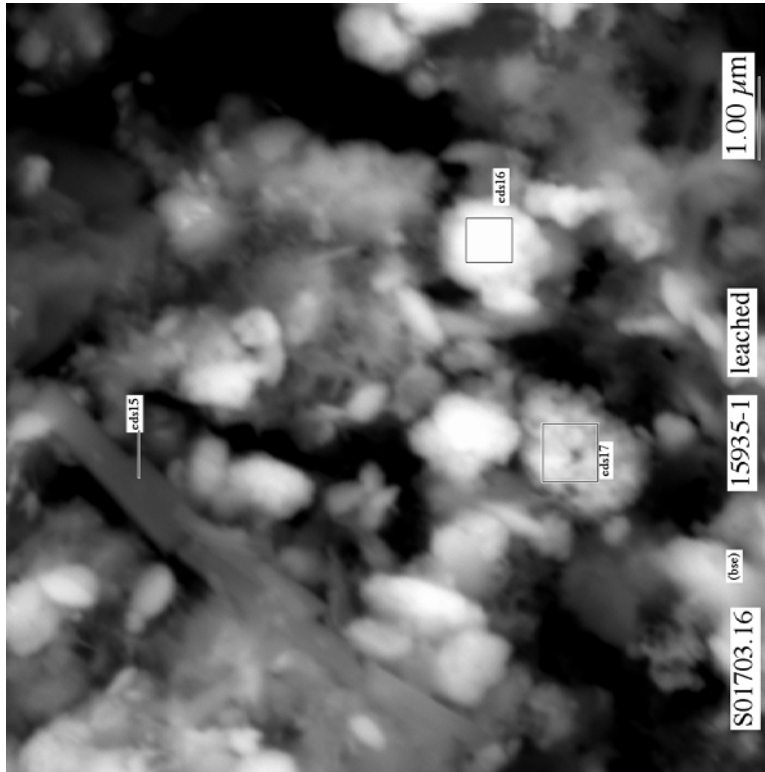


Figure 3-41. Micrograph showing range of typical particle types in subsample “leached 15935-1”

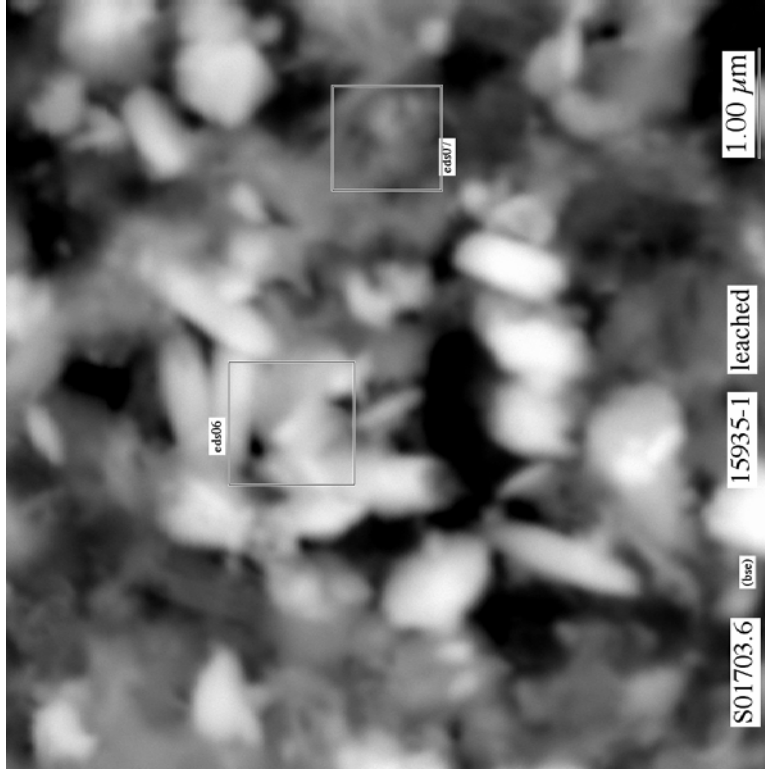


Figure 3-42. Micrograph showing range of typical particle types in subsample “leached 15935-1”

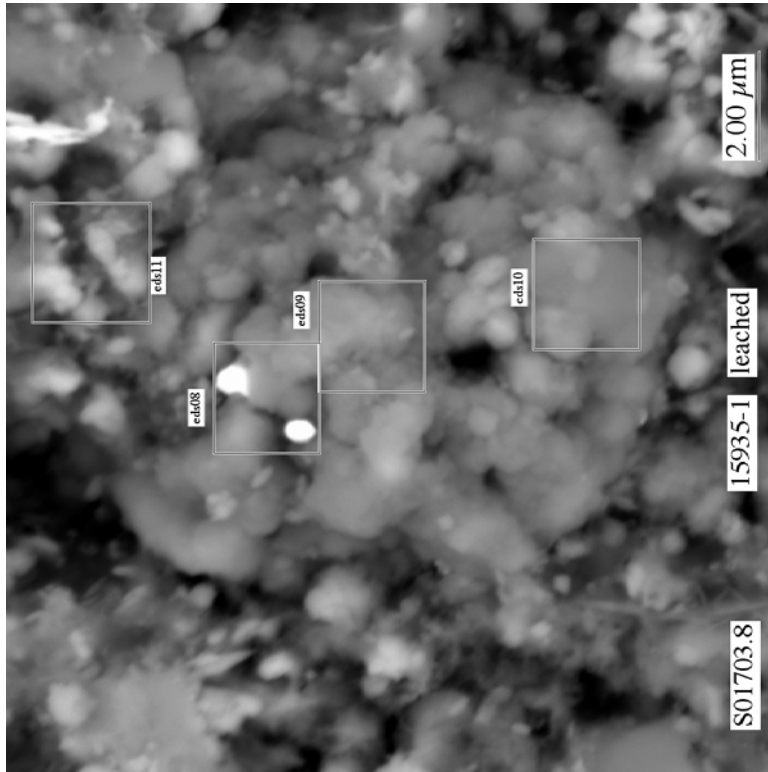


Figure 3-43. Micrograph showing range of typical particle types in subsample “leached 15935-1”

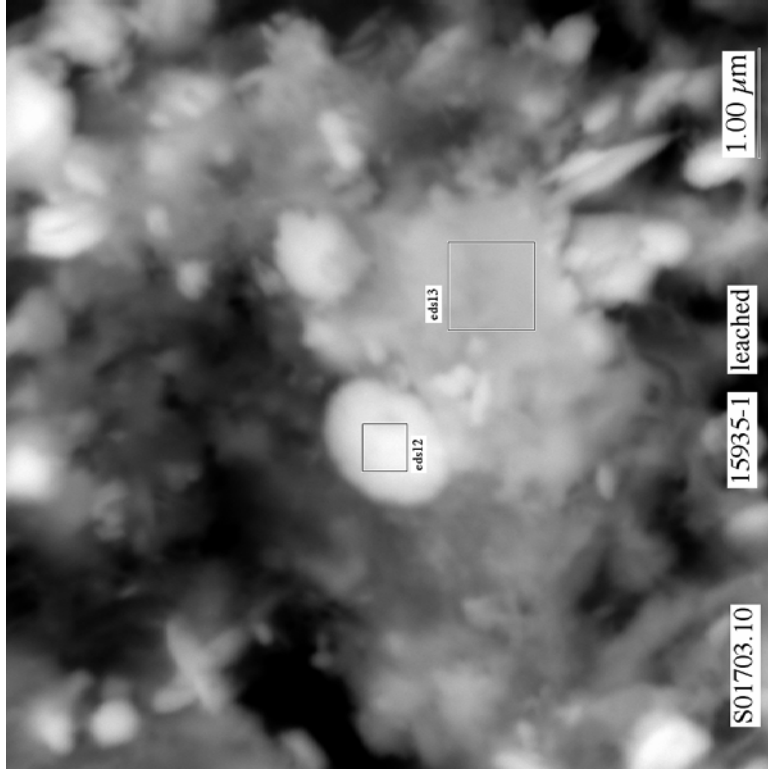


Figure 3-44. Micrograph showing range of typical particle types in subsample “leached 15935-1”

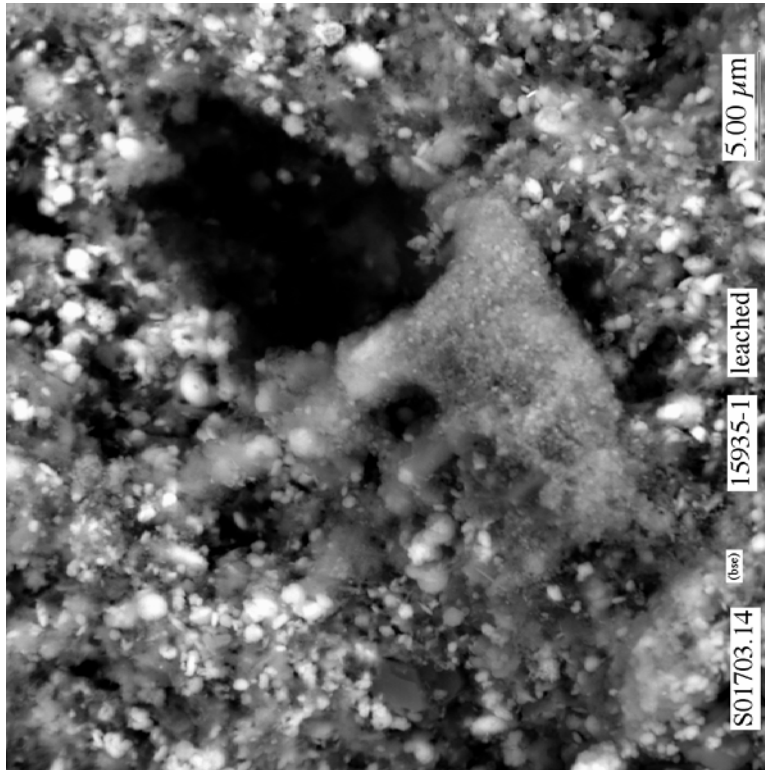


Figure 3-45. Micrograph showing range of typical particle types and crust-like aggregate in subsample “leached 15935-1”

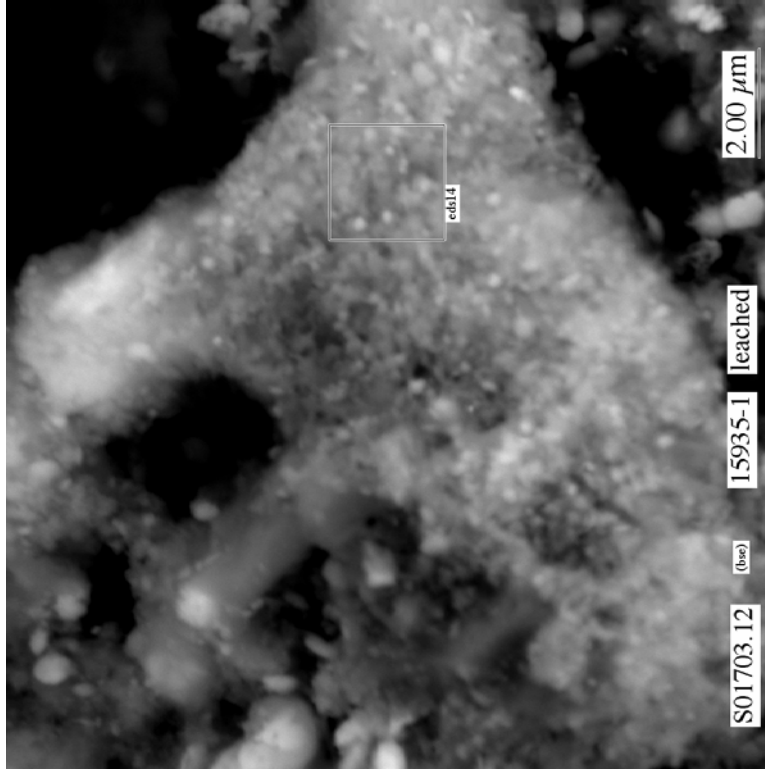


Figure 3-46. Micrograph showing at higher magnification crust-like particle aggregate in center of Figure 3-45 of subsample “leached 15935-1”

Table 3-18. Qualitative compositions determined by SEM/EDS that include the emission peak for carbon for particles observed in leached subsample 15935-1 of AY-102 tank sludge (jar 15935)

Figure and Spectrum Label	Major Metals (>5 wt%)	wt%													
		C	O	Na	Al	Si	P	S	Ca	Cr	Mn	Fe	Ni	Ag	U
Figure 3-40 eds01	Fe-Al	16.0	28.9	0.9	6.0	1.1	1.1	0.1	0.5	0.5	2.0	41.9	0.7	0.2	0.2
Figure 3-40 eds02	Al-Fe	16.1	51.0	0.5	21.3	0.8	0.4	0.1	0.4	0.5	1.0	7.6	0.3	0.2	-0.1
Figure 3-40 eds03	Fe-Mn	15.6	34.1	1.8	4.3	1.4	0.8	0.1	0.8	0.5	5.9	33.0	1.2	0.2	0.4
Figure 3-40 eds04	Fe-Mn	5.5	9.5	0.7	2.6	1.8	0.7	0.0	2.8	1.8	5.6	67.2	1.8	0.0	0.1
Figure 3-40 eds05	Fe-Al	14.6	34.0	1.2	8.4	2.6	1.2	0.1	1.5	4.4	2.7	28.5	0.7	0.0	0.2
Figure 3-42 eds06	Fe	17.5	39.4	0.9	4.2	1.8	3.7	0.1	2.7	0.1	1.7	26.2	1.2	0.1	0.2
Figure 3-42 eds07	Fe-Al	11.3	33.1	1.1	5.9	2.9	2.0	0.1	3.1	1.4	3.3	34.0	1.4	0.1	0.4
Figure 3-43 eds08	Ca-Ag-P-Fe	14.4	46.8	1.9	1.1	0.4	6.9	0.1	14.0	0.1	0.4	5.2	0.3	7.5	0.8
Figure 3-43 eds09	Ca-P-Fe	15.0	47.6	2.2	1.2	0.4	8.1	0.2	15.7	0.1	0.4	5.9	0.4	2.0	1.0
Figure 3-43 eds10	Ca-Fe-P	14.7	48.8	4.5	3.6	2.6	5.3	0.1	10.4	0.1	0.6	8.3	0.3	0.2	0.5
Figure 3-43 eds11	Fe-Ca	13.5	38.3	1.1	4.7	2.0	3.1	0.0	6.4	0.9	2.2	26.4	0.9	0.2	0.5
Figure 3-44 eds12	Fe-Al	17.3	43.9	0.7	6.5	1.8	1.1	0.1	0.9	2.1	1.4	23.5	0.6	0.1	0.2
Figure 3-44 eds13	Fe-Al	17.2	47.3	0.7	9.4	2.6	1.3	0.0	1.4	3.5	1.9	13.8	0.5	0.1	0.2
Figure 3-46 eds14	Fe-Si	17.4	52.0	3.2	4.8	5.1	0.8	0.1	1.3	0.3	3.6	10.7	0.5	0.2	0.1
Figure 3-41 eds15	Fe-Al	15.9	37.2	1.4	8.7	1.2	1.0	0.1	1.4	0.8	3.3	27.9	0.9	0.2	0.1
Figure 3-41 eds16	Fe	15.5	45.8	1.0	4.2	1.3	1.1	0.1	1.2	0.3	1.1	27.2	0.8	0.3	0.2
Figure 3-41 eds17	Fe	14.9	33.9	0.8	4.2	1.6	1.0	0.1	0.8	0.6	1.8	39.2	0.7	0.2	0.2
Fig. not shown eds18	Fe-Al	20.7	47.8	0.7	9.6	2.6	1.1	0.1	1.4	3.4	1.3	10.9	0.4	0.1	0.1

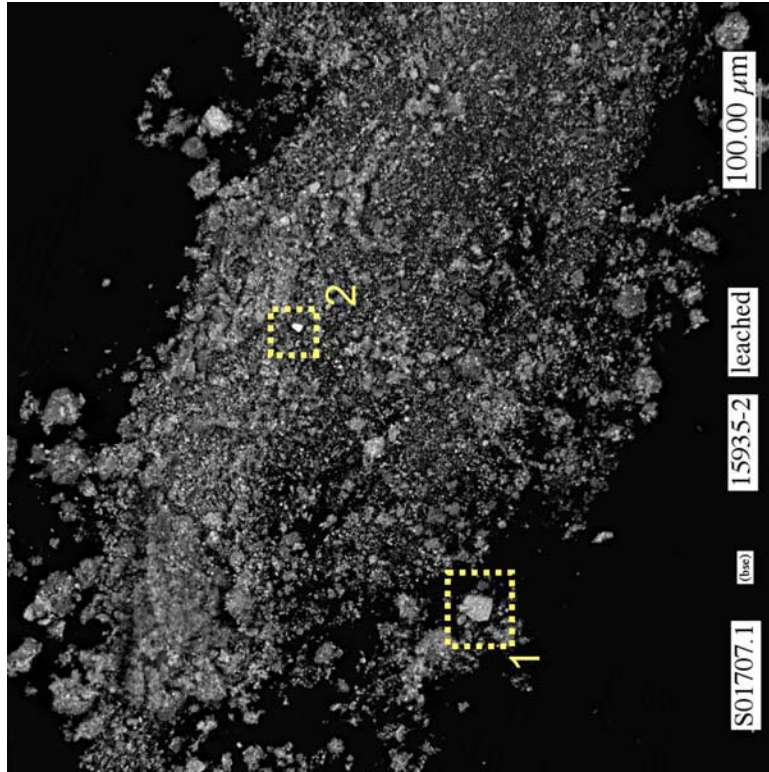


Figure 3-47. Low magnification scanning electron micrograph showing general morphology of particles in subsample “leached 15935-2”

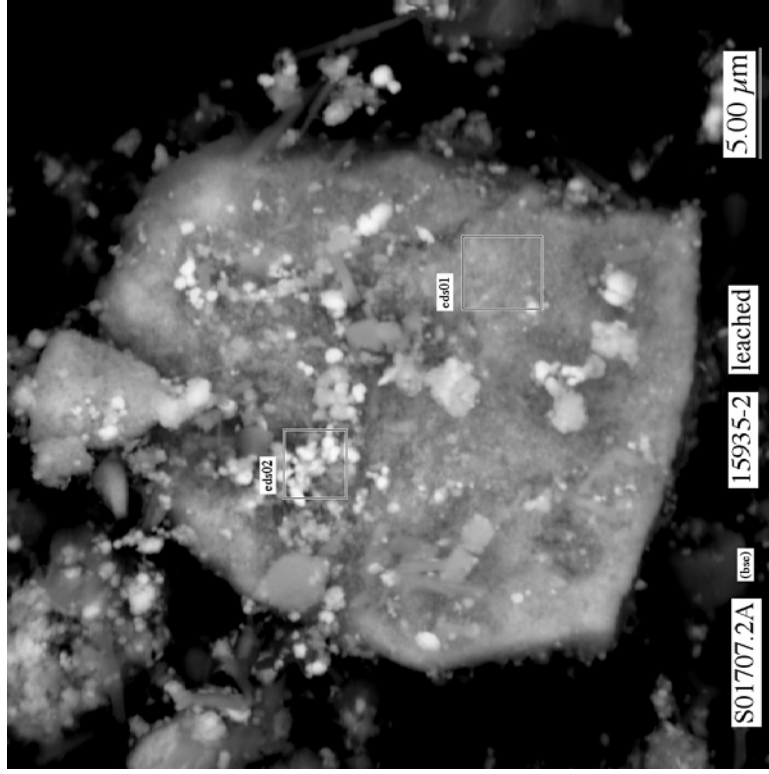


Figure 3-48. Micrograph showing at higher magnification the crust-like particle aggregate (area indicated by the yellow-dotted square #1) in Figure 3-47 of subsample “leached 15935-2”

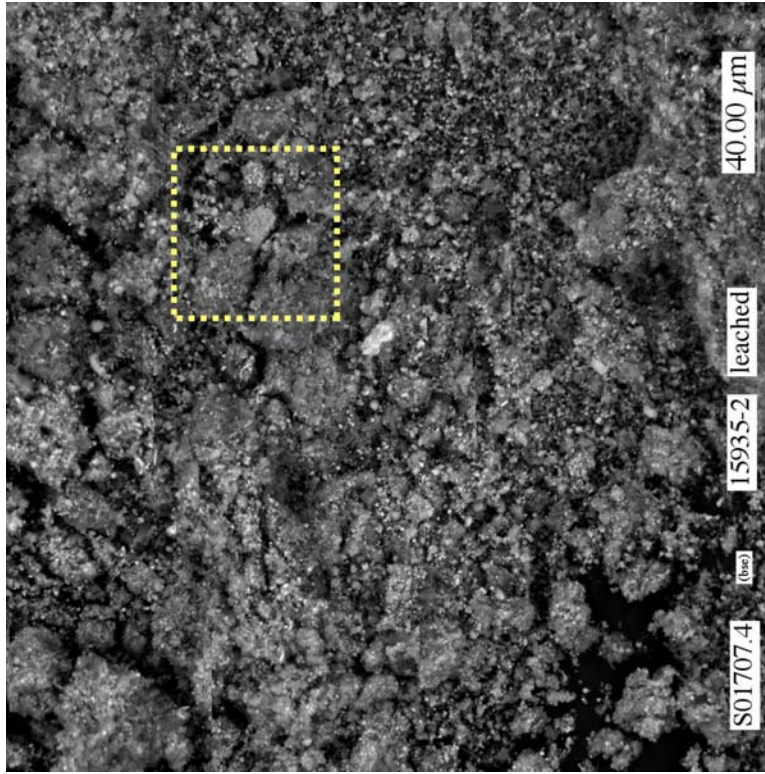


Figure 3-50. Low magnification scanning electron micrograph showing general morphology of particle aggregates in subsample “leached 15935-2”

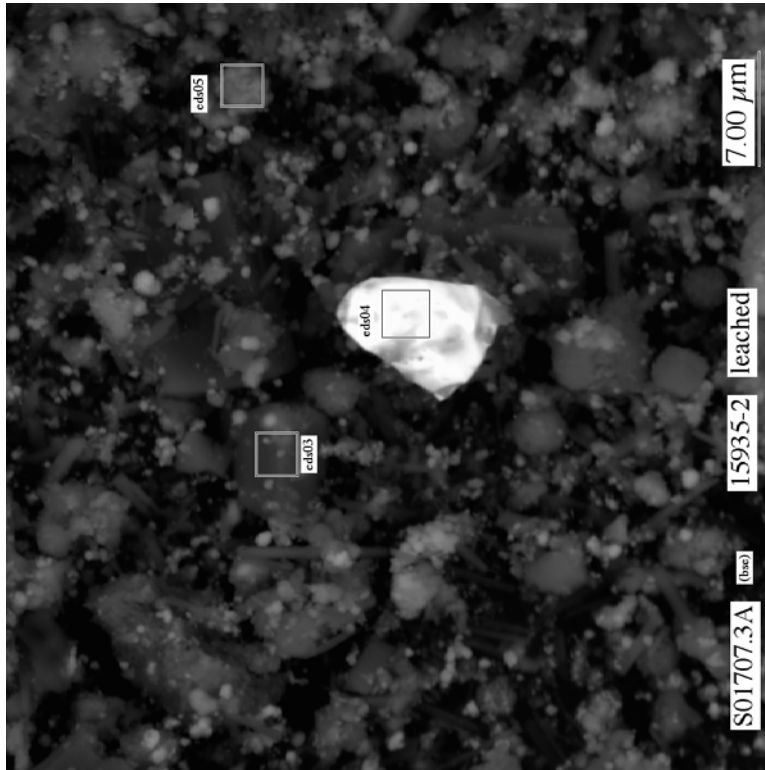


Figure 3-49. Micrograph showing at higher magnification particles in area indicated by the yellow-dotted square #2 in Figure 3-47 of subsample “leached 15935-2”

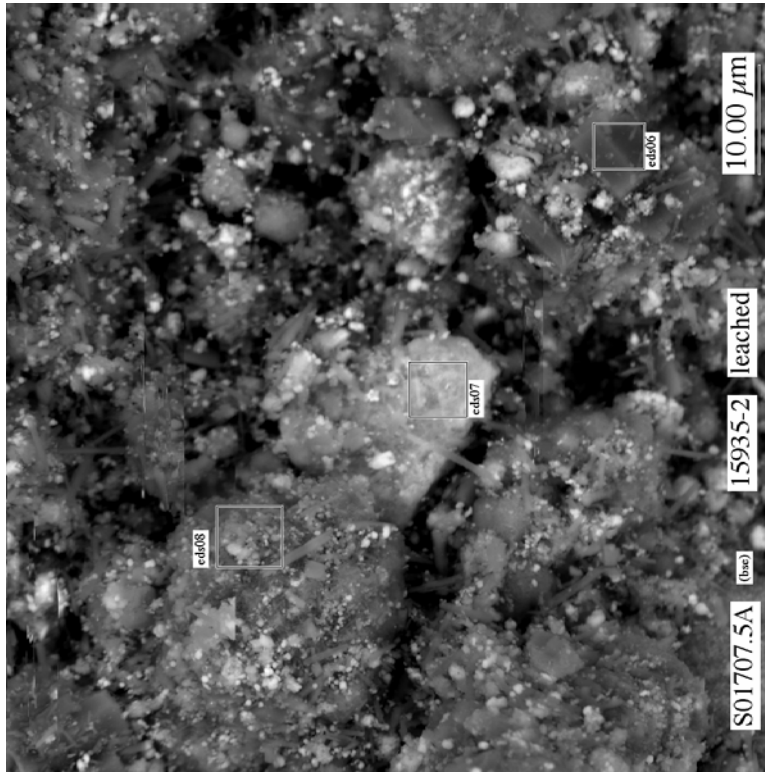


Figure 3-51. Micrograph showing at higher magnification particles in area indicated by the yellow-dotted square in Figure 3-50 of subsample “leached 15935-2”

Table 3-19. Qualitative compositions determined by SEM/EDS that include the emission peak for carbon for particles observed in leached subsample 15935-2 of AY-102 tank sludge (jar 15935)

Figure and Spectrum Label	Major Metals (>5 wt%)	----- wt% -----													
		C	O	Na	Al	Si	P	S	Ca	Cr	Mn	Fe	Ni	Ag	U
Figure 3-48 eds01	Fe-Mn	10.1	41.9	0.8	4.2	2.0	0.5	0.1	0.4	0.6	11.1	26.8	1.6	0.1	0.0
Figure 3-48 eds02	Fe-Mn	10.5	39.3	1.6	4.1	2.0	0.6	0.2	0.5	0.6	11.4	27.9	1.4	0.1	-0.1
Figure 3-49 eds03	Al-Na-Fe	12.3	53.6	9.7	11.8	0.3	0.2	0.0	0.2	0.1	1.8	8.3	1.2	0.5	0.1
Figure 3-49 eds04	Ag	15.6	25.9	0.9	1.1	0.3	0.0	0.5	0.4	0.1	0.5	2.0	0.4	51.0	1.3
Figure 3-49 eds05	Fe-Mn	0.4	5.4	0.5	2.0	0.6	0.3	0.1	0.5	1.4	38.5	46.3	3.5	0.5	-0.1
Figure 3-51 eds06	Al	6.4	66.7	1.0	23.7	0.2	0.2	0.0	0.1	0.0	0.4	1.2	0.1	0.1	-0.1
Figure 3-51 eds07	Fe-Mn	5.0	43.8	1.7	4.7	1.2	0.6	0.2	0.3	1.4	5.4	34.0	1.3	0.2	0.2
Figure 3-51 eds08	Al-Na-Si-Fe	7.0	53.4	9.9	10.3	9.0	0.3	0.3	0.5	0.1	2.0	5.6	0.3	1.4	0.1

3.3.3 Unleached BX-101 Sludge

Two subsamples (i.e., two SEM mounts) of unleached BX-101 (jar 16503) sludge were inspected by SEM/EDS. The two subsamples were designated “unleached 16503-1” and “unleached 16503-2.” Table 3-20 summarizes the number of micrographs and EDS spectra recorded in this study for the two subsamples of unleached BX-101 (jar 16503) sludge, and identifies the specific figures, tables, and appendix containing the relevant results for these subsamples.

Table 3-20. Summary of SEM/EDS data recorded in this study and listed in this report for the two subsamples of unleached BX-101 (jar 16503) sludge

	Subsample Identification	
	Unleached 16503-1	Unleached 16503-2
Number of recorded micrographs	13	14
Number of recorded EDS spectra	15	25
Figures of SEM micrographs showing typical particle morphologies and types	Figure 3-52 to Figure 3-61	Figure 3-62 to Figure 3-71
Tables of calculated EDS compositions (with carbon)	Table 3-21	Table 3-22
Appendix containing tables of calculated EDS compositions (without carbon) and figures of EDS spectra	Appendix D	

The sizes of discrete particles and particles that form aggregates in the unleached BX-101 (jar 16503) sludge typically range from a few micrometers to several micrometers in size (Figure 3-55, Figure 3-59, Figure 3-64, and Figure 3-71). Compared to the samples of unleached and water-leached AY-102 (jar 15935) sludge, the particles in the unleached BX-101 (jar 16503) sludge sample appear to be more dispersed (i.e., less intergrown or cemented-like aggregates) (Figure 3-52, Figure 3-54, and Figure 3-62).

Based on the SEM micrographs and EDS analyses, the unleached BX-101 (jar 16503) sludge contains primarily four types of particles. The most prevalent type of particle in both SEM mounts is the well faceted, tabular-shaped^a crystals that are shown plainly in Figure 3-52, Figure 3-53, and Figure 3-71. These particles contain primarily aluminum (as well as oxygen, and possibly carbon and/or hydrogen) (Figure 3-53 [eds15] and Figure 3-63 [eds03 and 04]), and often exhibit pseudo-hexagonal symmetry elements (e.g., see particle indicated by arrow at top of Figure 3-53). This composition and morphology are consistent with gibbsite [Al(OH)₃] (Deer et al. 1967).

Although relatively rare in the unleached BX-101 (jar 16503) sludge, one of the most obvious types of particles is the long (tens of micrometers), rod-shaped crystals shown in Figure 3-54, Figure 3-62, and Figure 3-63 (eds01). These rods are composed primarily of aluminum (Figure 3-55 [eds04] and

^a Tabular-shaped (or prismatic-shaped) refers to particles with lengths that are approximately 1.5 to 3 times their thickness.

Figure 3-63 [eds01]), and are thought to be a different aluminum-containing phase than the tabular-shaped crystals seen in Figure 3-52, Figure 3-53, and Figure 3-71.

The SEM analysis also revealed a third type of particle that consisted of clusters of ball-shaped crystals that were typically less than 5 μm in diameter (Figure 3-60, Figure 3-64, Figure 3-65, Figure 3-69, and Figure 3-70). The particles contained primarily sodium, aluminum, and silicon, and no calcium and nitrogen (Figure 3-65 [eds07 and eds08] and Figure 3-70 [eds20]). At higher SEM magnification, these ball-shaped crystals look like “balls of twine” (Figure 3-65 and Figure 3-66). Particles with similar crystal habit have been identified as the mineral cancrinite by others (Bickmore et al. 2001; Bredt et al. 2003) in studies of Hanford tank waste materials. If the particles shaped like “balls of twine” observed in our study are a member of the cancrinite mineral group, their composition best corresponds to the calcium-free mineral member cancrisilite [$\text{Na}_7\text{Al}_5\text{Si}_7\text{O}_{24}(\text{CO}_3)\cdot 2\text{H}_2\text{O}$].

Uranium-containing particles were common in all areas of the two subsamples of unleached BX-101 (jar 16503) sludge. When imaged using backscattered electrons, the uranium-rich particles appeared as bright white, globular or botryoidal groupings of particles (similar to a bunch of cotton balls or grapes) (Figure 3-57, Figure 3-58, Figure 3-63, and Figure 3-67). Compared to the bright white tone of the uranium-rich particles (Figure 3-65 [eds09 and eds11]), the particles tentatively identified as cancrisilite (or cancrinite) all appear as gray clusters of ball-shaped crystals (Figure 3-65 [eds07 and eds08]) in backscattered electron mode. All of the bright white particles shown in Figure 3-52 to Figure 3-71 and probed by EDS have a significant content of uranium (11 to 55 wt% uranium) with lesser amounts of sodium and aluminum.

The sodium uranate $\text{Na}_2\text{U}_2\text{O}_7$ has been identified by others (Temer and Villareal 1997, 1995, 1996; Herting et al. 2002) based on XRD and/or SEM/EDS studies of tank sludge materials from the Hanford Site. As discussed in Section 3.3.5, the morphology of the uranium-rich particles observed in our unleached BX-101 (jar 16503) sludge sample appears to be different than those shown in the SEM(bse) micrographs in Herting et al. (2002). The EDS compositions determined for the uranium-containing particles in our study moreover are not entirely consistent with these particles being $\text{Na}_2\text{U}_2\text{O}_7$. In addition to the presence of aluminum which typically ranged from 1% to 10% (Table 3-21 and Table 3-22) in the uranium-rich particles, the maximum uranium concentration measured by EDS was 55 wt% (subsample 16503-2, eds25) and more typically less than 50 wt%, whereas $\text{Na}_2\text{U}_2\text{O}_7$ ideally consists of 75 wt% uranium and 7.3 wt% sodium. However, as noted previously, EDS-derived compositions are qualitative and have a large uncertainty associated with them. Atomic sodium/uranium ratios were also calculated from the weight percentages of sodium and uranium for the uranium-rich (i.e., >10 wt%) particles listed in Table 3-21 and Table 3-22. About half of the uranium-rich particles had sodium/uranium atomic ratios of approximately one (e.g., 0.8 to 1.2), whereas the other half of these particles had sodium/uranium atomic ratios from 1.5 to 5.6. A sodium/uranium atomic ratio of one is consistent with the composition of $\text{Na}_2\text{U}_2\text{O}_7$. However, many of the uranium-rich particles with a sodium/uranium ratio of one also contained several weight percent of aluminum, which is not part of the ideal composition of $\text{Na}_2\text{U}_2\text{O}_7$.

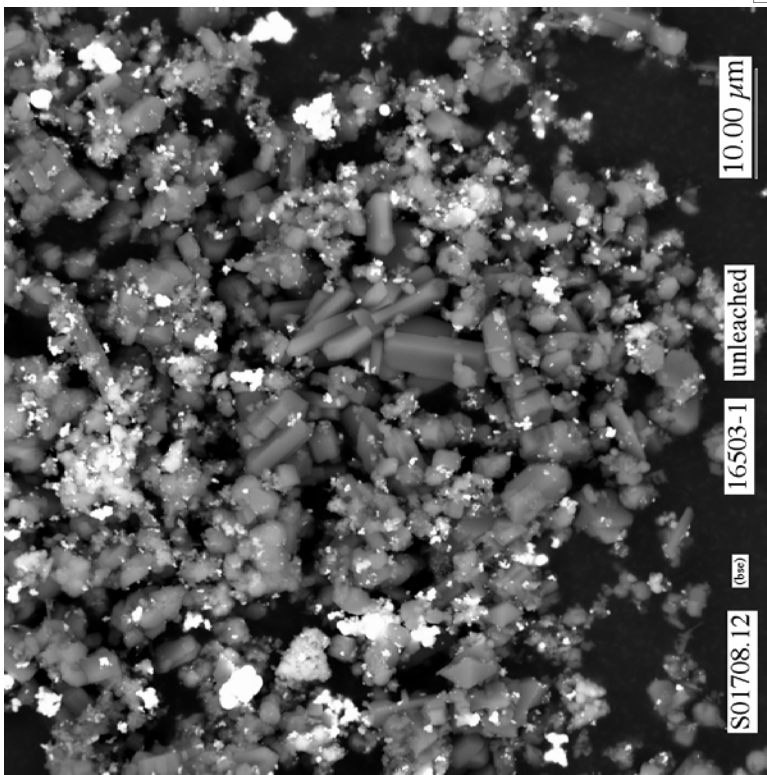


Figure 3-52. Low magnification scanning electron micrograph showing general morphology of particles in subsample “unleached 16503-1”

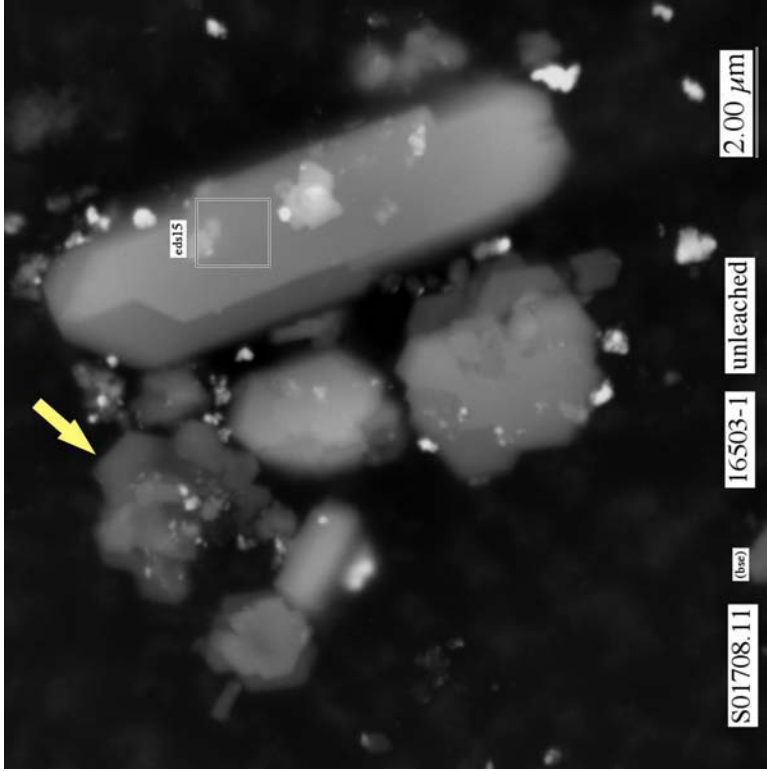


Figure 3-53. Micrograph showing prismatic-like particles with hexagonal-like symmetry features in subsample “unleached 16503-1”

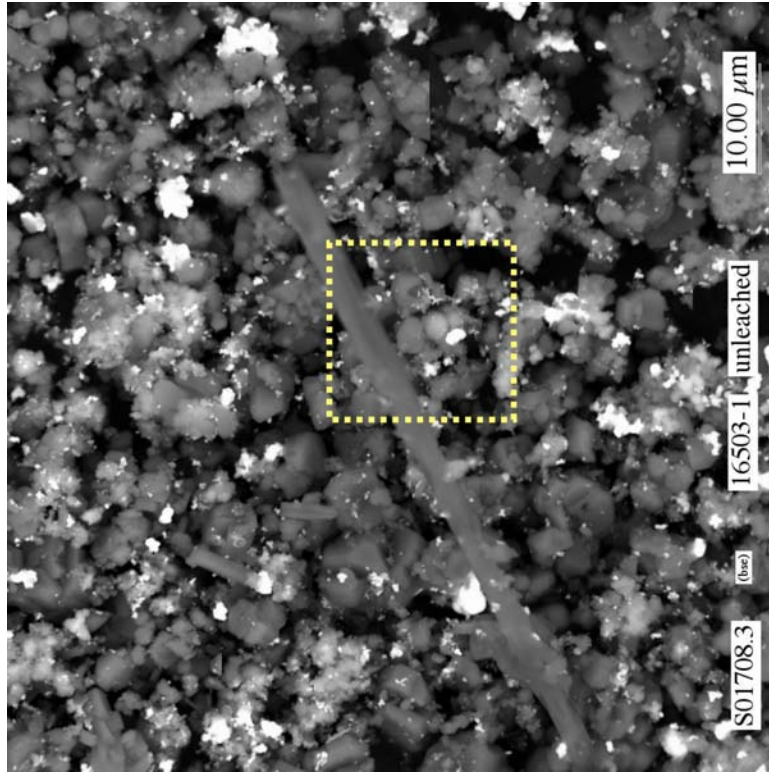


Figure 3-54. Micrograph showing range of typical particle types, including large needle-like grains, in subsample “unleached 16053-1”

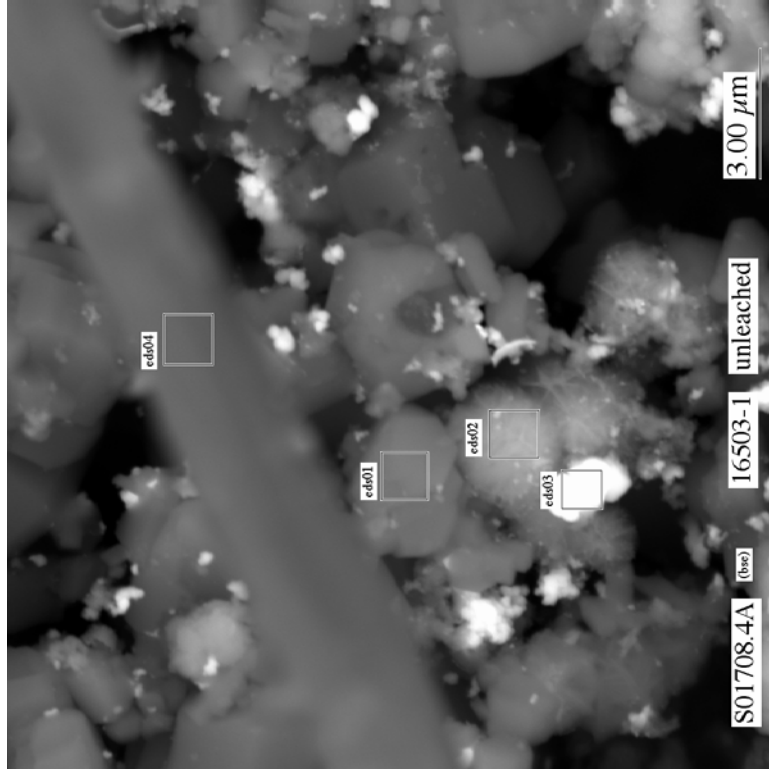


Figure 3-55. Micrograph showing at higher magnification particles, including “ball-of-twine”-like crystals (see eds 02), in area indicated by the yellow-dotted square in Figure 3-54 of subsample “unleached 16503-1”

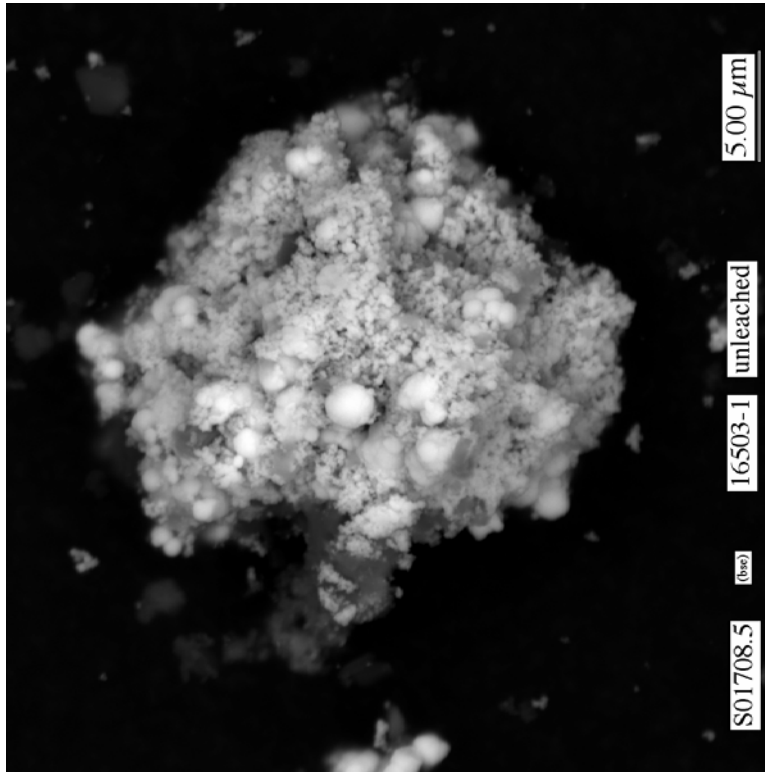


Figure 3-56. Micrograph showing typical botryoidal-shaped, uranium-rich particle aggregates in subsample “unleached 16503-1”

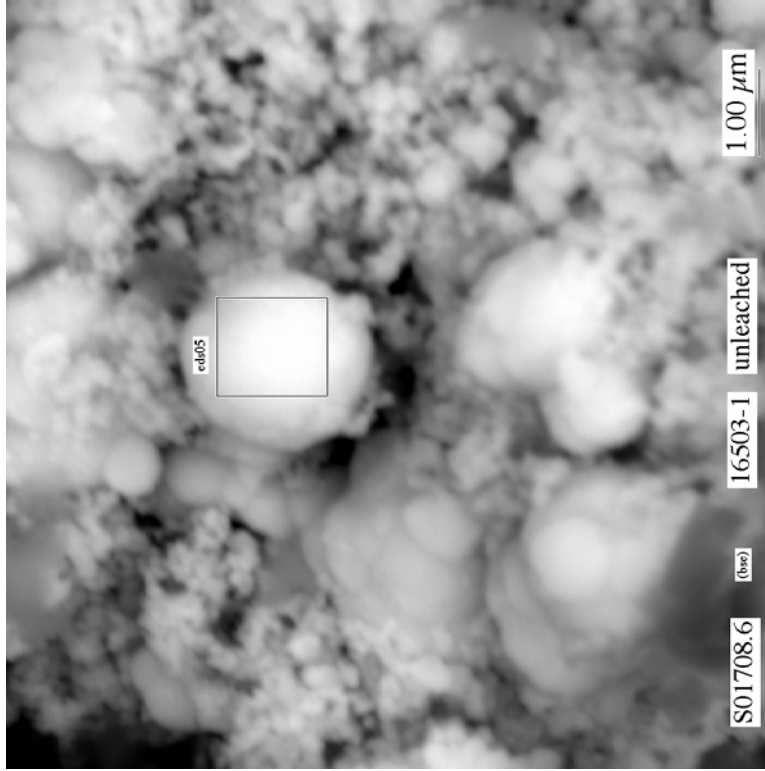


Figure 3-57. Micrograph showing at higher magnification botryoidal-shaped, uranium-rich particles at center of Figure 3-56 of subsample “unleached 16503-1”

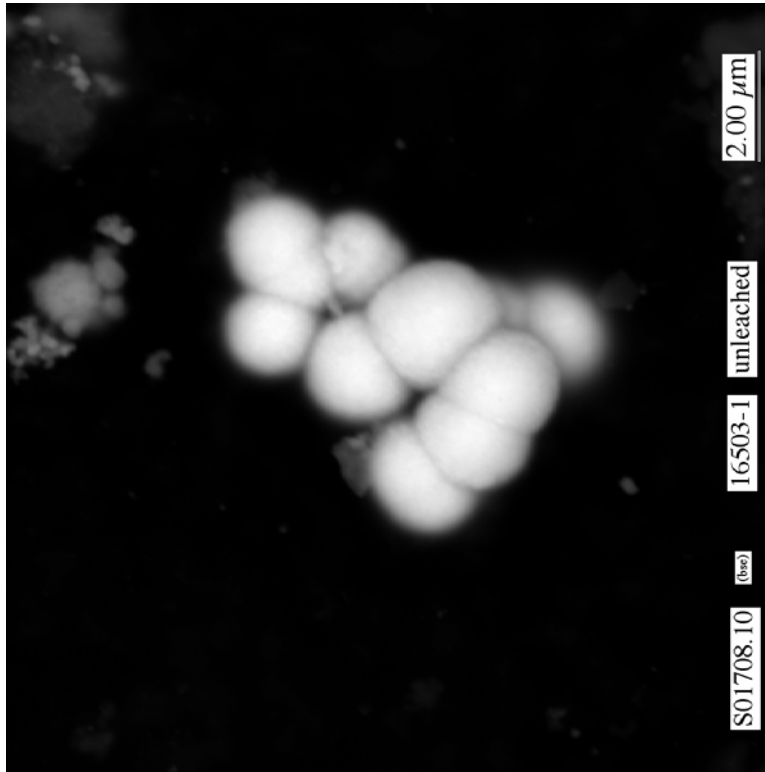


Figure 3-58. Micrograph showing botryoidal-shaped, uranium-rich particles in subsample “unleached 16503-1”

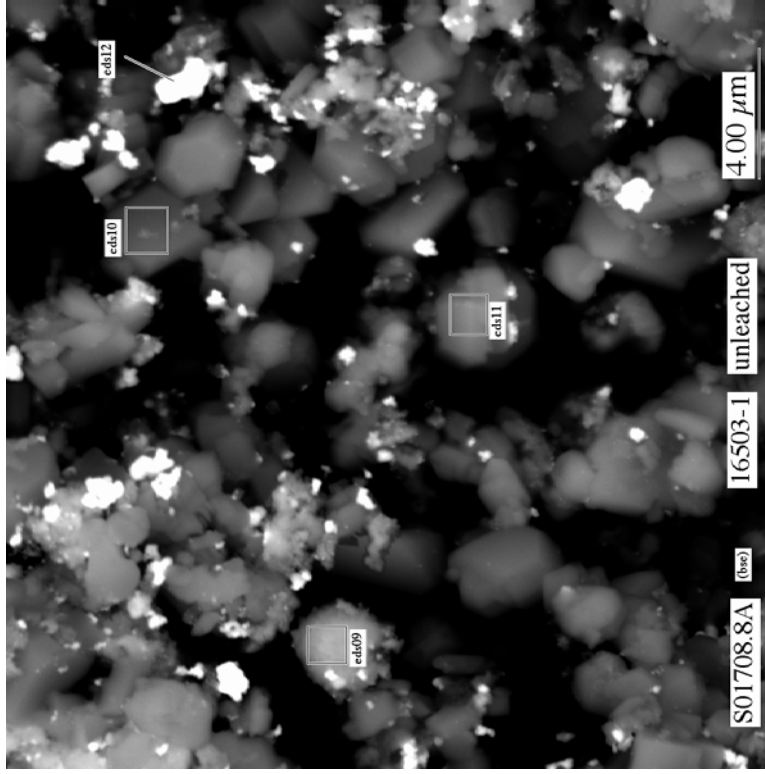


Figure 3-59. Micrograph showing typical particle types in subsample “unleached 16503-1”

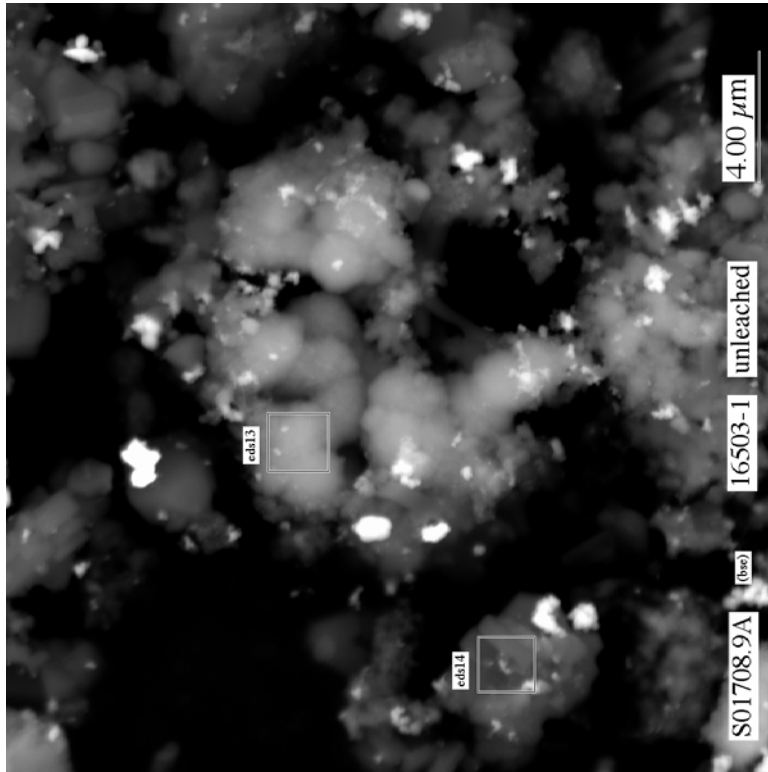


Figure 3-60. Micrograph showing typical particle types in sub-sample “unleached 16503-1”

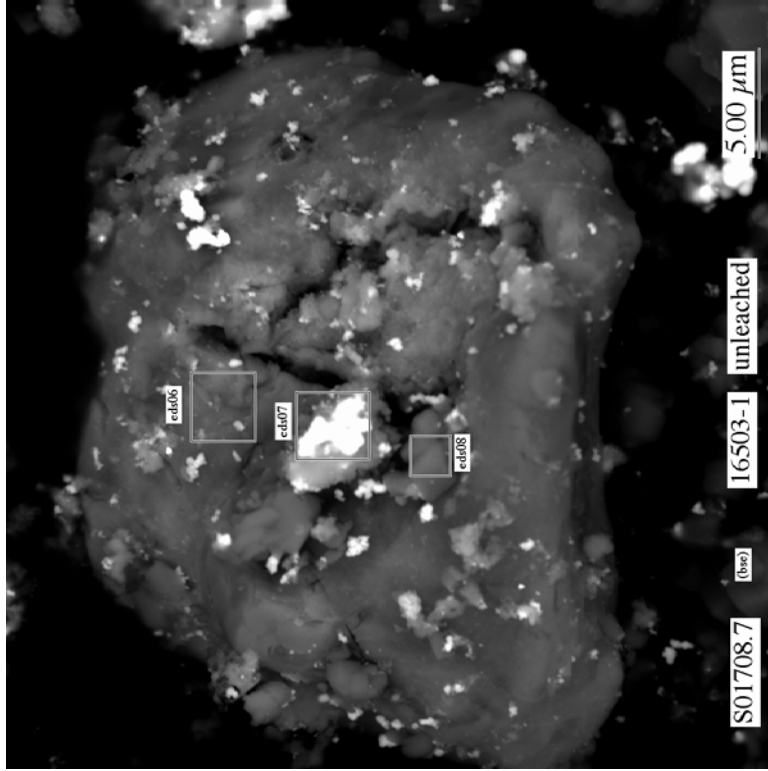


Figure 3-61. Micrograph showing typical large particle aggregate in sub-sample “unleached 16503-1”

Table 3-21. Qualitative compositions determined by SEM/EDS that include the emission peak for carbon for particles observed in unleached subsample 16503-1 of BX-101 tank sludge (jar 16503)

Figure and Spectrum Label	Major Metals (>5 wt%)	----- wt% -----												
		C	O	Na	Al	Si	P	S	Ca	Cr	Mn	Fe	Ni	U
Figure 3-55 eds01	Al	11.9	60.1	1.0	23.5	0.2	0.2	0.0	0.0	0.5	1.0	0.7	0.0	1.0
Figure 3-55 eds02	Mn-Al	13.4	47.7	2.9	12.9	0.4	0.2	0.1	0.0	4.3	13.0	2.5	0.1	2.5
Figure 3-55 eds03	U-Al-Mn	7.6	39.8	3.3	8.0	0.6	0.6	0.1	0.1	2.0	5.0	1.3	0.0	31.6
Figure 3-55 eds04	Al	21.9	55.9	4.5	13.5	0.3	0.1	0.1	0.1	0.5	0.8	0.7	0.0	1.6
Figure 3-57 eds05	U-Na	9.1	31.3	5.5	0.6	0.2	0.6	0.0	0.0	0.4	0.2	0.2	0.2	51.7
Figure 3-61 eds06	Si-Al	18.7	50.9	3.7	5.9	9.7	0.4	0.1	2.0	1.3	1.7	5.5	0.1	0.1
Figure 3-61 eds07	U-Na	22.4	45.8	5.1	3.1	2.3	0.5	0.1	0.3	1.2	1.7	2.1	0.0	15.6
Figure 3-61 eds08	Al	15.3	62.0	1.6	14.9	2.7	0.2	0.1	0.3	0.4	0.6	1.1	0.0	0.8
Figure 3-59 eds09	Al-Na-Si	16.4	52.8	8.9	11.6	5.6	0.2	0.1	0.1	0.5	0.7	1.4	0.0	1.7
Figure 3-59 eds10	Al	29.0	55.6	0.4	14.2	0.1	0.1	0.1	0.0	0.0	0.1	0.1	0.0	0.4
Figure 3-59 eds11	Al	16.4	59.9	0.9	22.0	0.3	0.1	0.0	0.0	0.0	0.1	0.1	0.0	0.2
Figure 3-59 eds12	U-Al	19.6	50.0	3.3	8.7	0.3	0.3	0.1	0.0	0.4	0.5	0.5	0.0	16.5
Figure 3-60 eds13	Mn-Cr-Na-Fe	18.5	42.2	7.0	1.8	1.9	0.5	0.3	0.1	7.6	14.6	5.6	0.1	0.0
Figure 3-60 eds14	Al	28.0	51.6	3.1	12.6	1.5	0.2	0.1	0.1	0.4	0.6	1.2	0.0	0.7
Figure 3-53 eds15	Al	32.0	53.4	0.2	13.8	0.1	0.1	0.1	0.0	0.1	0.0	0.1	0.0	0.1

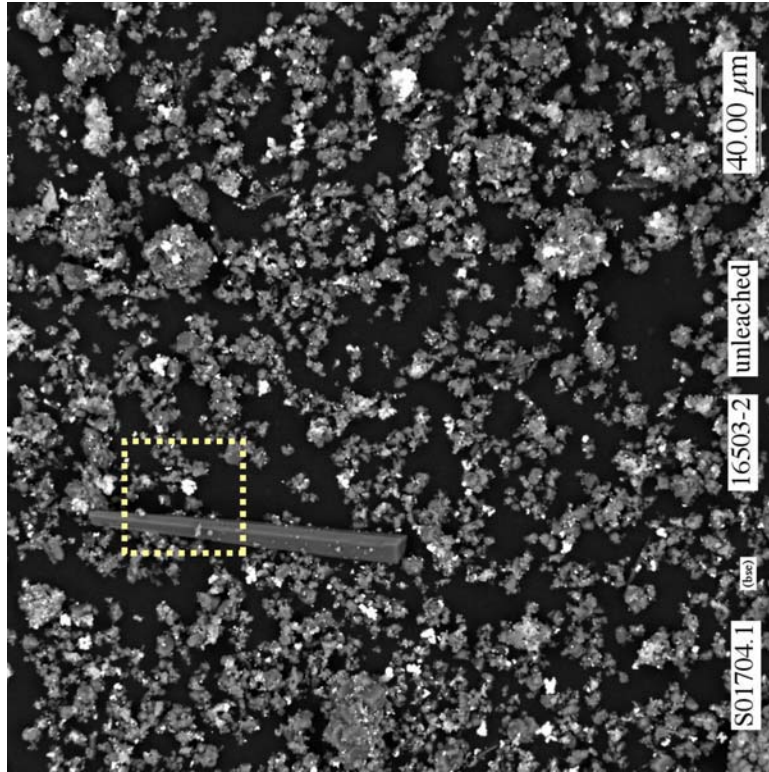


Figure 3-62. Micrograph showing range of typical particle types, including large needle-like grains, in subsample “unleached 16503-2”

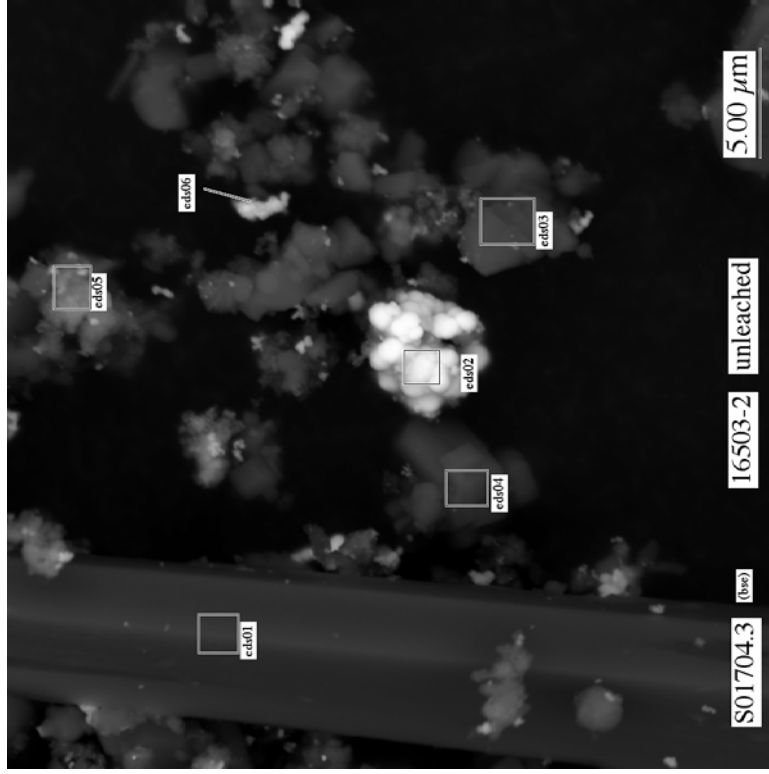


Figure 3-63. Micrograph showing at higher magnification particles, including botryoidal-shaped, uranium-rich particle aggregate (bright particles at center), in area indicated by the yellow-dotted square in Figure 3-62 of subsample “unleached 16503-2”

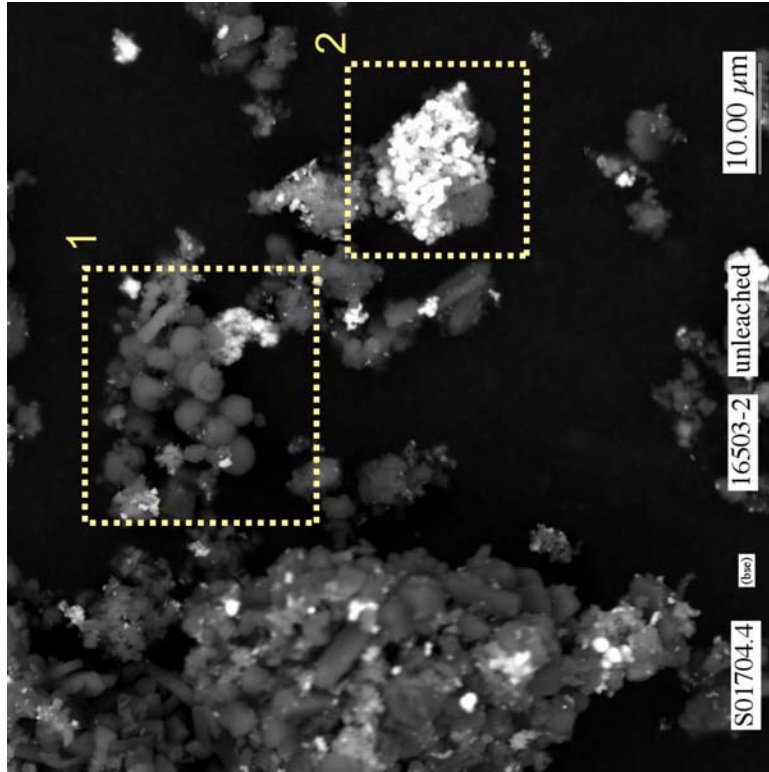


Figure 3-64. Micrograph showing typical particle types and aggregates in subsample “unleached 16053-2”

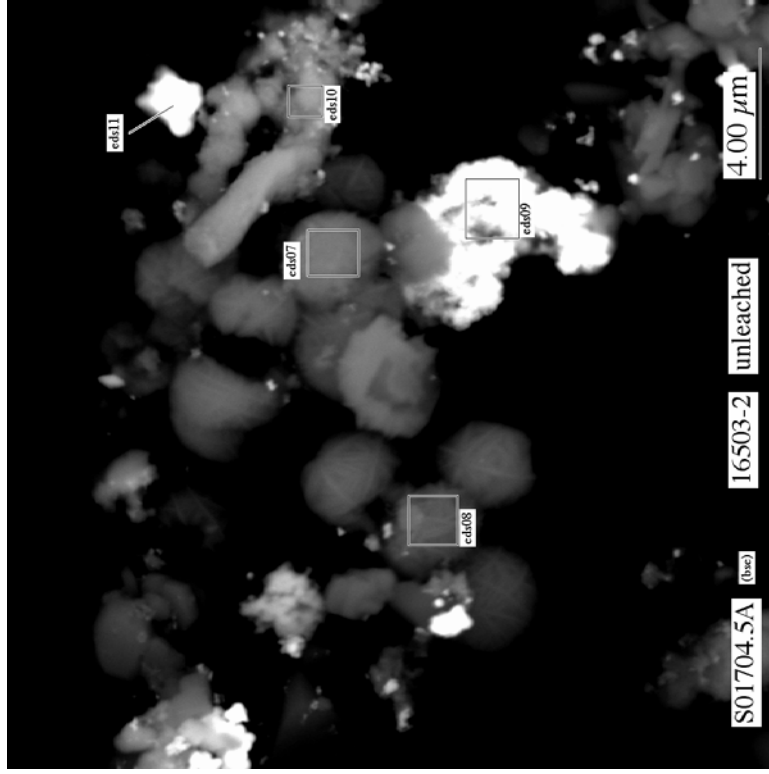


Figure 3-65. Micrograph showing at higher magnification particles, including “ball-of-twine”-like crystals (see eds06 and eds07), in area indicated by the yellow-dotted square #1 in Figure 3-64 of subsample “unleached 16503-2”

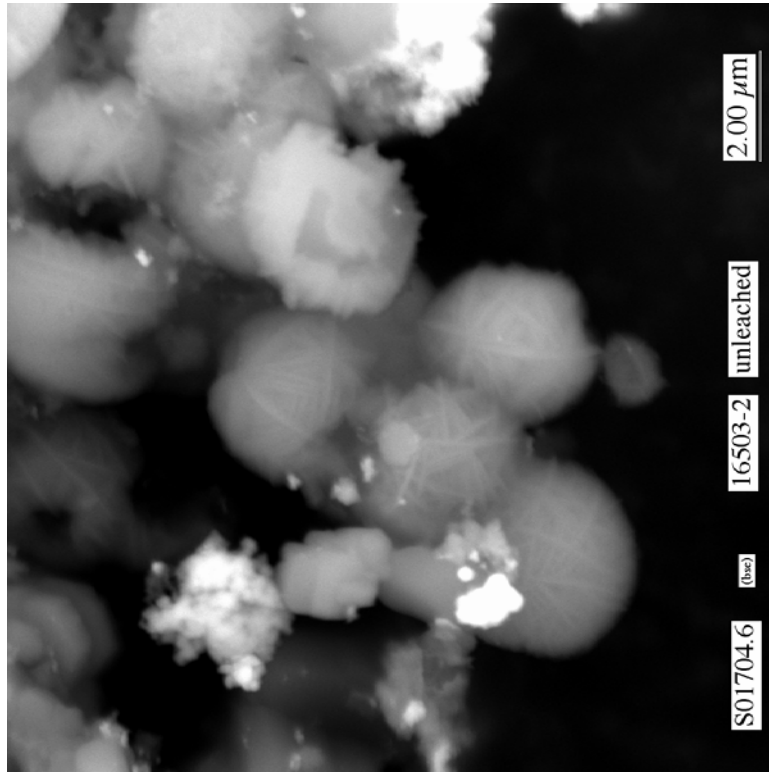


Figure 3-66. Micrograph showing at higher magnification “ball-of-twine”-like crystals in left-center area of Figure 3-65 in subsample “unleached 16503-2”

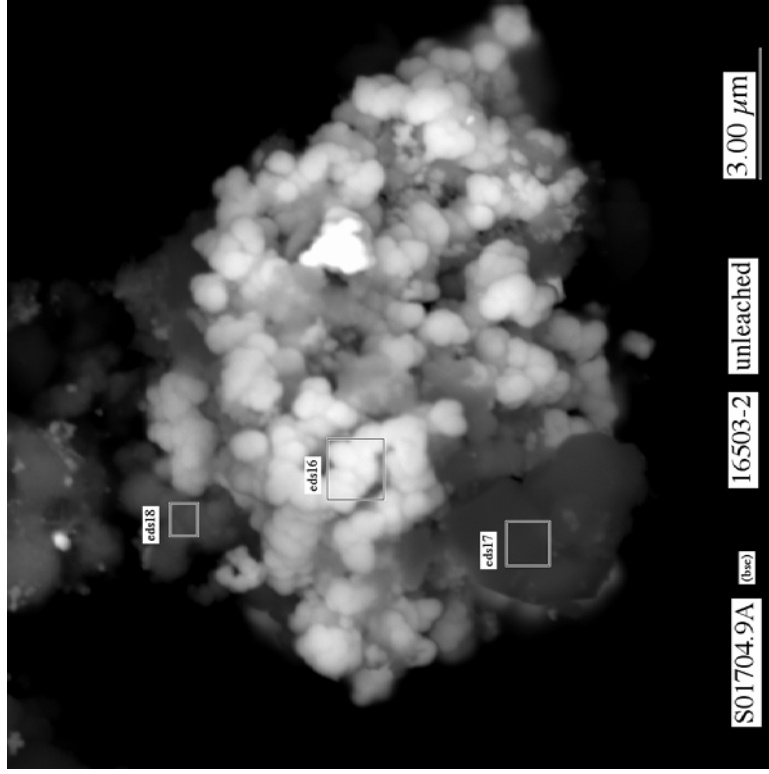


Figure 3-67. Micrograph showing at higher magnification botryoidal-shaped, uranium-rich particle aggregate in area indicated by the yellow-dotted square #2 in Figure 3-64 of subsample “unleached 16503-2”

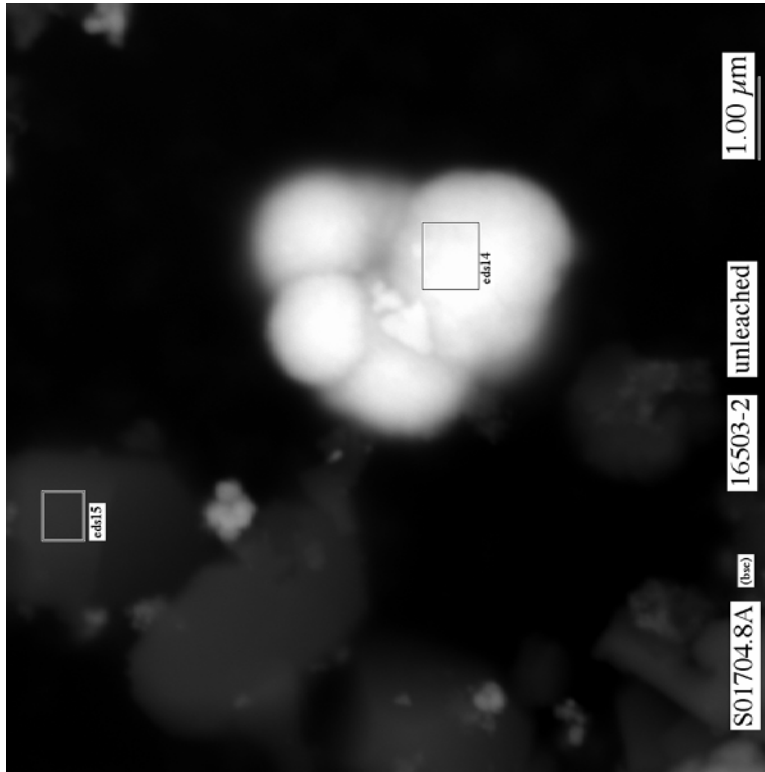


Figure 3-68. Micrograph showing botryoidal-shaped, uranium-rich particles (eds14) in subsample “unleached 16503-2”

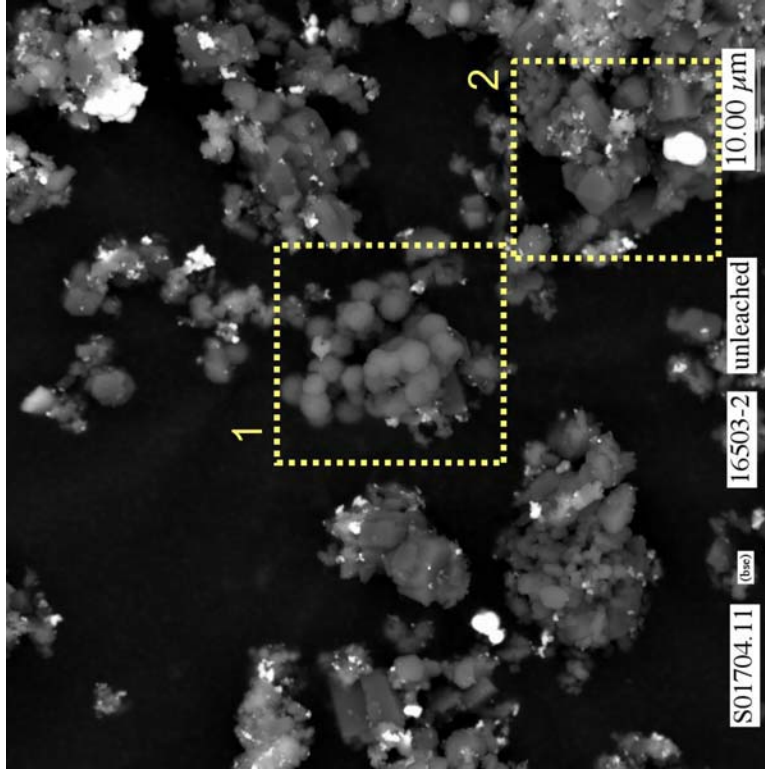


Figure 3-69. Micrograph showing typical particle types in subsample “unleached 16503-2”

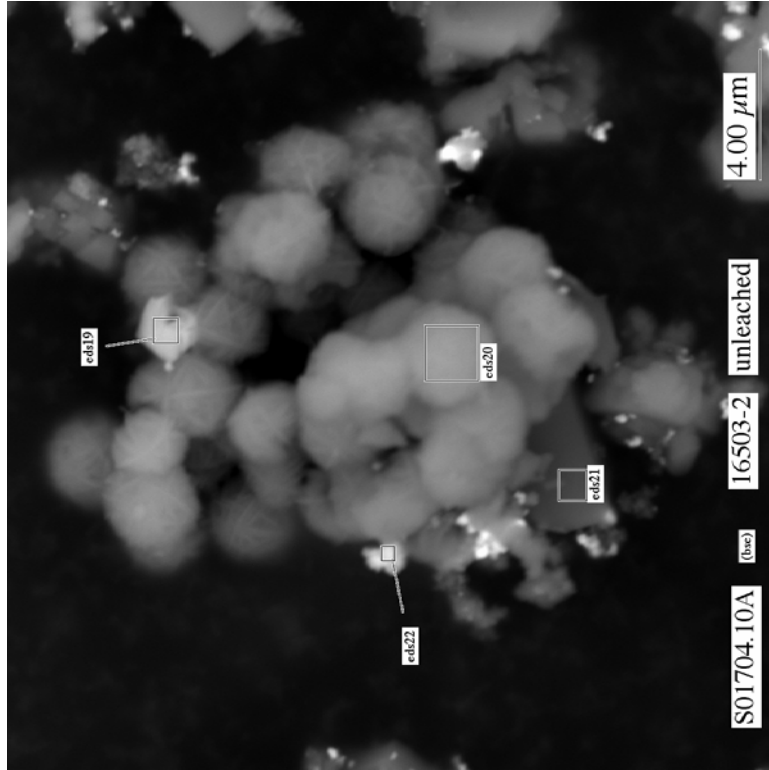


Figure 3-70. Micrograph showing at higher magnification “ball-of-twine”-like crystals in area indicated by the yellow-dotted square #1 in Figure 3-69 of subsample “unleached 16503-2”

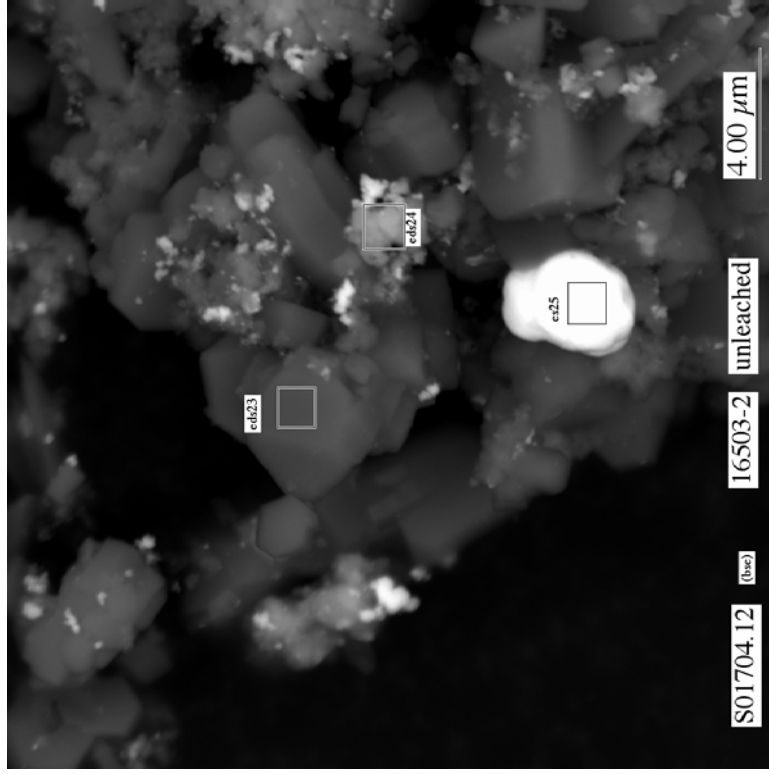


Figure 3-71. Micrograph showing at higher magnification prismatic-shaped crystals in the area indicated by the yellow-dotted square #2 in Figure 3-69 of subsample “unleached 16503-2”

Table 3-22. Qualitative compositions determined by SEM/EDS that include the emission peak for carbon for particles observed in unleached subsample 16503-2 of BX-101 tank sludge (jar 16503)

Figure and Spectrum Label	Major Metals (>5 wt%)	----- wt%-----												
		C	O	Na	Al	Si	P	S	Ca	Cr	Mn	Fe	Ni	U
Figure 3-63 eds01	Na	23.2	47.8	27.6	1.0	0.1	0.0	0.0	0.0	0.0	0.1	0.1	0.0	0.1
Figure 3-63 eds02	U-Na	10.9	28.0	5.4	2.0	0.1	0.5	1.5	0.1	0.4	0.5	1.3	0.0	49.4
Figure 3-63 eds03	Al	25.0	60.0	1.1	13.2	0.1	0.1	0.0	0.0	0.1	0.1	0.1	0.0	0.4
Figure 3-63 eds04	Al	18.2	60.7	1.4	19.1	0.1	0.1	0.0	0.0	0.0	0.1	0.1	0.1	0.2
Figure 3-63 eds05	Fe	32.7	42.8	3.6	3.6	0.5	0.7	0.4	0.1	1.9	2.7	10.1	0.0	1.0
Figure 3-63 eds06	U	34.9	35.0	3.0	3.3	0.2	0.4	0.2	0.0	0.3	0.2	0.3	0.0	22.2
Figure 3-65 eds07	Na-Al-Si	22.9	48.5	10.6	8.5	7.4	0.2	0.1	0.0	0.3	0.2	0.5	0.0	0.9
Figure 3-65 eds08	Al-Na-Si	23.0	48.3	9.7	10.1	7.9	0.2	0.1	0.0	0.2	0.1	0.3	0.0	0.2
Figure 3-65 eds09	U-Fe	28.3	30.7	3.6	1.4	0.5	0.9	0.3	0.4	0.7	1.0	8.1	0.1	24.1
Figure 3-65 eds10	Mn	38.0	39.8	3.4	2.7	0.6	0.4	0.2	0.1	1.9	8.1	3.8	0.1	1.0
Figure 3-65 eds11	U	32.2	32.3	3.6	2.3	0.3	0.5	0.1	0.0	0.4	0.5	0.5	0.0	27.1
Fig. not shown eds12	Al	15.2	61.4	0.5	21.2	0.1	0.1	0.0	0.0	0.7	0.2	0.4	0.0	0.2
Fig. not shown eds13	U-Al	21.1	44.7	3.1	10.3	0.5	0.3	0.1	0.0	0.6	0.3	0.5	0.1	18.5
Figure 3-68 eds14	U	16.6	30.7	3.6	1.1	0.1	0.6	0.1	0.1	0.4	0.2	0.2	0.1	46.2
Figure 3-68 eds15	Al	40.0	45.8	0.3	13.4	0.1	0.1	0.1	0.0	0.0	0.0	0.1	0.0	0.2
Figure 3-67 eds16	U-Na	12.9	30.3	5.0	2.3	0.7	0.6	0.2	0.1	0.7	0.2	0.5	0.0	46.7
Figure 3-67 eds17	U-Al	27.6	40.6	0.8	10.0	0.2	0.1	0.2	0.2	0.5	0.5	0.7	0.1	18.5
Figure 3-67 eds18	U-Mn-Na	26.2	42.5	5.5	2.4	0.5	0.5	0.2	0.3	2.8	6.2	2.5	0.1	10.5
Figure 3-70 eds19	Ca	33.7	44.0	4.1	3.6	2.6	4.0	0.2	7.1	0.1	0.0	0.4	0.0	0.1
Figure 3-70 eds20	Na-Al-Si	25.4	50.2	9.4	7.9	6.2	0.1	0.1	0.1	0.2	0.1	0.2	0.0	0.1
Figure 3-70 eds21	Al-U	10.3	33.9	0.9	38.1	0.7	0.1	0.4	0.2	1.8	3.5	3.8	0.3	6.1
Figure 3-70 eds22	Fe-Al	36.5	26.4	3.3	5.1	2.3	0.2	0.1	0.1	0.2	0.9	23.9	0.7	0.4
Figure 3-71 eds23	Al	14.5	64.3	0.6	20.2	0.1	0.1	0.0	0.0	0.1	0.0	0.1	0.0	0.1
Figure 3-71 eds24	Al-Fe	20.8	51.4	4.0	8.3	1.3	1.3	0.2	1.9	0.8	1.4	5.0	0.4	3.1
Figure 3-71 eds25	U	7.5	28.7	4.5	2.4	0.4	0.6	0.0	0.2	0.5	0.2	0.1	-0.1	55.0

3.3.4 General Observations

The EDS analyses obtained in this study are also important from the perspective of what elements of interest were not detected. As noted previously, SEM/EDS analyses are limited to elements with atomic weights heavier than boron. Therefore, it was not possible to detect the presence of hydrogen, such as in solids containing structural hydroxide, using SEM/EDS. Relative to the sludge samples analyzed in this study, it is important to note that iodine (based on the $L_{\alpha 1}$ and $L_{\beta 1}$ X-ray emissions at 3.938 and 4.221 keV, respectively), technetium (based on the $L_{\alpha 1}$ and $L_{\beta 1}$ X-ray emissions at 2.424 and 2.538 keV, respectively), and nitrogen (based on the $K_{\alpha 1}$ X-ray emission at 0.392 keV) were not detected in the EDS spectra for any of the particles of the untreated or treated sludge samples (X-ray emission data from Thompson et al. 2001). The principal X-ray emission line for nitrogen (0.392 keV) would occur approximately half way between the principal X-ray emission lines for carbon ($K_{\alpha 1}$) and oxygen ($K_{\alpha 1}$) at 0.277 and 0.525 keV, respectively.

Carbon was detected in essentially every EDS spectra. The carbon content (specific results discussed in previous sections) typically ranged from 5 to 40 wt% for particles in the unleached sludge samples, and 5 to 20 wt% for the water-leached AY-102 (jar 15935) sludge sample. The primary source for the carbon in the EDS spectra has not been identified. Given the uncertainties regarding the carbon content of these sludge particles, two sets of tables of EDS-determined qualitative compositions were presented for each sludge sample. The estimated carbon content of each probed particle is included in the composition summary tables in Section 3.0, whereas the carbon peak was excluded from the compositions calculated and re-normalized to 100 wt% in the EDS summary tables included in the respective appendices as an aid to readers reviewing these results.

Possible sources of carbon include the carbon coating applied to the SEM mounts, the carbon tape used for attaching the sludge particles to the aluminum mounting stubs, or carbon that might exist in carbonate-containing solids. EDS probes of carbon-coated areas of the aluminum mounting stubs that did not contain carbon tape and of the carbon-coated, carbon tape void of sludge particles indicated carbon emission peaks that were too low and too great, respectively, compared to the carbon peaks measured for the sludge particles. Carbon contents greater than 20 wt% are also larger than those expected for most oxalate- and carbonate-containing solid phases. For example, the carbon contents of $\text{Na}_2(\text{C}_2\text{O}_4)$ (natroxalate), Na_2CO_3 (natrite), and $\text{NaAl}(\text{CO}_3)(\text{OH})_2$ (dawsonite) are ideally 17.9, 11.3, and 8.3 wt%, respectively. Because most metals in the periodic table have atomic weights greater than sodium, it is safe to assume that the carbon content of other carbonate- or oxalate-containing solids will be significantly less than 20 wt%. When the EDS results for each sludge sample are sorted as a function of carbon content, there is no obvious relationship between an increase in carbon content with respect to a change in the content of any of the other detected elements, such as sodium, aluminum, or iron.

Computer modeling simulations were conducted to assess the potential for X-ray emissions that might result from penetration of the SEM electron beam through small sludge particles into the carbon tape substrate. When an electron beam hits a solid material, the electrons penetrate some depth into the solid and continue traveling in a straight line until they are scattered by atoms in the solid. This process repeats itself for each electron in the beam. The electrons continue to penetrate and be scattered in the solid until they run out of energy and stop. If the electrons being scattered have sufficient energy to produce a given X-ray transition, the scattering process can result in the generation of X-rays with

energies characteristic of the elements that make up the solid, which is the basis for EDS analysis. The volume of solid material through which the electron beam is able to penetrate and scatter is often referred to as the interaction volume. The depth and diameter of the interaction volume is dependent on the force of the electron beam and the composition of the solid material. The force of the electron beam is determined by the accelerating voltage, with the depth of the interaction volume increasing with increasing accelerating voltage. The extent of beam penetration however decreases with increasing atomic number of the elements that comprise the solid material. Solids containing elements with higher atomic numbers are more effective at stopping the electrons and reducing the extent of the interaction volume. If the particle thicknesses or diameters of a certain solid being studied by SEM/EDS are less than the actual interaction volume resulting from a particular accelerating voltage, then the EDS analyses may contain unwanted X-ray signals from adjacent grains and/or the supporting substrate if the scattered electrons have sufficient energy to produce a given X-ray transition.

The Electron Flight Simulator™ modeling software was used to estimate the depth and diameter of the interaction volume resulting from electron-beam penetration in solid particles with four compositions identified by our SEM/EDS analyses. The Electron Flight Simulator™ software is based on a Monte Carlo model developed by Dr. David Joy, University of Tennessee. Interaction volumes were simulated for dawsonite [NaAl(CO₃)(OH)₂], gibbsite [Al(OH)₃], hematite (Fe₂O₃), and Na₂U₂O₇ using an accelerating voltage of 20 keV and 32,000 electron trajectories. The densities used in the simulation calculations were 2.43 g/cm³ for dawsonite [NaAl(CO₃)(OH)₂] (ICDD PDF #45-1359), 2.44 g/cm³ for gibbsite [Al(OH)₃] (Robie et al. 1967), 5.27 g/cm³ for hematite (Fe₂O₃) (Robie et al. 1967), and 6.57 g/cm³ for Na₂U₂O₇ (ICDD PDF #43-0347). The estimated interaction volumes are shown as the blue half-ellipsoidal areas in each frame in Figure 3-72. The red vertical line shown at the top of each frame in Figure 3-72 represents the incoming electron beam at the surface of the solid. These Monte Carlo simulations show that the depth and diameter of electron-beam penetration and scatter will be greater for particles of dawsonite and gibbsite, which are less dense and composed of elements of lower atomic number, compared to particles of hematite and Na₂U₂O₇. These calculations indicate that the EDS spectra for particles of dawsonite, gibbsite, hematite, and Na₂U₂O₇ with thicknesses less than approximately 3.5, 2.0, 1.5, and 0.6 μm, respectively, could contain X-ray emissions from the carbon-tape substrate, such as those observed in the EDS spectra obtained in this study. That is, the carbon tape can be a contributor of carbon in the EDS analyses, especially with the examination of sludge particles that are submicron in thickness.

3.3.5 Comparison of XRD and SEM/EDS Results to Published Results of Others

Bechtold et al. (2003) used XRD and SEM/EDS to characterize untreated samples of AY-102 (jar 19406) sludge. This is the only other published source of characterization data for solids in AY-102 sludge. No sources were identified for characterization data of solids in BX-101 sludge material.

The results of our XRD and SEM/EDS analyses are summarized in Table 3-23, and are in good agreement with the results of Bechtold et al. (2003). Bechtold et al. (2003) identified dawsonite, hematite, gibbsite, and the silicate-carbonate phase cancrinite [Na₆Ca_{1.5}Al₆Si₆O₂₄(CO₃)_{1.6}] in their AY-102 (jar 19406) sludge sample. A cancrinite phase was also tentatively identified by XRD in our unleached AY-102 (jar 18686) sludge sample, but not in our unleached or water-leached AY-102 (jar 15935) sludge

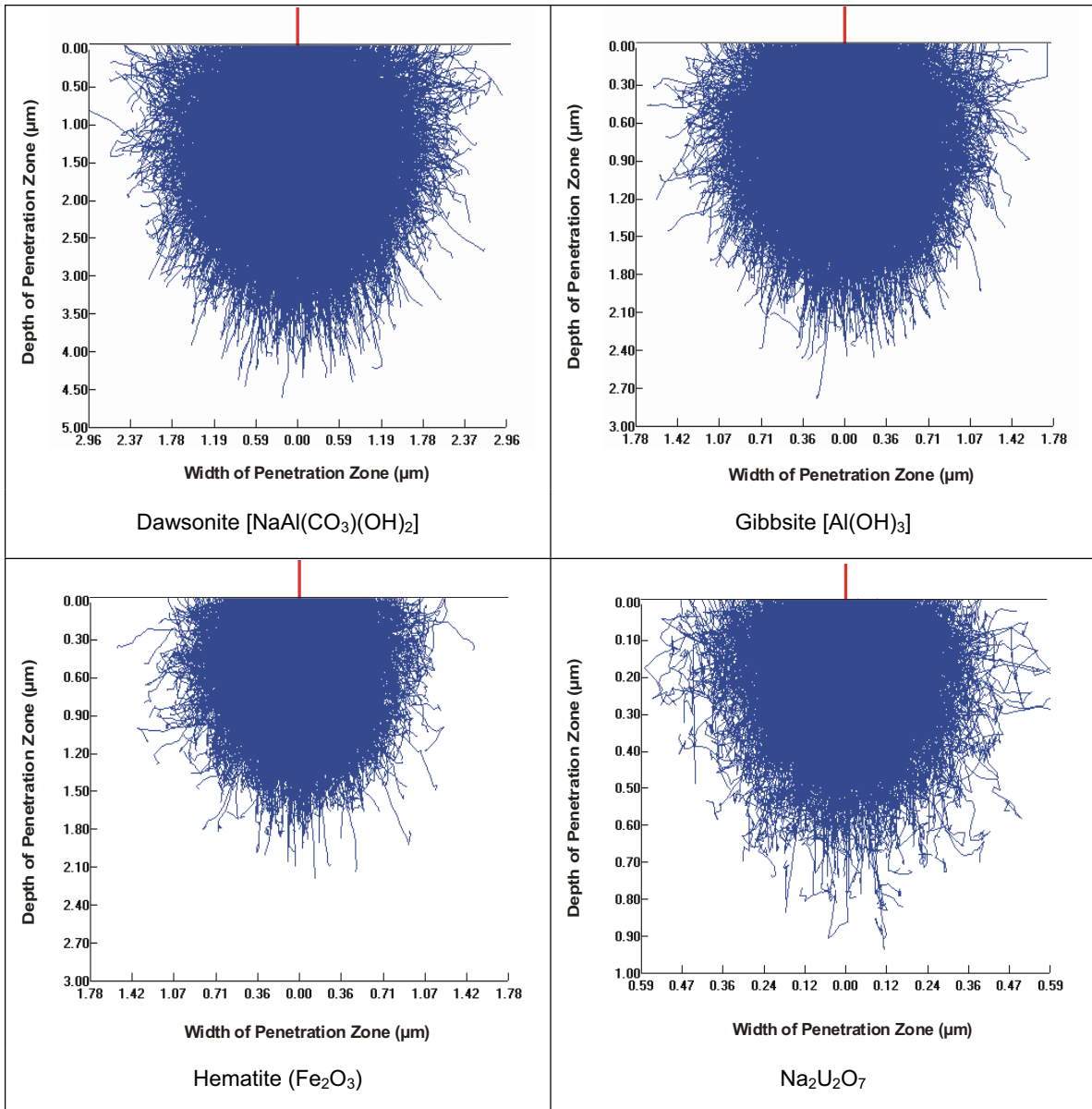


Figure 3-72. Estimated sizes of interaction volumes resulting from electron-beam penetration in four types of solids identified in the SEM/EDS analyses (Note differences in scale.)

sample. Identification of the presence of cancrinite in our study was based on a match to the XRD pattern PDF #71-0776 [cancrinite, $\text{Na}_6(\text{Al}_6\text{Si}_6\text{O}_{24})(\text{CaCO}_3)(\text{H}_2\text{O})_2$], whereas that in Bechtold et al. (2003) was determined from a match to pattern PDF #34-0176 [cancrinite, $\text{Na}_6\text{Ca}_{1.5}\text{Al}_6\text{Si}_6\text{O}_{24}(\text{CO}_3)_{1.6}$]. Because the AY-102 (jar 18686) sludge sample was not analyzed by SEM/EDS, there are no additional data to corroborate our identification of cancrinite in this sludge sample. The reason why cancrinite was not detected in our samples of AY-102 (jar 15935) sludge is not known, although heterogeneity potentially exists with respect to the solids present in the different samples of AY-102 sludge. Our SEM/EDS analyses of unleached (raw) and water-leached AY-102 (jar 15935) sludge samples show that particles

Table 3-23. Comparison of XRD and SEM/EDS results for this study and for Bechtold et al. (2003)

Sample Identification	This Study		Bechtold et al. (2003) AY-102 (jar 19406)
	XRD Analyses	SEM/EDS Analyses	SEM/EDS and XRD Analyses
Unleached AY-102 (jar 15935)	Dawsonite [NaAlCO ₃ (OH) ₂]	Lath-shaped, Na ±Al ±Fe particles	Dawsonite
	Hematite (Fe ₂ O ₃)	Globular aggregates of Fe ±Na ±Mn particles	Hematite
	Gibbsite [Al(OH) ₃]		Gibbsite
		Na,Al,Si-rich particles	Cancrinite [Na ₆ Ca _{1.5} Al ₆ Si ₆ O ₂₄ (CO ₃) _{1.6}]
		Na-rich particles	
		Ag-containing particles	
		U,Na-containing crusty particles	
Water-leached AY-102 (jar 15935)	Same phases as identified by XRD for unleached AY-102	Globular aggregates of Fe ±Al ±Mn particles	Water-leached material was not studied
		Ca ±Fe ±P particles	
		Lath-shaped, Na ±Al ±Fe particles	
		Ag-containing particles	
Unleached AY-102 (jar 18686)	Same phases as identified by XRD for unleached AY-102 (jar 15935) and cancrinite [Na ₆ (Al ₆ Si ₆ O ₂₄)(CaCO ₃)(H ₂ O) ₂]	Not analyzed by SEM/EDS	Dawsonite, hematite, gibbsite, and cancrinite
Unleached BX-101 (jar 16503)	Gibbsite	Tabular-shaped Al-rich particles	Sludge from BX-101 not studied
		Long, rod-shaped Al-rich particles	
		Cancrinite [Na ₆ (Al ₆ Si ₆ O ₂₄)(CaCO ₃)(H ₂ O) ₂]	
		U-rich ±Na ±Al globular particles	

with more than 5 wt% silicon (a necessary constituent of cancrinite) were rare. The particle labeled “eds05” for subsample “unleached 15935-1” (Figure 3-15) contains approximately 12 wt% sodium, 9 wt% aluminum, and 9 wt% silicon based on the SEM/EDS analyses, and thus may be a silicate particle such as cancrinite. However, this particle lacks any distinguishing morphological features that would be indicative of cancrinite or any other specific silicate phase.

A nitrate form of cancrinite $\{(Na,Ca,K)_{6-9}(Si,Al)_{12}O_{24}[(CO_3),(SO_4),Cl_2,(NO_3)_2,(OH)_2]_{2-4}n\}$ has been identified by others in studies of Hanford tank waste materials (Bickmore et al. 2001, Bredt et al. 2003). Their SEM images indicate that the cancrinite particles typically occur as clusters of ball-shaped crystals that look like “balls of twine.” Bickmore et al. (2001) observed such crystals in studies of mineral

precipitation on quartz sand in simulated Hanford tank solutions. Bredt et al. (2003) identified these “balls of twine” in a study of the rheological and physical properties of pretreated waste stream and melter feed materials for AP-101 low-activity waste.

The morphologies of the cancrinite particles observed in the studies by Bickmore et al. (2001) and Bredt et al. (2003) however are similar to the particles shaped like “balls of twine” observed in the SEM micrographs for the unleached BX-101 (jar 16503) sludge samples (see Section 3.3.3). Moreover, minor reflections observed in our XRD pattern for this sludge sample correlated well with the pattern PDF #71-0776 for cancrinite, which suggested that a trace amount of this mineral was present in this sludge sample. The composition of the particles shaped like “balls of twine” consisted primarily of sodium, aluminum, and silicon, but no detectable calcium or nitrogen (such as nitrate). This composition corresponds best to the calcium-free member cancrisilite [$\text{Na}_7\text{Al}_5\text{Si}_7\text{O}_{24}(\text{CO}_3)\cdot 2\text{H}_2\text{O}$] of the cancrinite mineral group.

Particles containing uranium with lesser amounts of sodium and aluminum were common in the unleached BX-101 (jar 16503) sludge samples analyzed by SEM/EDS. However, identification of any crystalline uranium/sodium-rich solids present in this sludge by XRD was problematic for the issues discussed in Section 3.2. Sodium uranate solids have been identified by others in tank sludge materials from the Hanford Site (Rapko and Lumetta 2000). For example, Temer and Villareal (1997, 1995, and 1996) used XRD to identify sodium diuranate ($\text{Na}_2\text{U}_2\text{O}_7$) in sludge samples from Hanford Tanks BX-103, BX-105, and BX-109, respectively. Herting et al. (2002) observed using SEM(bse)/EDS a “sodium/uranium-particulate” in saltcake from Hanford Tank BY-109 and in residues from water and NaOH washing of saltcake from Hanford Tank S-112. Their XRD analysis of these samples indicated that the uranium phase was $\text{Na}_2\text{U}_2\text{O}_7$. The SEM images and EDS spectra for the “sodium/uranium-particulate” are shown in Herting et al. (2002) (Figures 3.8.2-1 through 3.8.2-4) for the Tank BY-109 saltcake and in Herting et al. (2002) (Figures 3.8.3-1 through 3.8.3-2) for Tank S-112 saltcake residue. Like the EDS spectra measured for uranium-containing particles in our study of unleached BX-101 (jar 16503) sludge, the EDS spectra reported by Herting et al. (2002) (Figures 3.8.2-2, 3.8.2-4, and 3.8.3-2) also contain detectable concentrations of aluminum. However, the SEM images given for the “sodium/uranium-particulate” by Herting et al. (2002) (Figures 3.8.2-1, 3.8.2-3, and 3.8.3-1) do not closely resemble those for the uranium/sodium-rich phase detected in our study of unleached BX-101 (jar 16503) sludge. In two SEM images in Herting et al. (2002) (Figures 3.8.2-1 and 3.8.3-1), the “sodium/uranium-particulate” looks like a single sphere approximately 5 to 7 μm in diameter composed of intersecting platelets radiating from the center of the sphere. In the third SEM image (Herting et al. 2002) (Figure 3.8.2-3), the “sodium/uranium-particulate” is approximately 20 μm in diameter, and has generally an anhedral, indeterminate form. At the submicrometer scale, the particle in Figure 3.8.2-3 in Herting et al. (2002) appears possibly to be an aggregate of rounded platelets intergrown and stacked in the plane of the SEM image. These are the only SEM images and EDS spectra that have been reported in the published literature for an uranium/sodium-rich phase identified as $\text{Na}_2\text{U}_2\text{O}_7$ in Hanford tank-related waste materials.

The results of tank solution simulant experiments pertinent to Hanford storage tank wastes also suggest that uranium may be immobilized as a sodium uranate phase in the tank waste. Experiments reported by Traina et al. (2001) showed that mixing 10^{-3} M UO_2^{2+} in a NaOH solution resulted in precipitation of yellow solid that they identified as “ $\text{Na}_2\text{U}_2\text{O}_7$ (clarkeite)” by XRD. Their study indicated that the $\text{Na}_2\text{U}_2\text{O}_7$ phase was stable at high pH conditions and high sodium concentrations, and resulted in a decrease of >99.5% of the initial concentrations of dissolved uranium. The morphology of an “ $\text{Na}_2\text{U}_2\text{O}_7$

(clarkeite)” particle shown in an SEM micrograph in Traina et al. (2001, Figure 2A) is very nondescript and unlike the uranium/sodium particles that we observed in the unleached BX-101 (jar 16503) sludge samples by SEM/EDS. The summary progress report by Traina et al. (2001) does not provide any additional details regarding their XRD analysis of this uranium precipitate and the XRD database pattern(s) used to identify the “ $\text{Na}_2\text{U}_2\text{O}_7$ (clarkeite)” phase. Clarkeite is isostructural with $\text{Na}_2\text{U}_2\text{O}_7$ and $\text{Na}_6\text{U}_7\text{O}_{24}$, and is therefore difficult to distinguish using XRD (Finch and Ewing 1997). Based on new chemical and structural data, Finch and Ewing (1997) suggest that the “ideal formula for the ideal end-member” clarkeite is $\text{Na}[(\text{UO}_2)\text{O}(\text{OH})](\text{H}_2\text{O})_{0-1}$.

3.4 XAS Results – AY-102 Drainable Liquid

The shape of technetium XANES spectrum of tank AY-102 drainable liquid is compared to Tc(VII) (pertechnetate), Tc(V), and Tc(IV) standards in Figure 3-73. A pre-edge feature, identified in the AY-102 sample, is only found in Tc(V) and Tc(VII) standards. This pre-edge feature results from $1s \rightarrow 4d$ electronic transitions which are electric dipole forbidden in compounds with centrosymmetric site

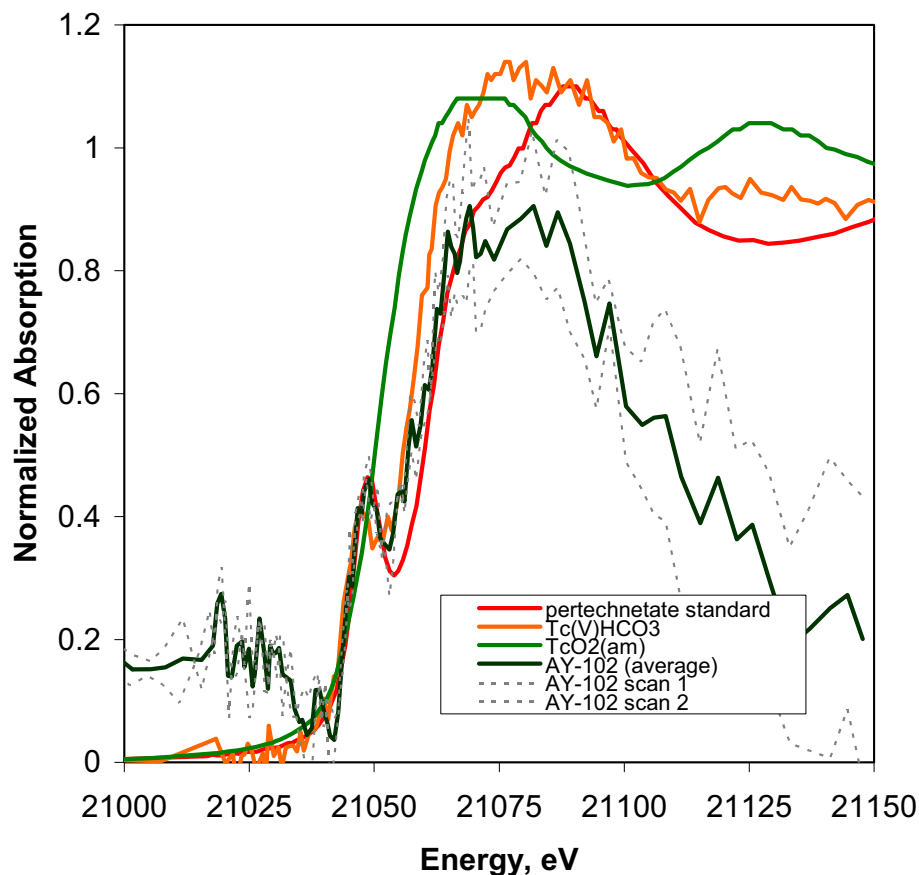


Figure 3-73. Technetium K-edge XANES spectra. The XANES of the drainable liquid from tank AY-102 is compared to a pertechnetate standard, Tc(V)-bicarbonate solution complex, and Tc(IV) amorphous solid sample.

symmetries. This feature is observed in the Tc(VII) and Tc(V) standards, because Tc(VII)O_4^- and Tc(V) compounds are nonscentrosymmetric with tetrahedral and square pyramidal or pentagonal pyramidal site symmetries, respectively. In centrosymmetric compounds $1s \rightarrow 4d$ electronic transitions can be weakly observed if the bound state is a de-localized molecular orbital and has p-orbital contributions from nearest neighbor atoms. In addition, although not apparent in Figure 3-73 due to the energy scale, the energy of the absorption edge shifts to higher value with increasing oxidation state of Tc. While the signal-to-noise ratio of the AY-102 sample is quite low, the shape of the XANES profile and the energy of the absorption pre-edge show a close correspondence to both the pertechnetate standard and the Tc(V) bicarbonate solution. This suggests that the technetium oxidation state in the drainable liquid is either Tc(VII) or Tc(V), but clearly not Tc(IV). The definitive distinction between Tc(VII) and Tc(V) oxidation states would be possible if XANES spectra with higher signal-to-noise ratio were available for both the drainable liquid samples and the Tc(V) standard.

3.5 Tier 1 Results – BX-101

The results of Tier 1 testing of sludge samples from tank BX-101 are discussed in this section. In some cases, comparisons are made with Tier 1 tests conducted on samples of sludge from tank AY-102. Tier 1 testing of AY-102 samples is documented in Lindberg and Deutsch (2003).

3.5.1 Digestion Factors and Moisture Contents

The digestion factors for BX-101 sludge samples used for water and acid extractions are listed in Table 3-24. These digestion factors are the ratios of wet weight of sludge to volume of extractant used to dissolve the soluble portion of the solid. The digestion factors were then multiplied by the percent solids, as determined from moisture content analysis, to convert to a dry weight basis. The variability is a

Table 3-24. Preparation data and moisture content

Sample Number	Preparation Type	Dry Weight Corrected Digest Factor (g/L)
S02T001253	Water Extract	10.85
S02T001253 DUP	Water Extract	9.85
S02T001254	Water Extract	20.88
S02T001255	Water Extract	6.47
S02T001253	Acid Extract	8.35
S02T001253 DUP	Acid Extract	4.48
S02T001254	Acid Extract	12.41
S02T001255	Acid Extract	5.57
Sample Number	Preparation Type	% Moisture
S02T001253	Moisture Content	2.82
S02T001253 DUP	Moisture Content	3.56
S02T001254	Moisture Content	4.17
S02T001255	Moisture Content	5.73

function of the mass of sludge used, which ranged from approximately 0.3 to 0.6 g. For the water extracts, 30 mL of DDI water was used, and for the acid extracts, 50 mL of acid was used.

The moisture contents listed in Table 3-24 show that the sludge samples were very dry. It is likely that much of the water initially in the sludge samples collected from the tank in 1994 would have evaporated during storage of the samples in the hot cells in the 222-S Laboratory.

3.5.2 Water Extract pH and Alkalinity

The pH values of the water extracts of the sludge samples are listed in Table 3-25. The high pH values are associated with neutralization of tank wastes with NaOH to minimize corrosion of the carbon steel tank liner.

Table 3-25. Water extract pH values

Sample Number	pH
S02T001253	10.08
S02T001253 DUP	10.12
S02T001254	9.70
S02T001255	9.94

The alkalinities of the sludge samples are listed in Table 3-26. These alkalinities were measured for the water extract samples of the sludge and, therefore, represent the water-soluble, acid neutralizing ability of the solids. Alkalinity is reported in terms of equivalent CaCO₃ content at pH values of 8.3 and 4.5. The digestion factors and moisture contents (Table 3-24) were used to convert concentrations in solution to a per gram of dry solid basis.

Table 3-26. Alkalinities from water extracts

Sample Number	Alkalinity CaCO ₃ at pH 8.3 Endpoint	Total Alkalinity CaCO ₃ at pH 4.5 Endpoint	Alkalinity CaCO ₃ at pH 8.3 Endpoint	Total Alkalinity CaCO ₃ at pH 4.5 Endpoint
	----- mg/L -----		----- mg/g -----	
S02T001253	222	713	21	68
S02T001253 DUP	166	570	18	60
S02T001254	444	1,402	22	70
S02T001255	253	618	42	101
PREP-BLK	0	5	0	5

“PREP-BLK” refers to the preparation blank sample which was used to monitor contamination resulting from the sample preparation process. The “PREP-BLK” sample was prepared from deionized water that was subjected to the same processing as the samples, including all reagent additions.

3.5.3 Technetium-99 and Uranium-238 – Water and Acid Extracts

Technetium-99 and uranium-238 are two of the more important potential long-term risk constituents of tank sludge because of their long half-lives and high mobility once dissolved in water. Table 3-27 lists the concentrations of these two radionuclides in units of $\mu\text{g/g}$ -solid and pCi/g -solid for the water and acid extracts. A comparison of the water extract concentrations with the acid extract concentrations shows that approximately 100% of the technetium-99 and 4.5% to 8.9% of the uranium-238 in the solid is water soluble (Table 3-28). (This assumes that the acid extraction method removes all of the radionuclide from the solid.) Table 3-28 also includes calculated water leachable percentages of technetium-99 and uranium-238 for Tier 1 testing of sludge from tank AY-102 reported in Lindberg and Deutsch (2003). In the case of tank AY-102, only about 20% of the technetium-99 was water leachable whereas most (65% and 90%) of the uranium-238 was water leachable. This is opposite of the pattern for tank BX-101, and shows the variability in mobile contaminant sources from these two tanks.

Table 3-27. Technetium-99 and uranium-238 concentrations in BX-101 sludge from water and acid extracts

Sample Number	Tc-99	U-238	Tc-99	U-238
	----- $\mu\text{g/g}$ -----		----- pCi/g -----	
Water Leach				
S02T001253 WE	1.95	2.97E+03	3.31E+04	1.00E+03
S02T001253 DUP WE	2.22	2.69E+03	3.76E+04	9.05E+02
S02T001254 WE	3.02	2.91E+03	5.13E+04	9.78E+02
S02T001255 WE	2.89	2.90E+03	4.90E+04	9.76E+02
Acid Extract				
S02T001253 AE	1.68	4.03E+04	2.86E+04	1.35E+04
S02T001253 DUP AE	1.91	4.49E+04	3.23E+04	1.51E+04
S02T001254 AE	2.57	3.26E+04	4.37E+04	1.10E+04
S02T001255 AE	3.18	6.50E+04	5.39E+04	2.19E+04

Table 3-28. Water leachable percentages of technetium-99 and uranium-238 in BX-101 and AY-102 sludge samples

Sample Number	Tc-99	U-238
	Percent Water Leachable	
S02T001253 WE (BX-101)	116	7.3
S02T001253 DUP WE (BX-101)	116	6.0
S02T001254 WE (BX-101)	118	8.9
S02T001255 WE (BX-101)	91	4.5
AY-102 15935 WE	21	90
AY-102 18686 WE	20	65

3.5.4 Selected Metal Concentrations – Water and Acid Extracts

Metals detected at measurable concentrations in one or more samples in the water extracts or the acid extracts are listed in Table 3-29. A discussion of the meaning of the less than values (<) and the values in parentheses is provided in Section 3.1. The acid extracts show that aluminum, sodium, iron, manganese, and chromium are the dominant metals present in the BX-101 sludge. The water extracts show that sodium and chromium are the primary water soluble constituents. Phosphorus is present at low concentrations in the solid, but it is also very water soluble.

Table 3-29. Metal concentrations in BX-101 sludge – ICP-OES analysis

Sample Number	Al	Ba	Cd	Cr	Fe	Mn	Ni	P	Na
	----- µg/g -----								
Water Leach									
S02T001253-WE	(149)	107	<142	6,247	(119)	(8)	(6)	1,181	132,242
S02T001253-Dup-WE	(171)	150	<158	2,176	163	(7)	(12)	535	59,529
S02T001254-WE	(91)	262	229	1,046	118	(4)	(3)	290	26,657
S02T001255-WE	(418)	242	<246	2,639	254	(15)	(7)	629	77,378
AY-102 15935 WE (avg)	2,165	(504)	(152)	(359)	(728)	(186)	(922)	(6,980)	97,270
AY-102 18686 WE (avg)	2,968	(141)	(74)	(338)	(848)	(90)	(612)	(2817)	45,640
Acid Extract									
S02T001253-AE	174,764	178	(49)	5,704	16,844	9,382	264	914	54,525
S02T001253-Dup-AE	214,690	268	1,479	6,727	19,853	10,893	348	1,055	65,176
S02T001254-AE	159,455	167	1,220	9,028	19,529	15,136	417	1,443	96,273
S02T001255-AE	155,930	301	562	9,422	10,136	12,443	326	1,394	127,553
AY-102 15935 AE (avg)	121,000	(1,390)	(462)	(5,770)	141,000	70,900	9,560	5,130	213,000
AY-102 18686 AE	91,200	(1,280)	(167)	(3,300)	116,000	25,700	4,180	1,630	123,000

Table 3-29 also provides the water and acid extractable metals concentrations for sludge samples of tank AY-102 reported in Lindberg and Deutsch (2003). Although the water leachable concentrations for the two tank samples are similar for most of the compounds, it is apparent from the acid extractable concentrations that AY-102 has much higher concentrations of iron (8x), manganese (4x), nickel (20x) and sodium (2x). The aluminum concentration in tank AY-102 is less by a factor of about 1.7 than the concentration in BX-101 sludge. It is possible that the recalcitrant technetium-99 in tank AY-102 is associated with these metals with the most likely candidates being iron and manganese oxide/hydroxide. Iron and manganese are present at high concentrations in AY-102, their solids have strong adsorption properties, and they are resistant to water dissolution.

3.5.5 Anion Concentrations – Water Extracts

The anion concentrations in the BX-101 sludge samples as estimated from the concentrations in the water extracts are listed in Table 3-30. The primary anions are carbonate, nitrate, and nitrite with all other

anions at least a factor of ten lower in concentration. The carbonate concentrations closely track the water extract alkalinity values (Table 3-26). The majority of the alkalinity is due to dissolved carbonate and bicarbonate. The relatively high concentrations of nitrite in the water extracts (23,600 to 31,680 µg/g) and presence of organic acids (acetate, formate, and oxalate) show that the sludge has the capacity to act as a reductant for more oxidized species.

Table 3-30. Anion concentrations in BX-101 sludge from water extracts

Sample Number	Fluoride	Acetate	Formate	Chloride	Nitrite	Nitrate	Carbonate	Sulfate	Oxalate	Phosphate
	----- µg/g -----									
S02T001253	141	756	107	993	23,600	37,990	51,600	1,460	839	1,230
S02T001253 DUP 1-100	84	519	119	1,080	28,750	41,160	47,750	1,520	852	1,440
S02T001254	489	1,170	62	1,750	31,680	46,990	56,200	2,310	3,540	1,200
S02T001255	<46	1,130	825	1,580	28,180	54,225	92,800	1,790	2,640	1,620

3.5.6 BX-101 Tier 1 Radioanalytical Results

The results of the GEA analysis of raw sludge and the water and acid extracts of the sludge for cobalt-60, cesium-137, europium-154, and europium-155 are listed in Table 3-31. Comparing the results of the sludge to acid extract values, these results show that acid extraction is a reasonably good method of removing these radionuclides from this sludge material. Comparing the cesium-137 water extract results with those for the sludge and acid extracts shows that 14% to 89% of the cesium is released into water.

Table 3-31. BX-101 Gamma Energy Analysis

Sample Number	Co-60	Cs-137	Eu-154	Eu-155
	----- pCi/g -----			
Sludge				
S02T001253	ND	4.83E+07	4.98E+05	ND
S02T001254	1.81E+04	1.59E+08	1.16E+06	5.98E+05
S02T001255	ND	1.44E+08	5.55E+05	ND
Water Extract				
S02T001253_WE	ND	2.70E+07	ND	ND
S02T001253Dup_WE	ND	2.90E+07	ND	ND
S02T001254_WE	ND	2.15E+07	ND	ND
S02T001255_WE	ND	6.11E+07	ND	ND
Acid Extract				
S02T001253_AE	ND	3.03E+07	3.82E+05	6.01E+06
S02T001253_AE_Dup	ND	3.50E+07	3.98E+05	4.48E+06
S02T001254_AE	1.52E+04	8.78E+07	6.82E+05	5.77E+06
S02T001255_AE	ND	9.78E+07	4.51E+05	ND

Gross alpha and gross beta levels for the water leach and acid extractions are listed in Table 3-32. These results show that approximately 10% of the gross alpha and 25% of the gross beta are water leachable.

Table 3-32. BX-101 Gross Alpha and Beta Analysis from water and acid extracts

Sample Number	Gross Alpha	Gross Beta
	----- pCi/g -----	
Water Leach		
S02T001253_WE	1.087E+07	1.492E+08
S02T001253DUP_WE	1.220E+07	1.705E+08
S02T001254_WE	1.607E+07	2.302E+08
S02T001255_WE	2.011E+07	3.154E+08
Acid Extract		
S02T001253_AE	9.558E+07	5.617E+08
S02T001253Dup_AE	8.359E+07	6.845E+08
S02T001254_AE	2.821E+08	1.243E+09
S02T001255_AE	1.396E+08	8.581E+08

3.6 Periodic Replenishment Test Results – AY-102

The water leachable percentages of several radionuclides of interest measured in the replenishment tests are listed in Table 3-33. These results show that the majority of the water leachable proportion of

Table 3-33. Percentages of radionuclides in Tank AY-102 sludge that are soluble in sequential water leaches (relative to the amount leachable by acid digestion of the sludge)

Sample and Contact Duration	Sludge Sample	Water Leachable (%)			
		Tc-99	U-238	Am-241	Pu-239
Sample 1 - 1 Day	15935-1	23.83	79.29	0.51	0.89
	15935-1 dup	24.57	83.50	0.42	0.88
Sample 2 - 2 Days	15935-1	0.76	0.83	0.39	0.28
	15935-1 dup	0.48	0.68	0.41	0.25
Sample 3 - 3 Days	15935-1	0.25	0.22	0.23	0.23
	15935-1 dup	0.23	0.19	0.23	0.17
Sample 4 - 3 Days	15935-1	0.16	0.14	0.20	0.22
	15935-1 dup	0.18	0.12	0.24	0.20
Sample 5 - 4 Days	15935-1	0.18	0.12	0.15	0.16
	15935-1 dup	0.18	0.10	0.19	0.18
Total 15935-1		25.19	80.61	1.48	1.78
Total 15935-1DUP		25.65	84.59	1.51	1.68

technetium-99 and uranium-238 are present as readily soluble materials that dissolve into the initial water contacting the sludge. After this initial contact, very little of these residual radionuclides are water leachable. For americium-241 and plutonium-239, the leachable amount is somewhat elevated in the initial solution, but, in general, these radionuclides in AY-102 sludge are not water soluble.

The water leachable percentages of dissolved metals measured in the replenishment tests are listed in Table 3-34. Approximately 50% of the sodium is water leachable in the initial contact water and over 65% is leachable after five consecutive contacts. The other four metals listed in Table 3-34 (aluminum, chromium, iron and manganese) are not very water leachable from AY-102 sludge.

Table 3-34. Percentages of metals in Tank AY-102 sludge that are soluble in sequential water leaches (relative to the amount leachable by acid digestion of the sludge)

Sample and Contact Duration	Sludge Sample	Water Leachable (%)				
		Al	Cr	Fe	Mn	Na
Sample 1 - 1 Day	15935-1	1.20	1.69	0.23	0.38	51.49
	15935-1 dup	0.78	1.58	0.24	0.34	51.35
Sample 2 - 2 Days	15935-1	1.30	0.68	0.13	0.27	6.42
	15935-1 dup	1.07	0.62	0.16	0.29	5.36
Sample 3 - 3 Days	15935-1	1.12	0.58	0.10	0.16	3.41
	15935-1 dup	0.90	0.48	0.07	0.17	3.20
Sample 4 - 3 Days	15935-1	1.18	0.35	0.08	0.14	2.35
	15935-1 dup	1.00	0.35	0.08	0.18	2.19
Sample 5 - 4 Days	15935-1	1.25	0.23	0.06	0.12	2.07
	15935-1 dup	1.06	0.25	0.08	0.15	1.86
Total 15935-1		6.06	3.54	0.61	1.07	65.75
Total 15935-1DUP		4.80	3.28	0.64	1.13	63.96

3.7 Selective Extraction Results – AY-102

Results for the first set of Tier 2 selective extractions are shown in Table 3-35. The pH of the initial extraction solutions along with those of the extractions after one day of contact are shown along with the percentage release of technetium-99, aluminum and iron. The percent release is relative to that determined by acid digestion (EPA 2000, Method 3050B) based on the average of four measurements conducted on sludge sample 15935. Two of these results were presented in Lindberg and Deutsch (2003); the other two are presented elsewhere in this document. These average total concentrations are $4.0 \pm 1.0 \mu\text{g/g}$ for technetium-99, $1.06 \pm 0.20 \times 10^5 \mu\text{g/g}$ for aluminum, and $1.35 \pm 0.13 \times 10^5 \mu\text{g/g}$ for iron.

As can be seen from these results, approximately 15% of the technetium-99 is removed during the first extraction with the NaHCO_3/Al solution. Only minor amounts of technetium-99 were removed during subsequent extractions with the NaHCO_3/Al solution and the acetate buffer. These results suggest

that the readily soluble technetium-99 is not associated with dawsonite, but that it precipitated along with other readily soluble salts such as NaNO_3 , that precipitated when the sludge was dried.

Table 3-35. Selective extraction results for a NaHCO_3/Al extractant solution followed by an acetate buffer solution (sludge sample 15935)

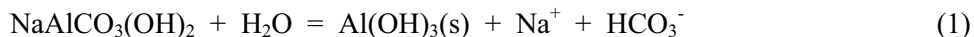
Sample Number	Extractant	pH	Tc-99 (% AE)	Al (% AE)	Fe (% AE)
Initial Soln	NaHCO_3/Al	8.57			
Initial Soln	Acetate Buffer	4.52			
SE-1 Day 1	NaHCO_3/Al	10.05	13.9	0.3	0.10
SE-1 Dup Day 1	NaHCO_3/Al	9.94	14.5	0.3	0.23
SE-1 Day 2	NaHCO_3/Al	9.34	0.4	0.1	0.04
SE-1 Dup Day 2	NaHCO_3/Al	9.27	0.2	0.2	0.07
SE-1 Day 3	Acetate Buffer	4.74	0.9	10.7	0.06
SE-1 Dup Day 3	Acetate Buffer	4.71	0.9	11.5	0.04
SE-1 Day 4	Acetate Buffer	4.63	0.3	2.0	0.04
SE-1 Dup Day 4	Acetate Buffer	4.67	0.3	1.9	0.02
Total (Ave)			15.7	13.5	0.3

Results for the second set of Tier 2 selective extractions are shown in Table 3-36. The release of technetium-99 by the acetate buffer is similar to that released by the NaHCO_3/Al solution in the previous set of sequential extraction experiments. This is consistent with expectations because in this case the

Table 3-36. Selective extraction results for a sequence of extractions starting with an acetate buffer, followed by a formate buffer, and then 8 M HNO_3 (sludge sample AY-102 [15935])

Sample Number	Extractant	pH	Tc-99 (% AE)	Al (% AE)	Fe (% AE)
Initial Soln	Acetate Buffer	4.52			
Initial Soln	Formate Buffer	3.51			
SE-2 Day 1	Acetate Buffer	5.03	10.5	5.5	0.0
SE-2 Dup Day 1	Acetate Buffer	5.01	13.7	5.8	0.0
SE-2 Day 2	Acetate Buffer	4.66	0.4	2.0	0.0
SE-2 Dup Day 2	Acetate Buffer	4.65	0.4	1.9	0.1
SE-2 Day 3	Formate Buffer	3.69	0.7	6.9	0.1
SE-2 Dup Day 3	Formate Buffer	3.69	0.6	7.1	0.0
SE-2 Day 4	Formate Buffer	3.63	0.7	4.0	0.0
SE-2 Dup Day 4	Formate Buffer	3.65	0.7	4.7	0.0
SE-2 Day 5	Formate Buffer	3.68	1.1	5.9	0.0
SE-2 Dup Day 5	Formate Buffer	3.67	1.2	6.1	0.0
SE-2 Day 6	8 M HNO_3	NA*	32.9	32.0	32.6
SE-2 Dup Day 6	8 M HNO_3	NA*	34.3	34.0	34.0
Total (Ave)			48.5	58.0	33.5

acetate buffer would be expected to remove any readily-soluble salts along with dawsonite. A somewhat unexpected result is that approximately 6% of the aluminum was dissolved by the first extraction with the acetate buffer. At this pH (at equilibrium), the dawsonite was expected to dissolve incongruently to form gibbsite as in the following equation:



A better explanation of the observed results appears to be congruent dissolution of dawsonite followed by slow precipitation of gibbsite, such that the aluminum remains in solution for more than one day.

During the formate buffer extractions, the total amount of aluminum that dissolved was approximately 17%. At equilibrium, all the aluminum would be expected to dissolve in this buffer solution if it occurs in the sludge as an aluminum oxyhydroxide phase. Two possible reasons could explain the low degree of aluminum dissolution. One possibility is slow dissolution kinetics, with equilibrium requiring significantly longer than one day. Another possible explanation is that aluminum occurs as a more insoluble aluminosilicate phase; however, this explanation seems unlikely because the sludge contains only 0.5 ± 0.7 % silicon (by acid digestion) or 2.8 % as determined by fusion. Along with the 17% of the aluminum that dissolved in the formate buffer extracts, 2.5% of the technetium-99 dissolved.

During the 8 M HNO_3 extraction step, only approximately 34% of the iron dissolved, and an additional 33% of the aluminum dissolved. Along with the iron, approximately 34% of the technetium-99 in the sludge was released. These results suggest that most of the refractory technetium-99 in the sludge is associated with iron hydroxides/oxides. However, association of technetium-99 with aluminum hydroxides/oxides cannot be discounted. These results also indicate that a one day extraction with 8 M HNO_3 is significantly less effective at dissolving the aluminum and iron phases in the sludge than the acid digestion procedure (EPA 2000, Method 3050B). Briefly, in Method 3050B the sample is digested with 8 M HNO_3 at $95 \pm 5^\circ\text{C}$ for 10 to 15 minutes, followed by addition of concentrated HNO_3 and refluxing until no further oxidation of the sample is observed. After this, 30% H_2O_2 is added to the sample and it is heated at $95 \pm 5^\circ\text{C}$ for an additional 2 hours. This more vigorous digestion process apparently dissolved significantly more of the iron- and aluminum-containing phases than is achieved with 8 M HNO_3 alone at room temperature.

3.8 Oxidation Test Results – AY-102 and BX-101

Results of the batch oxidation leaches (see Section 2.9) are compiled in Table 3-37. The cumulative percentage of technetium extracted is relative to that determined by extraction with the acid digestion procedure (EPA 2000, Method 3050B). For sample AY-102 (jar 15935), the cumulative percentage of technetium-99 that was extracted was 20%. This is essentially the same as that determined through water extraction. This indicates that oxidative leaching of AY-102 (jar 15935) sludge does not mobilize any more technetium-99 than is mobilized by water extraction. Results for BX-101 (jar 16503) are also consistent with the water extraction results. In this case, the cumulative technetium-99 extracted was 121% of that determined through 8 M nitric acid extraction. This higher value is likely the result of a combination of sample heterogeneity and analytical error.

Table 3-37. Batch oxidation leach results

Tank Sludge	Sample Number	Vol. H ₂ O ₂ (mL)	Extraction Time (Days)	Tc Extracted (µg/g)	Final pH	Cumulative Percent Tc Extracted
AY-102	15935	30	1	0.74	9.5	15
	15935	40	1	0.13	8.0	18
	15935	40	5	0.12	7.0	20
BX-101	16503	25	1	2.98	9.5	116
	16503	40	1	0.10	8.0	120
	16503	40	5	0.04	8.0	121

Subsequent total organic carbon (TOC) analysis of the AY-102 sludge from the batch oxidation leach experiments indicate that 30% of the TOC in the sludge was removed by the H₂O₂ oxidation treatment. This suggests that the organic carbon and any reduced technetium contained within the sludges may not have been completely oxidized; however, it does not imply that the technetium is necessarily associated with the organic carbon. As discussed above (Section 3.7), the technetium is likely associated with the metal oxyhydroxide solids in the sludge.

3.9 Reduction Capacity Test Results – AY-102 and BX-101

For sample AY-102 (jar 15935), the reduction capacity was determined to be 28 µeq/g sludge. This suggests that the sludge has very little reduction capacity. For example, the sample AY-102 (jar 15935), sludge contains an average of 14% by weight of iron. If 1% of the iron was reduced, ferrous iron, then this would result in a reduction capacity of 25 µeq/g sludge. Sample AY-102 (jar 15935) also contains 1.8×10^3 µg TOC/g sludge. If this organic carbon is assumed to occur as oxalate that acts as a reductant, this would be equivalent to a reducing capacity of 150 µeq/g sludge. The low reduction capacity measured using the chromate method suggests that the organic carbon is recalcitrant and not readily susceptible to oxidation.

For sample BX-101 (jar 16503), the reduction capacity was found to be negative. This indicates that the final concentration of chromate in the solution in contact with the sludge was higher than the amount of chromate added. The additional chromate concentrations resulted from dissolved chromate that was initially sorbed to the sludge. Because of this negative number, the experiment was repeated in duplicate. The average of the three sample results was -119 µeq/g sludge indicating no apparent reducing capacity for this material.

4.0 Conclusions

This report provides the results of laboratory tests on sludge samples from Hanford tanks AY-102 and BX-101 and supernatant from tank AY-102. The major conclusions from these tests are:

- Leaching tests of sludge from tank AY-102 that showed that only 25% of the technetium-99 and greater than 60% of the uranium-238 was water leachable. Leach tests of sludge from BX-101 show that all of the technetium-99 but less than 10% of the uranium-238 is water leachable.
- Comparison of the fusion method with the acid extraction method of quantifying metals and radionuclides in tank AY-102 sludge samples showed that acid extraction was an effective method for most of the components of the solid phase. Elements apparently not fully extracted by the acid method were silicon, boron, selenium, copper, arsenic, and bismuth. The acid extraction method resulted in significantly higher concentrations (>20%) of phosphorous, nickel, lithium, and strontium compared to the fusion method.
- XRD analysis showed a significant difference in the mineralogy of the sludge solids for tanks AY-102 and BX-101. The minerals identified in AY-102 sludge were dawsonite, hematite, gibbsite, and cancrinite (tentative), whereas BX-101 sludge contained only gibbsite and cancrinite (trace). The presence of hematite in AY-102 sludge may explain the occurrence of less mobile technetium-99 in this tank compared to BX-101. That is, a significant portion of the technetium-99 may be incorporated into the hematite mineral structure and tightly sequestered when in contact with water.
- SEM/EDS analysis of AY-102 sludge indicated the presence of several solid phases not detected by XRD. These solids included Na,Al,Si-rich particles; Na-rich particles; Ag-containing particles; U,Na-containing particles; and large carbon-rich particles. If any of these phases were crystalline, then they were present at levels below the detection limit (about 5%) of XRD analysis. Many of these phases were removed by water leaching of the AY-102 sludge. These phases may represent precipitates from supernatant or pore water that evaporated during long-term (~10 years) storage of the sludge.
- SEM/EDS analysis of BX-101 sludge showed the presence of three aluminum-rich crystalline phases with the predominant phase having a composition and morphology consistent with gibbsite. In addition, uranium-containing phases were common in this sludge. This is consistent with the high total uranium concentration (several weight percent [Table 3-27]) for this sludge. It was not possible to determine if these uranium-containing phases were crystalline or amorphous, because the SEM micrographs of these particles did not indicate any obvious crystal faces and the XRD results did not identify any uranium phases.
- Although the sludge has relatively high concentrations of reduced compounds (nitrite and organic anions), technetium in the drainable liquid from AY-102 was shown by XANES analysis to be either in the oxidized pertechnetate [Tc(VII)] or Tc(V) valence states, but not as reduced Tc(IV).

- The predominant metals in BX-101 sludge are aluminum, sodium, uranium-238, iron, manganese, and chromium. The predominant anions are carbonate/bicarbonate, nitrate, nitrite, sulfate, phosphate, and oxalate.
- Sludge from AY-102 has much higher concentrations of iron (8x), manganese(4x), nickel (20x), and sodium (2x) than sludge from BX-101. On the other hand, sludge from BX-101 has higher aluminum (1.7x) and uranium-238 (31x) concentrations.
- Periodic replenishment water leach tests of AY-102 sludge showed that the majority of the leachable technetium-99 and uranium-238 is present in very soluble sodium-salts that dissolve during the first water contact. However, most (75%) of the technetium-99 in AY-102 sludge is not water leachable.
- Selective extraction tests of AY-102 sludge suggest that most of the recalcitrant technetium-99 is associated with iron (and possibly aluminum) oxyhydroxide phases that were not completely soluble in strong acid (8 M HNO₃) solutions.
- AY-102 sludge has a very low reduction capacity (28 µeq/g-sludge) and oxidation of the sludge does not enhance the removal of technetium-99 from the solid. There was no measurable reduction capacity for the BX-101 sludge sample.

5.0 References

- ASTM. 1998. *D2216-98 Standard Test Method for Laboratory Determination of Water (Moisture) Content of Soil and Rock by Mass*. American Society for Testing and Materials, West Conshohocken, Pennsylvania.
- ASTM. 1999. *D3987-85 Standard Test Method for Shake Extraction of Solid Waste with Water*. American Society for Testing and Materials, West Conshohocken, Pennsylvania.
- Bechtold, DB, GA Cooke, DL Herting, JC Person, RS Viswanath, and RW Warant. 2003. *Laboratory Testing of Oxalic Acid Dissolution of Tank 241-C-106 Sludge*. RPP-17158, Rev. 0, Fluor Hanford, Inc., Richland, Washington.
- Bickmore, BR, KL Nagy, JS Young, and JW Drexler. 2001. "Nitrate-Cancrinite Precipitation on Quartz Sand in Simulated Hanford Tank Solutions." *Environmental Science and Technology* 35(22):4481-4486.
- Blanchard, DL, Jr, GN Brown, SD Conradson, SK Fadeff, GR Golcar, NJ Hess, GS Klinger, and DE Kurath. 1997. *Technetium in Alkaline, High-Salt, Radioactive Tank Waste Supernate: Preliminary Characterization and Removal*. PNNL-11386, Pacific Northwest National Laboratory, Richland, Washington.
- Bredt, PR, BK McNamara, BW Arey, AP Poloski, EC Buck, RG Swoboda, and ED Jenson. 2003. *Rheological and Physical Properties of AP-101 LAW Pretreated Waste and Melter Feed*. PNWD-3279 (WTP-RPT-064, Rev. 0), prepared by Battelle – Pacific Northwest Division for Bechtel National, Inc., Richland, Washington.
- Brown, GE, Jr, G Calas, GA Waychunas, and J Petiau. 1988. "X-ray Absorption Spectroscopy: Applications in Mineralogy and Geochemistry." In *Reviews in Mineralogy*, Volume 18, of *Spectroscopic Methods in Mineralogy and Geology*, FC Hawthorne (ed.), pp. 431-512, Mineralogical Society of America, Washington, D.C.
- Clesceri, LS, AE Greenberg, and AD Eaton. 1998. *Standard Methods for the Examination of Water and Wastewater*, 20th Edition. American Public Health Association, American Water Works Association, and Water Environment Federation, Washington, D.C.
- De Lorenzo, DS, AT DiCenso, DB Hiller, KW Johnson, JH Rutherford, DJ Smith, and BC Simpson. 1994. *Tank Characterization Reference Guide*. WHC-SD-WM-TI-648 REV 0, prepared by Los Alamos Technical Associates for Westinghouse Hanford Company, Richland, Washington.
- Deer, WA, RA Howie, and J Zussman. 1967. *Rock-Forming Minerals. Vol. 5. Non-Silicates*. Longmans, London, England.

EPA (U.S. Environmental Protection Agency). 2000. "Method 3050B. Acid Digestion of Sediments, Sludges, and Soils. Revision 2 (December 1996)." In *Test Methods for Evaluating Solid Wastes: Physical/Chemical Methods*. EPA SW-846, Third Edition, Volume I, Section A, Chapter 3, pp. 3050B-1–3050B-12. U.S. Environmental Protection Agency, Office of Solid Waste and Emergency Response, Washington, D.C. Available at <http://www.epa.gov/epaoswer/hazwaste/test/pdfs/3050b.pdf>

Ferrante, MJ, JM Stuve, and DW Richardson. 1976. *Thermodynamic Data for Synthetic Dawsonite*. U.S. Bureau of Mines Report Investigation 8129, U.S. Bureau of Mines, Washington, D.C.

Finch, RJ and RC Ewing. 1997. "Clarkeite: New Chemical and Structural Data." *American Mineralogist* 82:607-619.

Fiskum, SK, CJ Barinaga, JP Bramson, KJ Carson, JR DesChane, OT Farmer, LR Greenwood, FV Hoopes, RT Ratner, DR Sanders, MJ Steele, RT Steele, CZ Soderquist, RG Swoboda, KK Thomas, TL Trang-Le, MW Urie, and JJ Wagner. 2000. *Inorganic and Radiochemical Analysis of 241-C-104 Tank Waste*. PNNL-13364 (WTP-RPT-007-Rev. 0) (formerly BNFL-RPT-043), prepared by Pacific Northwest National Laboratory for CH2M HILL Hanford Group, Inc., Richland, Washington.

Herting, DL, RW Warrant, and GA Cooke. 2002. *Identification of Solid Phases in Saltcake from Hanford Site Waste Tanks*. HNF-11585, Rev. 0 (HNF-EDC-02-12376), Fluor Hanford, Inc., Richland, Washington.

Kopunec, R, FN Abudeab, and S Skrašková. 1998. "Extraction of Pertechetate with Tetraphenylphosphonium in the Presence of Various Acids, Salts, and Hydroxides." *Journal of Radioanalytical and Nuclear Chemistry* 230(1-2):51-60.

Lee, W and B Batchelor. 2003. "Reductive Capacity of Natural Reductants." *Environmental Science and Technology* 37:535-541.

Lee, W, B Batchelor, and MA Schlautman. 2000. "Reductive Capacity of Soils for Chromium." *Environmental Technology* 21(8):953-963.

Lindberg, MJ and WJ Deutsch. 2003. *Tank 241-AY-102 Data Report*. PNNL-14344, Pacific Northwest National Laboratory, Richland, Washington.

Patello, GK, TL Almeida, JA Campbell, OT Farmer, EW Hoppe, CZ Soderquist, RG Swoboda, MW Urie, JJ Wagner, and D Blumenkranz. 2001. *Regulatory DQO Test Plan for Determining Method Detection Limits, Estimated Quantitation Limits, and Quality Assurance Criteria for Specified Analytes*. PNNL-13429 (TP-41500-003-Rev 0), prepared by Pacific Northwest National Laboratory for CH2M HILL Hanford Group, Inc., Richland, Washington.

Rapko, BM and GJ Lumetta. 2000. *Status Report on Phase Identification in Hanford Tank Sludges*. PNNL-13394, Pacific Northwest National Laboratory, Richland, Washington.

Robie, RA and BS Hemingway. 1995. *Thermodynamic Properties of Minerals and Related Substances at 298.15 K and 1 bar (10⁵ Pascals) Pressure and at Higher Temperatures*. U.S. Geological Survey Bulletin 2131, U.S. Geological Survey, Washington, D.C.

Robie, RA, PM Bethke, and KM Bearsley. 1967. *Selected X-Ray Crystallographic Data, Molar Volumes, and Densities of Minerals and Related Substances*. USGS Bulletin 1248, U.S. Geological Survey, Washington, D.C.

Schwertmann, U and RM Cornell. 1991. *Iron Oxides in the Laboratory. Preparation and Characterization*. VCH Publishers, Inc., New York.

Simpson, BC. 1994. *Tank 241-T-111 Characterization Report*. WHC-EP-0806, Westinghouse Hanford Company, Richland, Washington.

Smith, GL, DJ Bates, RW Goles, LR Greenwood, RC Lettau, GF Piepel, MJ Schweiger, HD Smith, MW Urie, and JJ Wagner. 2001. *Vitrification and Product Testing of C-104 and AZ-102 Pretreated Sludge Mixed with Flowsheet Quantities of Secondary Wastes*. PNNL-13452, Pacific Northwest National Laboratory, Richland, Washington.

Strachan, DM, HT Schaef, MJ Schweiger, KL Simmons, LJ Woodcock, and MK Krouse. 2003. "A Versatile and Inexpensive XRD Specimen Holder for Highly Radioactive or Hazardous Specimens." *Powder Diffraction* 18 (1):23-28.

Temer, DJ and R Villarreal. 1995. *Sludge Washing and Alkaline Leaching Tests on Actual Hanford Tank Sludge: A Status Report*. LAUR-95-2070, Los Alamos National Laboratory, Los Alamos, New Mexico.

Temer, DJ and R Villarreal. 1996. *Sludge Washing and Alkaline Leaching Tests on Actual Hanford Tank Sludge: FY 1996 Results*. LAUR-96-2839, Los Alamos National Laboratory, Los Alamos, New Mexico.

Temer, DJ and R Villarreal. 1997. *Sludge Washing and Alkaline Leaching Tests on Actual Hanford Tank Sludge: FY 1997 Results*. LAUR-97-2889, Los Alamos National Laboratory, Los Alamos, New Mexico.

Thompson, AC, DT Attwood, EM Gullikson, MR Howells, K-J Kim, J Kirz, JB Kortright, I Lindau, P Pianetta, AL Robinson, JH Scofield, JH Underwood, D Vaughan, GP Williams, and H Winick. 2001. *X-Ray Data Booklet*. LBNL/PUB-490 Rev. 2, Lawrence Berkeley National Laboratory, Berkeley, California.

Traina, SJ (lead principal investigator) and others. 2001. *Immobilization of Radionuclides in the Hanford Vadose Zone by Incorporation in Solid Phases*. 2001 Progress Report, Project DE-FG07-99ER15010, U.S. Department of Energy, Environmental Management Science Program (EMSP), Washington, D.C. Available at: http://emsp.em.doe.gov/EMSPprojects1996_2002/Subsurface/700812001.pdf

Appendix A

As-Measured XRD Patterns for Sludge Samples

Appendix A

As-Measured XRD Patterns for Sludge Samples

This appendix presents the as-measured X-ray powder diffractometry analysis (XRD) patterns for the unleached (raw) and water-leached AY-102 (jar 15935) sludge samples, and the unleached (raw) AY-102 (jar 18686) and BX-101 (jar 16503) sludge samples. The included patterns show the XRD traces for each sample prior to background subtraction.

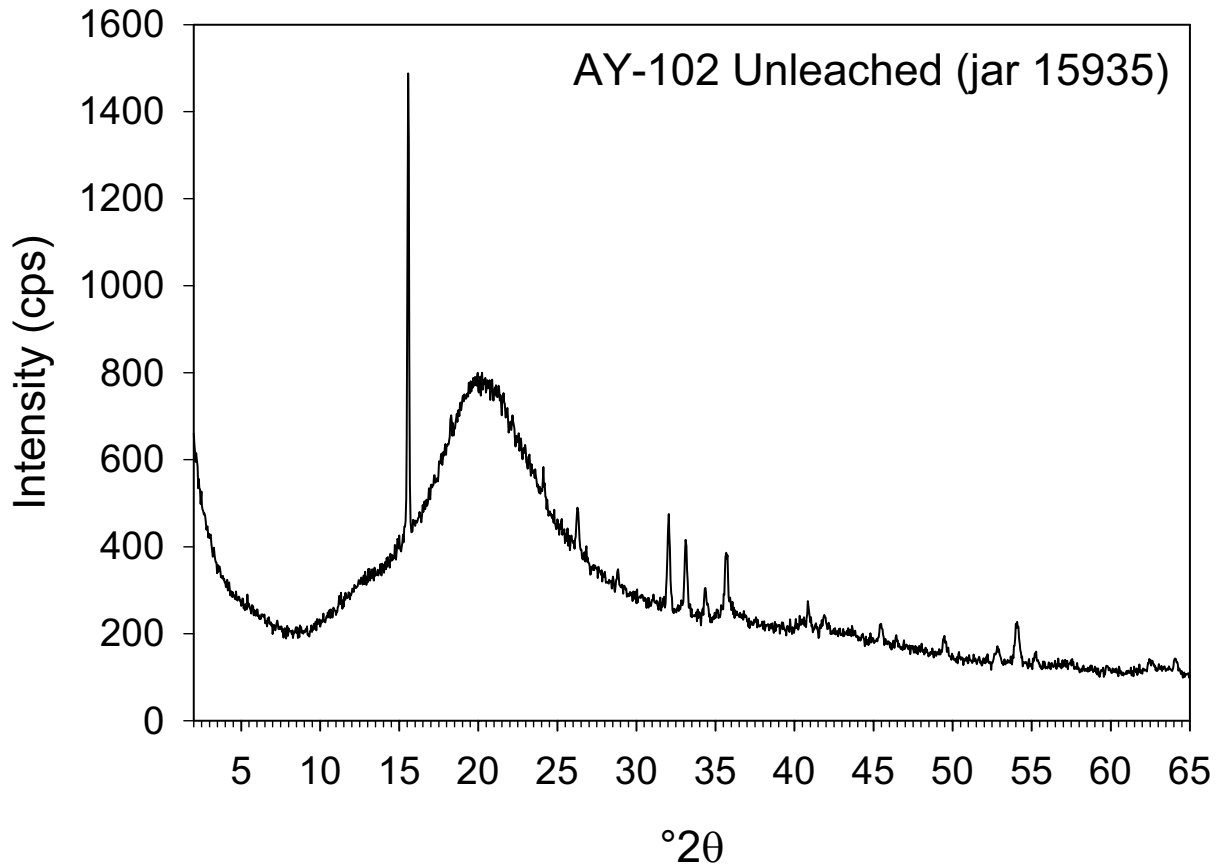


Figure A-1. As-measured XRD pattern (without background subtraction) for unleached AY-102 (jar 15935) sludge

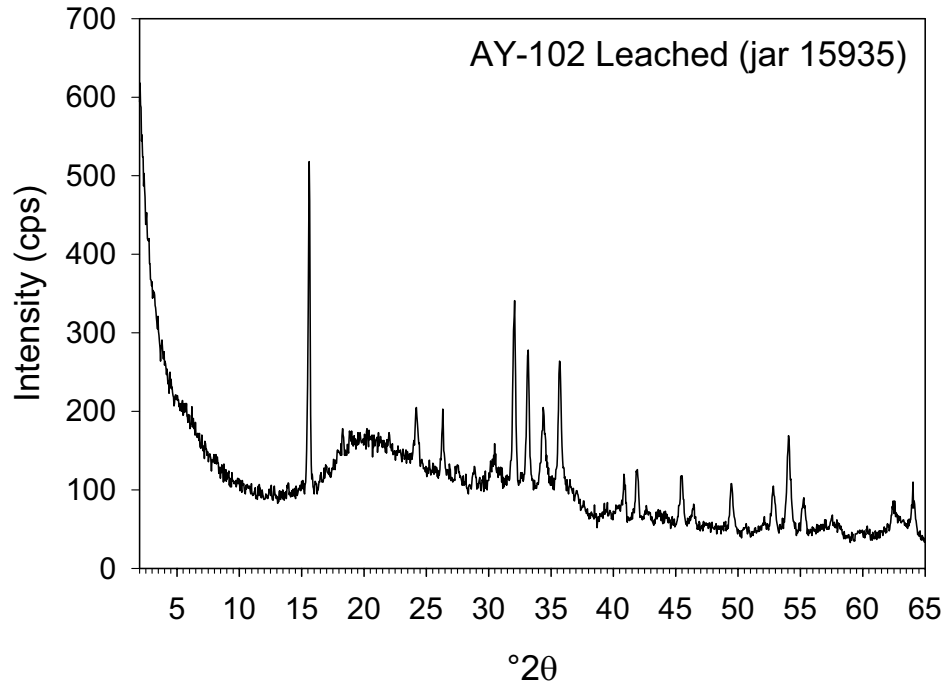


Figure A-2. As-measured XRD pattern (without background subtraction) for water-leached AY-102 (jar 15935) sludge

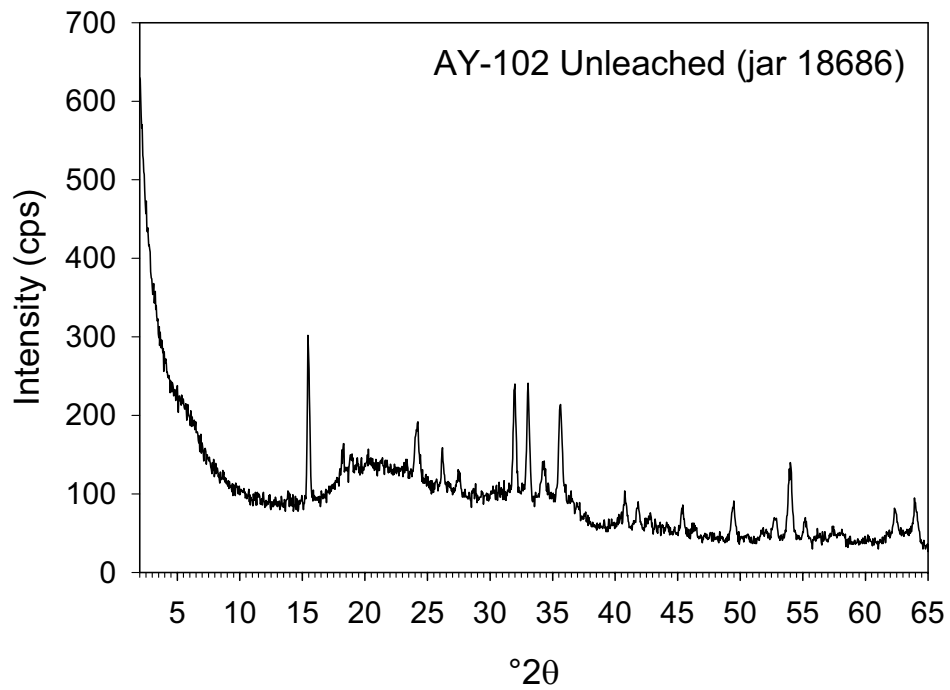


Figure A-3. As-measured XRD pattern (without background subtraction) for unleached AY-102 (jar 18686) sludge

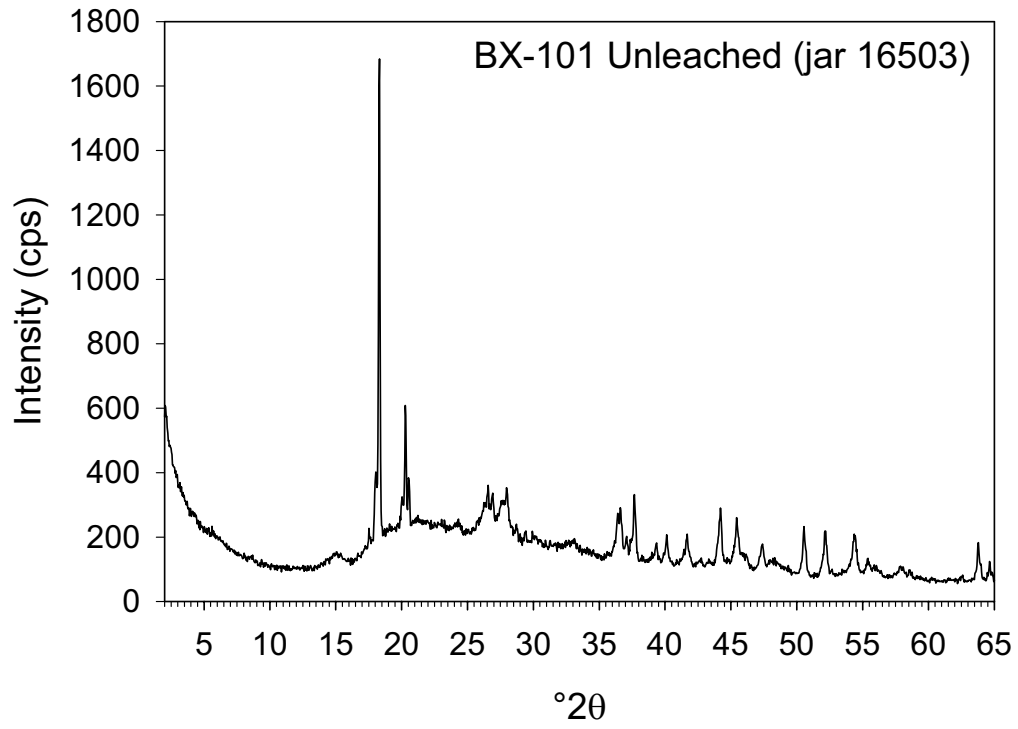


Figure A-4. As-measured XRD pattern (without background subtraction) for unleached BX-101 (jar 16503) sludge

Appendix B

EDS Results and Spectra for Unleached AY-102 (Jar 15935) Sludge

Appendix B

EDS Results and Spectra for Unleached AY-102 (Jar 15935) Sludge

This appendix includes an energy-dispersive X-ray spectrometry (EDS) summary table and all of the EDS spectra recorded for the three subsamples of unleached AY-102 (jar 15935) sludge examined by scanning electron microscopy (SEM)/EDS. The EDS summary table lists the qualitative compositions calculated without inclusion of the emission peak for carbon for particles in the unleached 15935 sludge sample.

Table B-1. Qualitative compositions determined by SEM/EDS for particles observed in the unleached 15935-1 sludge sample (calculated compositions do not include the emission peak for carbon and are normalized to 100 wt%)

Spectrum Label	O	Na	Al	Si	P	Ca	Mn	Fe	Ag	U
	----- wt% -----									
eds01	45.1	16.1	11.3	7.4	1.3	0.2	4.9	13.8	0.1	-0.3
eds02	56.0	15.0	10.2	0.6	1.3	0.3	4.2	12.5	0.0	0.1
eds03	34.7	10.9	9.0	3.2	1.8	0.8	9.4	29.2	0.9	0.2
eds04	39.5	4.8	6.7	0.7	0.3	0.1	1.7	5.0	41.4	-0.1
eds05	49.7	14.5	11.7	11.7	1.0	0.1	1.4	5.3	0.6	4.0
eds06	55.8	29.8	3.4	0.6	0.5	0.2	2.7	6.9	0.1	-0.1
eds07	56.2	17.3	9.4	1.4	1.2	0.2	3.3	11.2	0.1	-0.3
eds08	52.9	11.8	5.8	0.8	0.9	0.1	2.2	25.1	0.1	0.2
eds09	45.1	12.8	10.0	9.4	1.3	0.3	4.7	16.0	0.1	0.2
eds10	46.2	10.0	3.6	1.0	1.0	0.1	6.4	31.9	0.1	0.0
eds11	52.9	23.3	8.2	4.0	1.0	0.6	2.6	7.4	0.1	-0.1
eds12	53.1	28.7	5.2	1.6	1.0	0.2	2.9	7.3	0.1	0.0
eds13	52.0	25.9	5.0	0.6	1.0	0.2	4.4	10.7	0.1	0.0
eds14	51.9	33.6	4.4	1.9	0.5	0.1	2.1	5.8	0.1	-0.3
eds15	50.1	13.4	7.4	5.8	0.8	0.1	3.1	19.6	-0.1	-0.1
eds16	46.9	4.9	6.8	0.5	0.3	0.1	1.0	3.2	36.2	0.3
eds17	57.5	20.2	6.6	1.7	0.8	0.2	3.4	9.6	0.0	0.0
eds18	56.7	27.8	4.9	2.2	0.7	0.2	2.2	5.0	0.3	0.1
eds19	65.2	16.8	5.0	1.0	0.3	2.3	1.1	6.8	1.3	0.1
eds20	53.7	15.2	10.7	7.8	1.1	0.1	2.4	8.5	0.6	0.0
eds21	48.1	10.6	6.0	2.5	1.0	0.2	3.8	27.7	0.2	0.1
eds22	45.5	11.3	5.0	0.6	1.0	0.1	5.4	31.4	0.1	-0.3
eds23	6.9	2.3	0.8	0.4	0.7	0.1	5.5	83.7	-0.1	-0.3
eds24	34.4	8.4	2.2	0.8	1.0	0.2	6.1	46.7	0.2	0.1

Table B-2. Qualitative compositions determined by SEM/EDS for particles observed in the unleached 15935-2 sludge sample (calculated compositions do not include the emission peak for carbon and are normalized to 100 wt%)

Spectrum Label	O	Na	Al	Si	P	Ca	Mn	Fe	Ag	U
	----- wt% -----									
eds01	35.2	2.6	4.7	0.6	0.2	0.2	0.7	2.5	49.1	4.1
eds02	59.1	13.0	5.0	11.3	2.2	0.7	1.9	6.5	0.6	-0.2
eds03	52.4	7.3	6.9	4.0	0.8	0.3	2.2	4.3	21.0	1.0
eds04	56.0	37.3	1.9	0.5	0.3	0.1	1.0	2.9	0.2	-0.2
eds05	23.2	12.5	1.7	0.5	0.6	0.2	4.3	57.0	0.0	0.1
eds06	56.6	34.0	3.0	0.5	0.3	0.1	1.4	4.1	0.1	-0.2
eds07	57.0	16.2	17.8	0.6	0.6	0.1	2.0	5.7	0.1	-0.1
eds08	41.2	4.5	2.1	0.4	0.9	0.2	3.4	47.4	0.1	0.0
eds09	49.4	15.6	10.1	8.7	1.7	0.2	3.4	10.6	0.2	0.1
eds10	49.2	14.3	6.0	1.1	1.1	0.2	19.5	8.8	0.2	-0.1
eds11	52.1	29.5	5.2	1.0	0.4	1.3	0.7	2.9	3.5	3.4
eds12	Calculated composition not valid because particle contains essentially all carbon									
eds13	39.0	12.8	5.2	0.5	2.3	1.5	6.9	28.8	1.6	1.4
eds14	36.0	4.3	12.2	-0.1	0.2	0.0	1.1	2.8	43.0	0.4
eds15	55.7	16.2	4.4	0.5	0.9	2.3	4.4	15.4	0.4	-0.1

Table B-3. Qualitative compositions determined by SEM/EDS for particles observed in the unleached 15935-3 sludge sample (calculated compositions do not include the emission peak for carbon and are normalized to 100 wt%)

Spectrum Label	O	Na	Al	Si	P	Ca	Mn	Fe	Ag	U
	----- wt% -----									
eds01	39.1	6.3	3.4	9.3	1.3	0.0	1.9	3.8	0.4	34.7
eds02	51.6	13.3	21.8	1.4	0.6	0.1	2.5	8.9	0.0	-0.2
eds03	37.8	11.1	12.4	1.2	0.8	0.2	5.6	30.8	0.2	-0.1
eds04	35.7	8.8	6.1	1.5	1.0	0.4	8.6	37.7	0.2	-0.1
eds05	51.6	12.0	3.2	8.5	0.7	0.0	0.6	1.6	0.2	21.6
eds06	59.1	12.1	7.4	17.5	2.0	0.1	0.7	1.6	-0.5	0.1
eds07	48.6	7.6	4.4	8.2	1.8	0.9	3.1	26.0	0.0	-0.6
eds08	56.9	14.3	5.8	8.6	1.3	0.1	2.9	10.7	-0.2	-0.2
eds09	Calculated composition not valid because particle contains essentially all carbon									
eds10	58.2	16.5	8.2	7.2	1.6	0.1	2.9	5.3	0.1	0.0
eds11	48.8	9.6	3.6	4.5	1.0	0.1	3.1	29.2	0.0	0.0
eds12	Calculated composition not valid because particle contains essentially all carbon									
eds13	51.0	13.3	9.0	3.4	1.8	0.4	5.4	15.6	0.1	0.1
eds14	53.8	14.0	8.6	3.8	1.7	0.2	4.0	13.6	0.2	-0.1
eds15	50.2	13.8	2.5	1.2	1.5	0.1	2.6	10.0	0.0	18.0
eds16	53.6	14.0	10.0	0.8	1.3	0.4	4.7	15.2	0.0	0.1
eds17	53.7	9.7	7.1	0.5	0.8	0.1	3.2	7.5	17.8	-0.3
eds18	39.0	10.3	4.8	1.9	1.2	0.6	8.9	33.4	-0.1	0.0
eds19	67.3	1.7	29.3	0.2	0.2	0.0	0.4	0.9	0.0	-0.1
eds20	55.2	16.9	9.9	7.9	0.9	0.2	1.9	7.1	0.0	0.0
eds21	57.8	16.5	7.3	2.4	0.9	2.6	2.3	9.6	0.4	0.2
eds22	66.8	2.0	28.1	0.2	0.3	0.1	0.7	1.9	0.0	-0.1

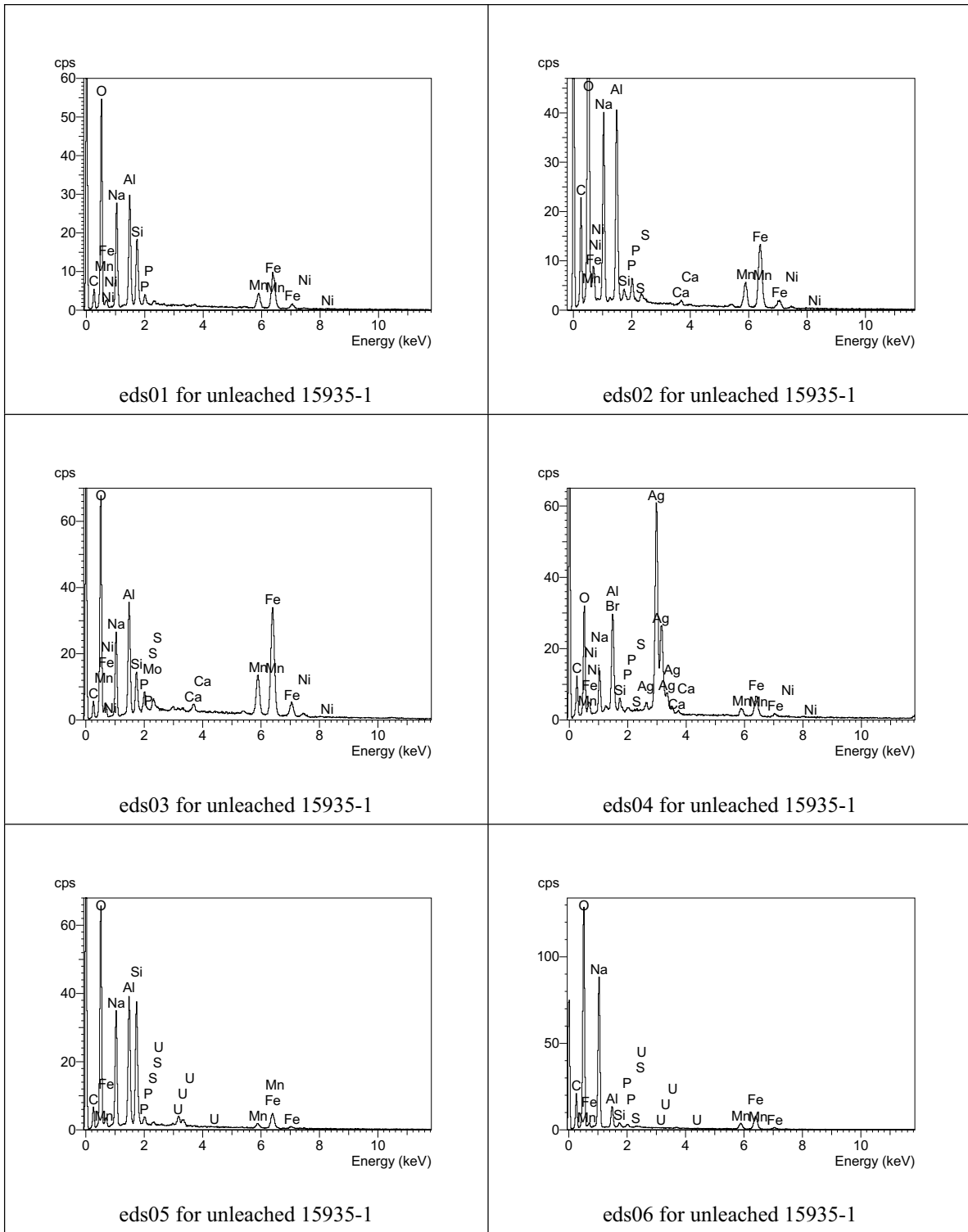


Figure B-1. EDS spectra for analyses eds01 through eds06 for unleached subsample 15935-1 of AY-102 tank sludge (jar 15935)

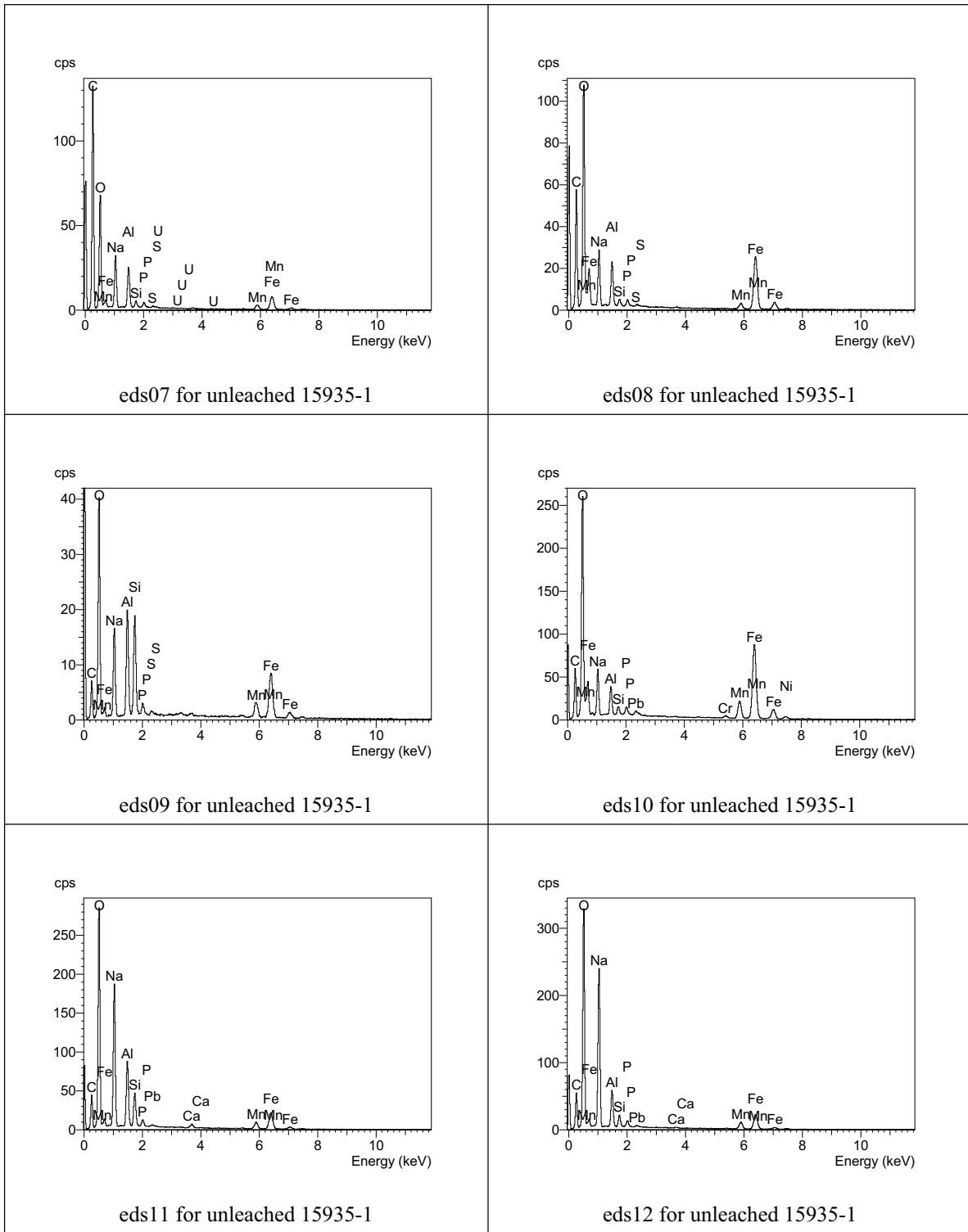


Figure B-2. EDS spectra for analyses eds07 through eds12 for unleached subsample 15935-1 of AY-102 tank sludge (jar 15935)

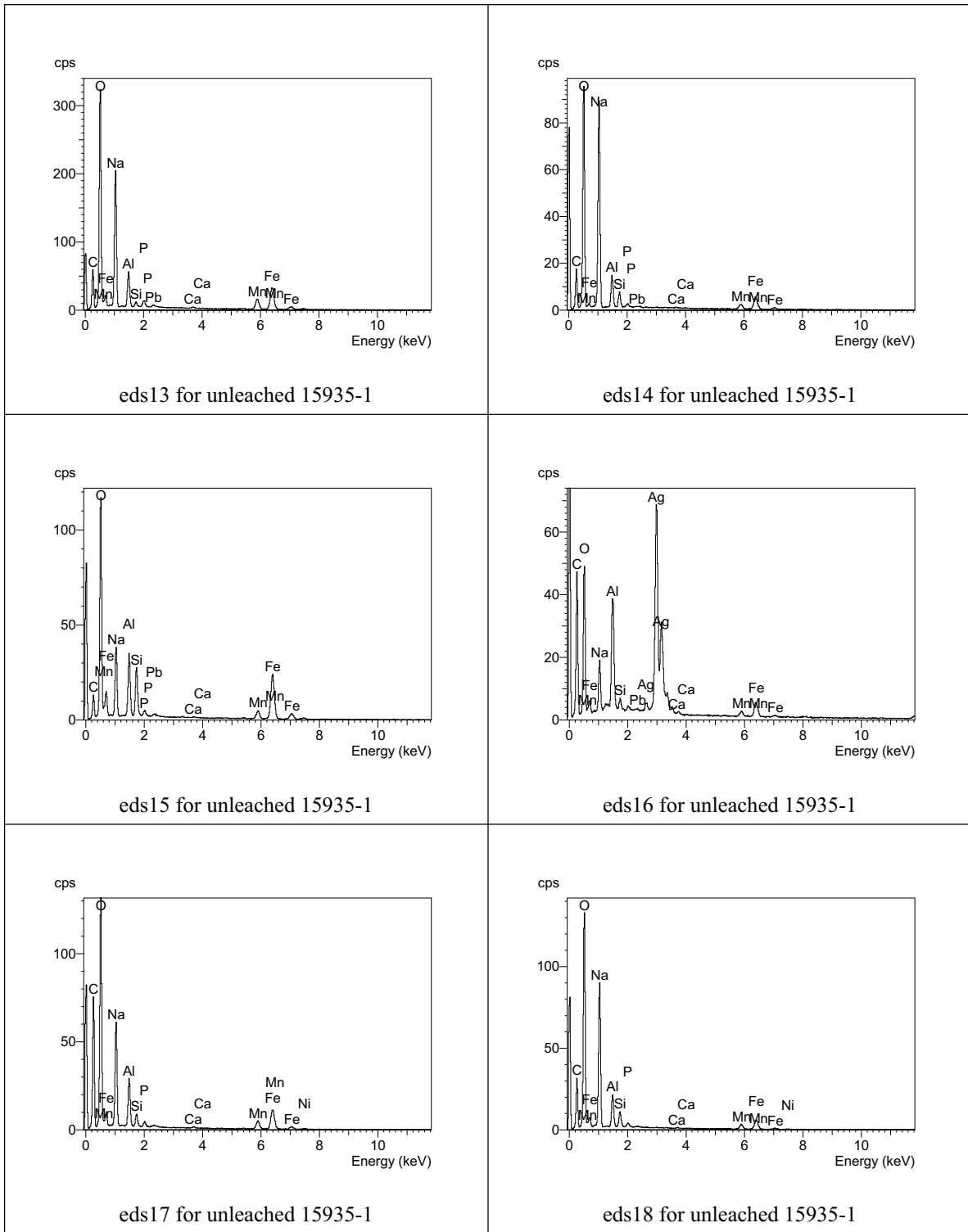


Figure B-3. EDS spectra for analyses eds13 through eds18 for unleached subsample 15935-1 of AY-102 tank sludge (jar 15935)

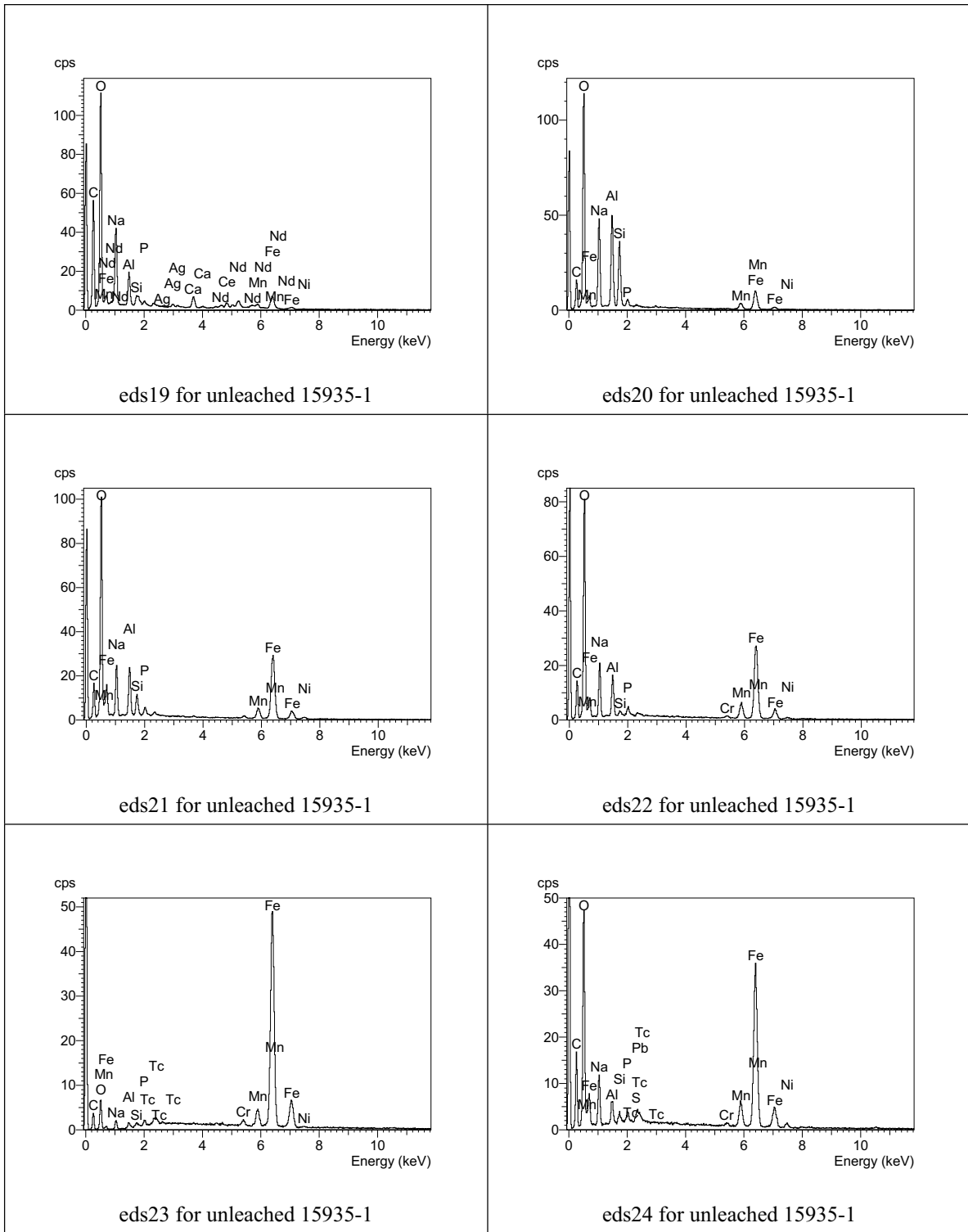


Figure B-4. EDS spectra for analyses eds19 through eds24 for unleached subsample 15935-1 of AY-102 tank sludge (jar 15935)

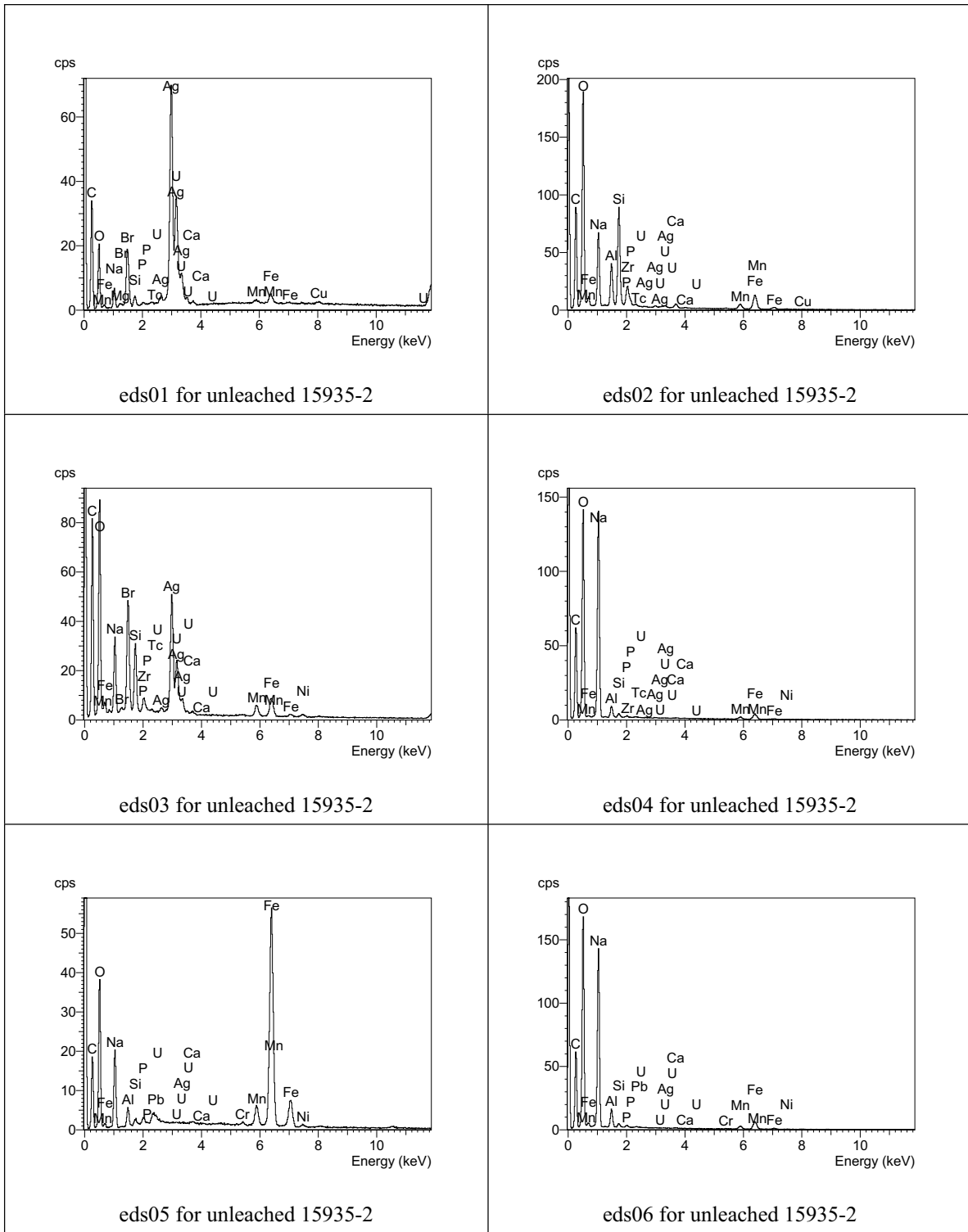


Figure B-5. EDS spectra for analyses eds01 through eds06 for unleached subsample 15935-2 of AY-102 tank sludge (jar 15935)

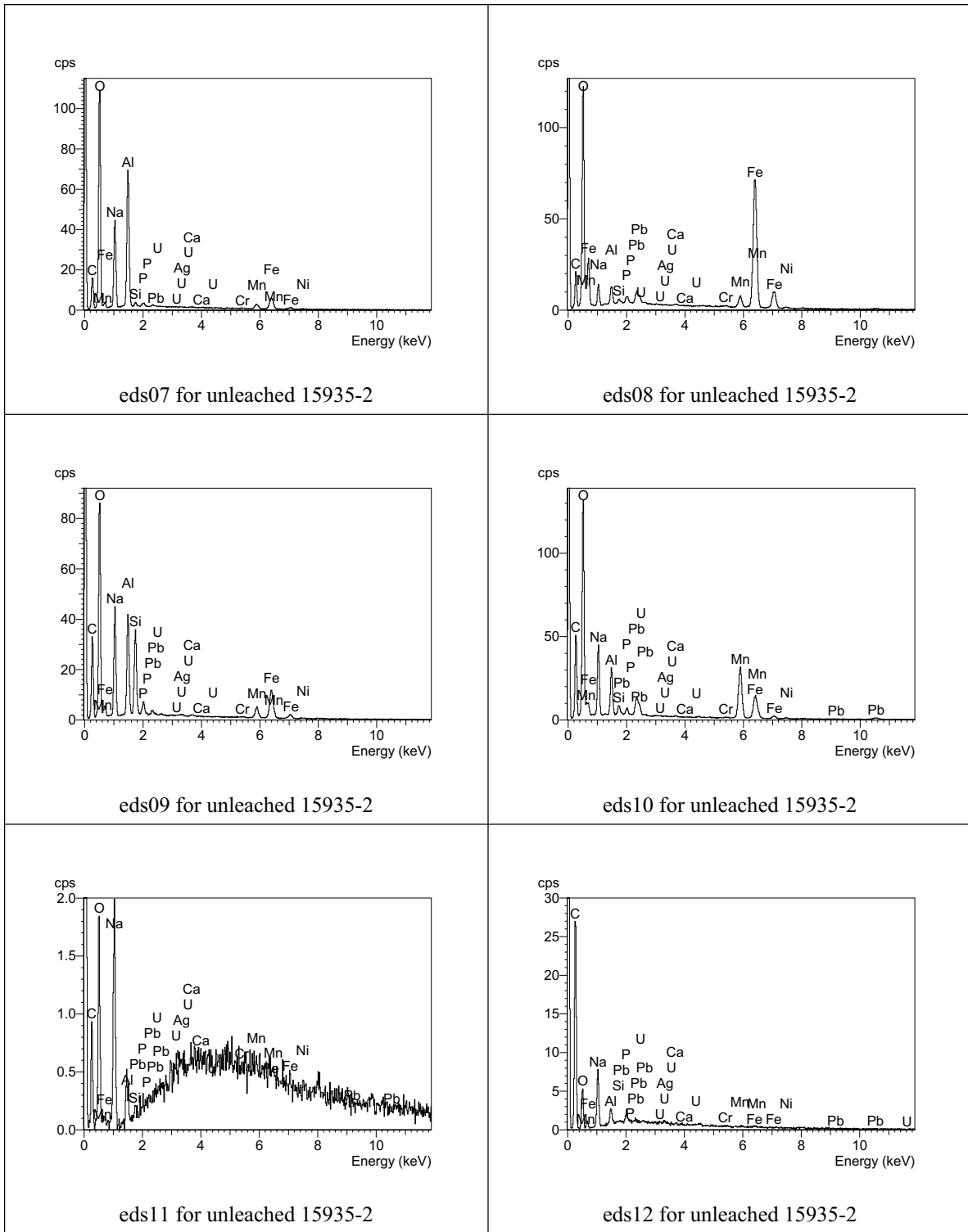


Figure B-6. EDS spectra for analyses eds07 through eds12 for unleached subsample 15935-2 of AY-102 tank sludge (jar 15935)

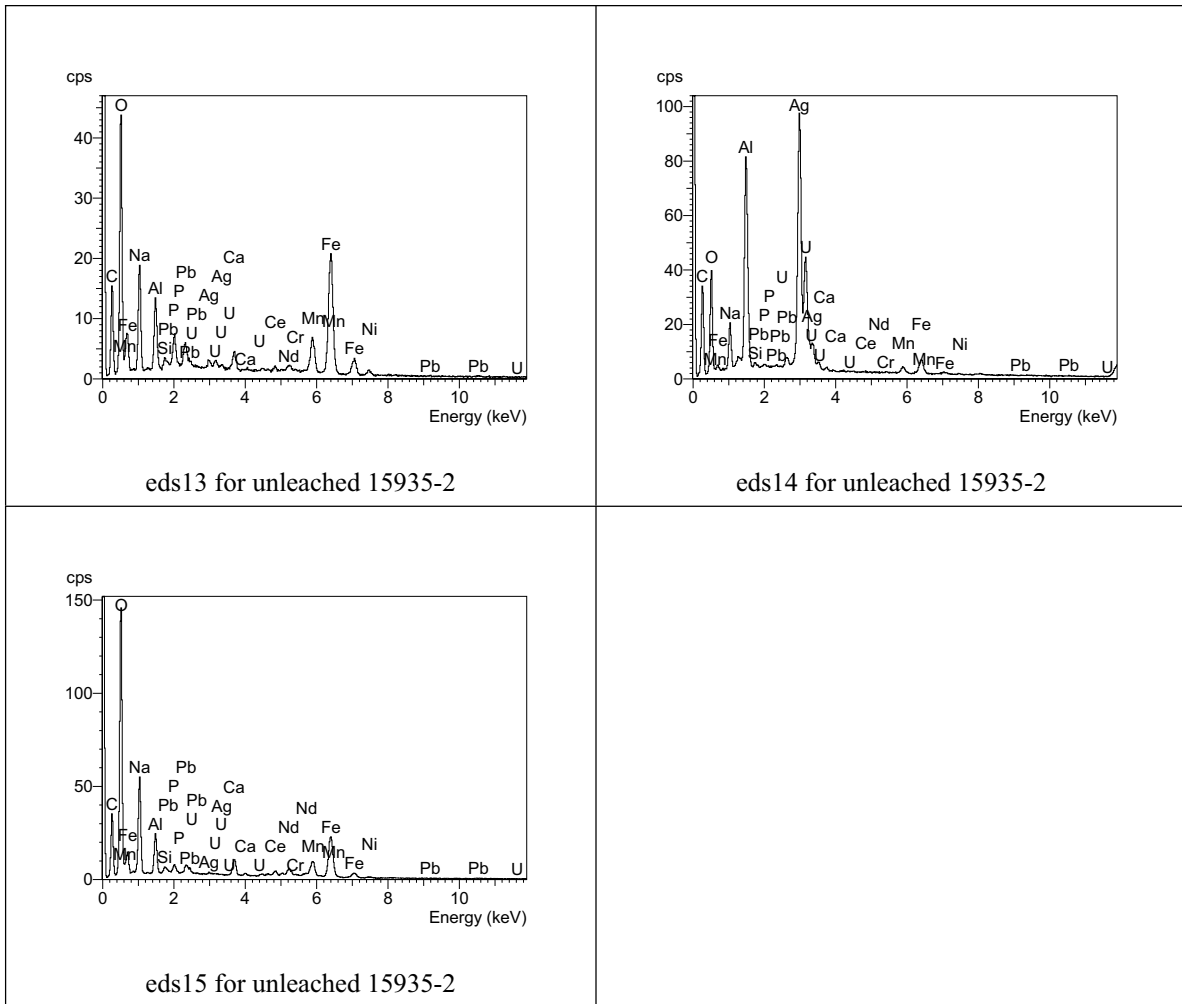


Figure B-7. EDS spectra for analyses eds13 through eds15 for unleached subsample 15935-2 of AY-102 tank sludge (jar 15935)

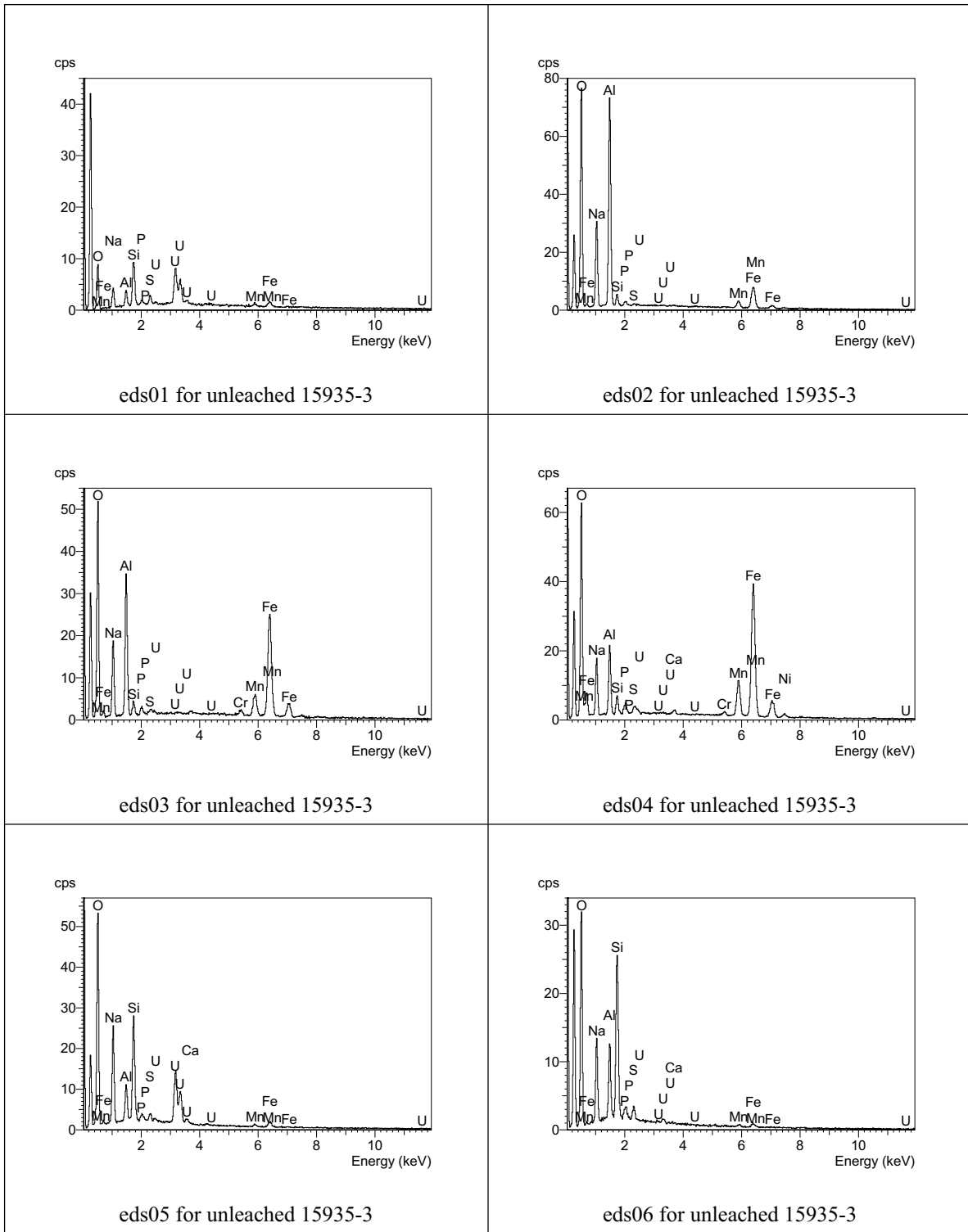


Figure B-8. EDS spectra for analyses eds01 through eds06 for unleached subsample 15935-3 of AY-102 tank sludge (jar 15935)

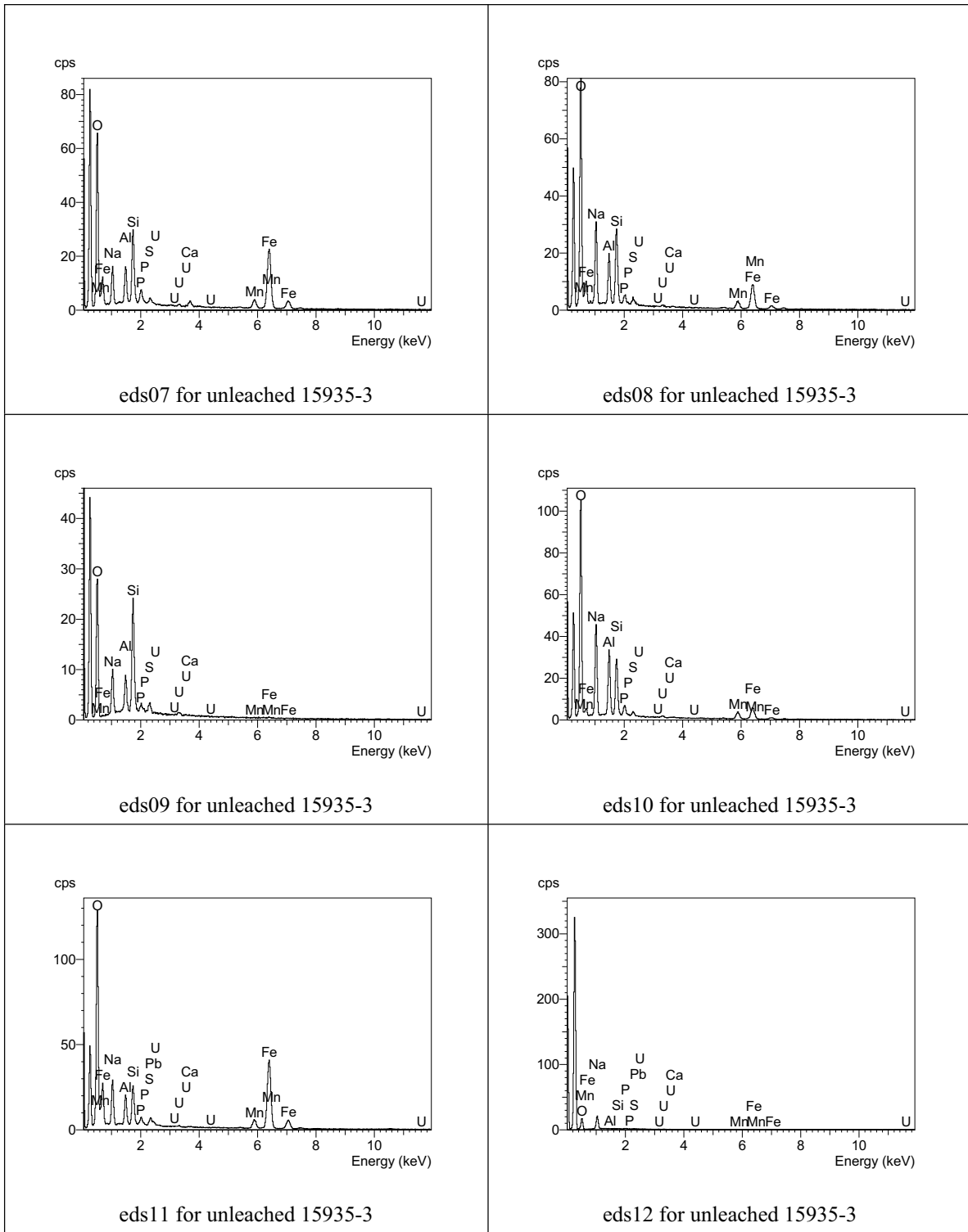


Figure B-9. EDS spectra for analyses eds07 through eds12 for unleached subsample 15935-3 of AY-102 tank sludge (jar 15935)

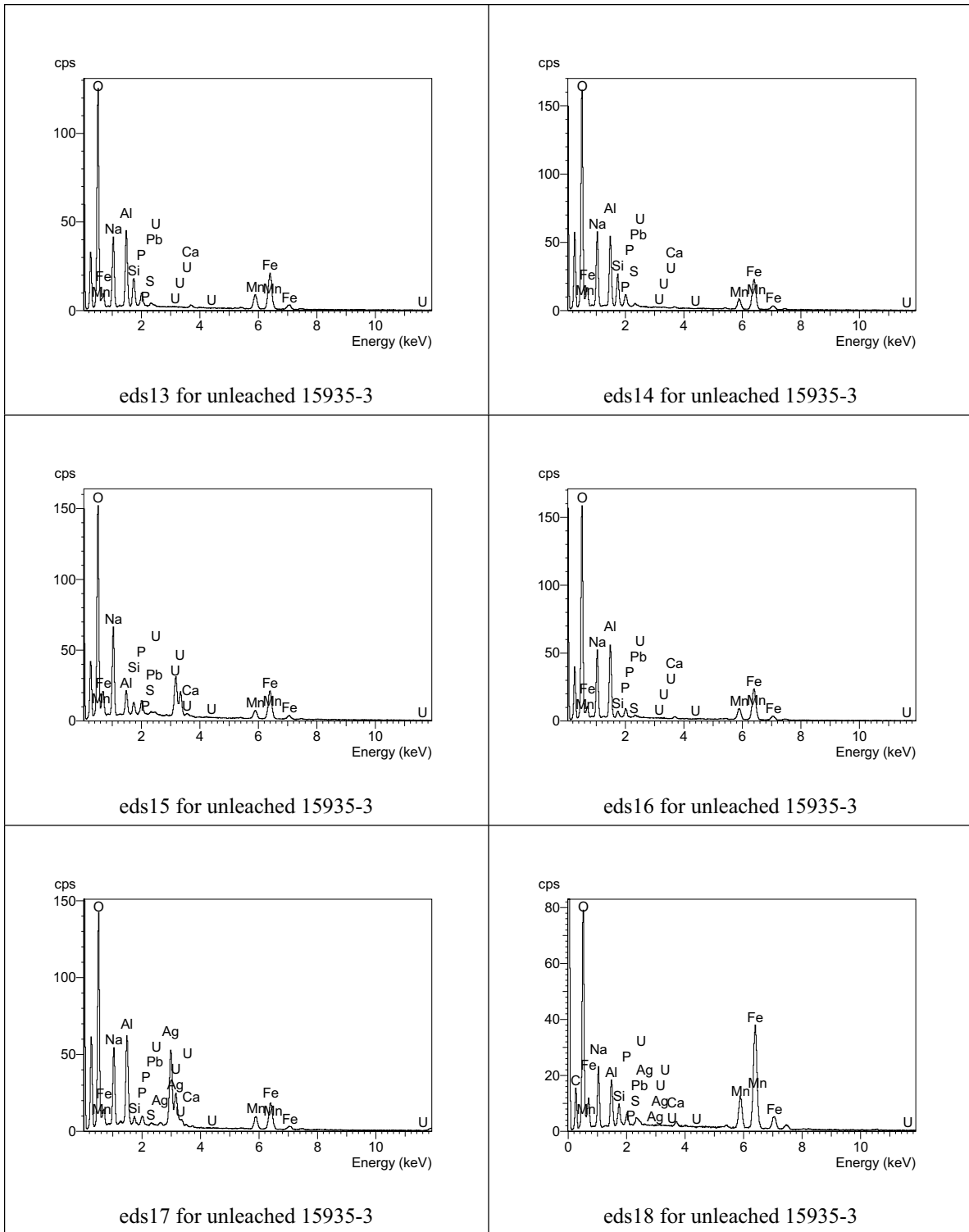


Figure B-10. EDS spectra for analyses eds13 through eds18 for unleached subsample 15935-3 of AY-102 tank sludge (jar 15935)

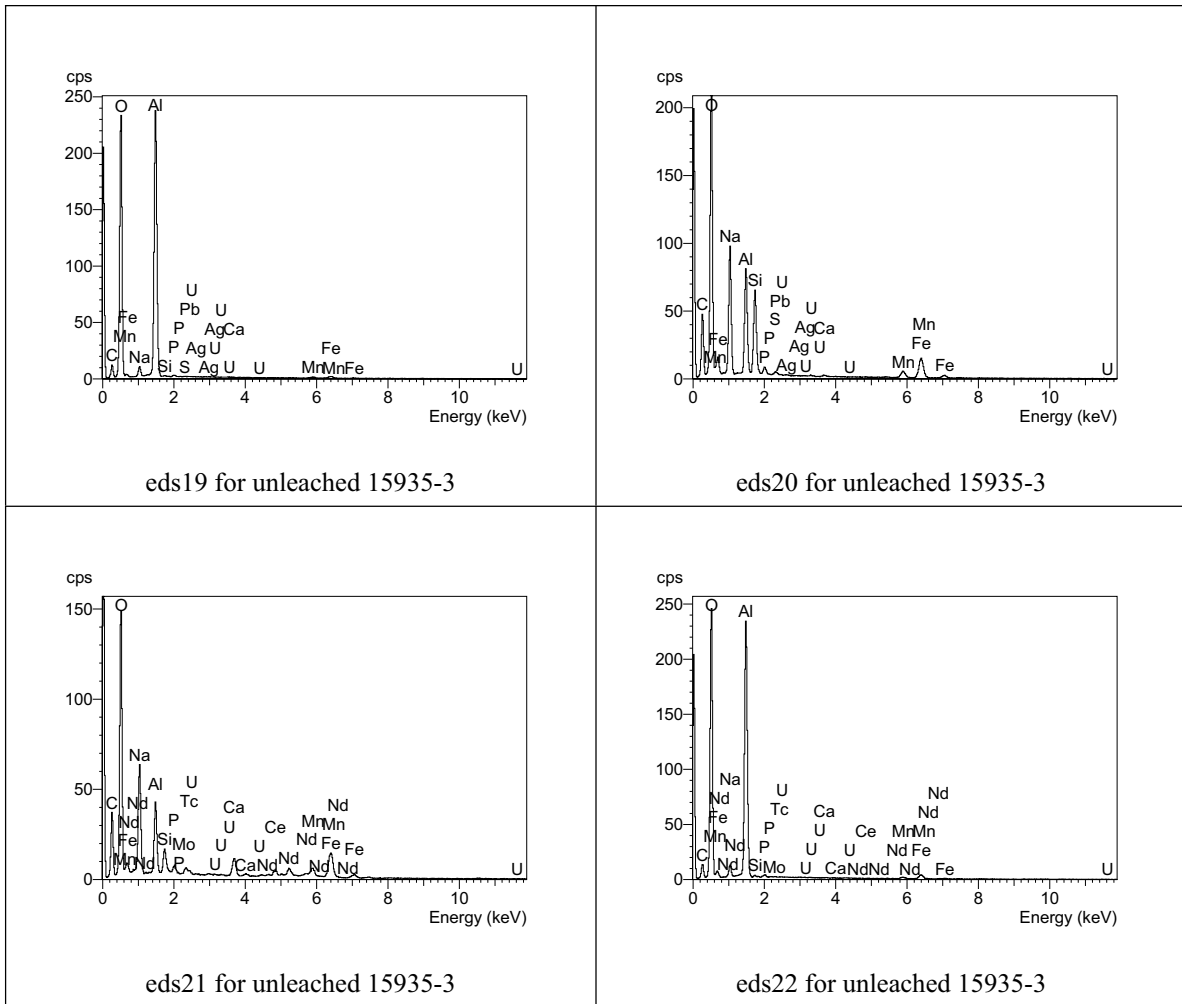


Figure B-11. EDS spectra for analyses eds19 through eds22 for unleached subsample 15935-3 of AY-102 tank sludge (jar 15935)

Appendix C

EDS Results and Spectra for Water-Leached AY-102 (Jar 15935) Sludge

Appendix C

EDS Results and Spectra for Water-Leached AY-102 (Jar 15935) Sludge

This appendix includes an energy-dispersive X-ray spectrometry (EDS) summary table and all of the EDS spectra recorded for the two subsamples of water-leached AY-102 (jar 15935) sludge examined by scanning electron microscopy (SEM)/EDS. The EDS summary table lists the qualitative compositions calculated without inclusion of the emission peak for carbon for particles in the water-leached 15935 sludge sample.

Table C-1. Qualitative compositions determined by SEM/EDS for particles observed in the leached 15935-1 sludge sample (calculated compositions do not include the emission peak for carbon and are normalized to 100 wt%)

Spectrum Label	O	Na	Al	Si	P	Ca	Mn	Fe	Ag	U
	----- wt% -----									
eds01	31.0	1.2	8.2	1.5	1.4	0.6	2.6	53.1	0.3	0.2
eds02	56.1	0.6	29.3	1.2	0.6	0.6	1.4	10.2	0.2	-0.3
eds03	37.3	2.3	5.8	1.9	1.1	1.1	7.6	42.2	0.3	0.5
eds04	10.6	0.8	2.9	2.0	0.7	3.0	6.3	73.7	0.0	0.1
eds05	39.0	1.6	11.4	3.5	1.6	1.9	4.1	36.7	0.0	0.2
eds06	44.7	1.3	5.9	2.5	5.1	3.5	2.3	34.3	0.2	0.3
eds07	36.6	1.3	7.3	3.6	2.5	3.6	4.2	40.3	0.2	0.5
eds08	54.4	2.3	1.3	0.5	8.3	16.7	0.5	6.2	8.9	0.9
eds09	55.2	2.8	1.5	0.5	10.0	19.0	0.5	7.1	2.4	1.1
eds10	55.1	5.7	4.6	3.3	6.7	12.8	0.7	10.1	0.3	0.6
eds11	43.2	1.4	5.9	2.4	3.8	7.7	2.8	31.9	0.3	0.7
eds12	49.5	1.1	9.4	2.7	1.6	1.3	2.2	32.1	0.1	0.2
eds13	54.3	1.1	13.8	3.9	1.9	2.0	3.2	19.4	0.2	0.3
eds14	57.1	4.7	7.2	7.5	1.3	1.8	5.0	15.1	0.3	0.1
eds15	40.3	2.0	11.9	1.7	1.3	1.8	4.4	36.1	0.3	0.1
eds16	50.4	1.3	5.8	1.8	1.5	1.5	1.5	35.4	0.5	0.3
eds17	37.3	1.1	5.6	2.1	1.3	1.0	2.4	48.9	0.2	0.3
eds18	56.3	1.1	15.2	4.2	1.8	2.2	2.5	16.5	0.1	0.1

Table C-2. Qualitative compositions determined by SEM/EDS for particles observed in the leached 15935-2 sludge sample (calculated compositions do not include the emission peak for carbon and are normalized to 100 wt%)

Spectrum Label	O	Na	Al	Si	P	Ca	Mn	Fe	Ag	U
	----- wt% -----									
eds01	43.1	1.0	5.3	2.5	0.6	0.5	13.8	33.2	0.1	0.0
eds02	40.5	2.0	5.3	2.5	0.7	0.6	14.0	34.3	0.2	-0.1
eds03	56.1	12.7	16.1	0.4	0.3	0.3	2.3	11.1	0.7	0.1
eds04	39.2	0.9	1.2	0.3	0.1	0.5	0.5	2.1	53.9	1.4
eds05	5.0	0.6	2.1	0.6	0.3	0.5	41.1	49.3	0.5	-0.1
eds06	68.8	1.1	27.7	0.2	0.2	0.1	0.5	1.4	0.1	0.0
eds07	46.0	1.8	5.3	1.4	0.7	0.3	6.2	37.9	0.2	0.2
eds08	55.4	11.2	11.9	10.5	0.4	0.5	2.3	6.3	1.6	0.0

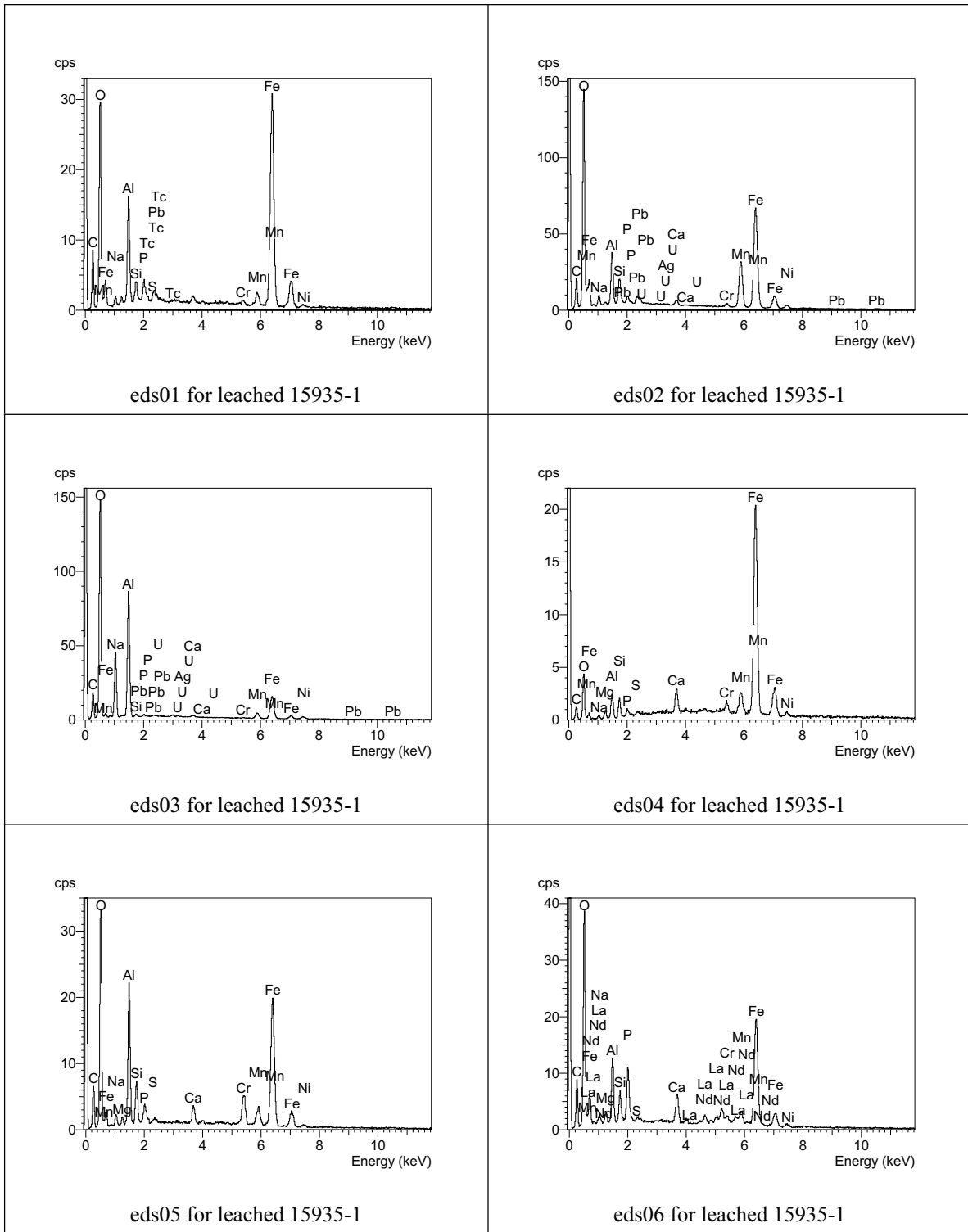


Figure C-1. EDS spectra for analyses eds01 through eds06 for leached subsample 15935-1 of AY-102 tank sludge (jar 15935)

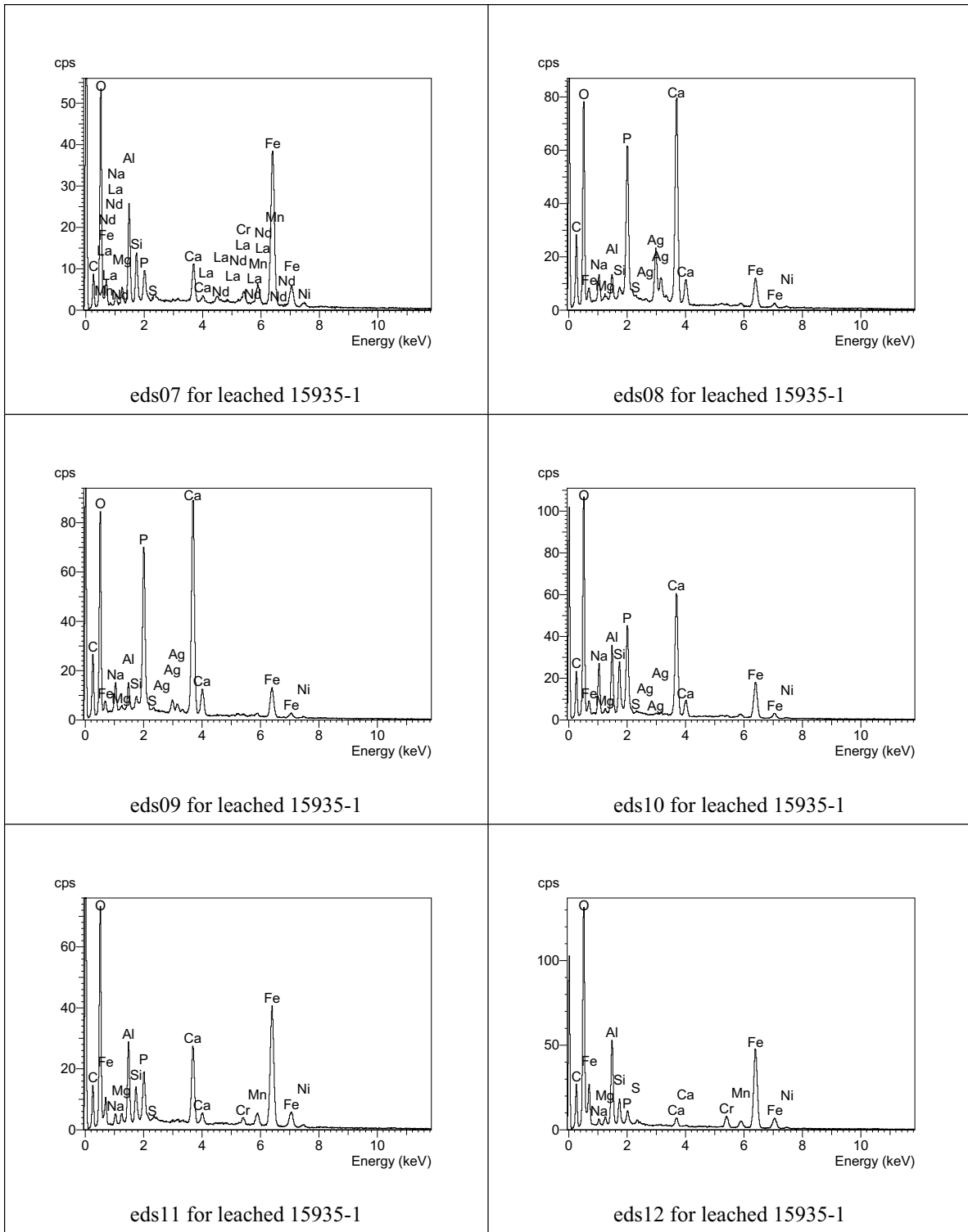


Figure C-2. EDS spectra for analyses eds07 through eds12 for leached subsample 15935-1 of AY-102 tank sludge (jar 15935)

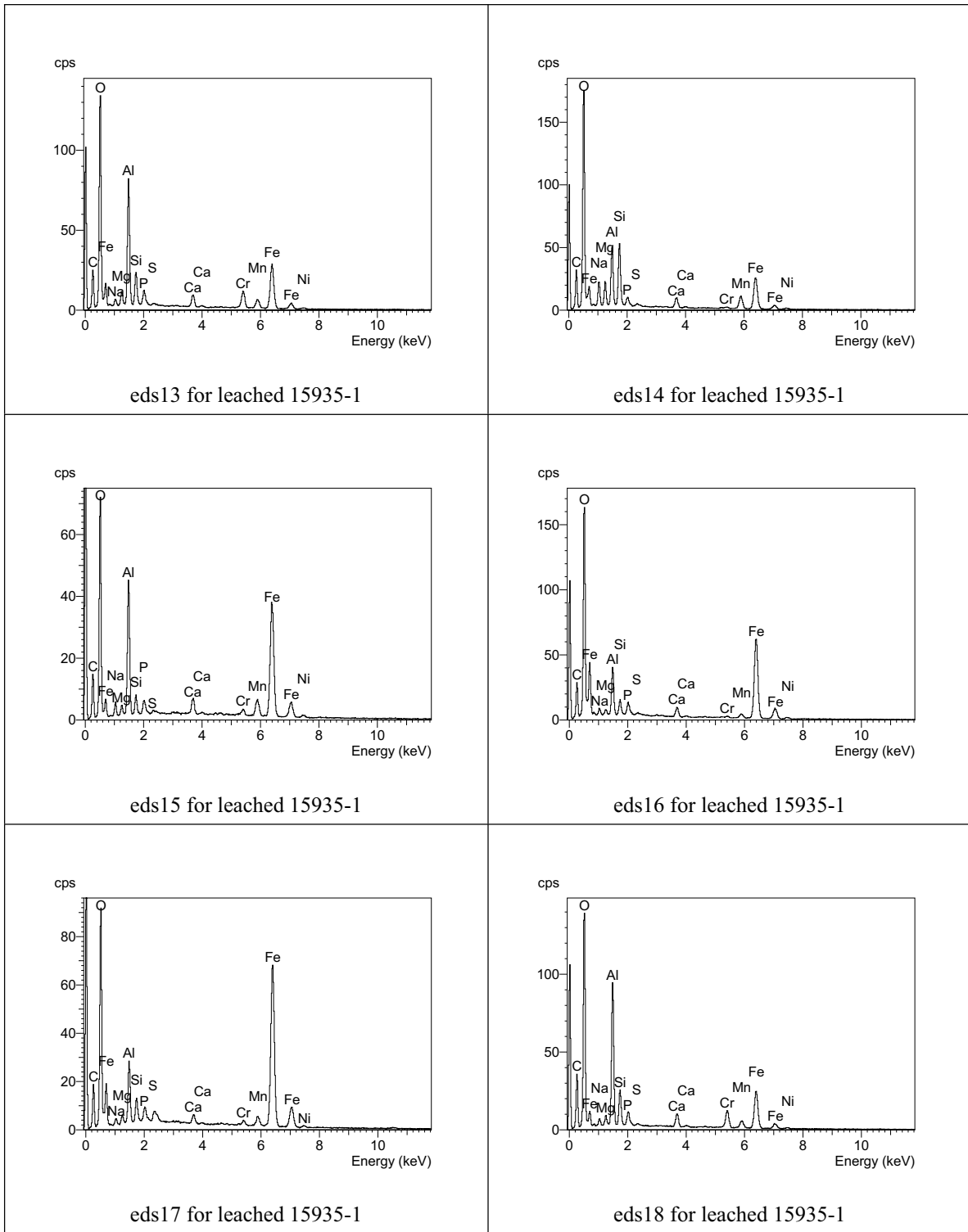


Figure C-3. EDS spectra for analyses eds13 through eds18 for leached subsample 15935-1 of AY-102 tank sludge (jar 15935)

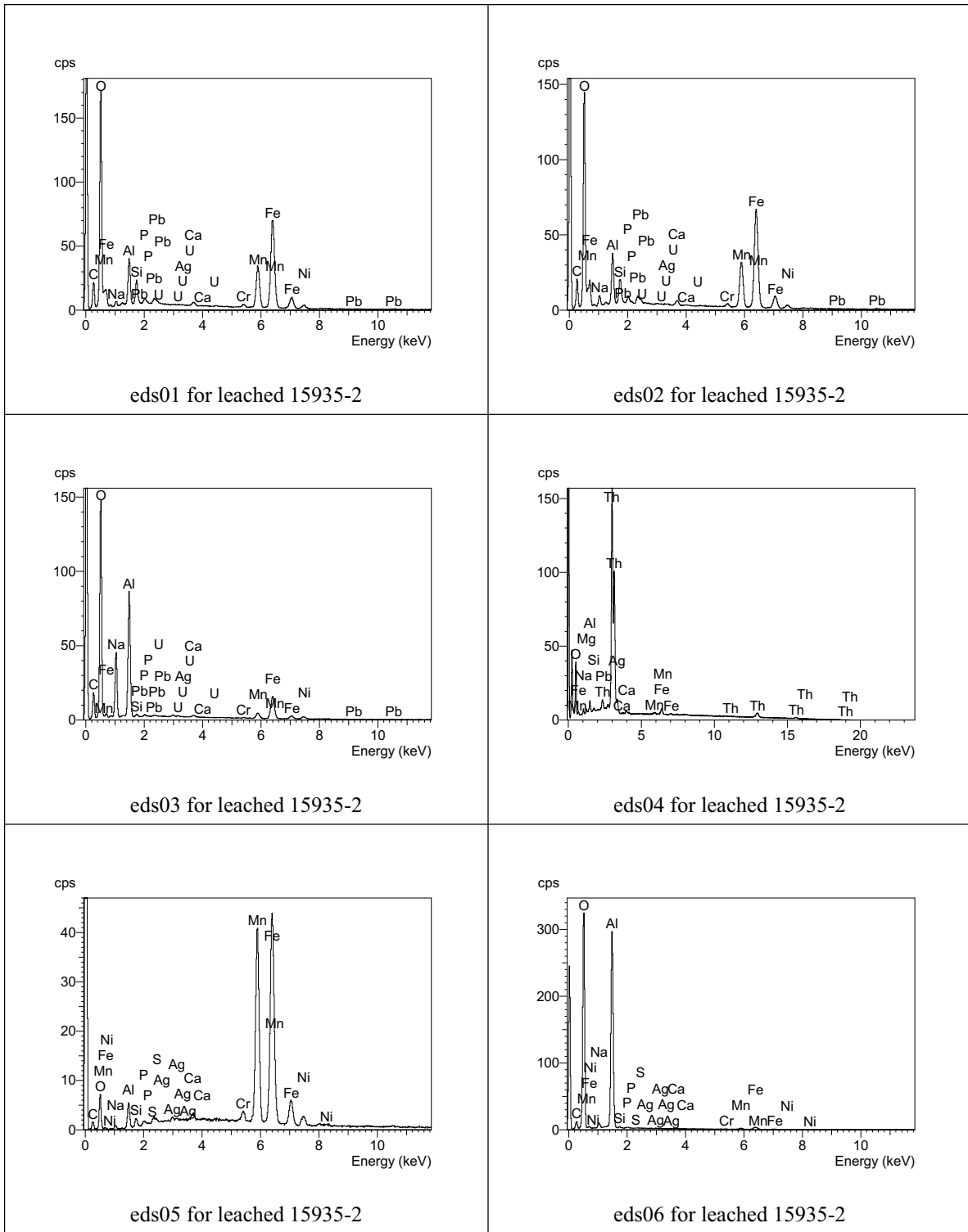


Figure C-4. EDS spectra for analyses eds01 through eds06 for leached subsample 15935-2 of AY-102 tank sludge (jar 15935)

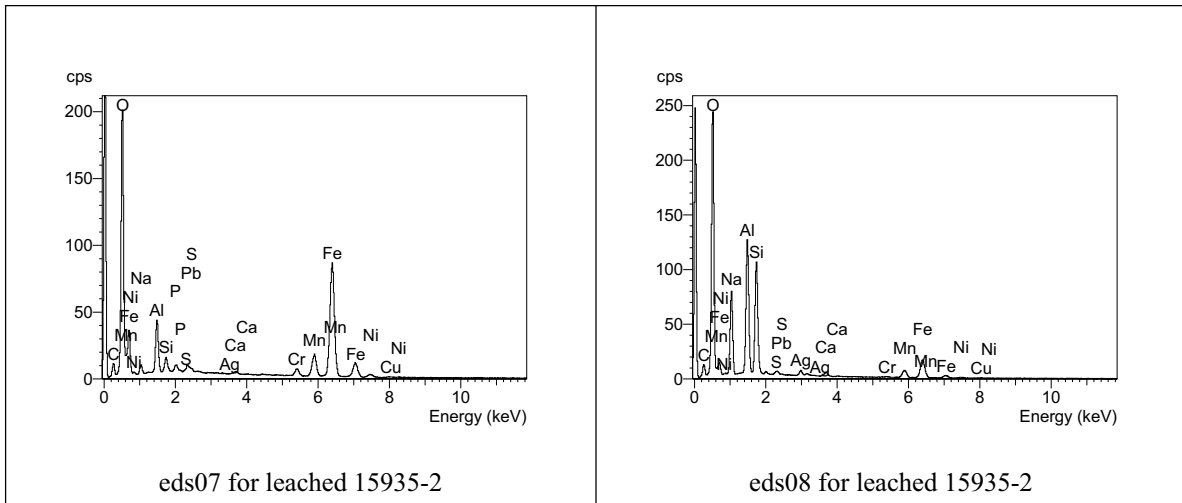


Figure C-5. EDS spectra for analyses eds07 through eds08 for leached subsample 15935-2 of AY-102 tank sludge (jar 15935)

Appendix D

EDS Results and Spectra for Unleached BX-101 (Jar 16503) Sludge

Appendix D

EDS Results and Spectra for Unleached BX-101 (Jar 16503) Sludge

This appendix includes an energy-dispersive X-ray spectrometry (EDS) summary table and all of the EDS spectra recorded for the two subsamples of unleached BX-101 (jar 16503) sludge examined by scanning electron microscopy (SEM)/EDS. The EDS summary table lists the qualitative compositions calculated without inclusion of the emission peak for carbon for particles in the water-leached 16503 sludge sample.

Table D-1. Qualitative compositions determined by SEM/EDS for particles observed in the unleached 16503-1 sludge sample (calculated compositions do not include the emission peak for carbon and are normalized to 100 wt%)

Spectrum Label	O	Na	Al	Si	P	Ca	Mn	Fe	Ag	U
	----- wt% -----									
eds01	63.7	1.3	30.7	0.3	0.2	0.1	1.3	0.9	0.2	1.4
eds02	51.6	3.9	18.0	0.6	0.3	0.1	18.3	3.3	0.3	3.5
eds03	42.4	3.8	9.2	0.7	0.7	0.1	5.9	1.5	0.1	35.7
eds04	62.7	7.5	23.2	0.6	0.2	0.1	1.5	1.1	0.3	2.8
eds05	33.7	6.4	0.7	0.3	0.7	0.0	0.2	0.2	-0.2	58.0
eds06	56.8	5.5	8.7	14.5	0.6	2.9	2.7	7.8	0.3	0.3
eds07	52.4	7.9	5.1	3.7	0.7	0.4	2.7	3.2	0.4	23.6
eds08	67.3	2.2	21.7	4.2	0.4	0.4	0.9	1.6	0.1	1.2
eds09	56.5	12.3	16.7	8.4	0.4	0.1	1.0	2.0	0.3	2.5
eds10	67.8	0.8	29.8	0.2	0.2	0.1	0.1	0.2	0.1	0.8
eds11	65.2	1.2	32.3	0.5	0.1	0.0	0.1	0.2	0.1	0.3
eds12	56.0	4.9	13.0	0.4	0.5	0.0	0.7	0.6	0.2	23.7
eds13	47.7	11.4	3.1	3.2	0.8	0.1	24.1	8.6	0.9	0.2
eds14	60.9	5.8	24.6	3.2	0.4	0.1	1.2	2.2	0.3	1.5
eds15	67.1	0.5	31.4	0.2	0.2	0.0	0.0	0.3	0.1	0.2

Table D-2. Qualitative compositions determined by SEM/EDS for particles observed in the unleached 16503-2 sludge sample (calculated compositions do not include the emission peak for carbon and are normalized to 100 wt%)

Spectrum Label	O	Na	Al	Si	P	Ca	Mn	Fe	Ag	U
	----- wt% -----									
eds01	52.5	44.8	2.0	0.1	0.0	0.1	0.1	0.2	0.1	0.1
eds02	31.7	6.3	2.3	0.1	0.8	0.2	0.6	1.5	0.4	56.1
eds03	71.0	2.0	25.5	0.1	0.1	0.0	0.1	0.3	0.1	0.7
eds04	67.3	2.1	29.6	0.2	0.1	0.0	0.1	0.1	0.1	0.4
eds05	52.4	8.0	7.9	1.0	1.6	0.1	5.5	19.3	1.6	2.5
eds06	46.5	5.8	6.4	0.4	0.9	0.0	0.3	0.5	0.0	39.2
eds07	54.3	16.2	13.8	12.6	0.3	0.0	0.3	0.8	0.2	1.4
eds08	53.7	14.7	16.4	13.6	0.3	0.0	0.1	0.5	0.2	0.4
eds09	39.0	5.8	2.2	0.8	1.5	0.5	1.6	11.9	0.4	36.3
eds10	50.3	8.6	7.1	1.5	1.0	0.2	18.5	8.4	1.5	3.0
eds11	41.9	6.3	4.1	0.5	0.9	0.1	0.9	0.9	0.4	44.1
eds12	67.3	0.7	30.5	0.2	0.2	0.1	0.3	0.5	0.0	0.3
eds13	51.5	4.4	15.2	0.7	0.5	0.0	0.5	0.7	0.2	26.2
eds14	36.0	4.6	1.4	0.1	0.7	0.1	0.3	0.3	0.1	56.3
eds15	62.8	0.8	35.1	0.3	0.2	0.0	0.1	0.2	0.1	0.5
eds16	34.6	5.9	2.7	0.8	0.7	0.1	0.2	0.6	0.5	53.9
eds17	49.7	1.4	16.6	0.4	0.3	0.3	0.9	1.1	0.4	29.2
eds18	51.7	9.4	4.2	0.8	1.0	0.4	10.4	3.9	0.7	17.4
eds19	59.2	7.6	6.8	5.0	7.6	12.7	0.1	0.7	0.1	0.2
eds20	57.3	15.6	14.3	11.8	0.3	0.1	0.2	0.3	0.0	0.2
eds21	35.1	1.1	46.3	0.9	0.2	0.2	4.5	4.6	-0.2	7.4
eds22	30.6	7.0	10.8	5.0	0.5	0.1	1.7	43.5	0.1	0.8
eds23	69.7	0.8	28.9	0.2	0.1	0.0	0.1	0.1	0.0	0.2
eds24	58.0	6.1	13.0	2.1	2.2	2.9	2.3	7.5	0.9	5.1
eds25	31.0	5.0	2.6	0.4	0.6	0.2	0.3	0.1	0.1	59.7

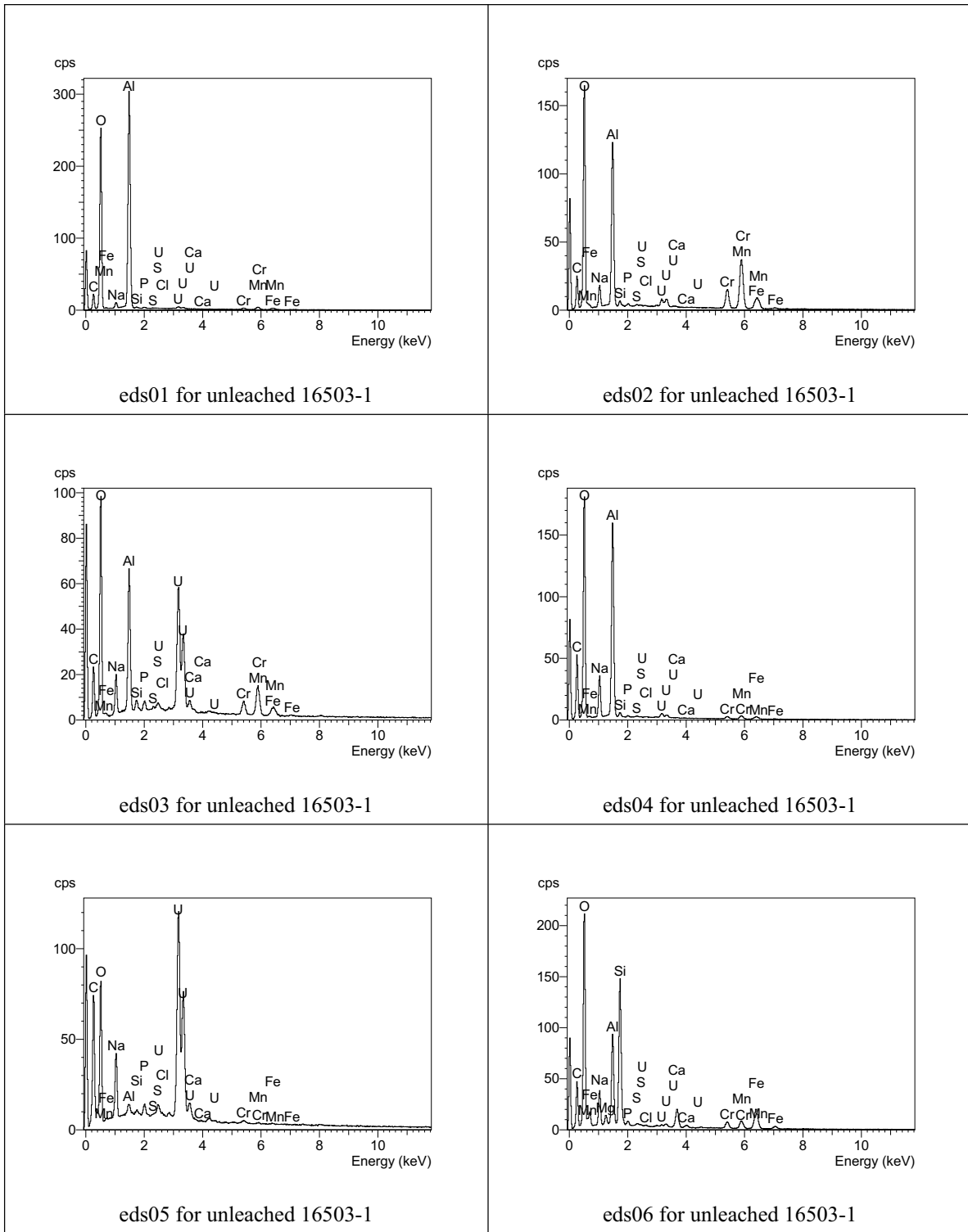


Figure D-1. EDS spectra for analyses eds01 through eds06 for unbleached subsample 16503-1 of BX-101 tank sludge (jar 16503)

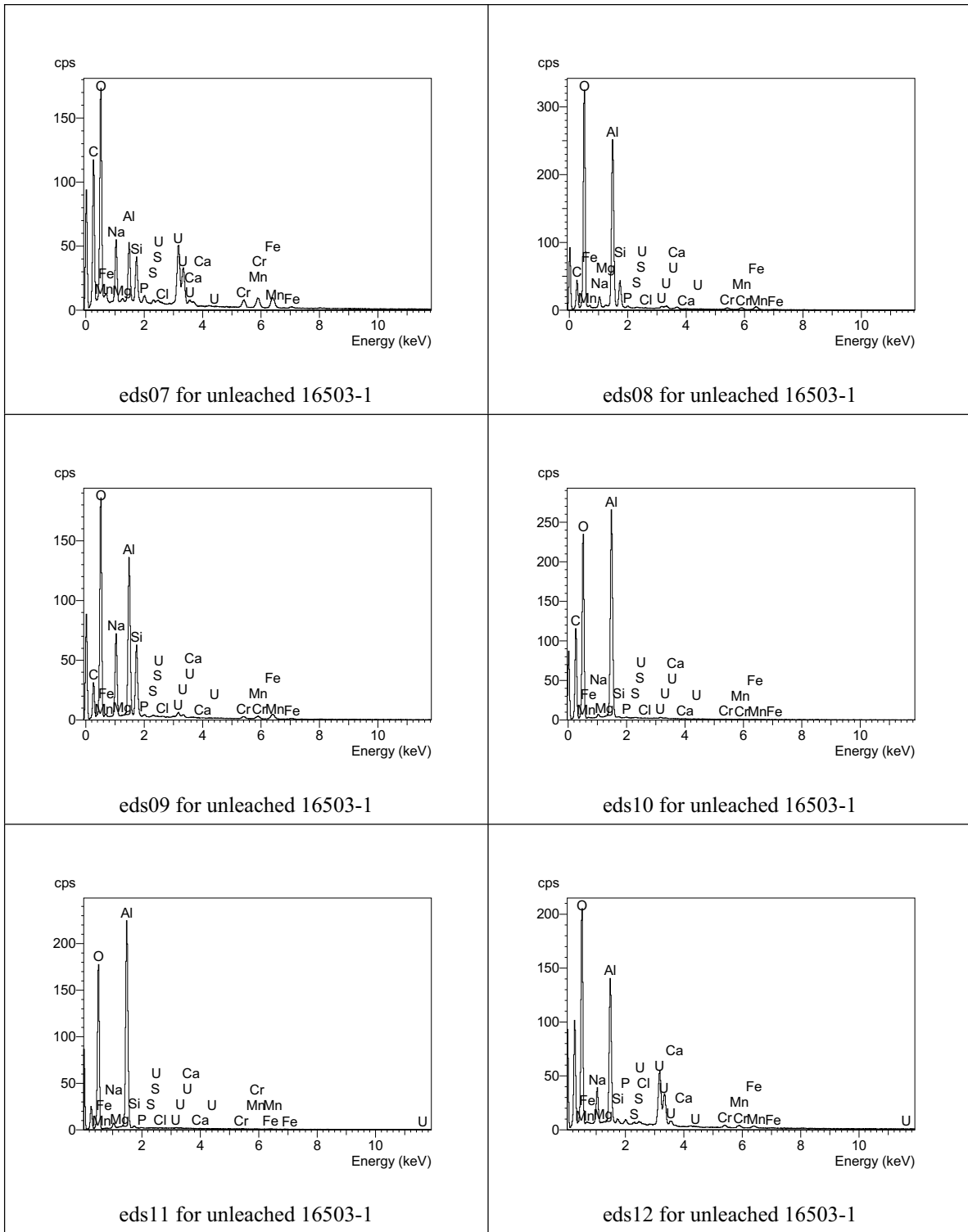


Figure D-2. EDS spectra for analyses eds07 through eds12 for unleached subsample 16503-1 of BX-101 tank sludge (jar 16503)

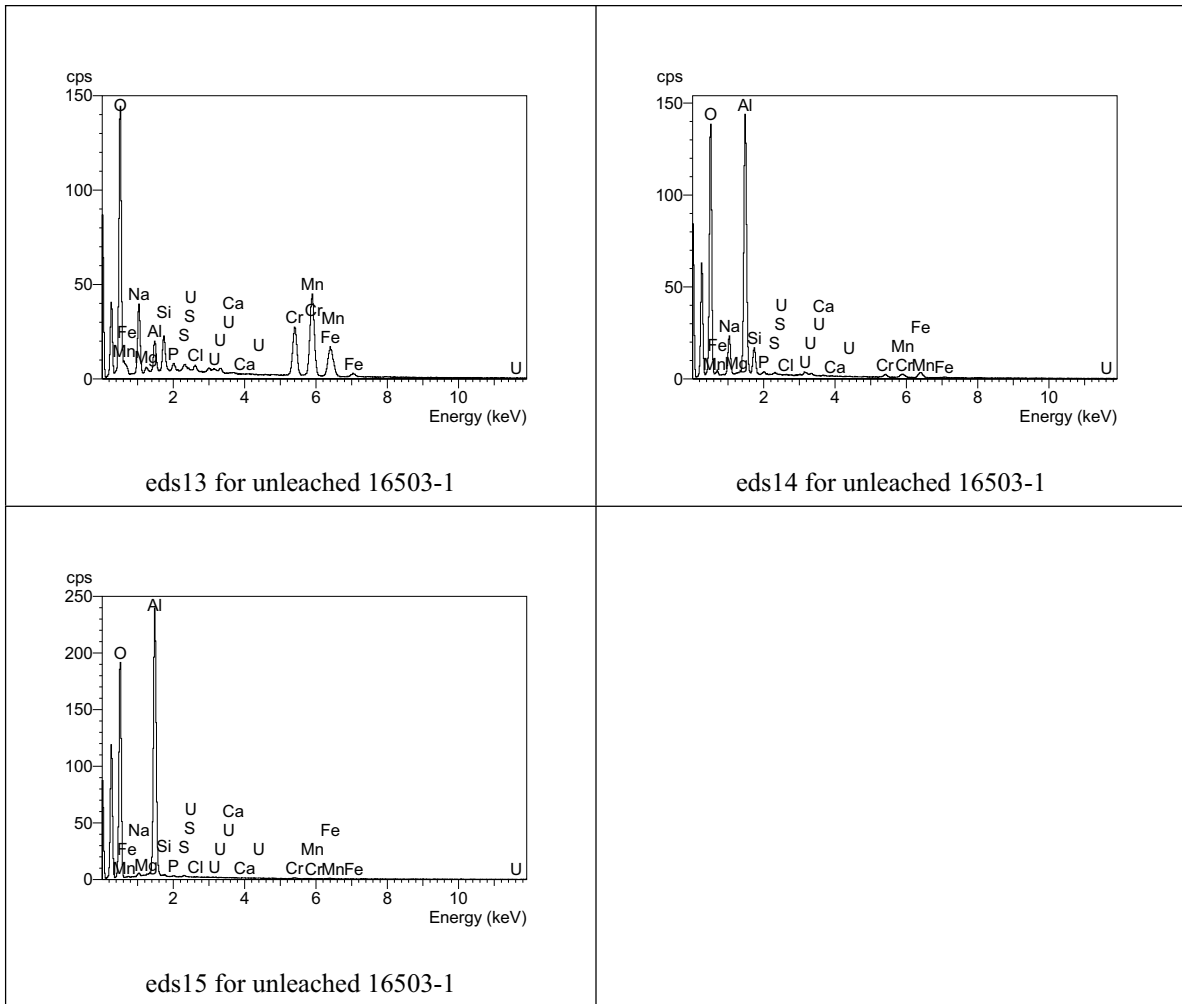


Figure D-3. EDS spectra for analyses eds13 through eds15 for unleached subsample 16503-1 of BX-101 tank sludge (jar 16503)

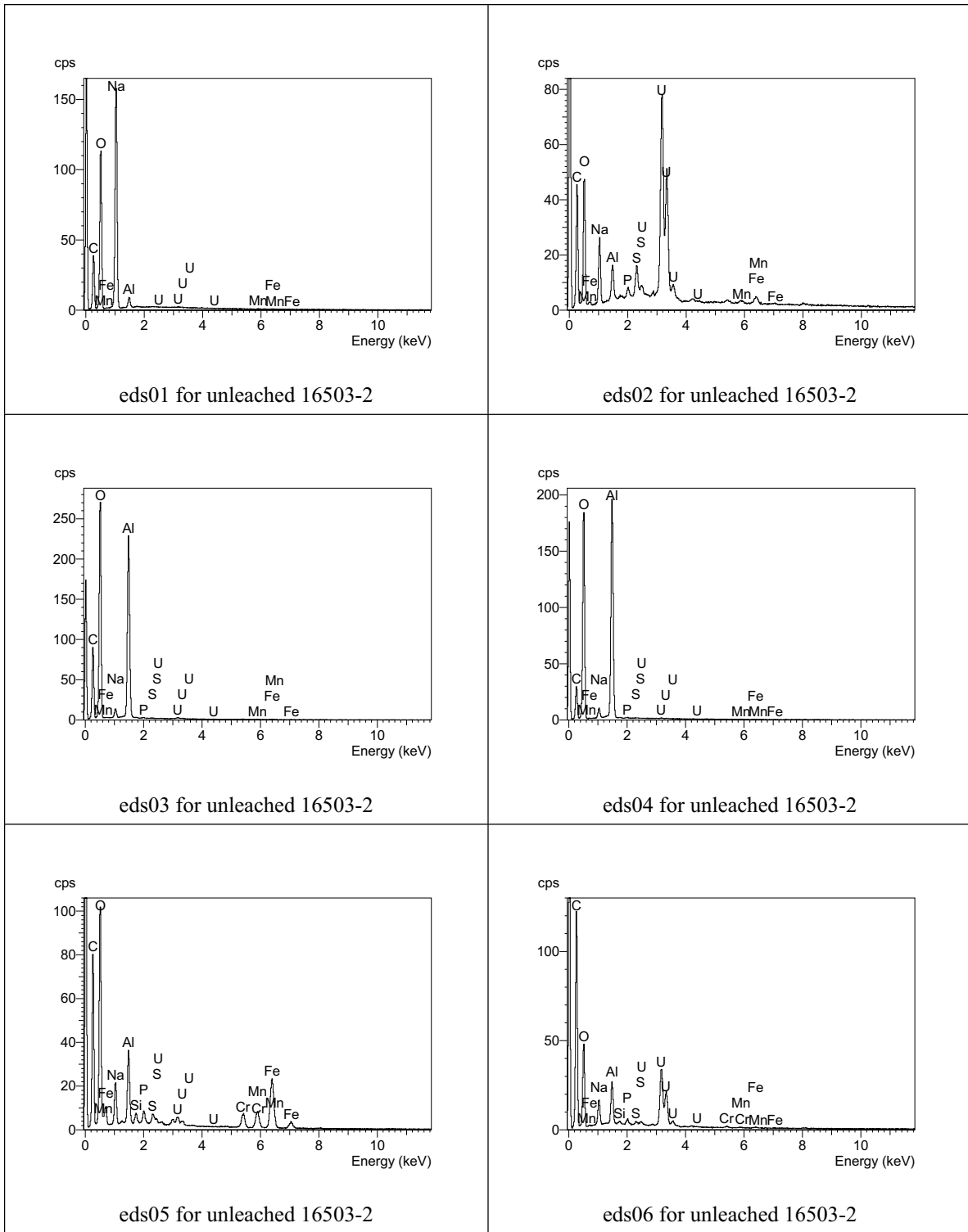


Figure D-4. EDS spectra for analyses eds01 through eds06 for unleached subsample 16503-2 of BX-101 tank sludge (jar 16503)

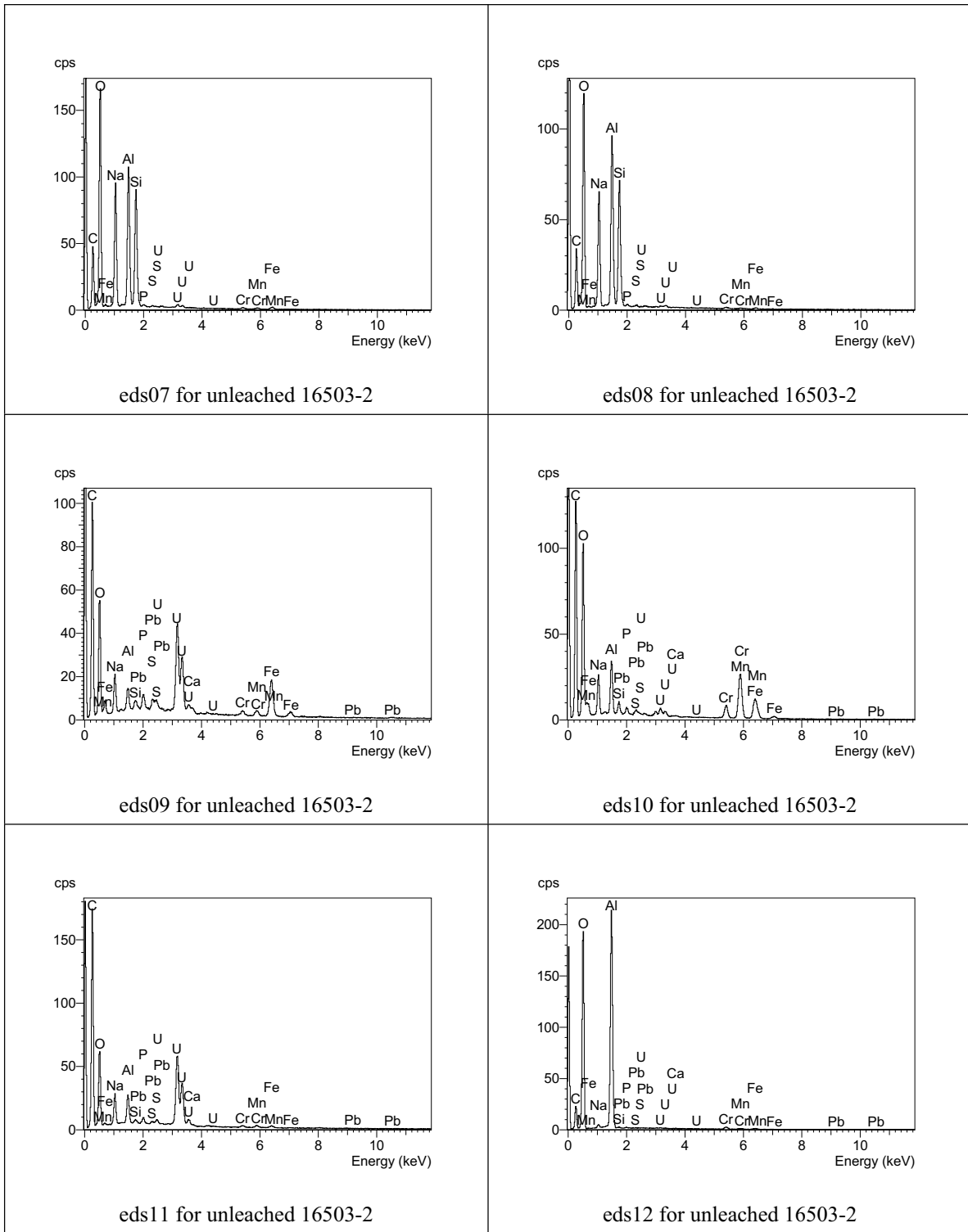


Figure D-5. EDS spectra for analyses eds07 through eds12 for unleached subsample 16503-2 of BX-101 tank sludge (jar 16503)

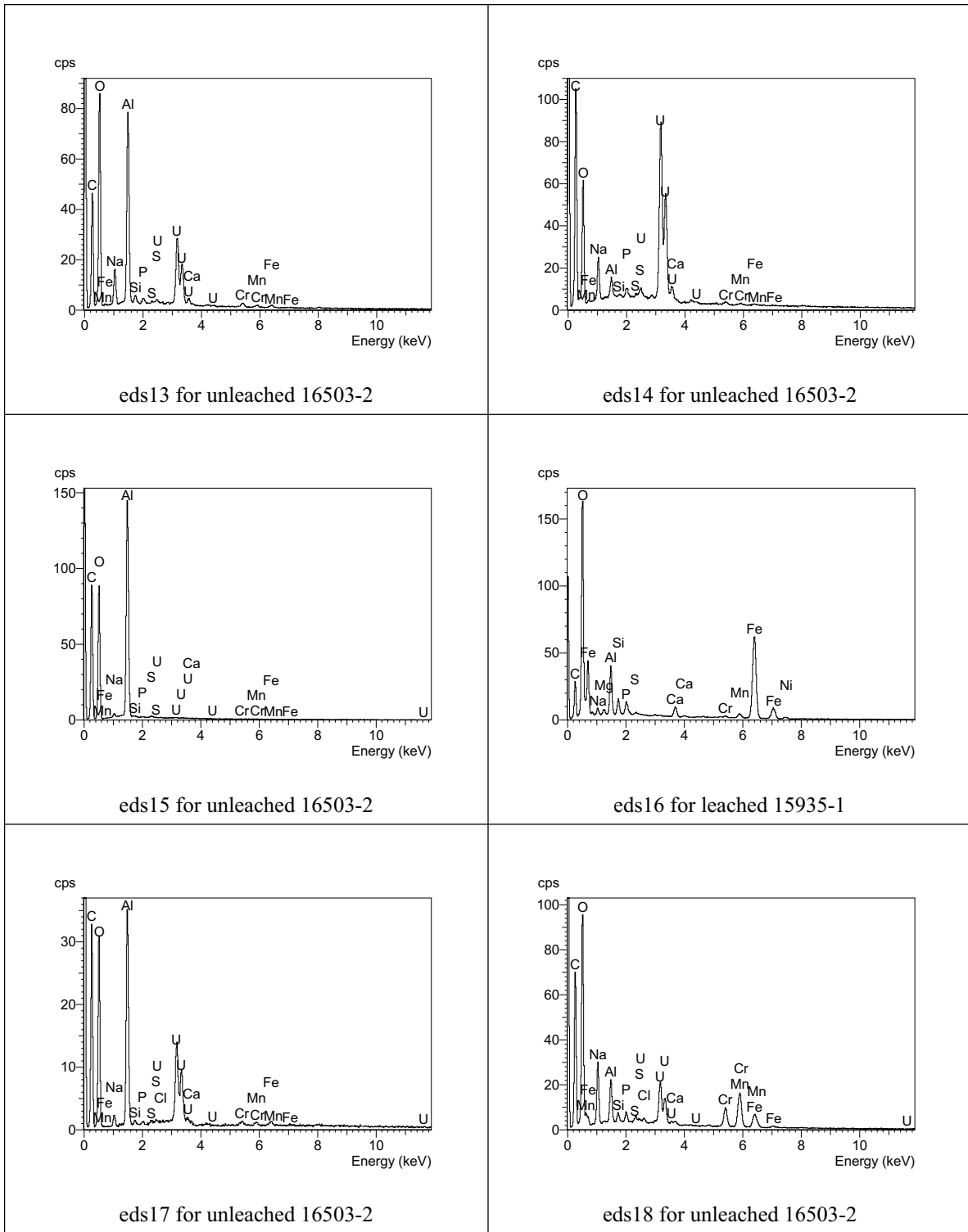


Figure D-6. EDS spectra for analyses eds13 through eds18 for unleached subsample 16503-2 of BX-101 tank sludge (jar 16503)

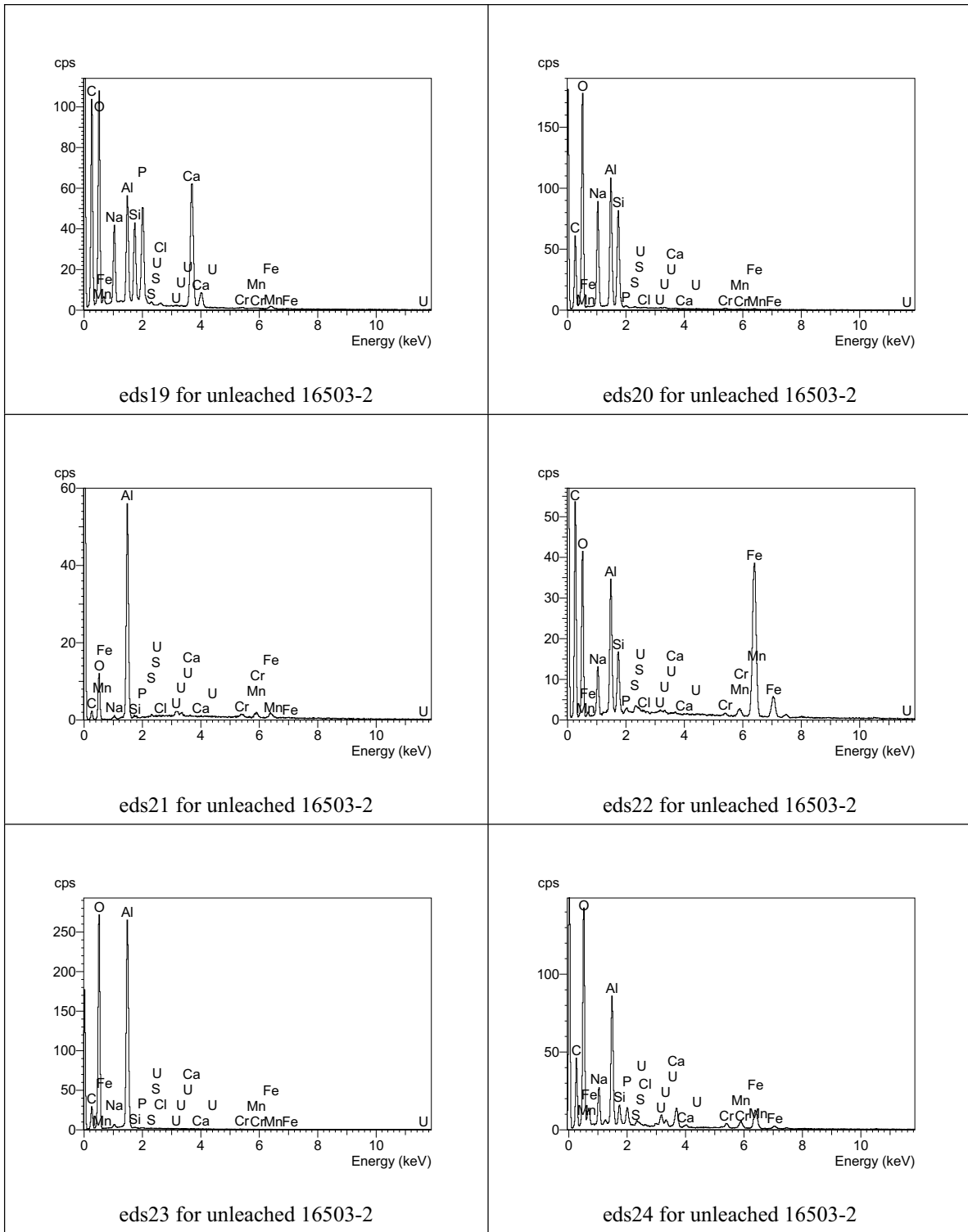


Figure D-7. EDS spectra for analyses eds19 through eds24 for unleached subsample 16503-2 of BX-101 tank sludge (jar 16503)

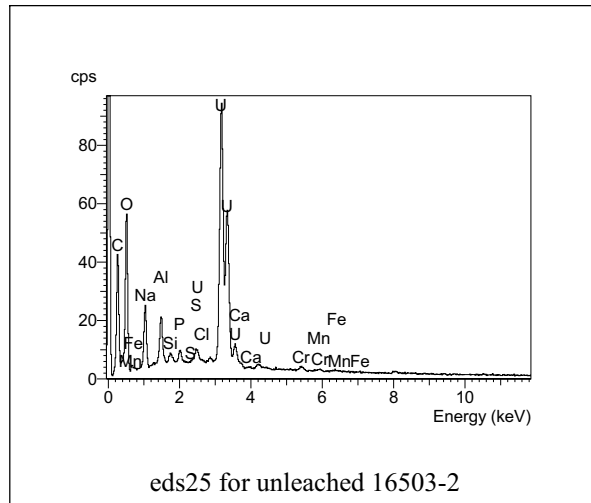


Figure D-8. EDS spectra for analysis eds25 for unleached subsample 16503-2 of BX-101 tank sludge (jar 16503)

Distribution

No. of Copies

No. of Copies

OFFSITE

Steve Airhart
Freestone Environmental Services
1933 Jadwin, Suite 225
Richland, WA 99352-1609

Dr. Harry Babad
2540 Cordoba Court
Richland, WA 99352-1609

Pat Brady
Geochemistry Department, 6118
Sandia National Laboratories
P.O. Box 5800
Albuquerque, NM 87185-0750

Jon Chorover
Associate Professor – Environmental
Chemistry
Department of Soil, Water, and
Environmental Science
Shantz 429, Building #38
University of Arizona
Tucson, AZ 85721-0038

Dirk A. Dunning
Oregon Office of Energy
625 Mariona Street, N.E.
Salem, OR 97301-3742

Jim Harsh
Department of Crop & Soil Sciences
Washington State University
Johnson Hall, Room 249
Pullman, WA 99164-6420

Dr. Daniel I. Kaplan
Westinghouse Savannah River Company
Building 774-43A, Room 215
Aiken, SC 29808

Dr. Kathryn L. Nagy
Department of Earth and Environmental
Sciences
University of Illinois at Chicago (MC-186)
845 West Taylor Street
Chicago, IL 60607-7059

Phil Reed
U.S. Nuclear Regulatory Commission
Office of Nuclear Regulatory Research
Division of Systems Analysis and
Regulatory Effectiveness
Radiation Protection, Env. Risk and Waste
Management Branch
MS T9-F31
Washington, D.C. 20555-0001

Al Robinson
68705, E 715 PRNE
Richland, WA 99352

Doug Sherwood
Rivers Edge Environmental
1616 Riverside Drive
West Richland, WA 99353

David K. Shuh
Lawrence Berkeley National Laboratory
1 Cyclotron Road
MS 70A-1150
Berkeley, CA 94720

**No. of
Copies**

Dan Tyler
Freestone Environmental Services
1933 Jadwin, Suite 225
Richland, WA 99352-1609

Dr. Jiamin Wan
Lawrence Berkeley National Laboratory
1 Cyclotron Road, MS 70-0127A
Berkeley, CA 94720

Mr. Ronald G. Wilhelm
Office of Radiation and Indoor Air
401 M Street, S.W.
Mail Code 6603J
Washington, D.C. 20460

W. Alexander Williams
U.S. Department of Energy
Office of Environmental Restoration
EM-33
19901 Germantown Road
Germantown, MD 20874-1290

ONSITE**4 DOE Office of River Protection**

C. A. Babel	H6-60
P. E. LaMont	H6-60
R. W. Lober	H6-60
R. B. Yasek	H6-60

6 DOE Richland Operations Office

J. P. Hanson	A5-13
K. A. Kapsi	A5-13
J. G. Morse	A6-38
K. M. Thompson	A6-38
DOE Public Reading Room (2)	H2-53

**No. of
Copies****18 CH2M HILL Hanford Group, Inc.**

F. J. Anderson	E6-35
K. C. Burgard	L6-57
M. P. Connelly (5)	E6-35
J. G. Field	H6-62
D. L. Herting	T6-07
T. E. Jones	E6-35
A. J. Knepp	H6-60
S. Lambert	E6-35
J. E. Laurenz	H6-62
T. A. Lee	H9-01
F. M. Mann	E6-35
C. W. Miller	H9-03
D. A. Myers	E6-35
T. L. Sams	H6-05

3 Environmental Protection Agency

N. Ceto	B5-01
D. A. Faulk	B5-01
M. L. Goldstein	B5-01

2 Fluor Federal Services

R. Khaleel	E6-17
R. J. Puigh	E6-17

4 Fluor Hanford, Inc.

T. W. Fogwell	E6-35
B. H. Ford	E6-35
V. G. Johnson	E6-35
M. I. Wood	H8-44

3 Washington State Department of Ecology

S. Dahl	B5-18
J. A. Caggiano	B5-18
E. Rochette	B5-18

**No. of
Copies****No. of
Copies****55 Pacific Northwest National Laboratory**

B. W. Arey	P8-16
S. R. Baum	P7-22
T. M. Brouns	K9-69
C. F. Brown	P7-22
R. W. Bryce	E6-35
K. J. Cantrell	K6-81
R. E. Clayton	P7-22
W. J. Deutsch (10)	K6-81
P. E. Dresel	K6-96
K. M. Geiszler	P7-22
M. J. Fayer	K9-33
A. R. Felmy	K8-96
V. L. Freedman	K9-36
M. D. Freshley	K9-33
J. S. Fruchter	K6-96
G. W. Gee	K9-33
W. J. Hess	P7-50
D. G. Horton	K6-81
J. P. Icenhower	K6-81
C. T. Kincaid	E6-35

K. M. Krupka (5)	K6-81
I. V. Kutnyakov	P7-22
G. V. Last	K6-81
V. L. LeGore	P7-22
M. J. Lindberg	P7-22
C. W. Lindenmeier	P7-22
W. J. Martin	K6-81
S. V. Mattigod	K6-81
B. P. McGrail	K6-81
P. D. Meyer	BPO
E. M. Pierce	K6-81
R. G. Riley	K6-81
R. J. Serne	P7-22
H. T. Schaef	K6-81
W. Um	P7-22
M. Valenta	P7-22
T. S. Vickerman	P7-22
S. B. Yabusaki	K9-36
J. M. Zachara	K8-96
F. Zhang	K9-33
Hanford Technical Library (2)	P8-55